



**HAL**  
open science

# Erythroid differentiation in vitro under the lens of mathematical modelling

Ronan Duchesne

► **To cite this version:**

Ronan Duchesne. Erythroid differentiation in vitro under the lens of mathematical modelling. Bioinformatics [q-bio.QM]. Université de Lyon, 2019. English. NNT : 2019LYSEN082 . tel-02440831v2

**HAL Id: tel-02440831**

**<https://hal.science/tel-02440831v2>**

Submitted on 28 May 2020

**HAL** is a multi-disciplinary open access archive for the deposit and dissemination of scientific research documents, whether they are published or not. The documents may come from teaching and research institutions in France or abroad, or from public or private research centers.

L'archive ouverte pluridisciplinaire **HAL**, est destinée au dépôt et à la diffusion de documents scientifiques de niveau recherche, publiés ou non, émanant des établissements d'enseignement et de recherche français ou étrangers, des laboratoires publics ou privés.



Numéro National de Thèse : 2019LYSEN082

# THÈSE de DOCTORAT de L'UNIVERSITÉ DE LYON

opérée par

## **l'École Normale Supérieure de Lyon**

École Doctorale N° 340 :

**Biologie Moléculaire, Intégrative et Cellulaire (BMIC)**

**Spécialité de doctorat : Biologie**

Soutenue publiquement le 13/12/2019, par :

**Ronan DUCHESNE**

---

## **Erythroid differentiation *in vitro* under the lens of mathematical modelling**

**Modélisation mathématique de la différenciation érythrocytaire *in vitro***

---

Devant le jury composé de :

Geneviève Dupont	DR FNRS	Université Libre de Bruxelles	Rapporteure
Jérémie Guedj	CR INSERM	Université Paris Diderot	Rapporteur
Sophie Pantalacci	CR CNRS	ENS de Lyon	Examinatrice
Delphine Ropers	CR Inria	Centre Inria Grenoble - Rhône-Alpes	Examinatrice
Fabien Crauste	DR CNRS	Institut de Mathématiques de Bordeaux	Co-directeur
Olivier Gandrillon	DR CNRS	ENS de Lyon	Directeur



# Remerciements

Une thèse, c'est long et ça se fait rarement tout seul. Après quasiment quatre ans passés dans le même labo, la liste des personnes à remercier est donc substantielle. Elle s'allongerait d'autant plus si l'on considérait mes sept années passées à l'ENS. Je vais essayer de l'établir de façon à peu près exhaustive dans les pages qui suivent. Mais je pense que c'est une vaine entreprise, et je m'excuse d'avance auprès des personnes que je vais oublier. Pas d'inquiétude, je vous aime bien quand même.

Tout d'abord, il faut que je remercie Fabien et Olivier, qui ont accepté d'encadrer un stagiaire un peu paumé en février 2016 et qui n'ont depuis lors pas cessé de le supporter –dans tous les sens du terme– avec une patience dont j'aurais été incapable. Vous m'avez déjà énormément appris, mais je ne comprends toujours pas comment vous êtes capables de faire tout ce que vous faites. J'espère pouvoir vous ressembler un peu plus un jour (peut-être).

Ensuite, il faut mentionner l'équipe SBDM du LBMC, ainsi que l'équipe Dracula d'Inria, pour m'avoir accueilli pendant tout ce temps. Et en particulier les autres thésards, qui ont partagé mes interrogations et m'ont aidé dans la mesure du possible dès qu'ils le pouvaient. Je tiens aussi à remercier l'assistante de l'équipe Dracula, Claire Sauer, qui a su m'aider à surmonter ma phobie administrative avec humour. Parmi tout ces collègues, une personne en particulier mérite une place d'honneur dans ces remerciements. Pour avoir cohabité dans le même bureau que moi pendant l'essentiel de ces années. Pour avoir accompagné mes pauses. Pour m'avoir encouragé quand ça n'allait pas, et pour avoir partagé mon bonheur quand ça allait. Et surtout pour avoir as-

suré l'intégralité de la contrepartie expérimentale des travaux exposés dans ces pages. Anissa, rien de tout ceci n'aurait été possible sans toi et je considère que le contenu de ce manuscrit t'appartient tout autant qu'à moi.

Je dois aussi remercier les membres de mon comité de thèse, Adeline Leclercq-Samson et Arezki Boudaoud, pour avoir suivi mon travail à travers les années, ainsi que les deux rapporteurs de ma thèse, Geneviève Dupont et Jérémie Guedj, pour avoir accepté de relire mon manuscrit à un moment où je n'en étais honnêtement plus capable. Et bien sûr Sophie Pantalacci et Delphine Ropers qui ont accepté de faire partie de mon jury.

Une partie non-négligeable de mon temps de ces dernières années a été occupée par l'enseignement. Ça n'aurait pas été possible sans Cendrine Moskalenko et Arezki Boudaoud, qui ont défendu ma candidature face à un département qui ne semble toujours pas convaincu de l'intérêt d'enseignements pluri-disciplinaires en biologie. Je tiens aussi à remercier tous les profs qui m'ont ensuite aidé à remplir mon service (et souvent à le dépasser), en particulier Marie Sémon et Stéphane Vincent pour leurs conseils et les opportunités qu'ils m'ont offertes.

Je tiens aussi à saluer ici la performance de l'équipe de la pause café du Foyer, qui a su rester réglée comme une horloge malgré les années qui s'accumulent et les nombreux départs pour post-doc et chômages divers : Gram', Benji, Valou, et surtout Jason, pour toutes ses interrogations existentielles qui nous ont occupées à travers ces années. Plus généralement, je tiens à remercier tous les vieux thésards de l'ENS, qui m'ont montré ce qui m'attendait (Léo, Pinouz, Groliv', Baba, Raph', Gram', Benji, Karpi et sans doute beaucoup d'autres que j'oublie). À une époque, je pensais que je valais mieux que vous et que tout se passerait bien pour moi. L'expérience montre que je ne pouvais pas me tromper plus.

Tant que j'en suis rendu à remercier mes amis, il faut absolument que je mentionne Tomtom et Michou, qui m'ont soumis l'idée de faire de la musique un jour dans l'ancien Foyer. Ils ne s'en rappellent sans doute pas, mais ils ont eu ce jour-là un rôle déterminant dans ma vie, et dans ce qui allait se

## Remerciements

passer pendant cette thèse. Il y a ensuite eu la Fanfarovis (et l'ensemble de ses membres), qui m'a prêté un instrument et m'a appris à en jouer, comme à tant d'autres, dans la bonne ambiance et sans jugement. Notre périple à vélo reste gravé dans ma mémoire comme mon meilleur souvenir de vacances. Puis la Bërkaille, qui a partagé mon rêve électro-cuivré et l'a fait grandir bien au-delà de toutes mes espérances. J'ose espérer que vous continuerez à faire vibrer les murs de la festive bien après mon départ. Au fil des années, la gralternative m'a permis d'assouvir ma soif de tierces picardes et d'entretenir le parolier de l'ENS avec une originalité et une motivation que je ne pensais plus pouvoir y trouver. Il faut aussi mentionner Émilie Jaunie, comme étant le groupe au meilleur ratio style/visibilité, du haut de ses zéros performances publiques. Les répètes étaient cool quand même. J'aimerais ajouter (exceptionnellement) à cette liste un groupe dont je n'ai pas fait partie, le Bonk, pour son énergie et surtout pour l'ensemble de son œuvre, qui m'a fait changer d'avis sur la musique électronique (ce qui n'était pas gagné).

Au-delà de la musique, il y a énormément de personnes que je tiens à remercier pour les moments qu'on a partagés ces dernières années. La roroteam, et en particulier mon homonyme Roro Dudu, pour nos expériences de connexion mentale. Mes collègues les anciens RF pour avoir fait vivre le Foyer avec moi. Et les nouveaux, pour avoir démontré qu'il est plus que jamais, et malgré son déménagement, un concept et non pas un lieu. Tant qu'on parle du Foyer, il y a aussi la team de l'apéro, dont la liste exhaustive serait beaucoup trop longue, mais qui m'a fait passer un catalogue inépuisable de bons moments. Devoir vous quitter constituera la rupture la plus difficile de ma vie, et j'espère pouvoir retrouver des gens comme vous partout où j'irai. Les BDE successifs de ces dernières années (Kwaggas, Gorfous, Quokkas et Bilbys, mais on pourrait remonter plus loin, jusqu'aux Ouandjis, Krakens, Bongos et même jusqu'aux Dugongs) pour tous ces WEI et autres événements inoubliables dont je n'ai gardé aucun souvenir. Je tiens aussi à mentionner les amis particuliers qu'ont été Medhi, Tony, Sam et surtout Awax (the best <3), pour leur disponibilité et la qualité des services qu'ils m'ont rendus aux moments où ça n'allait

pas.

Il faudrait aussi que je parle des habitants successifs du déciBar (Briscard, Alicia, Fiona et Angèle) pour avoir supporté de vivre avec moi ; et ceux de la yoloc' (Antton, Christine, Jason, Clément, Juliette, Alassane, Sonia, Siméon, Yolaine et tous les nouveaux que je ne connais pas encore) pour avoir transcendé les frontières de nos apparts'. Une très grosse dédicace va à Antton, qui ne se rendra sans doute jamais compte à quel point il m'aura servi de modèle dans la vie. Pour le meilleur et pour le pire, apparemment.

Enfin, je tiens à adresser mes plus sincères remerciements à ma famille, qui a toujours su me soutenir et m'encourager à distance, peu importe les problèmes que j'ai pu rencontrer.

# Contents

<b>Remerciements</b>	<b>iii</b>
<b>Contents</b>	<b>vii</b>
<b>List of Figures</b>	<b>xiii</b>
<b>List of Tables</b>	<b>xvii</b>
<b>List of Abbreviations</b>	<b>xix</b>
<b>List of Mathematical Notations</b>	<b>xxi</b>
<b>1 Introduction</b>	<b>1</b>
1.1 <i>In vitro</i> erythropoiesis . . . . .	2
1.1.1 A classical view of haematopoiesis and erythropoiesis . .	2
1.1.2 The TGF- $\alpha$ /TGF- $\beta$ -induced Erythrocytic Cells (T2EC) . .	4
1.1.3 Modelling attempts . . . . .	6
1.2 Differentiation and decision-making at the single-cell level . . . .	8
1.2.1 Stochasticity of Gene Expression (SGE) . . . . .	9
1.2.2 SGE and decision-making . . . . .	10
1.2.3 Experimental manipulation of SGE . . . . .	15
1.3 Parameter estimation and identifiability in mathematical models	16
1.3.1 Definitions . . . . .	16
1.3.2 Maximum Likelihood Estimation (MLE) . . . . .	17

1.3.3	Structural identifiability . . . . .	19
1.3.4	Practical identifiability . . . . .	19
1.3.4.1	Profile likelihood . . . . .	20
1.3.4.2	The Fisher Information Matrix (FIM) . . . . .	21
1.3.4.3	Computational cost and precision of the methods	24
1.3.5	Related concepts . . . . .	24
1.3.5.1	Parameter sensitivity . . . . .	24
1.3.5.2	Experimental design . . . . .	25
1.3.5.3	Sloppiness . . . . .	26
1.3.5.4	Dynamical compensation . . . . .	27
1.4	Mixed Effects Models (MEM) . . . . .	28
1.4.1	General principle and definitions . . . . .	29
1.4.1.1	Structural model . . . . .	29
1.4.1.2	Parameter model . . . . .	29
1.4.1.3	Error model . . . . .	31
1.4.2	Parameter estimation . . . . .	31
1.4.2.1	Population parameters . . . . .	32
1.4.2.2	The Stochastic Approximation of the Expectation Maximization (SAEM) algorithm . . . . .	33
1.4.2.3	Individual parameters . . . . .	34
1.4.3	Model selection . . . . .	35
1.4.3.1	Bayesian Information Criterion (BIC) . . . . .	35
1.4.3.2	Akaike's Information Criterion (AIC) . . . . .	37
1.4.3.3	Likelihood Ratio Test (LRT) . . . . .	38
1.4.4	Identifiability in mixed effects models . . . . .	38
1.4.4.1	Population parameters . . . . .	39
1.4.4.2	Individual parameters . . . . .	40
1.5	Thesis outline . . . . .	41
<b>2</b>	<b>A deterministic model of <i>in vitro</i> erythropoiesis</b>	<b>43</b>
2.1	Introduction . . . . .	43
2.2	Paper . . . . .	44

## Contents

2.3	Conclusion . . . . .	69
<b>3</b>	<b>Drugs that modulate SGE and differentiation</b>	<b>71</b>
3.1	Introduction . . . . .	71
3.2	Paper . . . . .	72
3.3	Conclusion . . . . .	87
<b>4</b>	<b>From a deterministic model to a mixed effects model - The Standard Two-States approach (STS)</b>	<b>89</b>
4.1	Introduction . . . . .	89
4.2	Some considerations on the results of the previous chapters . . .	90
4.3	Calibrating the deterministic model on a larger dataset . . . . .	94
4.4	Conclusion . . . . .	96
<b>5</b>	<b>Elaboration of a mixed effects model for the <i>in vitro</i> erythropoiesis</b>	<b>99</b>
5.1	Introduction . . . . .	99
5.2	A first version of the model . . . . .	100
5.3	Selection of a distribution for $\delta_{SC}$ . . . . .	104
5.4	Identifiability analysis of our MEM . . . . .	107
5.4.1	Population parameters: Initial Guess Sampling (IGS) . . .	107
5.4.2	Individual parameters: $\eta$ -shrinkage . . . . .	110
5.5	Conclusion . . . . .	110
<b>6</b>	<b>Experimental design</b>	<b>113</b>
6.1	Methods . . . . .	115
6.1.1	Population size . . . . .	115
6.1.2	Generation of artificial datasets . . . . .	115
6.1.3	Model calibration . . . . .	117
6.2	Convergence . . . . .	117
6.3	Identifiability of the population parameters . . . . .	119
6.3.1	FIM-based identifiability . . . . .	119
6.3.2	Population parameter values. . . . .	121
6.4	Identifiability of the individual parameters . . . . .	121

6.5	Conclusion . . . . .	124
<b>7</b>	<b>Reduction procedure in mixed effect models</b>	<b>125</b>
7.1	Introduction . . . . .	125
7.2	Initial estimation of parameter values of the full model . . . . .	126
7.2.1	Convergence over 50 SAEM runs . . . . .	126
7.2.2	Population parameters . . . . .	126
7.3	Model with reduced $\delta_{SC}^{pop}$ and $\delta_{CB}^{pop}$ . . . . .	128
7.3.1	Convergence over 50 SAEM runs . . . . .	130
7.3.2	Population parameters . . . . .	131
7.3.3	Individual random effects . . . . .	133
7.4	Model with reduced $\delta_{SC}^{pop}$ , $\delta_{CB}^{pop}$ and a fixed $\rho_C$ . . . . .	134
7.4.1	Convergence over 50 SAEM runs . . . . .	134
7.4.2	Population parameters . . . . .	134
7.4.3	Individual parameters . . . . .	137
7.5	Final model with reduced $\delta_{SC}^{pop}$ , $\delta_{CB}^{pop}$ , and fixed $\rho_C$ and $\rho_B$ . . . . .	138
7.5.1	Convergence over 50 SAEM runs . . . . .	138
7.5.2	Population parameters . . . . .	139
7.5.3	Individual parameters . . . . .	139
7.5.4	Quality of the fit . . . . .	140
7.6	Discussion . . . . .	141
7.6.1	Parameter values in the final model . . . . .	141
7.6.2	About the final model . . . . .	146
7.6.3	Conclusion . . . . .	147
<b>8</b>	<b>Discussion and prospects</b>	<b>149</b>
8.1	A mathematical model of <i>in vitro</i> erythropoiesis . . . . .	149
8.2	Stochasticity of gene expression and differentiation . . . . .	151
8.3	Generalizing our reduction approach for mixed effect models . . . . .	152
8.4	Computing the effect of the drugs with the mixed effect model . . . . .	153
8.5	Source of experimental heterogeneity . . . . .	154
8.6	Conclusion . . . . .	155

Contents

**Bibliography**

**157**



# List of Figures

1.1	Overview of haematopoiesis and erythropoiesis . . . . .	3
1.2	Experimental context of this study . . . . .	5
1.3	A systems biology view on cell decision-making in a simplistic case . . . . .	12
1.4	Effects of the drugs that influence the extent of SGE on the <i>in vitro</i> erythroid proliferation and differentiation. . . . .	15
1.5	The different outcomes of profile-likelihood-based identifiability analysis . . . . .	22
1.6	Number of publications in relation with identifiability . . . . .	25
4.1	Experimental heterogeneity in the control condition . . . . .	91
4.2	Experimental heterogeneity in the treated condition . . . . .	92
4.3	Parameter values from the previous chapters . . . . .	93
4.4	Boxplots of the full dataset . . . . .	94
4.5	Spaghetti plots of the full dataset . . . . .	95
4.6	Parameter values in the full dataset . . . . .	96
5.1	Distribution of the optimal likelihood values of our MEM . . . . .	103
5.2	Optimal likelihood values of the model with two bounds and the <i>rate model</i> . . . . .	107
5.3	Initial guess sampling of the population parameters of the model with a lognormal $\delta_{SC}$ . . . . .	108
5.4	Parameter distributions for the <i>rate model</i> . . . . .	109

6.1	Number of convergent runs as a function of population size . . .	118
6.2	Fraction of correctly estimated FIMs as a function of population size . . . . .	119
6.3	FIM-based identifiability criteria as a function of population size	120
6.4	Estimated population parameters as a function of population size	122
6.5	$\eta$ -shrinkage as a function of population size . . . . .	123
7.1	Likelihood distribution over 50 SAEM runs on the full model . .	127
7.2	Normalized parameter values in the the full model . . . . .	128
7.3	Correlation heatmap of the unidentifiable population parameters for the full model . . . . .	129
7.4	Correlations between population parameters in the full model . .	129
7.5	Likelihood distribution of the model with reduced $\delta_{SC}^{pop}$ and $\delta_{CB}^{pop}$	131
7.6	Estimated parameter values for the model with reduced $\delta_{SC}^{pop}$ and $\delta_{CB}^{pop}$ . . . . .	132
7.7	Correlations between population parameters in the model with reduced $\delta_{SC}^{pop}$ and $\delta_{CB}^{pop}$ . . . . .	132
7.8	Distribution of $s_\eta$ values for the model with reduced $\delta_{SC}^{pop}$ and $\delta_{CB}^{pop}$	133
7.9	Likelihood distribution of the model with reduced $\delta_{SC}^{pop}$ , and $\delta_{CB}^{pop}$ , and no variability on $\rho_C$ . . . . .	135
7.10	Estimated parameter values for the model with reduced $\delta_{SC}^{pop}$ and $\delta_{CB}^{pop}$ , and no variability on $\rho_C$ . . . . .	136
7.11	Correlations in the model with reduced $\delta_{SC}^{pop}$ and $\delta_{CB}^{pop}$ , and no variability on $\rho_C$ . . . . .	136
7.12	Distribution of $s_\eta$ values for the model with reduced $\delta_{SC}^{pop}$ and $\delta_{CB}^{pop}$ , and no variability on $\rho_C$ . . . . .	137
7.13	Likelihood distribution of the model with reduced $\delta_{SC}^{pop}$ , and $\delta_{CB}^{pop}$ , and no variability on $\rho_C$ and $\rho_B$ . . . . .	139
7.14	Normalized parameter values for the model with reduced $\delta_{SC}^{pop}$ and $\delta_{CB}^{pop}$ , and no variability on $\rho_C$ and $\rho_B$ . . . . .	140
7.15	Distribution of $s_\eta$ values for the individual parameters in the 25 convergent runs of SAEM. . . . .	141

## List of Figures

7.16	Observation/Prediction Diagram of the reduced model . . . . .	142
7.17	Estimated parameter values for the model with reduced $\delta_{SC}^{pop}$ and $\delta_{CB}^{pop}$ , and no variability on $\rho_C$ and $\rho_B$ . . . . .	143
7.18	Parameter distributions in the reduced model . . . . .	143
7.19	Cell distributions in each replicate of the experiment . . . . .	145
8.1	Diagram of the model designed in Chapter 2 . . . . .	150



# List of Tables

5.1	Initial guess values and distributions in our MEM . . . . .	102
5.2	Parameters with a null-sensitivity . . . . .	104
5.3	Alternative MEM defined by relaxing the bounds of $\delta_{SC}$ . . . . .	105
5.4	Selection criteria evaluated for our alternative $\delta_{SC}$ distributions .	106
6.1	Parameter values used to generate the artificial datasets and cal- ibrate the model . . . . .	116



# List of Abbreviations

ABM	Agent-Based Model
DDE	Delay-differential Equation
DE	Differential Equation
DM17	Differentiation medium
EBE	Empirical Bayesian Estimates
Epo	Erythropoietin
FIM	Fisher Information Matrix
GRN	Gene Regulatory Network
IGS	Initial Guess Sampling
IWRES	Individual Weighted RESiduals
LM1	Self-renewal medium
LRT	Likelihood-Ration Test
MEM	Mixed-Effects Model
ODE	Ordinary Differential Equation
PDE	Partial Differential Equation
PK	Pharmacokinetic
PKPD	Pharmacokinetic/Pharmacodynamic
sc-RNAseq	single-cell RNA-sequencing
sc-RTqPCR	single-cell Retro-Transcription quantitative Polymerase Chain Reaction
SAEM	Stochastic Approximation Expectation Maximisation
SDE	Stochastic Differential Equation
s.e.	standard error
SGE	Stochasticity of Gene Expression
T2EC	TGF- $\alpha$ /TGF- $\beta$ -induced Erythrocytic Cells



# List of Mathematical Notations

## Model specification

$y$	Data
$y_{i,j}$	Data for the $i^{th}$ observable measured at the $j^{th}$ timepoint
$n_{tot} = nm$	Total sample size
$n$	Number of observables
$m$	Number of timepoints
$f(t, y_0, \theta)$	Prediction from the dynamic model
$f_i(t_j, y_0, \theta)$	Prediction for the $i^{th}$ observable at the $j^{th}$ timepoint.
$g(t, y_0, \theta, \psi)$	Error model
$g_i(t, y_0, \theta, \psi)$	Error for the $i^{th}$ observable at the $j^{th}$ timepoint.
$t$	Time
$t_j$	$j^{th}$ timepoint
$y_0$	Initial condition
$\theta$	Parameters of the dynamic model
$\psi$	Error parameters
$\Theta = (\theta, \psi)$	Parameter vector
$K = \#(\Theta)$	Number of parameters

## Parameter estimation and identifiability

$\mathcal{L}(y t, y_0, \theta, \psi)$	Likelihood
$\hat{\theta}$	Optimal parameter set

$PL_{\theta_i}$	Profile likelihood w.r.t. parameter $\theta_i$
$CI_{\theta_i}(\alpha)$	Confidence interval of parameter $\theta_i$ at level of confidence $\alpha$
$\chi^2(\alpha, K)$	$\alpha$ -quantile of a $\chi^2$ distribution with $K$ degrees of freedom

## Fisher information matrix

$\mathcal{I}$	Fisher Information Matrix
$\mathcal{I}_{i,j}$	Coefficient at the $i^{th}$ row and $j^{th}$ column of the Fisher Information Matrix
$D$	D-criterion (determinant of the FIM)
$A$	A-criterion (trace of the FIM inverse)
$A_{modified}$	Modified A-criterion (trace of the FIM)
$E$	E-criterion (smallest FIM eigenvalue)
$E_{modified}$	Modified E-criterion (ratio of the largest to smallest FIM eigenvalues)

## Model selection

$BIC$	Bayesian Information Criterion
$AIC$	Akaike's Information Criterion
$w_{AIC}$	Akaike's weights

## Mixed Effect Models

$y_{i,j,k}$	Data for the $i^{th}$ observable measured at time $t_j$ on the $k^{th}$ individual
$y_{\cdot, \cdot, k}$	Data for the $k^{th}$ individual
$n_{tot} = nmN$	Total sample size
$N$	Population size (number of individuals)
$\theta_k$	Individual value of parameter $\theta$ in the $k^{th}$ individual
$\eta_k$	Individual random effect of the $k^{th}$ individual
$\theta^{pop}$	Fixed effect of parameter $\theta$
$\omega_\theta$	Standard-deviation of the random effect on parameter $\theta$

## List of Mathematical Notations

$\Omega$	Variance-covariance matrix of the random effects
$\psi$	Error parameters
$f_i(t_j, y_0, \theta_k)$	Prediction for the $i^{\text{th}}$ observable at time $t_j$ for individual $k$ .
$g_i(t_j, y_0, \theta_k, \psi)$	Model error for the $i^{\text{th}}$ observable at time $t_j$ for individual $k$ .
$\epsilon_{i,j,k}$	Individual weighted residual for observable $i$ at time $t_j$ for individual $k$
$s_\eta$	$\eta$ -shrinkage



# Chapter 1

## Introduction

Throughout the pages of this manuscript, we will mainly try to build and study mathematical models of the *in vitro* erythroid differentiation. This work was realized in the context of the studies of the Systems Biology of Decision-Making team, which uses the modern tools of systems biology to characterize decision-making at the single-cell level. These studies make an extensive use of mathematical modelling in complement to experimental work, and this manuscript represents the modelling counterpart to the work of a former experimentalist PhD student in the group, Anissa Guillemin.

In this introduction, we first present erythroid differentiation *in vivo*, also known as *erythropoiesis*, and the *in vitro* system that we use to model it experimentally (Section 1.1). Then, we introduce the contemporary theoretical framework to study cell decision-making processes, such as differentiation, and how we use *in vitro* erythroid differentiation as an experimental tool to tackle it (Section 1.2). In particular, we present the current modelling tools used to study erythropoiesis (Section 1.2.2). As we will see, the assessment of parameter identifiability will be of critical importance for our models, so we will introduce this notion and the related concepts in Section 1.3. Finally, as the most part of this manuscript is dedicated to the elaboration of Mixed Effects Models (MEM) of *in vitro* erythropoiesis, we will introduce these models and the related methodologies in Section 1.4.

## 1.1 *In vitro* erythropoiesis

### 1.1.1 A classical view of haematopoiesis and erythropoiesis

Haematopoiesis is the process which generates all blood and immune cells of vertebrates. Because living organisms maintain a constant blood composition in terms of cell populations despite cell death –a phenomenon known as homeostasis– haematopoiesis is tightly regulated. For instance, an adult human body produces around  $200 \times 10^9$  red blood cells each day.

All blood cells originate from haematopoietic stem cells, which live in specific environments called *niches*, that are located in the bone marrow. As reviewed in Weissman and Shizuru (2008), Seita and Weissman (2010), and Haas et al. (2018), early experiments of bone marrow transplants in mice proved the existence of these multipotent (as they could generate all blood cell types), self-renewing (as they could sustainably repopulate blood cell types upon serial transplantations) stem cells. In the classical view of differentiation, haematopoietic stem cells can differentiate into two different lineages of progenitors: the myeloid and the lymphoid lineages (Figure 1.1A). Each progenitor type can then differentiate into discrete sub-divisions of the lineage with reduced potency and self-renewal, which has led to the tree-like representation of differentiation of Figure 1.1A, though with considerable debate regarding the position of the branchings (G. Brown et al., 1985; Singh, 1996; Görgens et al., 2013). Reviews about haematopoietic stem cells are given in Weissman and Shizuru (2008), Seita and Weissman (2010), and Haas et al. (2018).

A branch of haematopoiesis that will be of particular interest in this manuscript is erythropoiesis, that is the generation of mature red blood cells from erythropoietic progenitors from the myeloid lineage. It is controlled by the hormone erythropoietin (Epo). The classical view of differentiation represents erythropoiesis as a series of discrete transitions between more and more mature cell types (Figure 1.1B). This is accompanied by a progressive reduction of cell size (Dolznig et al., 1995), a decrease of the expression of genes involved in self-renewal (Bresson-Mazet et al., 2008), and an increase in the ex-

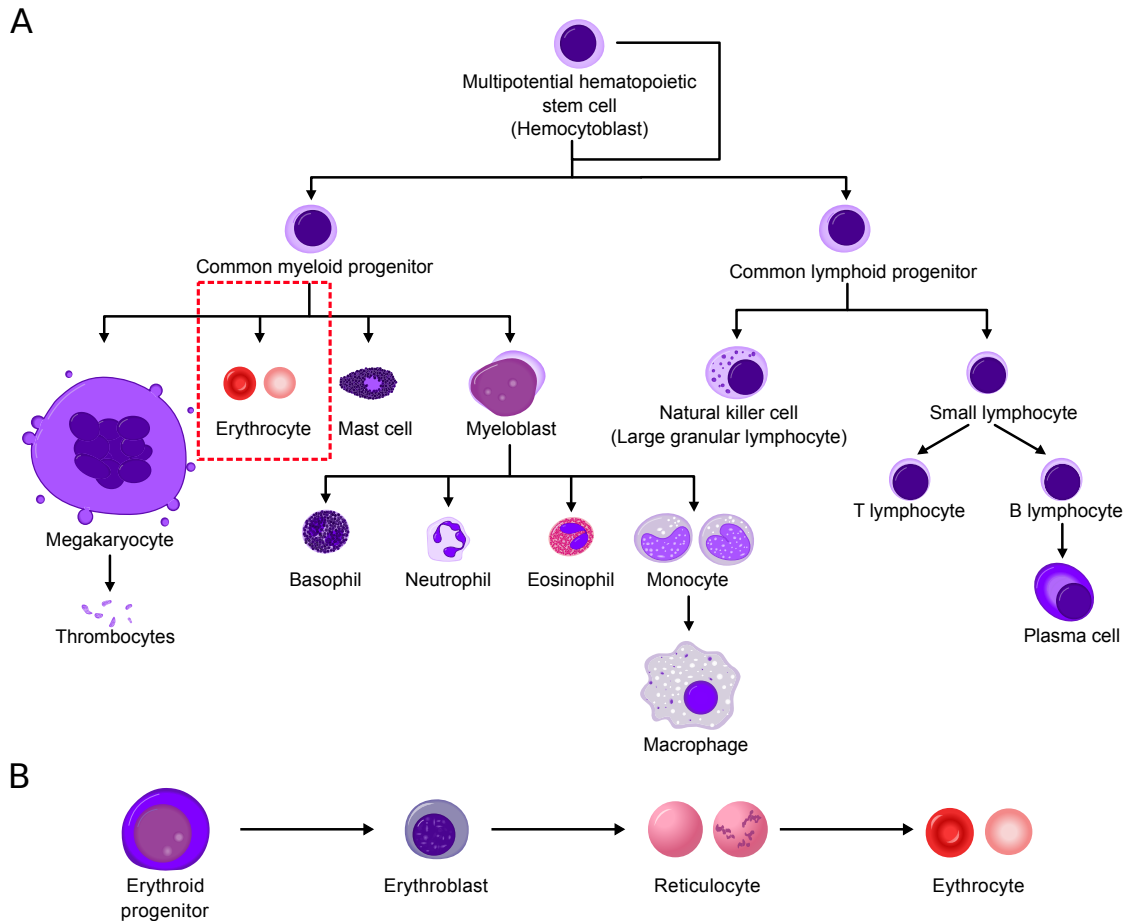


Figure 1.1: Overview of haematopoiesis and erythropoiesis. A: Classical tree-like representation of haematopoiesis. The portion of the tree corresponding to erythropoiesis is framed in red. B: Classical cascade representation of erythropoiesis. Sketches of each cell represent its typical morphology in humans. Both panels are adapted from Wikimedia Commons (Wikimedia Commons, 2019a,b, originals and the present figure are licensed under CC BY-SA 3.0.)

pression of  $\beta$ -globins (Baron and Maniatis, 1991). In mammals, the final steps of erythropoiesis involve the eviction of the cell nucleus and the degradation of mitochondria, while in birds the nucleus and mitochondria are conserved (Kowalski and Palyga, 2011), but the nucleus becomes so condensed that it is not able to show any transcriptional activity.

In order to study cellular differentiation *in vitro*, our group has made an extensive use of avian erythropoiesis as an experimental model (Gandrillon et al., 1999; Dazy et al., 2003; Bresson-Mazet et al., 2008; Gonin-Giraud et al., 2008; Richard et al., 2016; Guillemain et al., 2018), which we present in more details in the next section. Then, we review mathematical models of erythropoiesis in Section 1.1.3. Finally, we introduce why the modern view of cellular differentiation, based on contemporary single-cell experimental techniques, challenges this classical representation of differentiation (Figure 1.1) as a branching network of homogenous, discrete cell types of decreasing potential, in Section 1.2.

### 1.1.2 The TGF- $\alpha$ /TGF- $\beta$ -induced Erythrocytic Cells (T2EC)

The TGF- $\alpha$ /TGF- $\beta$ -induced Erythrocytic Cells (T2EC) are erythroid progenitors from the bone marrow of chicken embryos (Gandrillon et al., 1999). By placing bone marrow samples in a medium containing TGF- $\alpha$  and TGF- $\beta$  (two growth factors which influence various progenitors of the haematopoietic lineage) one can stimulate the proliferation of the erythroid progenitors while the other marrow cells decay. After a few days in the medium, the culture is composed of more than 99% erythroid progenitors (Gandrillon et al., 1999). This culture medium containing TGF- $\alpha$  and TGF- $\beta$ , in which T2EC are able to proliferate, will be referred to as the *LM1 medium*, or *self-renewal medium*.

The T2EC are also able to differentiate into fully mature erythrocytes if one replaces the LM1 medium with another one, which contains anaemic chicken serum. This culture medium will be referred to as the *DM17 medium*, or *differentiation medium*. After 6 days in DM17, the culture is fully differentiated (Gandrillon et al., 1999).

In LM1, the culture is a mixture of alive and dead progenitors. It is pos-

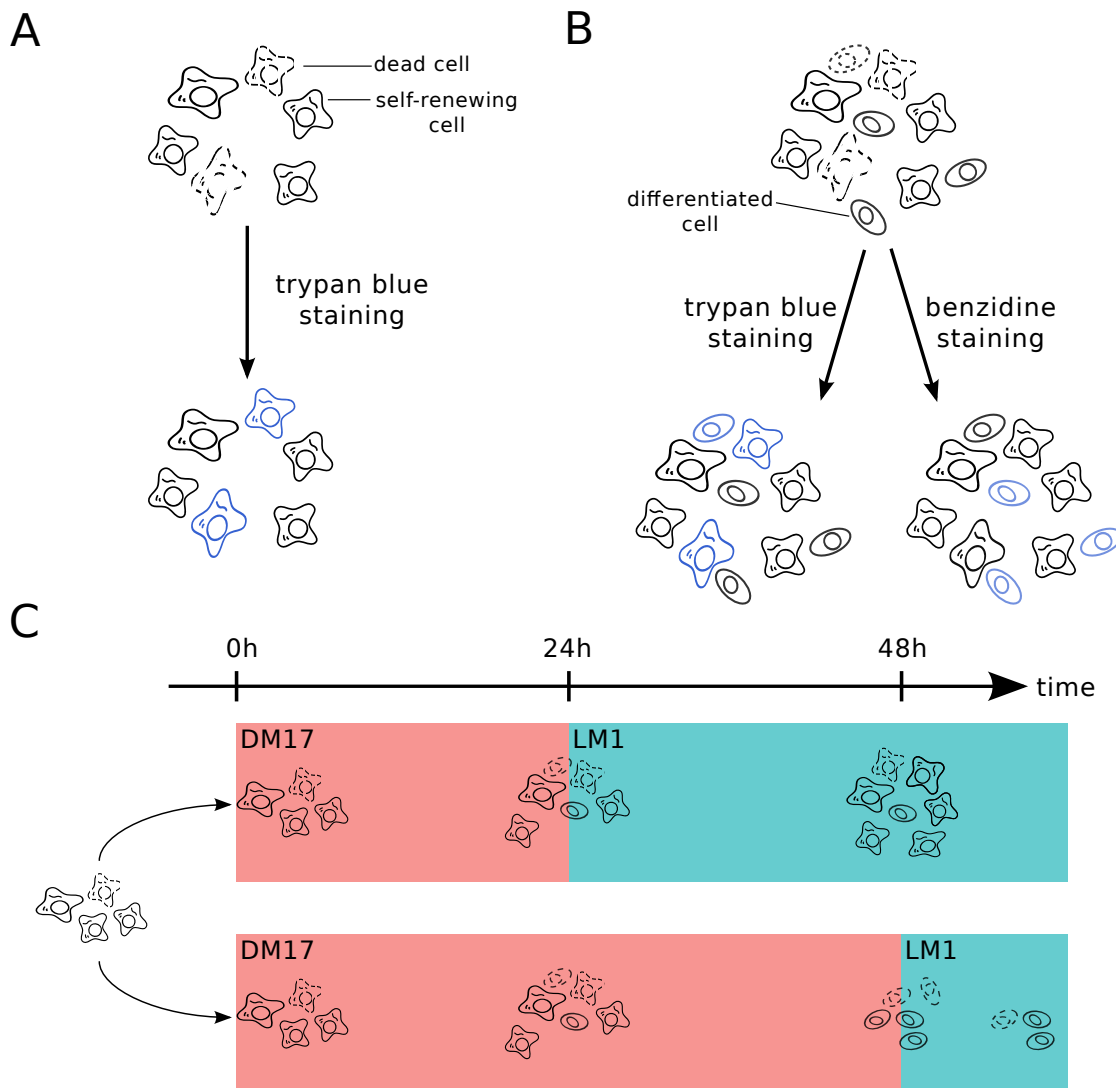


Figure 1.2: Experimental context of this study. A: In LM1 medium the culture is composed of living and dead cells in self-renewal. The population of living cells can be measured by trypan blue staining. B: In DM17 medium, the culture is composed of living and dead, self-renewing and differentiating cells. The amount of living cells can be measured by trypan blue staining. The amount of differentiated cells can be measured by benzidine staining. C: Commitment experiment. If the differentiating cells are switched back to LM1 after 24h of differentiation the culture starts proliferating again (upper trajectory). If the cells are switched back to LM1 after 48h, the culture stagnates (lower trajectory). Figure adapted from Figure 1 in Duchesne et al. (2019).

sible to measure the population of living progenitors by using trypan blue, a chemical dye which specifically stains dead cells (Figure 1.2A). In DM17, the culture is a mixture of progenitors, fully differentiated erythrocytes, and possibly differentiating cells which are not completely mature (Figure 1.1B). It is possible to assess the number of differentiated cells in the culture by using benzidine, a chemical dye which specifically binds haemoglobin. Considering that cells which contain haemoglobin are fully differentiated thus allows to link the number of benzidine-positive cells to the population of mature erythrocytes (Figure 1.2B). It is also possible to measure the total number of living cells in the culture using trypan blue.

Once a T2EC culture has been switched to DM17, it starts differentiating, but it can also be switched back to LM1. Doing so after 24h of differentiation does not alter the self-renewing ability of the culture (the culture proliferates), but doing it after 48h of differentiation cancels this ability: the culture does not proliferate (Figure 1.2C and Richard et al., 2016, Figure 10). This means that after 24h in the differentiation medium, some progenitors remain in the culture, that can proliferate in LM1. On the contrary, there are no progenitors in the culture after 48h in DM17, which means that they all have started differentiating. However, since it takes 6 days to differentiate the whole culture (Gandrillon et al., 1999), this also means that between day 2 and day 6, some cells have lost their self-renewing ability, and yet have not finished differentiating. This experiment has been used to prove the existence of a *commitment point* after which all the progenitors have started differentiating and cannot proliferate in LM1 anymore (Richard et al., 2016). We thus refer to this experiment as the *commitment experiment*.

### 1.1.3 Modelling attempts

Throughout the last decades, different modelling approaches have been used to describe erythropoiesis (Pujo-Menjouet, 2016). They accompanied biological discoveries and experimental advances which allowed to fit more and more complex models to an ever-extending set of data.

## 1.1. *In vitro* erythropoiesis

At first, and for the most part of the 20<sup>th</sup> century, a vast majority of these models were based on Differential Equations (DE), with the first models about iron kinetics in human blood cells from whole-body measurements published nearly 60 years ago (Sharney et al., 1963; Nooney, 1965). These models were formulated either as Partial Differential Equations (PDE, as in M. C. Mackey and Dörmer, 1982, who studied a PDE model of erythroid precursors *in vivo* in various species) which could in some cases be reduced to Delay Differential Equations (DDE, see for instance Bélair et al., 1995, who develop an age-structured PDE model of non-pathologic *in vivo* human erythropoiesis that they reduce to a 2-delay DDE, or Crauste et al., 2008, who try to adapt such models to account for data obtained in anaemic mice), or directly as DDE, as in Loeffler et al. (1989), who develop a model of *in vivo* erythropoiesis for mice. The design of these DE-based models since the second half of the 20<sup>th</sup> century accompanied the development of analytical methods to study the existence and unicity of the solutions, as well as to characterize their steady-states and bifurcations (Pujo-Menjouet, 2016).

Later, stochastic models started to be developed for erythropoiesis, see for instance Roeder et al. (2008), who develop a stochastic model of haematopoietic stem cells to account for bone marrow transplants in mice, and the design of Agent-Based Models (ABM) accompanied the rise of computing power, as in Bessonov et al. (2009) and Fischer et al. (2012), who design a multi-scale model of erythropoiesis including the internal molecular dynamics of the progenitors in the context of leukemia.

Apart from stimulating the development of new analytical and numerical tools for the study of mathematical models, all these works also helped improve our understanding of the diseases and perturbations of the haematopoietic system (Foley and M. Mackey, 2009; Pujo-Menjouet, 2016).

Current approaches for modelling erythropoiesis still involve DE-based models in a variety of context, e.g. Schirm et al. (2013), who develop a DDE of erythropoiesis coupled with a Pharmacokinetic (PK) model of erythropoietin and chemotherapy treatments in humans, and ABM, as Bouchnita et al.

(2014), who built a hybrid multi-scale model of human *in vivo* erythropoiesis with more detailed intracellular dynamics than the previous models. Methods based on multi-scale modelling, as reviewed in Bernard (2013), and hybrid modelling are increasingly being used to bridge the gap between different scales or processes. Again, we refer the reader to Bouchnita et al. (2014), as well as to Krinner et al. (2013), who developed a hybrid model based on an ABM of haematopoietic stem cells coupled to an ODE model of granulopoiesis (which is the formation of white blood cells) in humans. For a more detailed review of the history of haematopoiesis modelling, see Pujo-Menjouet (2016).

All these models helped understand haematopoiesis and its pathologies *in vivo*, and yet to our knowledge no mathematical model has actually been focused on *in vitro* erythropoiesis so far. Modelling the dynamics of *in vitro* erythropoiesis in T2ECs is thus the main motivation of this manuscript. We introduce our motivation in the next section.

## 1.2 Differentiation and decision-making at the single-cell level

During its life, each cell of a multicellular organism has roughly three possible fates: division, differentiation (into one or several lineages) or death. Cells choose between their accessible fates by integrating signals from their local environments and adapting gene expression, in a process called *cell decision-making*.

It is important to distinguish between the process of decision-making, which happens at the level of the single cell, and the ability of a whole cell population to differentiate. For instance, the ability of a pool of haematopoietic stem cells to generate all blood cell types upon transplantation, or the differentiation of a T2EC culture into erythrocytes, are population-scale processes, *i.e.* the macroscopic manifestation of fate decisions taken by a large number of cells at the microscopic level. In this section, we introduce the current theoretical framework for studying single-cell decision making.

## 1.2. Differentiation and decision-making at the single-cell level

### 1.2.1 Stochasticity of Gene Expression (SGE)

A fundamental aspect of single-cell biology is cell heterogeneity. It has been known since the development of flow cytometry that genetically identical cells placed within the same environment can display phenotypic heterogeneity, for instance with respect to the levels of membrane markers. But the historical demonstration of this fact was achieved by M. Elowitz et al. (2002), who measured the expression of a fluorescent protein across a population of isogenic *Escherichia coli*. This *Stochasticity of Gene Expression* (SGE) was later discovered across a wide spectrum of species (Eldar and M. B. Elowitz, 2010).

The sources of SGE are numerous, and universal (Haas et al., 2018). First and foremost, the low number of chemical species available to initiate transcription –such as the RNA-polymase complexes– results in substantial statistical fluctuations in the outcome of the chemical reaction. Once transcription is initiated, the unstability of the resulting molecular complex often leads to incomplete transcription (Sepúlveda et al., 2016). Finally, the accessibility of promoters is subject to the molecular crowding of the nucleus, and thus depends on epigenetic factors (Rinott et al., 2011), as well as DNA topology (Becskei et al., 2005).

The observation of SGE has been made possible by single-cell measurements of the protein or RNA levels. Historically, the use of fluorescent reporters allowed to characterize the distribution of a protein level across a population of cells, either by flow cytometry or by microscopy (M. Elowitz et al., 2002; Ozbudak et al., 2002). More recently, the development of single-cell transcriptomic technologies allowed for the measurement of the RNA counts of single cells, either for a restricted number of genes by single-cell Reverse-Transcription quantitative Polymerase Chain Reaction (sc-RTqPCR, A. K. White et al., 2011) or for the whole transcriptome by single-cell RNA-sequencing (sc-RNAseq, Goetz and Trimarchi, 2012).

All these experimental techniques provide the distribution of some molecular contents over a population of cells. The next step in the quantification of SGE usually involves a scalar metric, such as the coefficient of variation

(Ozbudak et al., 2002), the fano factor (Wong et al., 2018), the normalized variance (Viñuelas et al., 2013), or information-theoretic criteria such as Shannon’s entropy (Shannon, 1948).

The involvement of SGE has been demonstrated in numerous biological processes, e.g. the bet-hedging strategies of bacteria (Pradhan and Chatterjee, 2014) and cancer cells (Kreso et al., 2013), as well as several developmental processes (Rué and Martínez Arias, 2015), such as the patterning of the *Drosophila* retina (Heitzler and Simpson, 1991). Reviews about the involvement of SGE in biological processes are given in Huang (2009) and Eldar and M. B. Elowitz (2010). We are going to focus on one of these processes in particular –decision making– in the next section.

### 1.2.2 SGE and decision-making

The historical theory for single-cell decision making was introduced by Conrad Waddington (1957), based on the formalism of the theory of dynamical systems. In this metaphorical description, a cell is represented as a marble rolling down a rugged landscape, following a branching path, where each branching point is a decision-making event (Waddington, 1957 & Figure 1A in Moris et al., 2016). This is based on the introduction of the hypothetical *epigenetic landscape*<sup>1</sup>, which symbolizes the progressive restriction of the accessible fates of a differentiating cell. Moreover, the original description of Waddington’s landscapes already included the fact that the shape of the landscape, which determines what fates are possible for a cell, is fixed by interactions between genes (Waddington, 1957 & Figure 1B in Moris et al., 2016).

Even though it was introduced as a metaphor, the epigenetic landscape provided the first explanation of how cell fate decisions (and the associated developmental processes) rely on regulatory genetic interactions shaped during evolution. Furthermore, it served as a basis for a variety of more formal

---

<sup>1</sup>Here, the use of the word *epigenetic* has nothing to do with *epigenetics*, as in modifications of the chromatin. Actually, Waddington’s book was published several decades before epigenetic modifications were discovered.

## 1.2. Differentiation and decision-making at the single-cell level

descriptions, that are reviewed in Davila-Velderrain et al. (2015). Despite the various mathematical formalisms that these descriptions used to define and compute the epigenetic landscape, they all interpret decision-making as the outcome of a dynamical system, and thus they all have several features in common, that we are going to describe before introducing each method more precisely.

In these contemporary formalisms (Huang, 2009, 2010; Davila-Velderrain et al., 2015), a cell is seen as a dynamical system, characterized by the concentrations of its proteins, or the expression levels of its genes. Its state space thus has an enormous dimensionality (one dimension per gene), and the position of the cell within this space characterizes its identity in terms of a vector of gene expression levels. As time evolves, the cell moves through its state space, and its trajectory is defined by the structure of its *Gene Regulatory Network* (GRN). This means that modern formalisms for cell decision-making incorporate a function which maps the state of the system at time  $t$  to its state at time  $t + \delta t$ . The GRN allows certain stable states, associated with precise gene expression levels. These are called the *attractors* of the landscape, and are associated to the different possible fates of the cell (the proliferating state, and the accessible differentiated states of the cells are examples of such attractors, Figure 1.3).

Because gene expression is stochastic, a given cell doesn't have a straight, deterministic trajectory through its state space, but rather a noisy one (Chang et al., 2008). Consequently, a cell is rather described by the probability distribution of its presence over the state space, than by its precise position inside the space. Furthermore, a population of cells considered in the same state would rather be spread across the state space according to this distribution, with each cell randomly fluctuating around the attractors of the state space (Huang, 2009). Thus, studying the fate of cells in a population reduces to characterizing the dynamic distribution of their states in the state space, which is usually achieved by computing a formal equivalent of Waddington's landscape called the *quasi-potential* of the system (Figure 1.3, & Davila-Velderrain et al., 2015).

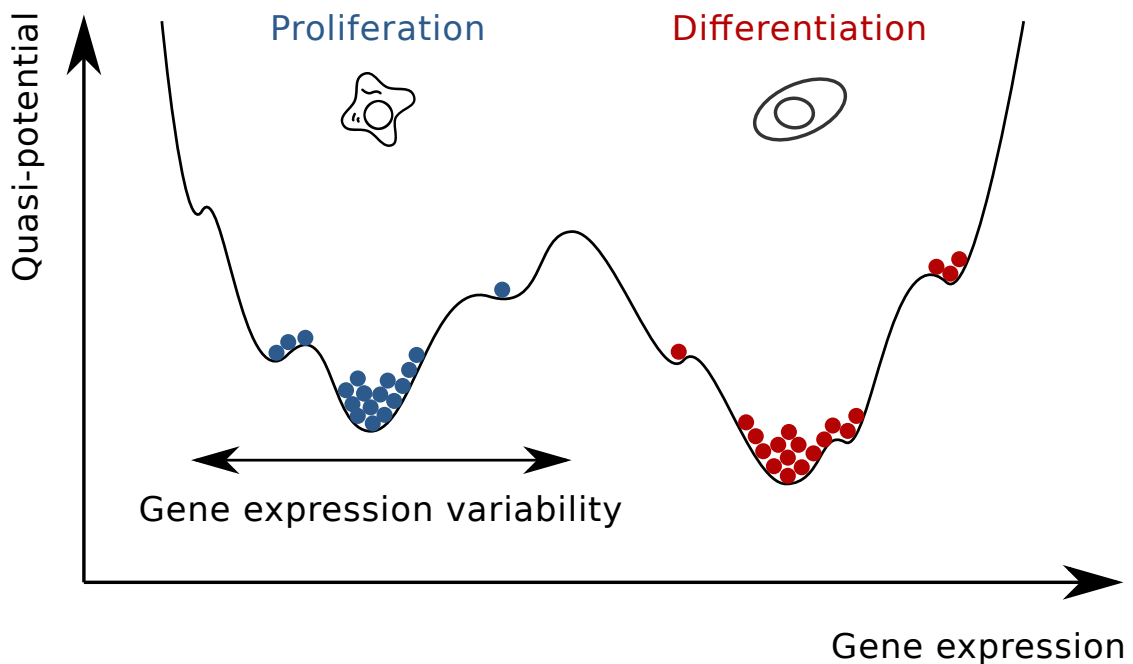


Figure 1.3: A systems biology view on cell decision-making in a simplistic case. The figure displays a hypothetical quasi-potential in a 1D state space with two attractors. Each circle represents a possible state of the associated Gene Regulatory Network. The most stable states are the most probable, as indicated by the stacking of circles in regions of low quasi-potential. Inspired by Huang (2009).

The quasi-potential maps every possible cellular state to its energy level (Davila-Velderrain et al., 2015). In this way, cells would progressively reduce their energy during their commitment, and converge to the local minima of energy (Figure 1.3).

However, the precise computation of an epigenetic landscape is far from an easy task, as the dynamical systems defined by GRNs are usually high-dimensional, non-linear, and thus non-integrable systems (Davila-Velderrain et al., 2015; Moris et al., 2016). Several approaches have been considered, depending on the precise modelling framework (considering discrete or continuous time, as well as discrete or continuous states of the system, result in different models).

## 1.2. Differentiation and decision-making at the single-cell level

In boolean networks, both the time and the system state are discrete variable (Kauffman, 1969). The attractors landscape can be characterized through an extensive simulation of the system, in order to sample its possible states (Davila-Velderrain et al., 2015). Then, one can relate the state distribution to the quasi-potential of the system (Villarreal et al., 2012).

In the case of continuous time and states, the study of the GRN dynamics and fate-decisions uses methods from statistical mechanics (Bertin, 2012; Davila-Velderrain et al., 2015). First, by adding a noise term to a deterministic ODE model of the GRN dynamics, one obtains a *Langevin equation* for the system, that is a Stochastic Differential Equation (SDE) which can be used to simulate the trajectories of individual cells and sample their distribution over time (J. Wang et al., 2010; Li and J. Wang, 2013). Then, one can re-write the Langevin equation as a *Fokker-Planck equation*, that is a PDE structured by the levels of expression of each gene in the network, which can be solved in order to characterize the distribution of the cells over time (J. Wang et al., 2010; Li and J. Wang, 2013). Finally, one can use the formalism of path integrals in order to compute the most probable paths for transitioning from one attractor to the other (Li and J. Wang, 2013). These methods have been applied to various GRNs, from the simple 2-gene toggle switch (J. Wang et al., 2010), to a 52-gene network controlling stemness and differentiation in human stem cells (Li and J. Wang, 2013). They also have motivated a lot of work regarding the computation of the quasi-potential landscape, because since GRNs are usually non-integrable, computing an epigenetic landscape requires to decompose the driving force of the system into an integrable and a non-integrable part (J. Wang et al., 2010; Zhou et al., 2012).

It should be noted that even though these numerical methods might allow to approximate a quasi-potential for a given GRN, their outcome is only an approximation because GRNs are non-integrable chemical systems, far from their equilibrium (Davila-Velderrain et al., 2015; Moris et al., 2016). Moreover, the continuous models of gene regulation from J. Wang et al. (2010) and Li and J. Wang (2013) consider SGE as an additive noise term in an ODE, *i.e.* as

a small external perturbation from the deterministic behaviour of the system. This is obviously not the case, as stochasticity is an inherent feature of gene expression.

As a consequence, our group has focused its efforts in incorporating stochasticity as a mechanistic feature of our models of gene expression (Herbach et al., 2017), and using these models to infer GRNs from experimental single-cell transcriptomics data (Bonnafox et al., 2018), without explicitly computing a quasi-potential. We thus consider the epigenetic landscape more as a metaphor, like Conrad Waddington used to, than as an actual biological feature to be extracted from data.

Our hypothesis is the following: since the extent of SGE defines how far cells can fluctuate from their attractor state (Figure 1.3), an increase in SGE should allow cells to explore a wider region of their state space, and thus potentially lead to an increased transition rate from an attractor to the others.

Such a causal link between SGE and state transitions has been observed in bacteria (Süel et al., 2006) and embryonic stem cells (Kalmar et al., 2009). Regarding haematopoiesis, a historical study by Chang et al. (2008) showed that haematopoietic progenitors with an extremely low or high expression level of stemness marker Sca-1 showed great variability in their potential to differentiate into the myeloid or erythroid lineages *in vitro*. The same kind of observations have been made *in vivo*, as single-cell transplantations of mice haematopoietic stem cells led to different composition of blood cell types (Haas et al., 2018), a process known as *lineage bias*. More recently, our group showed that in T2EC, the onset of differentiation was accompanied by an increase in SGE (Richard et al., 2016). And yet, a demonstration of the causative role of SGE in fate-decisions such as the commitment to differentiation is still lacking. In this manuscript, we propose to tackle this issue. We expose our strategy to achieve such a demonstration in the next section.

## 1.2. Differentiation and decision-making at the single-cell level

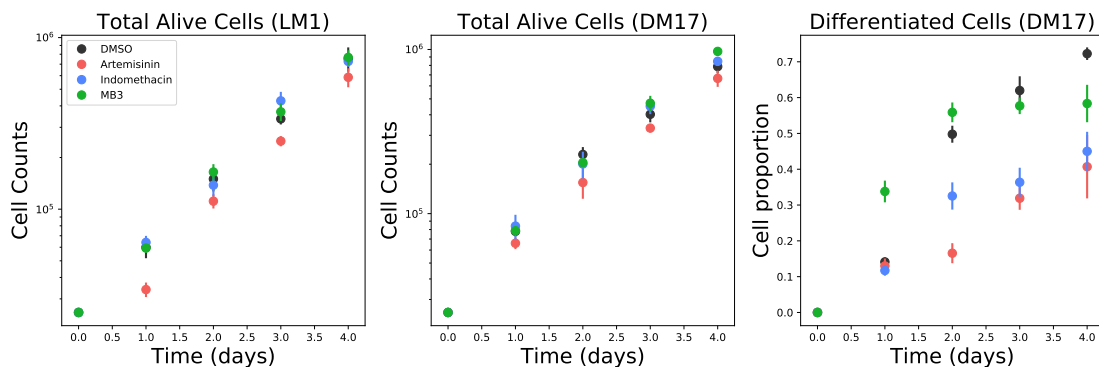


Figure 1.4: Effects of the drugs that influence the extent of SGE on the *in vitro* erythroid proliferation and differentiation. Displayed are the average cell counts and proportion of differentiated cells in 3 replicates of the T2EC differentiation experiment (Section 1.1.2) in 4 conditions (Artemisinin-, Indomethacin-, and MB3-treated, as well as in a DMSO control). Error bars display the standard-error of the measurements.

### 1.2.3 Experimental manipulation of SGE

In order to prove that SGE can influence differentiation, we need to be able to experimentally manipulate the level of SGE in T2EC, and assess its influence on cell differentiation. In this regard, an interesting prospect is provided by Dar et al. (2014), who identified a large panel of chemical drugs which modulate SGE. To do so, they used a systematic screening approach with a fluorescent reporter system.

Among these, our group selected two drugs, Artemisinin and Indomethacin, which reduced both the level of SGE and the fraction of differentiated cells in T2EC (Figure 1.4, and Guillemin et al., 2018). Moreover, we identified the chromatin modifier MB-3 (Raser and O’Shea, 2004; Moris et al., 2018) as a chemical drug which increases both the level of SGE and the fraction of differentiated T2EC (Figure 1.4, and Guillemin et al., 2018).

However, there is no proof that the precise effects of the drugs are limited to differentiation, as the number of differentiated cells that is measured in T2EC cultures typically depends on cell proliferation and cell death as well as on cell differentiation. Since the relative intensity of these processes is not accessible

to an experimental measure, we decided to infer these through mathematical modelling. If we could design a mechanistic model of T2EC differentiation that incorporates cell proliferation, death and differentiation, then it would be possible to compare its parameter values under each treatment. Such approach would allow us to assess the effect of each drug on differentiation.

Thus, 2 main questions will underlie this manuscript:

1. Can we define a mathematical model for the kinetics of T2EC differentiation?
2. How do its parameters vary under each drug treatments?

In such an approach, parameter identifiability will be a critical feature of our models. We thus introduce parameter identifiability, and its relevance to our work, in the next section.

## 1.3 Parameter estimation and identifiability in mathematical models

### 1.3.1 Definitions

When building a mathematical model of a biological process (say for example that we want to reproduce the behavior of an observable  $y$  as a function of time), one must define two things: the model prediction –often referred to as *the model*– and the model parameters. The model prediction is a function  $f(t, y_0, \theta)$  of time, the initial condition and the model parameters, which characterizes the output of the model. It is defined according to hypotheses about the biological process. The model parameters are scalars which quantify the behavior of the model. In order to reproduce biological data, they must be estimated, either by finding values in the literature, or by fitting the model to experimental data. In the latter case, an important step of the estimation is the analysis of the identifiability of the inferred values.

### 1.3. Parameter estimation and identifiability in mathematical models

The identifiability of a parameter describes the injectivity between the parameter space and the data. In other words, a parameter is identifiable if and only if there is only one parameter value that corresponds to a dataset (Raue et al., 2009). Otherwise, it is said to be unidentifiable. Then, the model is said to be identifiable if and only if all of its parameters are identifiable. Conversely, it is unidentifiable if and only if at least one of its parameters is unidentifiable. Even though identifiability is a property of the model under study, this definition means that the identifiability of a mathematical model also depends on the available data. For example, a model that is identifiable with ideal, noiseless data might become unidentifiable with actual data, which are subject to experimental noise.

Identifiability is especially important for partially observed models, which have more internal variables than available observables, and when the sample size  $n_{tot}$  is not large enough compared to the number of parameters  $K$ . Identifiability will be an important feature of our study, because in order to know how the parameters vary under treatment, we need to base our analysis on reliable estimates of their values.

Though very simple, the definition of identifiability is very hard to use in practice, so several methods have been developed to define and assess identifiability for the parameters of dynamic models (Villaverde and Barreiro, 2016). Depending on how parameters are estimated (bayesian or frequentist methods), different methods are available to assess their identifiability, each with its own limitations (Raue, Kreutz, Theis, et al., 2013).

#### 1.3.2 Maximum Likelihood Estimation (MLE)

A number of parameter estimation methods are based on the maximisation of the likelihood function, including the SAEM algorithm that we will use for calibrating our Mixed Effect Models (MEM) in Chapters 5 to 7, and the estimation procedure that we will define in Chapter 2. This means that if we want to model temporal data  $y$  with a dynamic model, we have to assume the distribution of the model residuals  $y_{i,j} - f_i(t_j, y_0, \theta)$ , where  $y_{i,j}$  is the data for

variable  $i$  at timepoint  $t_j$  and  $f_i$  its prediction from the dynamical model (which depends on time, the initial condition  $y_0$  and the parameters  $\theta$  of the model).

The model residuals are usually modelled by a centered gaussian distribution (Raue et al., 2009; Raue, Schilling, et al., 2013; Lavielle and Bleakley, 2014). Then, the standard deviation of the error remains to be characterized. To this aim, there are two main options (Raue, Schilling, et al., 2013):

- Estimate the standard deviation  $\sigma$  of the error from the data. For this estimate to be precise, one needs to have an extensive set of data. Then the error model is completely described as:  $y_{i,j} \hookrightarrow \mathcal{N}(f_i(t_j, y_0, \theta), \sigma)$ .
- Model the standard deviation of the error. This means finding a suitable function  $g$ , of the time  $t$ , the initial condition  $y_0$ , the dynamical parameters  $\theta$  and possibly other parameters  $\psi$  (which we will call the error parameters), to describe this variance. The error model is then completely described as:  $y_{i,j} \hookrightarrow \mathcal{N}(f_i(t_j, y_0, \theta), g_i(t_j, y_0, \theta, \psi))$ .

With this representation, the likelihood of the model follows:

$$\mathcal{L}(y|t, y_0, \theta, \psi) = \prod_{i=1}^n \prod_{j=1}^m \frac{1}{\sqrt{2\pi g_i^2(t_j, y_0, \theta, \psi)}} \exp\left(-\frac{(y_{i,j} - f_i(t_j, y_0, \theta))^2}{2g_i^2(t_j, y_0, \theta, \psi)}\right),$$

and its log-likelihood:

$$-2 \log(\mathcal{L}) = \sum_{i=1}^n \sum_{j=1}^m \frac{(y_{i,j} - f_i(t_j, y_0, \theta))^2}{g_i(t_j, y_0, \theta, \psi)^2} + 2 \log(g_i(t_j, y_0, \theta, \psi)) + \log(2\pi), \quad (1.1)$$

from which the  $\log(2\pi)$  term is dropped. In Equation (1.1),  $n$  refers to the number of observables of the model (indexed by  $i$ ),  $m$  refers to the number of timepoints (indexed by  $j$ ). In the end, the best-fit parameters of the model are the values of  $\theta$  and  $\psi$  which minimize the quantity defined in Equation (1.1).

The model is described by the vector of parameters:  $\Theta = (\theta, \psi)$ , which contains the parameters from both the dynamic and the error models.

### 1.3. Parameter estimation and identifiability in mathematical models

Such a model can be unidentifiable for various reasons, which means that one can define different kinds of identifiability (Villaverde and Barreiro, 2016). In this manuscript, we will only consider structural identifiability, which is a theoretical property of the model related to the definition of its outputs, and practical identifiability, which also depends on what actual data are being used for fitting the model.

#### 1.3.3 Structural identifiability

Structural identifiability is related to the structure of the model, and the observed variables. A model is structurally unidentifiable when several of its parameters are redundant, meaning that they can vary in such a manner that the measured output of the model is not affected (Raue et al., 2009; Chis et al., 2011; Villaverde and Barreiro, 2016). In the context of the maximum-likelihood estimation, a model is said to be structurally identifiable if and only if the likelihood optimum is unique.

A variety of methods, based on different approaches, can be used to assess the structural identifiability of a dynamic model. These include, non-exhaustively, the Taylor series method (Pohjanpalo, 1978), the similarity transformation (Vajda et al., 1989), the generating series method (Walter and Lecourtier, 1982), and the profile likelihood approach (Venzon and Moolgavkar, 1988; Raue et al., 2009; Fröhlich et al., 2014). A review of these methods is provided in Villaverde and Barreiro (2016) and their performance is assessed in Chis et al. (2011). We conclude as to which method should be used in our study in Section 1.3.4.3.

#### 1.3.4 Practical identifiability

Practical Identifiability is related to the quantity and quality of the data used for model calibration. If the data is too sparse or too noisy to estimate all parameters together, then the model is said to be practically unidentifiable (Raue et al., 2009; Villaverde and Barreiro, 2016). Essentially three kinds of frequentist

methods can be used to assess the practical identifiability of a model (Luzyanina et al., 2007): the profile likelihood approach, bootstrapping and methods based on the Fisher Information Matrix of the model. The profile likelihood approach is based on the constrained optimization of the likelihood function (Raue et al., 2009). Bootstrapping uses a resampling of the data to estimate parameter variability (Efron and Tibshirani, 1986). Finally, the Fisher Information Matrix allows to approximate the variance-covariance matrix of the parameter estimates (Villaverde and Barreiro, 2016). We introduce profile likelihood and the Fisher Information Matrix in the following sections, and we discuss their relative performance and the associated computational cost in Section 1.3.4.3.

#### 1.3.4.1 Profile likelihood

The first method for assessing the practical identifiability of dynamic models is the profile-likelihood approach, which uses constrained optimization (Venzon and Moolgavkar, 1988; Raue et al., 2009).

For a model with  $K$  parameters  $(\theta_1, \theta_2, \dots, \theta_K)$  and a likelihood  $\mathcal{L}$ , the *profile likelihood*  $PL_{\theta_i}$  of parameter  $\theta_i$  is defined as:

$$\forall x \in \mathbb{R} \quad PL_{\theta_i}(x) = \min_{\theta_{j \neq i}} (-2 \log(\mathcal{L}(\theta_i = x, \theta_j))). \quad (1.2)$$

Namely, the profile likelihood of a parameter at a certain value is the log-likelihood of the model, minimized with respect to all the other parameters. To compute the profile likelihood at a certain value  $x$  of a parameter  $\theta_i$  means to set  $\theta_i = x$  and to estimate the values of the other parameters  $\theta_j$  that minimize the log-likelihood in this setting. Consequently, the profile likelihood is minimal at the optimal parameter values set, and increases in both directions.

In a highly dimensional parameter space where the exact shape of the likelihood landscape is not straightforward, the profile likelihood summarizes this shape along the axis of  $\theta_i$ , by keeping the likelihood as high as possible in both directions. It is possible to define a confidence interval  $CI_{\theta_i}$  at a level of confidence  $\alpha \in [0, 1]$  for a parameter  $\theta_i$ , derived from the evaluation of the profile

### 1.3. Parameter estimation and identifiability in mathematical models

likelihood (Raue et al., 2009):

$$CI_{\theta_i}(\alpha) = \left\{ x \in \mathbb{R} \mid PL_{\theta_i}(x) - PL_{\theta_i}(\hat{x}) \leq \chi^2(\alpha, K) \right\}, \quad (1.3)$$

where  $\hat{x}$  is the optimal estimate of  $\theta_i$ ,  $K$  is the number of parameters being estimated and  $\chi^2(\alpha, K)$  is the  $\alpha$ -quantile of the  $\chi^2$  distribution with  $K$  degrees of freedom.

Namely, all the parameter sets that render a profile likelihood closer to its minimal value than a threshold  $\chi^2(\alpha, N)$  belong to the confidence interval. The threshold is equivalent to the threshold of a Likelihood Ratio Test (LRT) where the value of the likelihood at a given point of the profile is tested against the optimal likelihood. This threshold depends both on the number of parameters estimated (the more parameters, the higher the threshold and the wider the confidence interval) and on the requested confidence level (the higher the confidence level, the higher the threshold, and the wider the confidence intervals).

Once a confidence interval has been extracted for a parameter  $\theta_i$ , we say that  $\theta_i$  is practically identifiable at the level of confidence  $\alpha$  if and only if its confidence interval at the level  $\alpha$  is bounded (Raue et al., 2009).

Then we say that a model is practically identifiable at the level of confidence  $\alpha$  if and only if all its parameters are identifiable (Raue et al., 2009).

Apart from assessing the identifiability of a model parameter, the profile likelihood approach also allows to decipher between structural and practical unidentifiabilities (Figure 1.5).

#### 1.3.4.2 The Fisher Information Matrix (FIM)

Another method for assessing the practical identifiability of parameters is based on the observed Fisher Information Matrix (FIM), which is the opposite of the hessian of the loglikelihood observed at the likelihood maximum:

$$\mathcal{I}_{i,j}(\hat{\theta}) = -\frac{\partial^2 \log(\mathcal{L})}{\partial \theta_i \partial \theta_j}(\hat{\theta}), \quad (1.4)$$

where  $\mathcal{I}$  is the FIM ( $\mathcal{I}_{i,j}$  is the coefficient at its  $i^{th}$  row and  $j^{th}$  column), and

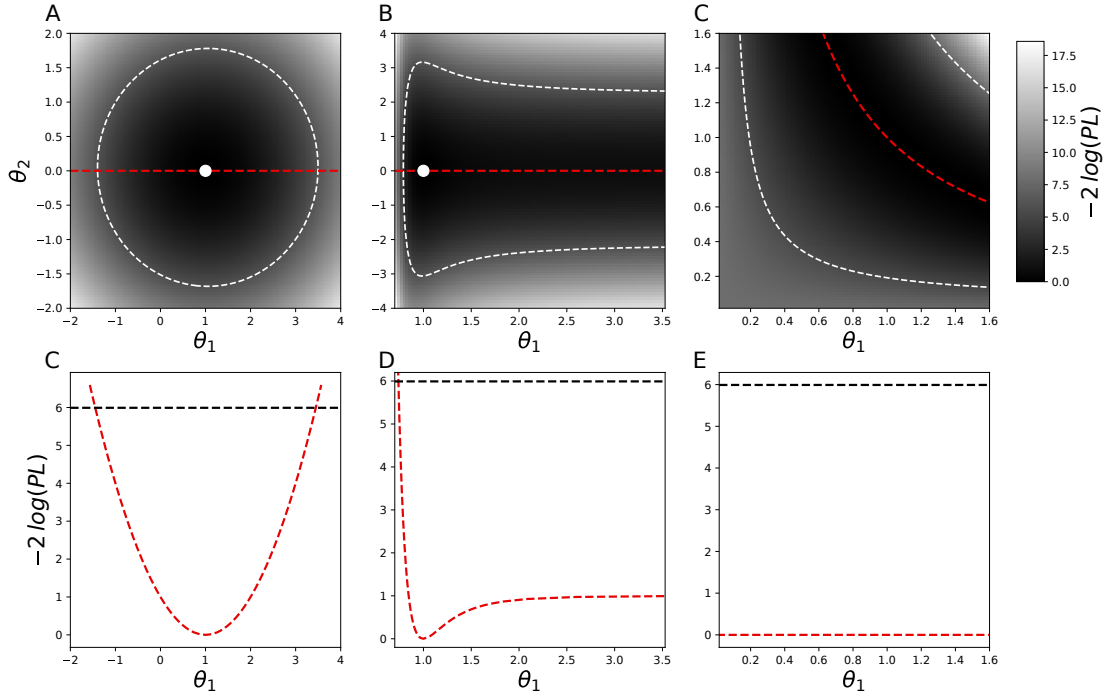


Figure 1.5: The different outcomes of profile-likelihood-based identifiability analysis. A-C: Contour plots of the log-likelihood  $-2\log(\mathcal{L})$  in an hypothetical two-parameters model in shades of grey, from low (darker grey) to high (lighter grey) values. The white dot indicates the coordinates of the likelihood optimum. The dashed white lines display the borders of the confidence interval. The dashed red line displays the minimal log-likelihood with respect to  $\theta_1$ . D-F: Profile-likelihood curves with respect to  $\theta_1$  (in red) in the corresponding models. The dashed black line shows the identifiability threshold from Equation (1.3). A,D: Practical Identifiability: The confidence interval is bounded, both parameters are identifiable and so is the model. B,E: Practical non-identifiability: due to the amount or quality of the data, the confidence intervals of the parameters are infinitely extended along one direction. The profile likelihood is not flat, but does not cross the  $\chi^2$  threshold on one direction. C,F: Structural non-identifiability: there is a relation that maximizes  $\mathcal{L}$  for every value of the parameters. The profile likelihood is completely flat. Inspired by Figure 1 in (Raue, Kreutz, Theis, et al., 2013).

### 1.3. Parameter estimation and identifiability in mathematical models

$\hat{\theta}$  is the optimal parameter set. The FIM can be used to define a quadratic approximation of the likelihood surface near its optimum. Different features of the geometry of the likelihood surface can then be assessed from the FIM.

The variance-covariance matrix of the parameter estimates can be approximated by  $\mathcal{I}^{-1}(\hat{\theta})$ , meaning that the standard errors of the parameter estimates are the square-roots of the diagonal elements of  $\mathcal{I}^{-1}(\hat{\theta})$  (Villaverde and Barreiro, 2016). A precisely estimated parameter will have a low standard error, and conversely, unidentifiable parameters are associated to high standard errors.

Approximating the standard errors of the estimates from the FIM requires that the FIM can be inverted. If it is singular, there are unidentifiable parameters, and if it is near-singular, some parameters are highly correlated and poorly estimated. As a consequence, the FIM eigenvalues are also informative regarding parameter identifiability, because low eigenvalues make the FIM near-singular, and thus characterize poorly identifiable parameters. Conversely, high eigenvalues are associated to identifiable parameters (Villaverde and Barreiro, 2016).

Other properties of the FIM are related to the geometrical features of the likelihood. These properties have been used to define scalar criteria, which quantify the information about parameter values stored in the FIM (Vanrolleghem and Dochain, 1998). Each criterion should be either minimized or maximized in order to maximize the information about each parameter (Vanrolleghem and Dochain, 1998):

$$\left\{ \begin{array}{l} D = \max \left( \det \left( \mathcal{I}_{i,j}(\hat{\theta}) \right) \right), \\ A = \min \left( \text{tr} \left( \mathcal{I}_{i,j}(\hat{\theta})^{-1} \right) \right), \\ A_{modified} = \max \left( \text{tr} \left( \mathcal{I}_{i,j}(\hat{\theta}) \right) \right), \\ E = \max \left( \lambda_{\min} \left( \mathcal{I}_{i,j}(\hat{\theta}) \right) \right), \\ E_{modified} = \min \left( \frac{\lambda_{\max}(\mathcal{I}_{i,j}(\hat{\theta}))}{\lambda_{\min}(\mathcal{I}_{i,j}(\hat{\theta}))} \right), \end{array} \right. \quad (1.5)$$

where  $\det(\mathcal{I}_{i,j}(\hat{\theta}))$  is the determinant of the FIM,  $\text{tr}(\mathcal{I}_{i,j}(\hat{\theta}))$  its trace and  $\lambda_{\min}$  (resp.  $\lambda_{\max}$ ) its smallest (resp. largest) eigenvalue.

### 1.3.4.3 Computational cost and precision of the methods

FIM-based methods are less computationally demanding, because they require the fewest parameter estimation steps (Luzyanina et al., 2007), but due to their parabolic approximation they are proven to render biased results, especially when the confidence intervals of the parameters are used to compute prediction intervals for the model observables (Raue et al., 2009). On the other hand, the profile likelihood-based method is computationally more expensive (Luzyanina et al., 2007), but it is proven to detect both structural and practical unidentifiabilities (Figure 1.5), and gives more accurate confidence intervals than the FIM Raue et al., 2009; Fröhlich et al., 2014).

We thus conclude that the profile likelihood is a good compromise between computation time and the precision of the confidence intervals estimation. It will be our method of choice for the analysis of the identifiability of our models. However, since the profile likelihood approach is based on a constrained optimization of the model, it is usually too costly to apply it when models have too many parameters, or a long estimation time (Fröhlich et al., 2018).

## 1.3.5 Related concepts

The arising interest for parameter identifiability in the literature (Figure 1.6) has led to the definition of various related concepts that we need to clarify in order to avoid confusion when reading this manuscript.

### 1.3.5.1 Parameter sensitivity

The sensitivity of a model to a parameter quantifies the influence of that parameter values on the model output (Villaverde and Barreiro, 2016). Sensitivities are related to the identifiability of a model, because a parameter with a

### 1.3. Parameter estimation and identifiability in mathematical models

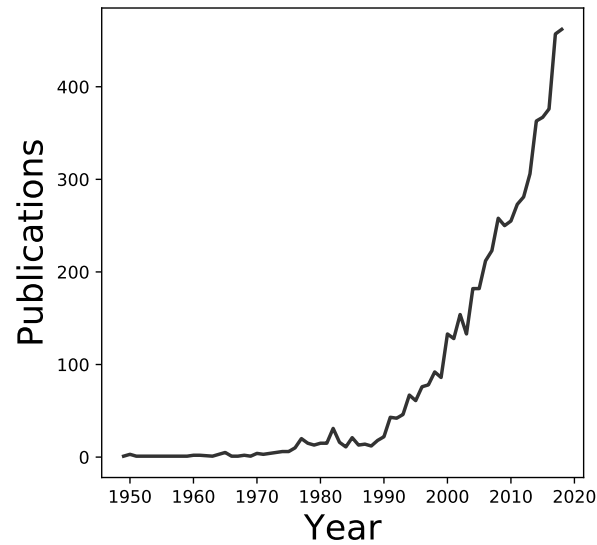


Figure 1.6: Number of publications in relation with identifiability. Displayed are the results of a search on WebOfScience for articles having identifiability as a topic. We found 5882 papers, published between 1949 and 2018.

null sensitivity has no influence on the model output, and is thus structurally unidentifiable since every possible value renders the same likelihood.

In detail, there are different definitions of sensitivity, which distinguish between absolute and relative, as well as local and global, sensitivities. A detailed introduction to these distinctions is beyond the scope of this manuscript, and is provided in (Villaverde and Barreiro, 2016)

#### 1.3.5.2 Experimental design

As we already explained, a practically unidentifiable parameter cannot be estimated because data are insufficient. In this context, the topic of optimal experimental design attempts to predict which experiments would be the most informative for determining all parameter values. This is made possible by the simulation of experiments and the optimization of an information criterion, such as those introduced in System (1.5).

Different methods, both frequentist and bayesian, have been developed

to this end (Faller et al., 2003; Weber et al., 2012; Busetto et al., 2013; Liepe et al., 2013). In certain cases, experimental design has successfully predicted which experiments to perform in order to make a model identifiable (Apgar et al., 2010). However, it should be noted that it is impossible to know *a priori* if the optimally designed experiments will actually make the model identifiable. This should be considered when the cost of actually performing the experiments is prohibitive.

### 1.3.5.3 Sloppiness

When models include too many parameters, they often become sloppy, meaning that their output is controlled by a limited number of parameters. More precisely, a model is said to be sloppy when the eigenvalues of the FIM are evenly spaced in the log-space across many orders of magnitude (Transtrum et al., 2015). This implies that the few parameters associated to the highest eigenvalues of the FIM are much more important than the many parameters associated to the lower eigenvalues in determining the model output. The parameters that are irrelevant to the model output are said to be sloppy, while the others are called stiff. Sloppiness is related to identifiability, because the values of sloppy parameters would normally be harder to estimate.

Sloppiness is a feature shared by many models from various fields of biology (K. Brown and Sethna, 2003; K. Brown et al., 2004) and physics (Waterfall et al., 2006). Basically, a sloppy model can be reduced to its most stiffest features, in order to make it identifiable (Transtrum et al., 2015). This reduced model can be seen as a macroscopic approximation of the microscopic phenomena that are being modeled. This connection has been verified for models in physics (Machta et al., 2013), because in physics the macroscopic theory often precedes the microscopic model. However, there is usually no established quantitative theory for biological process, which leaves modellers with the choice of what components to include in their models. This might lead to overly complex, unidentifiable and sloppy models.

Focusing on the estimation procedure and experimental design in sloppy

### 1.3. Parameter estimation and identifiability in mathematical models

models, A. White et al. (2016) showed that in biological models, the relevant mechanisms are often unknown and might be excluded. In this case it will be impossible to fit all observables from an experimental dataset and at the same time to identify all the parameters of the model.

Optimal design is used to define experiments which would allow to identify all parameter values. But fitting an approximate model to new data would change the quality of its fit to the original data, and usually reduce its predictive ability. Instead, the authors suggest the definition of a *sloppy system*, a sequence of sloppy models of increasing complexity that become unidentifiable in the microscopic limit. Considering a range of models of varying complexity would theoretically allow the modeller to optimally balance the quality of the fit and the identifiability of the parameters when the relevant mechanisms to a model output are unknown (A. White et al., 2016).

Sloppiness provides the modeller with interesting concepts, like the possibility to reduce a model to its identifiable parts (Transtrum et al., 2015), or to consider a range of models of varying complexity instead of focusing on estimation in a single model (A. White et al., 2016). Modellers should pay attention to these, especially at times when the complexity of biological models keeps increasing (Fröhlich et al., 2018).

#### 1.3.5.4 Dynamical compensation

Dynamical compensation has been described as the ability of a physiological system to keep the same dynamic output given varying parameters (Karin et al., 2016). This implies that a model exhibiting dynamical compensation would also be structurally unidentifiable, leading to considerable debate regarding potential reconciliations of dynamical compensation with structural identifiability (Karin et al., 2017; Sontag, 2017; Villaverde and Banga, 2017).

This debate originates from the dichotomy between two aspects of parameter sensitivity (Sontag, 2017). From the point of view of robustness, one would not want the model outputs to be affected by parameter values, and yet from the point of view of parameter identification, parameter sensitivities are critical

quantifiers of structural identifiability (Villaverde and Barreiro, 2016).

Villaverde and Banga (2017) proposed a solution to reconcile dynamical compensation with structural identifiability, noting that both structural identifiability and dynamical compensation are affected by which set of parameters are considered unknown and which observables are measured. They basically proposed a complementary definition for dynamical compensation by considering dynamical compensation for one observable of the model with respect to one parameter, while the original definition of Karin et al. (2016) lacked precision and considered dynamical compensation as a global feature of the whole model.

As a conclusion, aside from these technicalities, the story of dynamical compensation stresses the importance of proper identifiability analysis when using partially observed models to extract biological insight from experiments.

## 1.4 Mixed Effects Models (MEM)

Mixed Effects Models (MEM) form a class of statistical models that has been developed for the description of various kinds of data, which always include a lot of interindividual variability (Lavielle and Bleakley, 2014). They have been applied to a variety of fields, like demography (O'Brien et al., 2008), genomics (Haldermans et al., 2007), ecology and evolution (Bolker et al., 2009), psychophysiology (Bagiella et al., 2000), and single-cell studies (Gonzalez et al., 2013; Karlsson et al., 2015). But MEM are best-known for their widespread application to clinical trials (Andersen and Millen, 2013) and PKPD modelling (Rowland, 2005).

In this section, we introduce the rationale that underlies this modeling framework, and present the statistical and numerical methodologies that will be of interest for model calibration, selection and identifiability analysis in our study.

## 1.4. Mixed Effects Models (MEM)

### 1.4.1 General principle and definitions

#### 1.4.1.1 Structural model

Mixed effect models are used to describe the observation of the same quantitative features, measured repeatedly on different individuals that belong to the same population. The general idea of mixed effects modeling is to apply the same mathematical model, or *structural model*, to all the individuals of the population with different parameter values for each individual, in order to account for inter-individual variability. In the case of dynamic models, this means that the structural model for variable  $y_{i,j,k}$ —that is the  $i^{\text{th}}$  observable measured at time  $t_j$  on the  $k^{\text{th}}$  individual— is a function  $f_i$  which depends on time  $t_j$ , the initial condition  $y_0$  and the individual parameters  $\theta_k$ .

#### 1.4.1.2 Parameter model

The fundamental assumption of mixed effect modeling is that since all individuals come from the same population, their parameters should show some level of inter-individual variability around the average of the population. Mathematically, this writes as the decomposition of individual parameter  $\theta_k$  in 2 terms:

$$\theta_k = \theta^{pop} + \eta_k, \quad (1.6)$$

where  $\theta_k$  is the value of parameter  $\theta$  in the  $k^{\text{th}}$  individual of the population,  $\theta^{pop}$  is the population value of the parameter, or fixed effect, and  $\eta_k$  is the random effect of the  $k^{\text{th}}$  individual<sup>2</sup>. It is usually assumed to be drawn from a gaussian distribution:  $\eta_k \hookrightarrow \mathcal{N}(0, \omega_\theta)$ , where  $\omega_\theta$  is the standard-deviation of the random effect on parameter  $\theta$  and quantifies the inter-individual variability. In the end it follows naturally that:

$$\theta_k \hookrightarrow \mathcal{N}(\theta^{pop}, \omega_\theta). \quad (1.7)$$

---

<sup>2</sup>The use of the term *mixed effects model* is justified by the fact that individual parameters can be defined by a fixed effect alone, a random effect alone, or a combination of the two.

Equations (1.6) and (1.7) give two equivalent definitions of the *parameter model*, that is the description of which and how individual parameters vary in the population. When the structural model has more than one parameter, they can be re-written in a matrix form. In this case, we use  $\theta_k$  (resp.  $\theta^{pop}$  and  $\eta_k$ ) to designate the vector of the individual parameters for individual  $k$  (resp. the vector of the fixed effects and the vector of the individual random effects for individual  $k$ ), and  $\Omega$  to designate the variance-covariance matrix of the random effects.

Parameters  $\theta^{pop}$  and  $\omega_\theta$  are referred to as the population parameters of the model, because they fully characterize the distribution of parameter  $\theta$  across the population. Parameters  $(\theta_k)_{1 \leq k \leq N}$  are referred as the *individual parameters* of the model.

Equation (1.7) defines a gaussian distribution for parameter  $\theta$  in the population, but it might be useful to define another distribution. For instance, if one parameter is defined as being positive (e.g. rates of chemical reactions or state transitions) or bounded (e.g. probabilities of random events), then the gaussian distribution is not suited to model inter-individual variability because it can generate any value in  $\mathbb{R}$ . In this case, it is more comfortable to use a transformation  $h$  of the normal distribution (Lavielle and Bleakley, 2014):

$$\begin{cases} x_k \hookrightarrow \mathcal{N}(x^{pop}, \omega_x), \\ \theta_k = h(x_k), \end{cases}$$

from which it follows naturally that  $\theta_k \in h(\mathbb{R})$ . For instance, if  $h$  is the natural logarithm, then  $\theta$  is positive and follows a log-normal distribution. Moreover, if  $h$  is the repartition function of the standard normal gaussian distribution, then  $\theta \in [0, 1]$  and follows a probit-normal distribution. Other distributions could be considered (Lavielle and Bleakley, 2014), but they will not be used in this manuscript.

Usually, there is little evidence that a given distribution should be used in place of another, except for the parameter values that they allow. As a consequence, our choice of distribution in this manuscript will be limited to normal

## 1.4. Mixed Effects Models (MEM)

distributions for parameters that can take any real values, log-normal distributions for positive parameters, and probit-normal distributions for bounded parameters.

### 1.4.1.3 Error model

Finally, one last layer of modeling is used in MEM, in order to define an *error model*, or *observation model*. This part of the model quantifies the prediction error of the model using a gaussian error model, that we introduced in Section 1.3.2:

$$y_{i,j,k} = f_i(t_j, y_0, \theta_k) + g_i(t_j, y_0, \theta_k, \psi) \varepsilon_{i,j,k}, \quad \varepsilon_{i,j,k} \hookrightarrow \mathcal{N}(0, 1), \quad (1.8)$$

where  $g_i$  is the error function for observable  $i$ , which might depend on time, the initial condition, the individual parameters, and potentially other parameters, called the *error parameters*, that we denote as  $\psi$ . Since they do not vary between individuals, they can be estimated together with, and considered as part of the population parameters. In Equation (1.8),  $\varepsilon_{i,j,k}$  is the *Individual Weighted RESidual* (IWRES) for observable  $i$ , measured at time  $t_j$ , on individual  $k$ .

## 1.4.2 Parameter estimation

The fact that MEM are characterized by different kinds of parameters (population and individual parameters, fixed and random effects...) complicates their calibration. The population parameters are chosen in order to match the distribution of the model predictions to the distribution of the experimental data. Moreover, the individual parameters are fitted to the individual data, but at the same time their distribution across the population should match the distribution defined by the values of the population parameters.

In this section, we detail how we estimate the parameters of MEM. The first step of this estimation deals with the population parameters, and the second one concerns the individual parameters.

### 1.4.2.1 Population parameters

During the last decades, a variety of estimation methods, both frequentist and bayesian, have been developed for the computation of the population parameters. They are reviewed in (Pillai et al., 2005).

Frequentist methods for population parameters estimation comprise non-exhaustively the Laplacian method, the First-Order (FO) and First-Order Conditional Estimation (FOCE, Lindstrom and D. Bates, 1990; Pinheiro and D. M. Bates, 1995) methods, that are detailed in Y. Wang (2007), the Stochastic Approximation of the Expectation Maximization algorithm (Kuhn and Lavielle, 2005), and methods based on gaussian quadratures (Guedj et al., 2007).

Originally, bayesian estimation of population parameters were based on Markov Chain Monte Carlo (MCMC) sampling (Pillai et al., 2005). However, the timecost of this method has motivated the introduction of refinements like the Normal Approximation of the Posterior (NAP, Drylewicz et al., 2012; Prague et al., 2013).

Several pieces of software and packages have been developed to implement these estimation algorithms. The historical software NONMEM for instance (Kennedy, 1980), implements most of the algorithms that we mentioned (FO, FOCE, Laplacian approximation, SAEM and MCMC, as well as other methods and refinements of these, see Bauer, 2019). It is thus the standard for PKPD modeling in the industry. However, that fact that its sources are proprietary, and the prohibitive cost of its licence, are serious limitations to the use of such a software.

An alternative to NONMEM for the academia is Monolix, which is the historical implementation of the SAEM algorithm (Kuhn and Lavielle, 2005), and several of its refinements (Lavielle and Bleakley, 2014). The development of Monolix started as an open-source project, but it is now proprietary, and it also has a significant licence fee for industrials. However, it is free-of-use for the academia, which allowed us to use it in our study.

Another alternative is provided by the free R package nlmxir (Fidler et al., 2019), which has been developed as a solution for the increasing demand for

## 1.4. Mixed Effects Models (MEM)

a free mixed effects modeling platform (Conrado et al., 2017). It incorporates SAEM and FOCE, as well as a few variants and other methods.

Throughout the course of this project, we chose to use Monolix because of its reputation for being faster and more user-friendly than the other MEM softwares. The next section is thus dedicated to the introduction of the SAEM algorithm.

### 1.4.2.2 The Stochastic Approximation of the Expectation Maximization (SAEM) algorithm

The Stochastic Approximation of the Expectation Maximization (SAEM) algorithm has been proposed by Kuhn and Lavielle (2005) as a variant for nonlinear MEM of the Expectation Maximization (EM) algorithm of Dempster et al. (1977), which was already used in linear MEM. In this algorithm, the Expectation phase of the EM algorithm is replaced by a Stochastic Approximation step. This means that starting from an initial guess  $\theta_0$  of the population parameters, SAEM estimates the population parameters by iteratively applying the following steps:

1. Sampling  $N$  individuals according to their distribution conditioned by the data and the previously estimated population parameters:  $p(\theta_k^i | y, \theta^{i-1})$ , where  $\theta_k^i$  are the individual parameters of the  $k^{th}$  sampled individual at the  $i^{th}$  iteration of the algorithm,  $y$  designates the whole set of the data (all observables, at all timepoints, for all individuals) and  $\theta^{i-1}$  is the previously estimated population parameter vector. Since this conditional distribution has no general analytical expression, sampling is achieved by MCMC in Monolix. This step is referred to as the *simulation step*.
2. Updating quantity  $Q_i$  according to:

$$Q_i(\theta) = Q_{i-1}(\theta) + \gamma_i \left( p(y, z^i | \theta^{i-1}) - Q_{i-1}(\theta) \right),$$

where  $(\gamma_i)$  is a sequence of positive, decreasing, numbers, on which convergence depends (we will come back to this in a few lines). This step is

referred to as the *Stochastic Approximation step*.

3. Updating the estimate of the population parameters with the sampled data according to:

$$\theta_i = \arg \max_{\theta} Q_i(\theta).$$

This step is referred to as the *Maximization step*.

Theoretically, conditions for convergence depend on the sequence  $\gamma$  introduced at step 2. The choice of this sequence is thus critical to ensure as quick a convergence as possible. Specifically, the convergence of the algorithm requires two conditions on  $(\gamma_i)$  (Lavielle and Bleakley, 2014):

$$\begin{cases} \sum_{i=1}^{\infty} \gamma_i = \infty, \\ \sum_{i=1}^{\infty} \gamma_i^2 < \infty. \end{cases}$$

In practice, Monolix chooses the sequence  $(\gamma_i)$  such that the estimation involves two phases (Lavielle and Bleakley, 2014):

- In the *exploratory phase*, which lasts for the first  $K_1$  iterations,  $\gamma_i = 1$ , which ensures the convergence of the estimate to a neighborhood of the optimum in a relatively small amount of time.
- In the *smoothing phase*, which lasts for the last  $K_2$  iterations,  $\gamma_i = 1/(i - K_1)$ , which ensures the convergence of the estimate to the actual optimum.

Unless stated otherwise, we used  $K_1 = 5000$  and  $K_2 = 1000$  for all MEM in this manuscript.

We refer the reader to the web-tutorial by Lixoft (2019) for a graphical introduction to this algorithm.

### 1.4.2.3 Individual parameters

Once the population parameters have been estimated by SAEM, Monolix infers individual parameters for each individual using the Empirical Bayesian

## 1.4. Mixed Effects Models (MEM)

Estimates, which is based on the posterior distribution of the random effects using the population as a prior (Lavielle and Bleakley, 2014):

$$p(\eta_k|y_{\cdot,\cdot,k}) \propto p(y_{\cdot,\cdot,k}|\eta_k)p(\eta_k), \quad (1.9)$$

where  $y_{\cdot,\cdot,k}$  is the set of data corresponding to individual  $k$  (for all observables and at all timepoints),  $p(y_{\cdot,\cdot,k}|\eta_k)$  accounts for the fit to the individual data and is computed from Equation (1.8), and  $p(\eta_k)$  is the density distribution of the random effects in the population (from Equation (1.7)). It is then possible to define a value for the individual parameter by taking the mode of this distribution<sup>3</sup>.

### 1.4.3 Model selection

Because MEM have different kinds of parameters (population mean values, population variances, error parameters, individual parameters), classical model selection methods have been adapted for MEM.

#### 1.4.3.1 Bayesian Information Criterion (BIC)

For example, the Bayesian Information Criterion (BIC) has been classically defined by Schwarz (1978) as:

$$BIC = \log(n)K - 2\log(\hat{\mathcal{L}}), \quad (1.10)$$

where  $n$  is the sample size,  $K$  is the number of parameters of the model, and  $\hat{\mathcal{L}}$  is the optimal likelihood. In order to avoid overfitting, the BIC penalizes the likelihood with the number of parameters multiplied by the logarithm of the sample size. However, it is unclear in MEM if the sample size should be chosen as the population size  $N$  (number of individuals) or as the total number of observations  $n_{tot} = nmN$  (since there are  $n$  observables,  $m$  timepoints and  $N$

---

<sup>3</sup>Other definitions might be used, for instance the mean of the posterior, but they will not be used in this manuscript.

individuals in the dataset). As a consequence, the different available software for MEM estimation don't use the same definition for the BIC in MEM.

In order to tackle this problem, a formal corrective term for the Bayesian Information Criterion has been developed for the selection of covariates and random effects in MEM (Delattre et al., 2014; Delattre and Poursat, 2016), by decomposing the individual parameters between fixed parameters, that don't vary between individuals, and random ones, that have a different value for each individual:

$$\theta_k = \begin{pmatrix} \theta_{F,k} \\ \theta_{R,k} \end{pmatrix} = \begin{pmatrix} \theta_{F,pop} \\ \theta_{R,pop} \end{pmatrix} + \begin{pmatrix} 0 \\ \eta_{R,k} \end{pmatrix}, \quad \eta_{R,k} \hookrightarrow \mathcal{N}(0, \Omega_R),$$

where  $\theta_{F,k}$  (resp.  $\theta_{R,k}$ ) is the vector of fixed individual parameters of individual  $k$  (resp. the vector of random individual parameters),  $\theta_{F,pop}$  (resp.  $\theta_{R,pop}$ ) is the vector of fixed effects of the fixed parameters (resp. the vector of fixed effects of the random parameters),  $\eta_{R,k}$  is the vector of random effects of the the random parameters of individual  $k$  (the vector of random effects on the fixed parameters is null), and  $\Omega_R$  is the covariance matrix of the random effects of the random parameters.

Then, the population parameters can also be decomposed into population parameters of the fixed parameters, and population parameters of the random parameters:  $\theta = (\theta_F, \theta_R)$ , with:

$$\begin{cases} \theta_F = \theta_{F,pop}, \\ \theta_R = (\theta_{R,pop}, vec(\Omega_R)), \end{cases}$$

where  $vec(\Omega_R)$  is the vector containing the non-null elements of  $\Omega_R$ .

Then the BIC of the model is defined in Delattre and Poursat (2016), as:

$$BIC = -2 \log(\hat{\mathcal{L}}) + \#(\theta_R) \log(N) + \#(\theta_F) \log(n_{tot}), \quad (1.11)$$

where  $\#(x)$  is the cardinality of vector  $x$ .

## 1.4. Mixed Effects Models (MEM)

### 1.4.3.2 Akaike's Information Criterion (AIC)

Similarly, the classical Akaike's Information Criterion (AIC), introduced in detail in Burnham and Anderson (2010) as:

$$AIC = 2K - 2\log(\hat{\mathcal{L}}), \quad (1.12)$$

is referred as the *marginal AIC* (mAIC) in a MEM context (Vaida and Blanchard, 2005), and has been shown to be inappropriate for MEM. A *conditional AIC* (cAIC) has been derived for linear MEM Vaida and Blanchard, 2005; Liang et al., 2008.

Depending on the precise context, mAIC or cAIC might be the best-suited selection criterion (Vaida and Blanchard, 2005), but no matter which criterion is being used, a useful selection method is provided by the Akaike's weights (Burnham and Anderson, 2010):

$$w_i = \frac{\exp(-(AIC_i - \min(AIC))/2)}{\sum_{j=1}^R \exp(-(AIC_j - \min(AIC))/2)}, \quad (1.13)$$

where  $w_i$  is the Akaike's weight of the  $i$ -th model,  $AIC_i$  is its Akaike's Information Criterion and  $R$  is the number of competing models. The Akaike's weight of a given model in a given set of models can be seen as the probability that it is the best one among the set (Burnham and Anderson, 2010). In this setting, selecting the best models of a set of models means computing their Akaike's weights, sorting them, and keeping only the models whose weights add up to a significance probability (in this manuscript, 95%).

In this manuscript, we will essentially use the AIC and the corresponding Akaike's weights for selecting models with the same structure, that differ only by their parameter values (this will be developed in the next section, and in Chapters 5 to 7). In this context, differences in AIC originate from differences in the likelihood of the models, and are independent from the corrective term being used. For this reason, the choice of mAIC or cAIC is not relevant to our study, and we will use the marginal AIC, that is computed by Monolix by default (Lavielle and Bleakley, 2014).

### 1.4.3.3 Likelihood Ratio Test (LRT)

Another model selection tool that will be of use for our investigations is the Likelihood Ratio Test (LRT), which tests the difference in the log-likelihoods of two nested models  $\mathcal{M}_0$  and  $\mathcal{M}_1$  with numbers of parameters  $K_0$  and  $K_1 > K_0$ . Under the null hypothesis that  $-2\log\hat{\mathcal{L}}_1 = -2\log\hat{\mathcal{L}}_0$ , the statistic  $2(\log\hat{\mathcal{L}}_1 - \log\hat{\mathcal{L}}_0)$  follows a  $\chi^2$  distribution with  $K_1 - K_0$  degrees of freedom.

In MEM, the test statistic is more complex to compute, and can be a mixture of  $\chi^2$  and Dirac distributions (Lavielle and Bleakley, 2014), depending on the precise hypotheses of the test (*i.e.* whether the hypothesis is on a fixed effect, a random effect variance, or the covariance between two random effects).

### 1.4.4 Identifiability in mixed effects models

Mixed Effects Models are often proposed as a way of addressing the unidentifiability of a structural model, because if the parameters of some individuals are poorly characterized, the population information is used as a prior for their estimation (Karlsson et al., 2015). Provided that the population parameters are well determined, MEM could thus be used to better estimate the individual parameters.

However, as is often the case with MEM, things are more complex than this simplistic hypothesis. Especially, the intricate parameterization of MEM, where population parameters are estimated by sampling individual parameters first, and individual parameters are estimated using the population distribution as a prior in a second step, complicates the definition and assessment of identifiability. Lavielle and Aarons (2016) studied the identifiability of non-linear MEM. They decipher between *theoretical identifiability*, which is a feature of the parameter model (provided if different population parameter values render different individual parameter distribution), *structural identifiability* (that is the structural identifiability of the structural model), and *practical identifiability*, which is defined as previously (Section 1.3.3).

In this section, we present the existing framework for studying parametric

## 1.4. Mixed Effects Models (MEM)

identifiability in MEM, starting with the population parameters, before focusing on the individual parameters.

### 1.4.4.1 Population parameters

Regarding the assessment of the practical identifiability of population parameters, Lavielle and Aarons (2016) report two methods, that are essentially empirical.

The most frequent one estimates the FIM of the model, and defines identifiability either by the FIM eigenvalues, using the  $E$ -criterion (or its modified version  $E_{modified}$ ) as introduced in System (1.5), or by approximating the parameters standard errors and comparing the estimated value to the range of the standard error for each parameter.

The other method uses repeated parameter estimations, starting from different initial guesses. In this case, convergence to different parameter values with the same likelihood indicates unidentifiability. However, this requires repeated estimations of the model parameters, which can be time-consuming if the model is complex. This approach has also been termed the *multistart approach*, for instance by Fröhlich et al. (2014), who stress the fact that despite underlining parameter unidentifiabilities, the multistart approach does not provide any information regarding the actual values of parameter uncertainties. We will refer to the multistart approach as *Initial Guess Sampling* (IGS) in this manuscript.

To our knowledge, no implementation of the profile likelihood approach (Section 1.3.4.1) has been achieved for MEM. In the case of our models, we will thus try to use a combination of FIM-based strategies and IGS. Specifically, our approach to IGS is the following:

1. We perform a random sampling of the initial parameter guesses, which provides us with a sample of optimal parameter values.
2. We test the convergence of the SAEM runs: we only want to consider the runs which reached the global optimum. To this end, we use a selection

criterion ( $w_{AIC}$ , Section 1.4.3) to keep only the runs that converged to the lowest likelihood values.

3. We compare the parameter values of these convergent runs. If they're not the same, then the model is unidentifiable (several different parameter values give the same likelihood)

#### 1.4.4.2 Individual parameters

In the case where the individual parameters are not identifiable, the experimental data do not provide enough information to determine them precisely. In the case of the EBE defined in Equation (1.9), this means that the distribution  $p(y_{\cdot,\cdot,k}|\eta_k)$  will not be very important in the product  $p(y_{\cdot,\cdot,k}|\eta_k)p(\eta_k)$ . In turn, the posterior distribution  $p(\eta_k|y_{\cdot,\cdot,k})$  will be very close to  $p(\eta_k)$ , so its mode will be close to 0. As a consequence, the individual parameters will all be close to the population average.

This phenomenon is summarized by a scalar criterion called the  $\eta$ -shrinkage (Karlsson and Savic, 2007; Savic and Karlsson, 2009):

$$s_\eta = 1 - \frac{std(\eta_k)}{\omega_\theta}, \quad (1.14)$$

where  $std(\eta_k)$  is the standard deviation of the estimated individual random effects in the population, and  $\omega_\theta$  is their theoretical standard deviation. In the case where information about a parameter is insufficient, the random effects on this parameter shrink toward 0 in the population, and thus  $s_\eta$  increases. Equation (1.14) also implies that shrinkage values vary from parameter to parameter, and that some parameter might be more poorly characterized than the others.

Simulation studies have shown that shrinkage can generate false correlations between random effects, or mask the existing correlations, starting from 30% shrinkage (Savic and Karlsson, 2009). This number should be taken with care, since Savic and Karlsson (2009) did not test many distinct shrinkage values in their paper, and their results are very specific to the model they used for

## 1.5. Thesis outline

generating their simulations.

## 1.5 Thesis outline

This manuscript is divided in two parts. The first one is dedicated to the elaboration of a dynamic model of *in vitro* erythropoiesis. We first define the model in Chapter 2. Then, in Chapter 3, we apply it in to the data obtained under the drug treatments that we introduced in Section 1.2.3. In Chapter 4, we present why MEM will be of interest for modelling *in vitro* erythropoiesis, by introducing the notion of *experimental heterogeneity*, that is the variation of the outcome of the differentiation experiment obtained in the same conditions.

The second part of the manuscript aims at adapting the model defined in Chapter 2 in a mixed effects context, based on the data introduced in Chapter 4. We define this MEM in Chapter 5, and conclude that it is unidentifiable. Finally, we assess how to make our model identifiable, using experimental design (Chapter 6) and model reduction (Chapter 7).



# Chapter 2

## A deterministic model of *in vitro* erythropoiesis

### 2.1 Introduction

Our main goal throughout this work is to model the *in vitro* erythropoiesis. More precisely, we want to quantify the differentiation of the T2EC progenitors, that we presented in Section 1.1.2, in different conditions. In some conditions the cells were treated with chemical drugs, and we ask whether the treatment accelerates or decelerates differentiation. It seems that we cannot answer this question experimentally, since the number of differentiated cells that we presented in Section 1.2 results from the dynamic balance between cell proliferation, cell death and differentiation, which we cannot measure from experiments. Consequently, the first part of the project was to develop a dynamic model of *in vitro* erythropoiesis, explicitly accounting for the differentiation rate of the cells in culture. Since we want to compare parameter values between the different conditions, we need to estimate these parameter values as precisely as possible.

We thus propose to design the first model of *in vitro* erythroid differentiation. We test different possible forms for the ODE in this model and the distribution of its residuals, and select the best-one at fitting our data using

Akaike's weights (Burnham and Anderson, 2010). The data consist in the three measured quantities that we presented in Section 1.1. Then, in order to be able to compare parameter values between the treated and untreated conditions, we need to assess the identifiability of these values. We thus perform identifiability analysis based on the profile likelihood approach (which we presented in Section 1.3, Raue et al., 2009). Then, we test the ability of our model to assess the effect of chemical treatments on the parameter values. To this end, we use rapamycin, a chemical drug which is known to affect the number of cells in the culture as well as the proportion of differentiated cells (Dazy et al., 2003; Gonin-Giraud et al., 2008), and try to compute its effects on the parameter values. This work was published in *In Silico Biology* (Duchesne et al., 2019).

## 2.2 Paper

# Calibration, Selection and Identifiability Analysis of a Mathematical Model of the *in vitro* Erythropoiesis in Normal and Perturbed Contexts

Ronan Duchesne<sup>1,2,\*</sup>, Anissa Guillemin<sup>1</sup>, Fabien Crauste<sup>2,3</sup>, and Olivier Gandrillon<sup>1,2</sup>

<sup>1</sup>Laboratoire de Biologie et Modélisation de la Cellule, École Normale Supérieure de Lyon, 46 allée d'Italie, Lyon.

<sup>2</sup>Équipe Dracula, Inria, 56 Boulevard Niels Bohr, Villeurbanne

<sup>3</sup>Institut Camille Jordan, Université Claude Bernard Lyon 1, 43 Boulevard du 11 Novembre 1918, Villeurbanne

\*ronan.duchesne@ens-lyon.fr

## Abstract

The *in vivo* erythropoiesis, which is the generation of mature red blood cells in the bone marrow of whole organisms, has been described by a variety of mathematical models in the past decades. However, the *in vitro* erythropoiesis, which produces red blood cells in cultures, has received much less attention from the modelling community. In this paper, we propose the first mathematical model of *in vitro* erythropoiesis. We start by formulating different models and select the best one at fitting experimental data of *in vitro* erythropoietic differentiation obtained from chicken erythroid progenitor cells. It is based on a set of linear ODE, describing 3 hypothetical populations of cells at different stages of differentiation. We then compute confidence intervals for all of its parameters estimates, and conclude that our model is fully identifiable. Finally, we use this model to compute the effect of a chemical drug called Rapamycin, which affects all states of differentiation in the culture, and relate these effects to specific parameter variations. We provide the first model for the kinetics of *in vitro* cellular differentiation which is proven to be identifiable. It will serve as a basis for a model which will better account for the variability which is inherent to the experimental protocol used for the model calibration.

## 1 Introduction

Erythropoiesis is the process by which red blood cells are produced. It occurs within the broader frame of haematopoiesis, the process which generates all blood cells. The dynamics of haematopoiesis has been extensively modelled mathematically in the past decades, with the first historical models published as early as fifty years ago<sup>(1,2)</sup> (for a review of the history of haematopoiesis modelling in general, see<sup>(3)</sup>). Models of haematopoiesis have improved the understanding of both the processes they describe<sup>(4)</sup>, and the mathematical tools they use. These models comprise non-exhaustively Differential Equations (DE, either ordinary<sup>(1,2,5)</sup>, partial, which can be structured by age, maturity, or a combination of these<sup>(6)</sup>, or even delay differential equations<sup>(7)</sup>) and agent-based models<sup>(8)</sup>. They can be fully deterministic<sup>(5)</sup> or can include a more or less prominent stochastic component<sup>(9,10,11)</sup>.

Recent works specifically focusing on erythropoiesis comprise DE-based models<sup>(12,13)</sup> and multi-scale descriptions of these phenomena<sup>(14,15,16)</sup>.

All these works aim at modeling the *in vivo* physiological processes, *i.e.* the processes occurring in a whole organism. Those processes are related to numerous pathologies, for which clinical data are very sparse and must be acquired on experimentally prohibitive time-scales, which complicates their study. Modeling has therefore provided significant insights into these pathologies<sup>(4)</sup>. On the contrary, the *in*

*vitro* context, *i.e.* the process that takes place in cells grown in culture, is much simpler to characterize experimentally. Yet, to our knowledge, no modeling study has focused on it so far. Since the *in vitro* differentiation is an experimental tool of choice for the study of cellular decision-making<sup>(17,18,19)</sup>, we propose to develop a model for the dynamics of the *in vitro* erythropoiesis.

Moreover, the current models of erythropoiesis suffer from one major drawback: the weakness of their parameterization, which can fall within three categories.

A vast majority of the existing models of erythropoiesis are based on experimental parameter values from the literature. In some cases these values are used in other contexts than those in which they were obtained (typically, in other species<sup>(12)</sup>).

In other cases, the parameter values of a model are chosen arbitrarily to reproduce a qualitative behaviour. Apart from this qualitative fit, such approaches do not provide any information regarding the validity of the values<sup>(16)</sup>.

Finally, when the parameters of a model are estimated to reproduce a dataset, the precision of this estimation is seldom investigated<sup>(20)</sup>. By this, we mean that depending on the algorithmic details of the estimation, it is possible that several values of the parameters might render the same fit to the data. In this case the model is said to be unidentifiable.

A model is said to be identifiable if and only if it is possible to infer a unique value for each of its parameter by comparing its output to experimental data. Otherwise it is unidentifiable. A model can be non-identifiable for several reasons<sup>(21,22)</sup>.

Structural identifiability is related to the structure of the model, and the observed variables. A model is structurally unidentifiable when several of its parameters are redundant, meaning that they can vary in such a manner that the measured output of the model is not affected<sup>(21,22,23)</sup>. A variety of methods, based on different approaches, can be used to assess the structural identifiability of a dynamic model. These include, non-exhaustively, the Taylor series method<sup>(24)</sup>, the similarity transformation<sup>(25)</sup>, the generating series method<sup>(26)</sup>, and the profile likelihood approach<sup>(22,27,28)</sup>. A review of these methods is provided in<sup>(21)</sup> and their performance is assessed in<sup>(23)</sup>.

Practical Identifiability is related to the quantity and quality of the data used for model calibration. If the data is too sparse or too noisy to estimate all parameters together, then the model is said to be practically unidentifiable<sup>(21,22)</sup>. Essentially three kinds of frequentist methods can be used to assess the practical identifiability of a model: methods based on the Fisher Information Matrix (FIM)<sup>(29)</sup>, which use a parabolic approximation of the likelihood function, profile-likelihood-based methods<sup>(22,28)</sup>, and bootstrapping, which is based on the resampling of the data<sup>(30)</sup>. FIM-based methods are less computationally demanding, because they require the fewest parameter estimation steps<sup>(31)</sup>, but due to their parabolic approximation they are proven to render biased results<sup>(22)</sup>. On the other hand, the profile likelihood-based method is computationally cheaper than bootstrapping<sup>(31)</sup>, and is proven to detect both structural and practical unidentifiabilities<sup>(22,27)</sup>.

Despite the growth of the interest in identifiability and related concepts among the biological systems modelling community<sup>(21,32,33,34)</sup> the identifiability of models remains seldom investigated<sup>(20)</sup>. With this in mind, the most rigorous way to design and calibrate a model of erythropoiesis seems to use dedicated experiments to determine its parameter values. Once these values have been determined, one should then test the identifiability of the model before using it for any prediction.

In this paper, we aim at developing an identifiable model for the dynamics of the *in vitro* erythroid differentiation. The data that we generated to calibrate it consists in counts of different cell sub-populations at regularly spaced time-points during the course of proliferation and differentiation of chicken erythroid progenitors. We start by formulating different possible structures for the dynamics of the system, and for the distribution of residuals. We select the best structure and distribution using classical information criteria. We then assess the identifiability of our model using an approach based on the profile likelihood concept. Finally, we test the adaptation of our model in a perturbed context, when cells are exposed to rapamycin, a drug which is known to affect the dynamics of differentiation, although its precise effect on proliferation and differentiation remains unclear. Since our model is identifiable, it is possible to quantify the effect of the drug on each of its parameters.

## 2 Methods

### 2.1 Experimental Data

#### 2.1.1 T2EC cell culture

The experimental setting from which all the data used in this study were obtained consists in a culture of chicken erythroid progenitors called T2EC that were extracted from the bone marrow of 19 days-old SPAFAS white leghorn chickens embryos (INRA, Tours, France). They may either be maintained in a proliferative state or induced to differentiate into mature erythrocytes depending on the medium in which they are grown<sup>(35)</sup>.

#### 2.1.2 LM1 experiment

In the self-renewal medium (referred to as the LM1 medium) the progenitors self-renew, and undergo successive rounds of division. LM1 medium was composed of  $\alpha$ -MEM medium supplemented with 10 % Foetal bovine serum (FBS), 1 mM HEPES, 100 nM  $\beta$ -mercaptoethanol, 100 U/mL penicillin and streptomycin, 5 ng/mL TGF- $\alpha$ , 1 ng/mL TGF- $\beta$  and 1 mM dexamethasone as previously described<sup>(35)</sup>. After 10 days in LM1, the culture is composed at >99% of erythroid progenitors cells<sup>(36,37)</sup>. Cell population growth was evaluated by counting living cells in a 30  $\mu$ L sample of the 1mL culture using a Malassez cell and Trypan blue staining (SIGMA), which specifically dyes dead cells (Figure 1-A), each 24h after the beginning of the experiment.

#### 2.1.3 DM17 experiment

T2EC can be induced to differentiate by removing the LM1 medium and placing cells into 1mL of the differentiation medium, referred to as DM17 ( $\alpha$ -MEM, 10% foetal bovine serum (FBS), 1 mM HEPES, 100 nM  $\beta$ -mercaptoethanol, 100 U/mL penicillin and streptomycin, 10 ng/mL insulin and 5% anaemic chicken serum (ACS)). Upon the switching of culture medium, a fraction of the progenitors undergoes differentiation and becomes erythrocytes. The culture thus becomes a mixture of differentiated and undifferentiated cells, with some keeping proliferating. Cell population differentiation was evaluated by counting differentiated cells in a 30 $\mu$ L sample of the culture using a counting cell and benzidine (SIGMA) staining which stains haemoglobin in blue (Figure 1B). A parallel staining with trypan blue still gives access to the overall numbers of living cells (Figure 1B). Consequently, the data available from this experiment are the absolute numbers of differentiated cells, as well as the total number of living cells (which comprises both self-renewing and differentiated cells) at the same time points as in the LM1 experiment. The data presented on Figures 1C and 4A are the total number of living cells in the culture, and the fraction of differentiated cells, extrapolated from the counting.

#### 2.1.4 Rapamycin treatment

In the control condition, cells were grown in their regular medium with 0.1% DMSO (Figure 1C, black dots). In the treated condition, cells were grown in the presence of rapamycin (Calbiochem), a chemical drug known to affect both the number of living cells in culture, and the proportion of differentiated cells<sup>(36,38)</sup>, as displayed on Figure 1C. Cells were treated with Rapamycin at 50 nM just after switching them to the DM17 medium. It should be noticed that the very same original culture was used to initiate all the experiments presented on Figure 1C (in the LM1 and DM17 media, as well as in the treated and untreated conditions).

#### 2.1.5 Commitment experiment

Another piece of experimental data that will be of use for calibrating our models is the result of the commitment experiment. The full protocols and results of this experiment are described in Figure 10 of<sup>(17)</sup> and are summarized on Figure 1D. In this experiment, once a cell culture has been switched to the DM17 medium, it can be switched back to the LM1 medium. Switching back after 24 hours of differentiation does not cancel the self-renewing ability of the progenitors, but switching back after 48

hours does: instead of proliferating again, the culture stagnates. This means that there must remain some self-renewing cells in the culture after one day, but that they all have started differentiating after two days.

## 2.2 Models

### 2.2.1 Structural Model

We propose three alternative dynamic models of the erythroid differentiation, which are summarized on Figure 2.

The SB model comprises only two compartments (Figure 2A), a self-renewing one (S) and a differentiated one (B, which stands for *benzidine-positive*), whose dynamics are given by the equations:

$$\frac{dS}{dt} = \rho_S S(t) - \delta_{SB} S(t), \quad (1a)$$

$$\frac{dB}{dt} = \rho_B B(t) + \delta_{SB} S(t). \quad (1b)$$

This model is characterized by a set  $\theta = (\rho_S, \delta_{SB}, \rho_B)$  of three parameters, where  $\rho_i$  is the net proliferation rate of compartment  $i$ . For estimation-related reasons, it incorporates the balance between cell proliferation and cell death. This means that  $\rho_i$  can be either positive (more proliferation than death) or negative (more death than proliferation). On the other hand  $\delta_{ij}$  is the differentiation rate of cell type  $i$  into cell type  $j$ , which is positive.

The S2B model comprises also the S and B compartments (Figure 2B), but allows the self-renewing cells to change their net proliferation rate upon culture medium switching. This formulation arose from the consideration that proliferation is faster in the DM17 than in the LM1 medium (Figure 1C). The dynamics of this model are given by the equations:

$$\frac{dS_{LM1}}{dt} = \rho_{LM1} S_{LM1}(t), \quad (2a)$$

$$\frac{dS_{DM17}}{dt} = \rho_{DM17} S_{DM17}(t) - \delta_{SB} S_{DM17}(t), \quad (2b)$$

$$\frac{dB}{dt} = \rho_B B(t) + \delta_{SB} S_{DM17}(t). \quad (2c)$$

It is characterized by the set  $(\rho_{LM1}, \rho_{DM17}, \delta_{SB}, \rho_B)$  of four parameters, following the same notation convention as in the SB model.

Finally, the SCB model (Figure 2C) also comprises the same self-renewing and differentiated compartments as the SB model, as well as a hypothetical *committed cells* compartment  $C$ . This compartment comprises intermediary cells that are committed to differentiation, yet not fully differentiated. The dynamics of these three compartments are given by the equations:

$$\frac{dS}{dt} = \rho_S S(t) - \delta_{SC} S(t), \quad (3a)$$

$$\frac{dC}{dt} = \rho_C C(t) + \delta_{SC} S(t) - \delta_{CB} C(t), \quad (3b)$$

$$\frac{dB}{dt} = \rho_B B(t) + \delta_{CB} C(t). \quad (3c)$$

It is characterized by the set  $(\rho_S, \delta_{SC}, \rho_C, \delta_{CB}, \rho_B)$  of five parameters, following the same naming convention as the two other models.

Moreover, it should be noted that differential systems (1) to (3) are fully linear, and that their matrices are lower-triangular, which makes them easily solvable analytically. Their simulation is thus very fast. The detail of the analytical solutions to these systems is given as supplementary material.

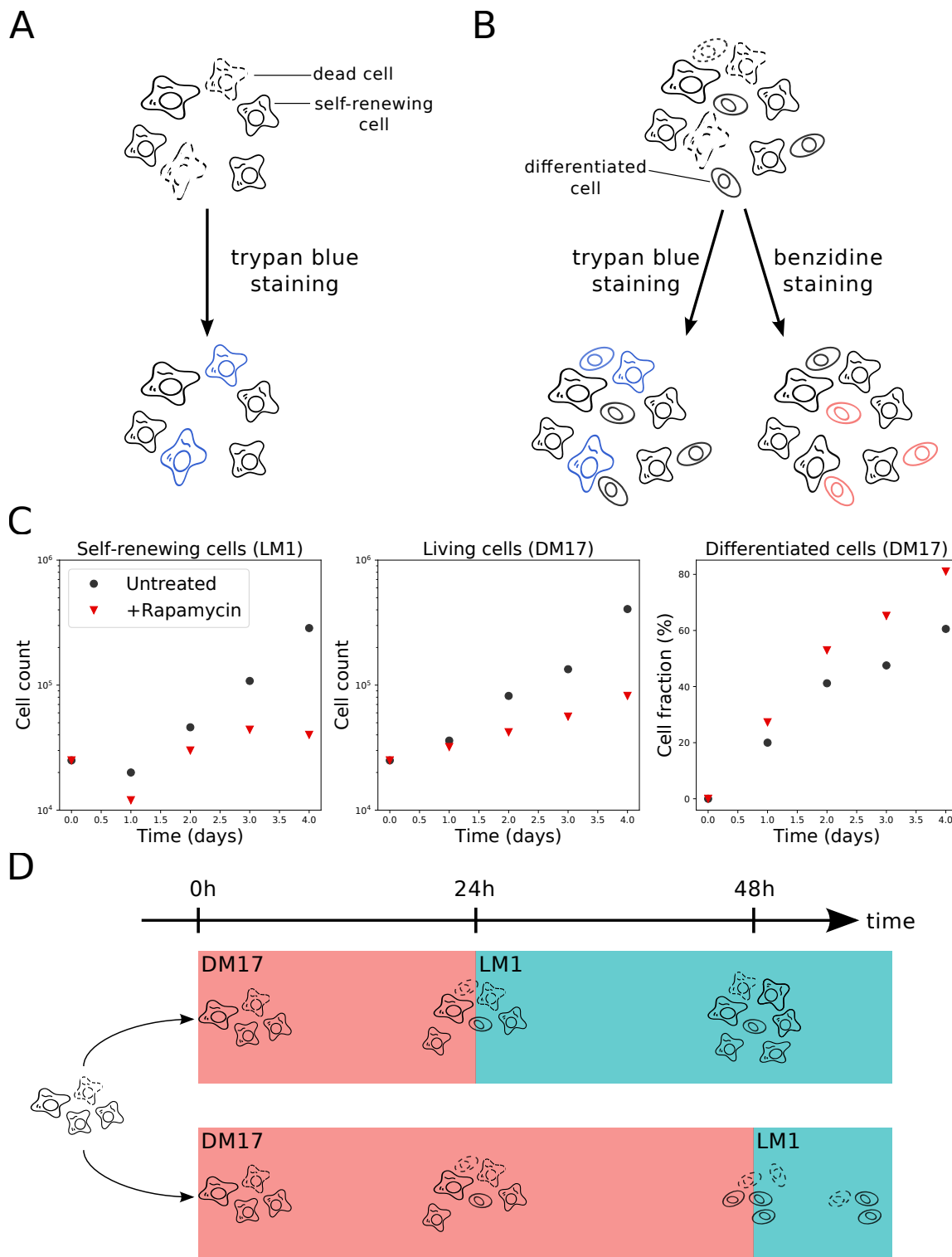


Figure 1: Experimental context. A: In LM1 medium the culture is only composed of living and dead cells in the self-renewal state. The amount of living cells can be measured by trypan blue staining. B: In DM17 medium, the culture is a mixture of living and dead, self-renewing and differentiating cells. The amount of living cells can be measured by trypan blue staining. The amount of differentiated cells can be measured by benzidine staining. C: Data used to calibrate the models. Black dots are the results of a single experiment in the control situation (no treatment). Red triangles are the results of the same experiment under rapamycin treatment. Both conditions were obtained with the same initial populations, so the black dot and red triangle are the same at  $t = 0$ . For readability, living cell counts are displayed in log-scale, and differentiated cell counts are displayed as a fraction of the total living cell count. D: Commitment experiment. If the differentiating cells are switched back to LM1 after 24h of differentiation the culture starts proliferating again (upper trajectory). If the cells are switched back to LM1 after 48h, the culture stagnates (lower trajectory).

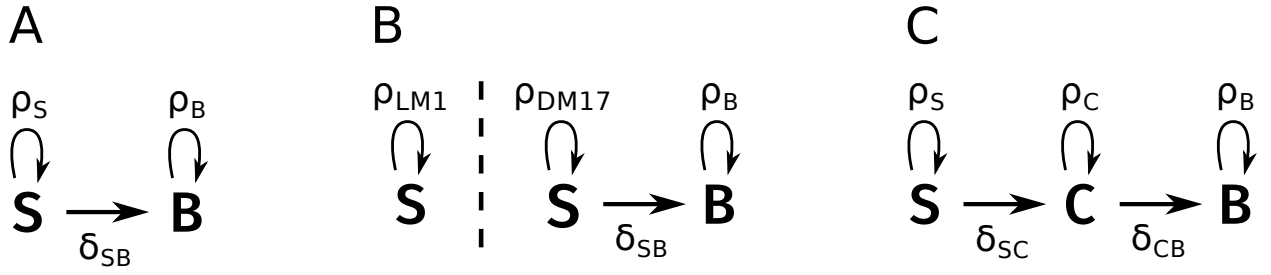


Figure 2: Diagrams of three possible dynamic models for our data. A: The SB model has no intermediary compartment. B: The S2B model has no intermediary compartment, but the self-renewing cells change proliferation rate in DM17. C: The SCB model has an intermediary compartment.

Finally, not all variables in the models can be measured through the experiments that we presented in section 2.1, and we only have access to two observables of the system: the total amount of living cells  $T(t)$  through trypan blue staining, and the amount of differentiated cells  $B$  through benzidine staining. The number of living cells  $T$  can be measured in LM1 and in DM17, yet in LM1 there is no differentiation, so in the LM1 experiment  $T = S$  (or  $T = S_{LM1}$  in the S2B model). The number of differentiated cells  $B$  can be measured in DM17 (it is null in LM1).

### 2.2.2 Error Model

In order to properly define the likelihood of our model, we need to define a statistical model for the prediction error of our dynamical model,  $y - f(t, y_0, \theta)$ , where  $y$  is the data and  $f$  the prediction from the dynamical model (which depends on time  $t$ , the initial condition  $y_0$  and the parameters  $\theta$  of the model). This prediction error is usually modelled by a gaussian distribution with a null mean<sup>(22,39,40)</sup>. Then, the standard deviation of the error remains to be characterized.

When dealing with small datasets, a reasonable option is to build an additional model layer for the standard deviation of the error<sup>(39)</sup>. This means finding a suitable function  $g$ , of the time  $t$ , the initial condition  $y_0$ , the dynamical parameters  $\theta$  and possibly other parameters  $\xi$  (which we will call the error parameters), to describe this variance. The error model is then completely described as:  $y_{i,j} \leftrightarrow \mathcal{N}(f_i(t_j, y_0, \theta), g_i(t_j, y_0, \theta, \xi))$ . Several simple forms have been proposed for the function  $g$ <sup>(40)</sup>, that we summarize in Table 1. However, it is not obvious whether one should be used in general, or if the choice of  $g$  should be context-specific.

Error model	Definition of $g$	Error parameters
Constant error	$\forall j \quad g_i(t_j) = a$	$\xi = (a)$
Proportional error	$\forall j \quad g_i(t_j, y_0, \theta) = b \cdot f_i(t_j, y_0, \theta)$	$\xi = (b)$
Combined error	$\forall j \quad g_i(t_j, y_0, \theta) = a + b \cdot f_i(t_j, y_0, \theta)$	$\xi = (a, b)$

Table 1: Definition of three different error models<sup>(40)</sup>.

With this representation, the log-likelihood of the model follows as:

$$-2 \log(L) = nm \log(2\pi) + \sum_{i=1}^n \sum_{j=1}^m \left( \frac{(y_{i,j} - f_i(t_j, \theta))}{g_i(t_j, \theta, \xi)} \right)^2 + 2 \log(g_i(t_j, \theta, \xi)), \quad (4)$$

where  $n$  is the number of variables of the dynamic model, and  $m$  the number of measurement points for each variable, and from which the  $\log(2\pi)$  term is dropped. In the end, the best-fit parameters of the model are the values of  $\theta$  and  $\xi$  which minimize the quantity defined in Equation (4). In this equation, the data  $y_{i,j}$  and the prediction  $f_i(t_j, \theta)$  are the total number of cells in each measured compartment of the model (without any transformation of the variables).

## 2.3 Parameter Estimation

Considering the data at our disposal, we adopted the following procedure for parameter estimation:

1. Estimate  $\rho_S$  (or  $\rho_{LM1}$  in the S2B model), and the corresponding error parameters  $\xi_1$  from the LM1 experiment. In LM1 there is no differentiation, so the  $S$  compartment just follows an exponential growth with rate  $\rho_S$ .
2. (a) In the SB model, set  $\delta_{SB}$  so that there are no more self-renewing cells after 2 days of differentiation (which we interpret as  $S(48h) \leq 1$ , i.e.  $\delta_{SB} \geq \rho_S + 1/2 \ln(S(0))$  from Equation (1a)).  
 (b) In the SCB model, set  $\delta_{SC}$  so that there are no more self-renewing cells after 2 days of differentiation (which we interpret as  $S(48h) \leq 1$ , i.e.  $\delta_{SC} \geq \rho_S + 1/2 \ln(S(0))$  from Equation (3a)).
3. Estimate the remaining parameters, and the corresponding error parameters  $\xi_2$ , using the data from the DM17 experiment. In the SB model, the only remaining parameter is  $\rho_B$ . In the S2B model, the remaining parameters are  $\rho_{DM17}$ ,  $\delta_{SB}$  and  $\rho_B$ . In the SCB model, these are  $\rho_C$ ,  $\delta_{CB}$ ,  $\rho_B$ .

The second step of this estimation sets  $\delta_{SC}$  ( $\delta_{SB}$  in the SB model) to a value such that there are no more self-renewing cells after 2 days of differentiation. This observation does not come from the cellular kinetics experiment that we presented on Figure 1C. It rather uses the results of the commitment experiment (Section 2.1.5 & Figure 1D), which shows that some self-renewing cells remain in the culture after one day, but that they all are differentiated after two days<sup>(17)</sup>.

In the SCB model, considering that the self-renewing compartment  $S$  is characterized by an exponential dynamic, and that there are no more self-renewing cells if and only if  $S \leq 1$ , this provides an upper and a lower bound for  $\delta_{SC}$ :

$$\rho_S + \frac{1}{2} \ln(S_0) \leq \delta_{SC} \leq \rho_S + \ln(S_0). \quad (5)$$

For the sake of simplicity, we will set  $\delta_{SC} = \rho_S + 1/2 \ln(S_0)$  in order to verify the equality:  $S(48h) = 1$  in the following. Figures S2 and S3 show that varying  $\delta_{SC}$  between its two bounds does not refute our conclusions.

These considerations do not affect the S2B model, in which the switching of the culture medium only affects the proliferation rate of the  $S$  compartment.

In both estimation steps, the  $-\log$  likelihood was minimized using the Truncated Newton's algorithm<sup>(41,42)</sup> implemented in the python package for scientific computing `scipy`<sup>(43)</sup>. Convergence to the global minimum was assured by a random sampling of the initial guesses for parameter values (Figure S1).

## 2.4 Model Selection

In order to choose a proper error model, one needs to adopt a selection criterion, which allows to rank models and keep only the best ones, by balancing the quality of the fit of the models with their complexity.

We used a selection approach based on the corrected Akaike's Information Criterion ( $AICc$ ,<sup>(44)</sup>):

$$AICc = -2 \log(L) + \frac{2kn}{n - k - 1}. \quad (6)$$

where  $k$  is the number of parameters of the model and  $n$  is the sample size. The corrective term in  $AICc$  has been developed for linear models and small samples. However, since there is no selection criterion derived from  $AIC$  for non-linear models, the literature recommends using  $AICc$  when in doubt<sup>(44)</sup>.

From the  $AICc$  values of a set of models, we compute the corresponding Akaike's weights<sup>(44)</sup>:

$$w_i = \frac{\exp(-(AICc_i - \min(AICc))/2)}{\sum_{j=1}^R \exp(-(AICc_j - \min(AICc))/2)}, \quad (7)$$

where  $w_i$  is the Akaike's weight of the  $i$ -th model, and  $R$  is the number of competing models. The Akaike's weight of a given model in a given set of models can be seen as the probability that it is the best

one among the set<sup>(44)</sup>. In this setting, selecting the best models of a set of models means computing their Akaike's weights, sorting them, and keeping only the models whose weights add up to a significance probability (for example, 95%).

## 2.5 Identifiability Analysis

We assessed the identifiability of our model using the method based on the statistical notion of profile likelihood<sup>(22,45)</sup>.

For a model with  $k$  parameters, a parameter space  $\Theta = \{(\theta_i, i \in \{1, 2, \dots, k\}), \theta_i \in \mathbb{R}\}$ , and a likelihood  $L$ , the **profile likelihood**  $PL_{\theta_i}$  with respect to parameter  $\theta_i$  is defined as:

$$\forall x \in \mathbb{R} \quad PL_{\theta_i}(x) = \max_{\theta_{j \neq i}} (L(\theta_i = x, \theta_j)). \quad (8)$$

Namely, the profile likelihood with respect to a parameter at a certain value is the likelihood of the model, maximized with respect to all the other parameters. Computing the profile likelihood at a certain value  $x$  of a parameter  $\theta_i$  means to set  $\theta_i = x$  and to estimate the values of the other parameters  $\theta_j$  that minimize the error  $-2 \log(L)$  in this setting. Consequently,  $-2 \log(PL)$  is minimal at the optimal parameter values set, and increases in both directions. It is possible to define a **confidence interval**  $CI_{\theta_i}$  at a level of confidence  $\alpha \in ]0, 1[$  for a parameter  $\theta_i$ , derived from the evaluation of the profile likelihood<sup>(22)</sup>:

$$CI_{\theta_i}(\alpha) = \{x \in \mathbb{R} \mid -2 \log(PL_{\theta_i}(x)) + 2 \log(PL_{\theta_i}(\hat{x})) \leq \chi^2(\alpha, k)\}, \quad (9)$$

where  $\hat{x}$  is the optimal estimate of  $\theta_i$ ,  $k$  is the number of parameters being estimated and  $\chi^2(\alpha, k)$  is the  $\alpha$ -quantile of the  $\chi^2$  distribution with  $k$  degrees of freedom.

Namely, all the parameter sets that render a profile likelihood closer to its minimal value than a threshold  $\chi^2(\alpha, k)$  belong to the confidence interval.

A model is then **practically identifiable at the level of confidence  $\alpha$**  if and only if the confidence intervals at level  $\alpha$  of all of its parameters are bounded<sup>(22)</sup>. In this study, we used  $\alpha = 0.95$ .

The profile likelihood approach is a good way of addressing the identifiability of a model, because it allows to detect both structural and practical unidentifiabilities. This feature makes the approach more efficient in practice than most of the other methods in the field<sup>(21,23,27,46)</sup>.

## 3 Results & Discussion

### 3.1 Measurement error

The data that we used for the calibration of our models are displayed on figure 1C. For readability, it displays the total cell counts in log scale, and the differentiated cell counts as a fraction of the total count. This representation emphasises the fact that the measured cell population in LM1 decreases between 0h and 24h, in both conditions (control, and rapamycin-treated).

Every time-point displayed on figure 1C was obtained by a single measurement, which increases the measurement error compared to a replicated experiment. We conclude that the observed decrease in the total living cell number in the LM1 medium (in both conditions) is due to the experimental error that the protocol suffers rather than to a hypothetical biological feature of the cells under study.

### 3.2 Fitting the Model with no Treatment: Model Design and Validation

#### 3.2.1 Choosing a structural and an error model: selection approach

By combining the three error models presented in Table 1 with the three dynamic models presented in Figure 2, it is possible to define 9 different models of our system. In order to choose the best one at reproducing the *in vitro* dynamics of erythropoiesis, we computed the maximum-likelihood estimates of the parameters of these nine models, (which are displayed in Table S1).

For each of these nine models, we computed the likelihood-based selection criteria that are displayed on Table 2. The S2B and SCB dynamic models with a proportional error appear as the best ones and offer very similar fits. All other models are far worse (their Akaike's weights add up to around  $4 \times 10^{-4}$ ) but it remains impossible, based on this criterion, to decipher which of the two remaining models should be used to best describe the *in vitro* erythropoiesis.

However, the S2B model does not describe the results of the commitment experiment (Figure 1D). In this model indeed, self-renewing cells switch between different self-renewing rates upon medium switching. As a consequence, switching the cells back and forth between the two media should just switch their proliferation rate, without affecting their proliferation ability. So the cells would never lose their proliferation ability, as opposed to the result of the commitment experiment.

On the other hand, the SCB model predicts that upon switching to the differentiation medium, the cells from the S compartment start differentiating. Once they are all differentiated, cells from the C and B compartments can still proliferate, but this proliferation might be cancelled by a switch back to the LM1 medium. It is thus impossible to describe the process of commitment with the S2B model, while it is possible with the SCB model.

As a conclusion, the SCB model with a proportional error is the best-fitting model which also accounts for the results of the commitment experiment, making it our dynamic model of choice for the rest of this study.

Dynamic model	Error model	$-2 \log(L_1)$	$-2 \log(L_2)$	k	AIC	$AIC_c$	$\Delta AIC_c$	$w_{AIC_c}$
SB	constant	107	228	4	343	347	45	$8.9 \times 10^{-11}$
SB	proportional	106	199	4	313	317	15	$2.5 \times 10^{-4}$
SB	combined	106	199	6	317	328	26	$1.3 \times 10^{-6}$
S2B	constant	107	195	6	314	324	22	$7.6 \times 10^{-6}$
S2B	proportional	106	174	6	291	302	0	0.55
S2B	combined	106	174	8	295	319	18	$8.7 \times 10^{-5}$
SCB	constant	107	195	6	314	325	23	$6.7 \times 10^{-6}$
SCB	proportional	106	174	6	292	302	0.40	0.45
SCB	combined	106	174	8	296	320	18	$7.1 \times 10^{-5}$

Table 2: Selection criteria evaluated for the nine possible pairs of error model and dynamic model.  $L_1$  is the log-likelihood of the model for the LM1 data.  $L_2$  is the log-likelihood of the model for the DM17 data.  $k$  is the number of estimated parameters in each of the models, according to the procedure described in section 2.3. For each model, the sample size is  $n = 15$ .  $AIC = -2 \log(L_1) - 2 \log(L_2) + 2k$  is the Akaike's Information Criterion<sup>(44)</sup>.  $AIC_c$  is the corrected AIC (Equation (6)).  $\Delta AIC_c = AIC_c - \min(AIC_c)$  is the  $AIC_c$  difference.  $w_{AIC_c}$  is the Akaike's weight (Equation (7)).

### 3.2.2 Identifiability analysis

In order to use a model for predictive purposes, one needs to assess its identifiability. The profile likelihood curves of all estimated parameters are displayed on Figure 3, for the SCB model with proportional error. For  $\rho_S$  and  $b_1$ , which are estimated together, the identifiability threshold at confidence  $\alpha = 0.95$  is  $\chi^2(0.95, 2) = 5.99$ . For  $\rho_C$ ,  $\delta_{CB}$ ,  $\rho_B$  and  $b_2$ , which are also estimated together, the threshold is  $\chi^2(0.95, 4) = 9.49$ .

For every parameter of the model, the profile likelihood curve crosses the threshold on both sides of the optimum, which means that every parameter of the model is identifiable, at the level of confidence  $\alpha = 0.95$ . The confidence intervals of the parameters<sup>(22)</sup>, extracted from these profiles (Equation (9)) are displayed in Table 3.

For a given parameter, the size of the confidence interval depends on the number of parameters that are estimated together, the required level of confidence, and the likelihood function used for the computation. By definition (Equation (8)), the profile likelihood renders as large of a confidence interval as possible, because it increases as slowly as possible on each side of the optimal parameter value. This means that identifiability is harder to satisfy with the profile likelihood approach than with other definitions, for example based on a linearization of the likelihood surface at the optimal parameter set<sup>(22)</sup>.

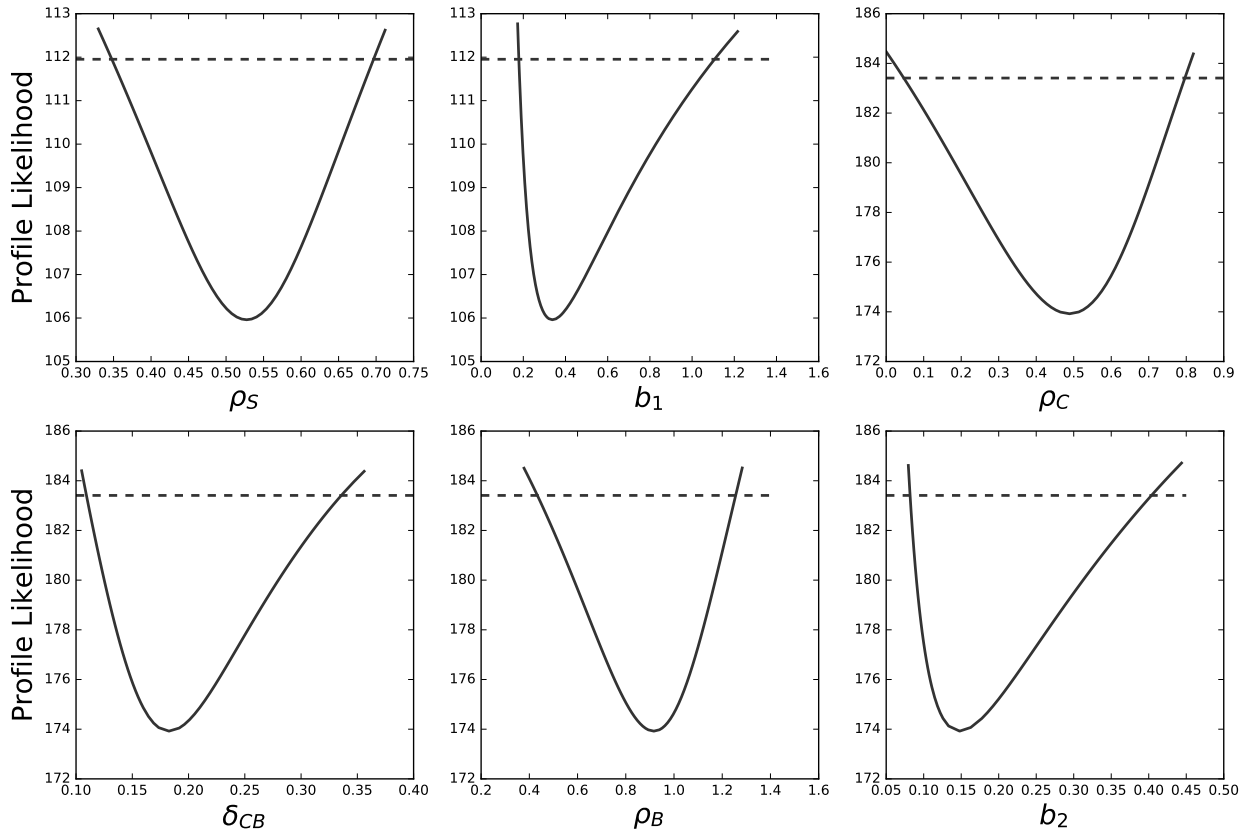


Figure 3: The SCB model with proportional error is fully identifiable. Solid curves are the profile likelihood curves of each estimated parameter of the model. Dashed lines give the identifiability threshold of each parameter at confidence level  $\alpha = 0.95$ .

As a consequence, the fact that the parameter confidence intervals presented in Table 3 may appear as quite large is not a sign that the parameters are poorly estimated. It is rather the evidence that they remain identifiable even with a very stringent definition of identifiability, and at a high level of confidence.

It is not possible to study the identifiability of  $\delta_{SC}$ , since it is not estimated from the data. However, the commitment experiment (figure 1D) give us access to a lower and an upper bounds for its value (Equation (5)). We determined the optimal likelihood of the model, and its optimal parameters in this range of value (figures S1 and S2), showing that the choice of  $\delta_{SC}$  does not influence the dynamics of our model.

### 3.3 Modelling differentiation in the control case

A simulation of the model with the identified values of its parameters is reproduced, with the corresponding experimental data, on Figure 4A. The overall quality of the fit is good, especially for the DM17 populations.

The precise values of each parameter of the model are reported in Table 3. The proliferation rate of the committed cells is slightly lower than the one of the self-renewing cells (the net doubling-time of the committed compartment is about 34h, whereas the doubling-time of the self-renewing compartment is around 31h). The differentiated cells proliferate with a higher rate (their doubling time is about 18h). Taken together, these doubling times explain the faster proliferation of cells in the DM17 medium than in the LM1, in agreement with previous data<sup>(35)</sup>. Finally, the self-renewing cell differentiation is very fast: the lowest possible value of  $\delta_{SC}$  gives them a half-life of 3h in DM17. This means that half of the S compartment would differentiate every 3h in the absence of proliferation. On the contrary, the differentiation of the committed cells is much slower (if they stopped proliferating, they would have a half-life of 90h).

Parameter	Lower bound	Optimal value	Upper bound
$\rho_S$	0.35	0.53	0.70
(doubling time)	24	31	48
$b_1$	0.18	0.34	1.1
$\delta_{SC}$	5.6	-	11
(half-life)	2	-	3
$\rho_C$	0.049	0.49	0.80
(doubling time)	21	31	340
$\delta_{CB}$	0.11	0.18	0.34
(half-life)	49	92	150
$\rho_B$	0.44	0.92	1.3
(doubling-time)	13	18	38
$b_2$	0.081	0.15	0.41

Table 3: Confidence Intervals of the parameters of the SCB model with proportional error. Highlighted in gray are the confidence interval boundaries at level  $\alpha = 0.95$ , extracted from figure 3, and the best-fit estimate of all the estimated parameters of the model (expressed in  $d^{-1}$ ). For  $\delta_{SC}$ , which is not estimated, no optimal value can be computed, but absolute bounds on its values can be computed with Equation (5). Parameters are grouped by their estimation step in our procedure:  $\rho_S$  and  $b_1$  are estimated together in the first step, then  $\delta_{SC}$  is set, and finally the four other parameters are estimated together. For the proliferation rates  $\rho_S$ ,  $\rho_C$  and  $\rho_B$ , we also give the corresponding doubling times of the populations in hours (*i.e.* how long would it take to double the population in the absence of differentiation?). For the differentiation rates  $\delta_{SC}$  and  $\delta_{CB}$ , we also give the half-life of the corresponding populations in hours (*i.e.* how long would it take to differentiate half the cells from the undifferentiated population, in the absence of proliferation?).

The timescales at which these processes occur are pictured on Figure 4B, which displays the number of cells in each state during a simulation of the model. As specified by the setting of the value of  $\delta_{SC}$ , the population of self-renewing cells quickly collapses, and the culture becomes a mixture of committed and differentiated cells. Both of these compartments then grow at their own rate.

At this stage, we have developed a very simple model of erythroid differentiation, that accounts well for the data used to calibrate it. Plus, it is fully identifiable (at confidence level 95%). We thus use it to study the effect of rapamycin, a drug known to affect the *in vitro* erythroid differentiation<sup>(36,38)</sup>.

### 3.4 Modelling differentiation under Rapamycin treatment

Rapamycin is known to increase the proportion of differentiated cells in cultures of chicken erythroid progenitors<sup>(36,38)</sup> (Figure 1C). Yet this effect might have several origins: a decreased mortality of the differentiated cells, or an increased differentiation rate for example. To decipher between these different possible effects of the rapamycin treatment, we estimated the values of the parameters of our model in the rapamycin treated case.

To avoid an overparameterization of the rapamycin effect, we considered that for each estimated parameter of the model, the value under rapamycin treatment could be either equal to the value in the untreated case, or equal to another value yet to be estimated. The first option would not introduce a new parameter in the model, but the latter would. Our model has seven parameters (5 dynamical parameters and 2 error parameters), of which 6 only are estimated (since  $\delta_{SC}$  is entirely determined by the value of  $\rho_S$ ). This means that we can define  $2^6 = 64$  models of rapamycin treatment, by keeping some of the parameters unchanged compared to the untreated case, and re-estimating the others with the data presented on Figure 1C.

We thus estimated the parameters of these 64 possible models of the treatment, and computed their likelihood-based selection criteria, the same way as we did for the dynamic model and the error model (see section 3.2). The Akaike's weights of the best three of these models are shown on Figure 5A. The best model of the treatment is responsible for 94 % of the weight of the 64 models, making it by far the best model for the rapamycin treatment. A simulation of this model is displayed on Figure 4, which indeed shows the quality of its fit to the data obtained under rapamycin treatment.

This model is obtained by varying all the parameter values except  $b_1$ , compared to the control case,

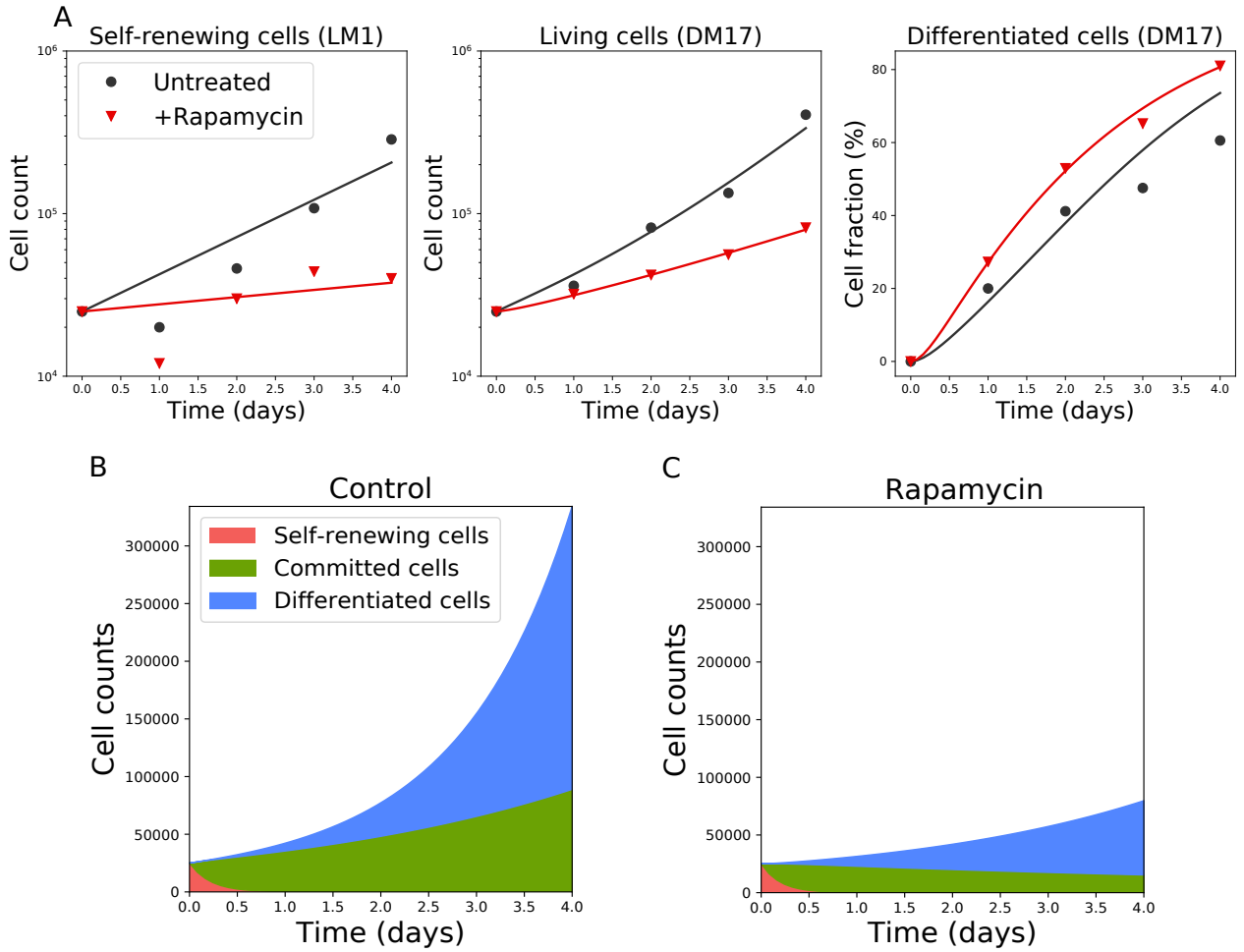


Figure 4: The model reproduces the cellular kinetics observed *in vitro*. A: Simulation of the SCB model with proportional error in the untreated (black) and rapamycin-treated cases (red). Solid lines represent a simulation of the SCB model with proportional error, with its best-fit parameters. Dots are the experimental data in the untreated condition. Triangles are the experimental data under rapamycin treatment. Displayed are the total number of living cells in LM1 and DM17 media (in log-scale), and the fraction of differentiated cells in DM17, although the fit was performed on the raw cell numbers. B-C: Numbers of cells in each compartment as a function of time in the untreated (B) and treated (C) cases.

as displayed on Figure 5B. Moreover, we computed confidence intervals for the parameters that vary under the treatment, showing that all these parameters are identifiable at  $\alpha = 0.95$  (Figure S4). The confidence intervals of  $\rho_S$ ,  $\delta_{CB}$ ,  $\rho_B$  and  $b_2$  show very little overlap with their confidence intervals in the control case, showing the strength of the treatment effects. The three proliferation rates  $\rho_S$ ,  $\rho_C$  and  $\rho_B$  are reduced under the treatment, while the differentiation rate  $\delta_{CB}$  is increased.

Finally, the effect of rapamycin on the distribution of cells between the different compartments is displayed on Figure 4C. Under rapamycin, the C compartment decays, when it proliferated in the control case. Moreover the B compartment has a longer doubling time under rapamycin treatment (48h instead of 18h in the untreated case). These two effects explain why the drug treatment reduces the overall amount of cells and increases the proportion of differentiated cells in the culture.

## 4 Discussion

We proposed a model for the *in vitro* erythroid differentiation, which comprises two components. First, the dynamic component is the set of ODE written in Equation (3), which describes the dynamics of three cell populations. Second, we added an error component which describes the distribution of the residuals

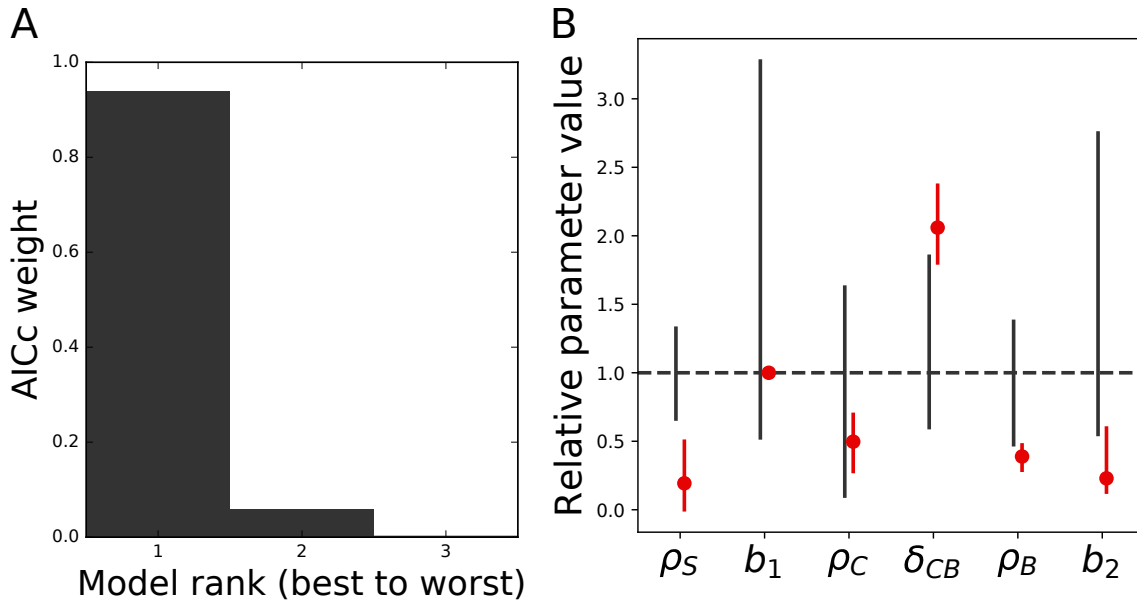


Figure 5: Modelling erythropoiesis under rapamycin treatment. A. Akaike's weights of the three best models of the rapamycin treatment. The 61 other models are not displayed for readability. B. Parameter values in the best model of rapamycin treatment. Red dots are the ratio of the parameter values under rapamycin treatment with their values in the untreated case. Black straight lines represent the confidence intervals of the values in the untreated case, computed from Figure 3. Red straight lines represent the confidence intervals at  $\alpha = 95\%$  of the values in the treated case, computed with the Profile Likelihood as well (Figure S4). The dashed line indicates the parameter values in the untreated case, by which all parameters are scaled for readability.

of the dynamic model,

The three populations of our dynamical model are related to three different stages of differentiation of the progenitors. The first one is in a self-renewal state S where differentiation has not started, and the third one has finished differentiating. The second population lies in the middle, in a state of commitment C where cells are not fully differentiated yet, but cannot go back to self-renewal.

Similar 3-states models have already been used to describe differentiation<sup>(19)</sup>. Their success probably stems from the fact that it would be difficult to describe differentiation as the transition between only 2 states, as we highlighted in the context of *in vitro* erythropoiesis with our SB model. Actually, differentiation from one cell type to another is a continuous process, so its best description would probably be a continuum of states, which would punctuate the transition between the two cell types<sup>(19,47)</sup>.

However, explicitly accounting for this continuum would require an infinity of intermediary states. For example, the levels of differentiation factors inside the cell could be used as a measure of its differentiation state<sup>(48,49)</sup>. Such kind of a model should be able to describe differentiation more faithfully than ours. Yet our model, though simplistic, reproduces our experimental data quite well, and is identifiable. Moreover, since it is fully linear and thus analytically integrable, its simulation and calibration are very quick.

Such simplicity and identifiability of our model would probably make it valuable to describe differentiation in other contexts.

Once the model was chosen, we verified the accuracy of its parameter estimates. We showed that among the seven parameters of our model, the six that are estimated by the maximum-likelihood approach are identifiable, and that the choice of the seventh one does not alter the behaviour of the others. Using the Profile Likelihood approach, we computed confidence intervals for our parameters. Even though their relatively large size might be interpreted as a lack of accuracy in the estimates of the parameters, it is not the case since the identifiability of a parameter is harder to satisfy by the Profile-Likelihood approach than using other methods. We thus showed that our model is fully identifiable, even using a very stringent criterion.

After demonstrating the validity of our model in the control case, we used it to study the effect of

rapamycin, a chemical drug which is known to impact the differentiation of erythroid progenitors<sup>(36,38)</sup>. We designed 64 different models of the rapamycin treatment, which differ by the combinations of parameters that are affected by the treatment. Evaluating the quality of their fit to the data allowed us to retain only the best model of rapamycin treatment. The parameter values in this model reveal that rapamycin increases the differentiation rate of the intermediary cell compartment, and reduces the net growth rates of the three other compartments. This means that rapamycin increases the differentiation of the cells in culture, and also affects the balance between their proliferation and mortality. The reduced net proliferation rates might be caused by a reduced proliferation, an increased mortality or any joint variation of the two processes equivalent to one of these effects (e.g. reduced mortality, and an even more reduced proliferation).

In the context of other perturbations of differentiation (for instance, treating cultures with a different drug than rapamycin), should the drug influence be less strong, we might need a more subtle means of parameter evaluation, such as the fused lasso penalized regression<sup>(50)</sup>.

At the moment, our approach suffers one major drawback that is the size of our dataset. Indeed, the precision of our prediction of cell numbers at one time-point relies on the precision of our measures of these numbers. And this measurement precision is directly related to the number of repetitions of the measurements.

Repeating the same experiment several times would thus increase measurement precision and average out measurement noise. This would allow a more precise estimation of the error model parameters, and in turn would increase the precision of the dynamic model. What we call *repeating the same experiment* here does not simply consist in counting cells from the same time point several times to average out sampling biases. It rather involves putting new cells in culture and following their populations over time, as two full replicates of the experiment.

In this setting, the measurement error would not just be limited to technical noise due to the sampling of cells from the culture for counting. It would rather be related to differences between the kinetic features of the cells in culture, *i.e.* to actual biological heterogeneity. This heterogeneity would be averaged by the estimation of one parameter set to fit all the data.

One way of accounting for this heterogeneity in a model, without averaging it out during parameter estimation, is through the use of a mixed effect model, that is a mathematical model (e.g. a set of deterministic ODE, like ours) whose parameters are modeled by distributions of random variables<sup>(40)</sup>. We are presently assessing the ability of such mixed effect models to characterize both the behaviour of the cells in culture on average, as well as their variability.

## 5 Acknowledgements

We thank La Ligue Nationale Contre le Cancer (Comité de la Loire) for funding.

The original design of the progenitor cell in Figure 1 was made available by Muharrem Fevzi Çelik, from the Noun Project.

We thank members of the SBDM and Dracula teams, as well as Dr. Boudaoud (ENS Lyon), Dr. Leclercq Samson (Laboratoire Jean Kuntzmann, Grenoble, France) and Dr. Raue (Merrimack Pharmaceuticals, Cambridge, Massachusetts) for enlightening discussions.

We also thank Pr. Saccomani (University of Padova, Italy) for providing the manuscript for reference<sup>(20)</sup>.

Finally, we want to thank the BioSyL Federation and the LabEx Ecofect (ANR-11-LABX-0048) of the University of Lyon for inspiring scientific events.

## 6 Supplementary Materials

The supplementary materials file shows the analytical solutions of our three dynamic models, the parameter values estimated for the three dynamic models (table S1) and the three error models (table S2), as well as the influence of our choice of  $\delta_{SC}$  on the likelihood of the model (figure S1) and on its parameter values (figure S2).

All the datasets and pieces of code analysed and generated during the current study are available in a public github repository, at [https://github.com/rduchesn/Dynamic\\_Model\\_Erythropoiesis](https://github.com/rduchesn/Dynamic_Model_Erythropoiesis).

## References

- [1] L. Sharney, L. R. Wasserman, L. Schwartz, and D. Tandler. Multiple pool analysis as applied to erythro-kinetics. *Annals of the New York Academy of Sciences*, 108:230–249, 1963.
- [2] G. C. Nooney. Iron kinetics and erythron development. *Biophysical Journal*, 5(6):755–765, 1965.
- [3] L. Pujo-Menjouet. Blood Cell Dynamics: Half of a Century of Modelling. *Mathematical Modelling of Natural Phenomena*, 11(1):92–115, 2016.
- [4] C. Foley and M. Mackey. Dynamic hematological disease: a review. *Journal of Mathematical Biology*, 58(1-2):285–322, 2009.
- [5] M. Loeffler, K. Pantel, H. Wulff, and H. E. Wichmann. A mathematical model of erythropoiesis in mice and rats. Part 1: Structure of the model. *Cell and Tissue Kinetics*, 22(1):13–30, 1989.
- [6] M. C. Mackey and P. Dörmer. Continuous maturation of proliferating erythroid precursors. *Cell and Tissue Kinetics*, 15(4):381–392, 1982.
- [7] F. Crauste, L. Pujo-Menjouet, S. Génieys, C. Molina, and O. Gandrillon. Adding self-renewal in committed erythroid progenitors improves the biological relevance of a mathematical model of erythropoiesis. *Journal of Theoretical Biology*, 250(2):322–338, 2008.
- [8] A. Krinner, I. Roeder, M. Loeffler, and M. Scholz. Merging concepts - coupling an agent-based model of hematopoietic stem cells with an ODE model of granulopoiesis. *BMC Systems Biology*, 7:117, 2013.
- [9] I. Roeder, L. Kamminga, K. Braesel, B. Dontje, G. Haan, and M. Loeffler. Competitive clonal hematopoiesis in mouse chimeras explained by a stochastic model of stem cell organization. *Blood*, 105(2):609–616, 2005.
- [10] D. Dingli and J. Pacheco. Modeling the architecture and dynamics of hematopoiesis. *Wiley Interdisciplinary Reviews. Systems Biology and Medicine*, 2(2):235–244, 2010.
- [11] M. Kimmel. Stochasticity and determinism in models of hematopoiesis. *Advances in Experimental Medicine and Biology*, 844:119–152, 2014.
- [12] S. Schirm, C. Engel, M. Loeffler, and M. Scholz. A Biomathematical Model of Human Erythropoiesis under Erythropoietin and Chemotherapy Administration. *PLOS ONE*, 8(6):e65630, 2013.
- [13] O. Angulo, O. Gandrillon, and F. Crauste. Investigating the role of the experimental protocol in phenylhydrazine-induced anemia on mice recovery. *Journal of Theoretical Biology*, 437:286–298, January 2018.
- [14] F. Crauste, I. Demin, O. Gandrillon, and V. Volpert. Mathematical study of feedback control roles and relevance in stress erythropoiesis. *Journal of Theoretical Biology*, 263(3):303–316, 2010.
- [15] S. Fischer, P. Kurbatova, N. Bessonov, O. Gandrillon, V. Volpert, and F. Crauste. Modeling erythroblastic islands: using a hybrid model to assess the function of central macrophage. *Journal of Theoretical Biology*, 298:92–106, 2012.
- [16] N. Eymard, N. Bessonov, O. Gandrillon, M. J. Koury, and V. Volpert. The role of spatial organization of cells in erythropoiesis. *J Math Biol*, 70(1-2):71–97, 2015.

- [17] A. Richard, L. Boullu, U. Herbach, A. Bonnafoux, V. Morin, E. Vallin, A. Guillemin, N. Papili Gao, R. Gunawan, J. Cosette, O. Arnaud, JJ. Kupiec, T. Espinasse, S. Gonin-Giraud, and O. Gandrillon. Single-Cell-Based Analysis Highlights a Surge in Cell-to-Cell Molecular Variability Preceding Irreversible Commitment in a Differentiation Process. *PLoS biology*, 14(12):e1002585, 2016.
- [18] S. Semrau, J. Goldmann, M. Soumillon, T. Mikkelsen, R. Jaenisch, and A. Oudenaarden. Dynamics of lineage commitment revealed by single-cell transcriptomics of differentiating embryonic stem cells. *Nature Communications*, 8(1):1096, 2017.
- [19] P. Stumpf, R. Smith, M. Lenz, A. Schuppert, FJ. Müller, A. Babbie, T. Chan, M. Stumpf, C. Please, S. Howison, F. Arai, and B. MacArthur. Stem Cell Differentiation as a Non-Markov Stochastic Process. *Cell Systems*, 5(3):268–282.e7, 2017.
- [20] C. Cobelli and M. P. Saccomani. Unappreciation of a priori identifiability in software packages causes ambiguities in numerical estimates. *American Journal of Physiology-Endocrinology and Metabolism*, 258(6):E1058–E1059, 1990.
- [21] A. Villaverde and A. Barreiro. Identifiability of Large Nonlinear Biochemical Networks. *MATCH Commun. Math. Comput. Chem.*, (76):259–296, 2016.
- [22] A. Raue, C. Kreutz, T. Maiwald, J. Bachmann, M. Schilling, U. Klingmüller, and J. Timmer. Structural and practical identifiability analysis of partially observed dynamical models by exploiting the profile likelihood. *Bioinformatics*, 25(15):1923–1929, 2009.
- [23] OT. Chis, J. Banga, and E. Balsa-Canto. Structural Identifiability of Systems Biology Models: A Critical Comparison of Methods. *PLOS ONE*, 6(11):e27755, 2011.
- [24] H. Pohjanpalo. System identifiability based on the power series expansion of the solution - ScienceDirect. *Mathematical Biosciences*, 41(1-2):21–33, 1978.
- [25] S. Vajda, K. R. Godfrey, and H. Rabitz. Similarity transformation approach to identifiability analysis of nonlinear compartmental models. *Mathematical Biosciences*, 93(2):217–248, 1989.
- [26] E. Walter and Y. Lecourtier. Global approaches to identifiability testing for linear and nonlinear state space models - ScienceDirect. *Mathematics and Computers in Simulation*, 24:472–482, 1982.
- [27] F. Fröhlich, F. Theis, and J. Hasenauer. Uncertainty Analysis for Non-identifiable Dynamical Systems: Profile Likelihoods, Bootstrapping and More. In P. Mendes, J. Dada, and K. Smallbone, editors, *CMSB*, pages 61–72, Cham, 2014. Springer International Publishing.
- [28] D. J. Venzon and S. H. Moolgavkar. A Method for Computing Profile-Likelihood-Based Confidence Intervals. *Journal of the Royal Statistical Society. Series C (Applied Statistics)*, 37(1):87–94, 1988.
- [29] Y. Bard. *Nonlinear parameter estimation*. Academic Press, San Diego, Calif., 1974.
- [30] B. Efron and R. Tibshirani. Bootstrap Methods for Standard Errors, Confidence Intervals, and Other Measures of Statistical Accuracy. *Statistical Science*, 1(1):54–75, 1986.
- [31] T. Luzyanina, S. Mrusek, J. Edwards, D. Roose, S. Ehl, and G. Bocharov. Computational analysis of CFSE proliferation assay. *Journal of Mathematical Biology*, 54(1):57–89, January 2007.
- [32] M. Transtrum, B. Machta, K. Brown, B. Daniels, C. Myers, and J. Sethna. Perspective: Sloppiness and emergent theories in physics, biology, and beyond. *The Journal of Chemical Physics*, 143(1):010901, 2015.
- [33] O. Karin, A. Swisa, B. Glaser, Y. Dor, and U. Alon. Dynamical compensation in physiological circuits. *Molecular Systems Biology*, 12(11):886, November 2016.

- [34] A. Villaverde and J. Banga. Dynamical compensation and structural identifiability of biological models: Analysis, implications, and reconciliation. *PLOS Computational Biology*, 13(11):e1005878, November 2017.
- [35] O. Gandrillon, U. Schmidt, H. Beug, and J. Samarut. TGF-beta cooperates with TGF-alpha to induce the self-renewal of normal erythrocytic progenitors: evidence for an autocrine mechanism. *The EMBO journal*, 18(10):2764–2781, 1999.
- [36] S. Dazy, F. Damiola, N. Parisey, H. Beug, and O. Gandrillon. The MEK-1/ERKs signalling pathway is differentially involved in the self-renewal of early and late avian erythroid progenitor cells. *Oncogene*, 22(58):9205–9216, 2003.
- [37] H. Dolznig, P. Bartunek, K. Nasmyth, E.W. Müllner, and H. Beug. Terminal differentiation of normal erythroid progenitors: shortening of g1 correlates with loss of d-cyclin/cdk4 expression and altered cell size control. *Cell Growth Differ.*, 6:1341–1352, 1995. p23.
- [38] S. Gonin-Giraud, C. Bresson-Mazet, and O. Gandrillon. Involvement of the TGF- $\beta$  and mTOR/p70s6kinase pathways in the transformation process induced by v-ErbA. *Leukemia Research*, 32(12):1878–1888, 2008.
- [39] A. Raue, M. Schilling, J. Bachmann, A. Matteson, M. Schelke, D. Kaschek, S. Hug, C. Kreutz, B. Harms, F. Theis, U. Klingmüller, and J. Timmer. Lessons learned from quantitative dynamical modeling in systems biology. *PloS One*, 8(9):e74335, 2013.
- [40] M. Lavielle and K. Bleakley. *Mixed Effects Models for the Population Approach: Models, Tasks, Methods and Tools*. Chapman & Hall/CRC Biostatistics Series. CRC Press/Taylor & Francis Group, Boca Raton, Florida, 2014.
- [41] J. Nocedal and S. Wright. *Numerical Optimization*. Springer series in operations research. Springer, New York, 2nd ed edition, 2006.
- [42] S. Nash. Newton-Type Minimization Via the Lanczos Method. *SIAM Journal on Numerical Analysis*, 21(4):770–788, 1984.
- [43] Jones E., Oliphant T., Peterson P., et al. SciPy: Open source scientific tools for Python, 2001–. [Online; accessed f].
- [44] K. Burnham and D. Anderson. *Model selection and multimodel inference: a practical information-theoretic approach*. Springer, New York, 2010.
- [45] S. A. Murphy and A. W. Van Der Vaart. On Profile Likelihood. *Journal of the American Statistical Association*, 95(450):449–465, 2000.
- [46] A. Raue, C. Kreutz, F. Theis, and J. Timmer. Joining forces of Bayesian and frequentist methodology: a study for inference in the presence of non-identifiability. *Phil. Trans. R. Soc. A*, 371(1984):20110544, 2013.
- [47] A. MacLean, T. Hong, and Q. Nie. Exploring intermediate cell states through the lens of single cells. *Current Opinion in Systems Biology*, 9:32–41, June 2018.
- [48] L. Barbarroux, P. Michel, M. Adimy, and F. Crauste. Multi-scale modeling of the CD8 immune response. In *ICNAAM 2015*, page 320002. AIP publishing, 2016.
- [49] A. Friedman, CY. Kao, and CW. Shih. Asymptotic phases in a cell differentiation model. *Journal of Differential Equations*, 247(3):736–769, 2009.
- [50] R. Tibshirani, M. Saunders, S. Rosset, J. Zhu, and K. Knight. Sparsity and smoothness via the fused lasso. *Journal of The Royal Statistical Society: Series B (Methodological)*, 67(1):91–108, 2005.

# Supplementary Material for

Calibration, Selection and Identifiability Analysis of a Mathematical Model of the *in vitro* Erythropoiesis  
in Normal and Perturbed Contexts

Ronan Duchesne<sup>1,2</sup>, Anissa Guillemain<sup>1</sup>, Fabien Crauste<sup>2,3</sup>, and Olivier Gandrillon<sup>1,2</sup>

<sup>1</sup>Laboratoire de Biologie et Modélisation de la Cellule, École Normale Supérieure de Lyon, 46 allée d'Italie, Lyon.

<sup>2</sup>Équipe Dracula, Inria, 56 Boulevard Niels Bohr, Villeurbanne

<sup>3</sup>Institut Mathématiques de Bordeaux, CNRS UMR5251, Université de Bordeaux, Talence, France

All the datasets and pieces of code analysed and generated during the current study are available in a public github repository, at [https://github.com/rduchesn/Dynamic\\_Model\\_Erythropoiesis](https://github.com/rduchesn/Dynamic_Model_Erythropoiesis).

## 1 Solutions of the dynamic models

Here, we give the solutions of the three dynamic models presented in systems (1) to (3) of the main text, which are represented graphically in figure 2. In all the following, we will note  $Y_0$  the initial condition at time  $t = 0$  for variable  $Y$ .

### 1.1 SB model

System (1) is written in matrix form as:

$$\begin{pmatrix} \frac{dS}{dt}(t) \\ \frac{dB}{dt}(t) \end{pmatrix} = \begin{pmatrix} \rho_S - \delta_{SB} & 0 \\ \delta_{SB} & \rho_B \end{pmatrix} \begin{pmatrix} S(t) \\ B(t) \end{pmatrix}.$$

We thus have immediate access to the eigenvalues of the system, and can solve it analytically. There are two possible cases, whether the two eigenvalues of the matrix are equal or not.

The dynamics of the self-renewing cells are described by the equation:

$$S(t) = S_0 e^{(\rho_S - \delta_{SB})t}.$$

Concerning the dynamics of the differentiated cells, we thus have :

$$\frac{dB}{dt}(t) - \rho_B B(t) = \delta_{SB} S_0 e^{(\rho_S - \delta_{SB})t}.$$

Then, there are two cases depending on the value of  $\rho_B$ :

1. If  $\rho_B \neq \rho_S - \delta_{SB}$ , then  $B$  writes as:

$$B(t) = b_1 e^{\rho_B t} + b_2 e^{(\rho_S - \delta_{SB})t},$$

with  $b_2 = \frac{\delta_{SB} S_0}{\rho_S - \delta_{SB} - \rho_B}$  and  $b_1 = B_0 - b_2$ .

2. If  $\rho_B = \rho_S - \delta_{SB}$ , then  $B$  writes as:

$$B(t) = (b_1 + b_2 t) e^{\rho_B t},$$

with  $b_2 = \delta_{SB} S_0$  and  $b_1 = B_0$ .

## 1.2 S2B model

System (2) is written in matrix form as:

$$\begin{pmatrix} \frac{dS_{LM1}}{dt}(t) \\ \frac{dS_{DM17}}{dt}(t) \\ \frac{dB}{dt}(t) \end{pmatrix} = \begin{pmatrix} \rho_{LM1} & 0 & 0 \\ 0 & \rho_{DM17} - \delta_{SB} & 0 \\ 0 & \delta_{SB} & \rho_B \end{pmatrix} \begin{pmatrix} S_{LM1}(t) \\ S_{DM17}(t) \\ B(t) \end{pmatrix}.$$

Again, the eigenvalues of the matrix of the system are its diagonal coefficients. The dynamics of the self-renewing cells still follow an exponential dynamic:

$$\begin{cases} S_{LM1}(t) = S_0 e^{\rho_{LM1}t}, \\ S_{DM17}(t) = S_0 e^{(\rho_{DM17} - \delta_{SB})t}, \end{cases}$$

and the differentiated cells follow the same dynamics as in the SB model (by replacing  $\rho_S$  by  $\rho_{DM17}$ ).

## 1.3 SCB model

System (3) is written in matrix form as:

$$\begin{pmatrix} \frac{dS}{dt}(t) \\ \frac{dC}{dt}(t) \\ \frac{dB}{dt}(t) \end{pmatrix} = \begin{pmatrix} \rho_S - \delta_{SC} & 0 & 0 \\ \delta_{SC} & \rho_C - \delta_{CB} & 0 \\ 0 & \delta_{CB} & \rho_B \end{pmatrix} \begin{pmatrix} S(t) \\ C(t) \\ B(t) \end{pmatrix}.$$

Again, the eigenvalues of the matrix of the system are its diagonal coefficients, and we can solve it analytically. There are several possible cases, depending on what eigenvalues are equal.

For the self-renewing cells, we have the same solution as in the two other models:

$$S(t) = S_0 e^{(\rho_S - \delta_{SC})t}.$$

Concerning the dynamics of the committed cells, we thus have :

$$\frac{dC}{dt}(t) - (\rho_C - \delta_{CB})C(t) = \delta_{SC} S_0 e^{(\rho_S - \delta_{SC})t}.$$

There are two cases depending on the respective values of  $\rho_C - \delta_{CB}$  and  $\rho_S - \delta_{SC}$ :

1. If  $\rho_C - \delta_{CB} \neq \rho_S - \delta_{SC}$ , then  $C$  writes as:

$$C(t) = c_1 e^{(\rho_C - \delta_{CB})t} + c_2 e^{(\rho_S - \delta_{SC})t},$$

with  $c_2 = \frac{\delta_{SC} S_0}{(\rho_S - \delta_{SC}) - (\rho_C - \delta_{CB})}$  and  $c_1 = C_0 - c_2$ .

2. If  $\rho_C - \delta_{CB} = \rho_S - \delta_{SC}$ , then  $C$  writes as:

$$C(t) = (c_1 + c_2 t) e^{(\rho_S - \delta_{SC})t},$$

with  $c_2 = \delta_{SC} S_0$  and  $c_1 = C_0$ .

Depending on the two previous cases, there are several possible solutions for the dynamics of differentiated cells:

1. If  $\rho_C - \delta_{CB} \neq \rho_S - \delta_{SC}$ , then:

$$\frac{dB}{dt}(t) - \rho_B B(t) = \delta_{CB} c_1 e^{(\rho_C - \delta_{CB})t} + \delta_{CB} c_2 e^{(\rho_S - \delta_{SC})t}.$$

Then, there are three possible sub-cases depending on the relative values of  $\rho_S - \delta_{SC}$ ,  $\rho_C - \delta_{CB}$  and  $\rho_B$ :

(a) If  $\rho_C - \delta_{CB} \neq \rho_S - \delta_{SC}$ ,  $\rho_S - \delta_{SC} \neq \rho_B$  and  $\rho_C - \delta_{CB} \neq \rho_B$ , then  $B$  writes as:

$$B(t) = b_1 e^{\rho_B t} + b_2 e^{(\rho_C - \delta_{CB})t} + b_3 e^{(\rho_S - \delta_{SC})t},$$

$$\text{with } b_2 = \frac{\delta_{CB} c_1}{\rho_C - \delta_{CB} - \rho_B}, b_3 = \frac{\delta_{CB} c_2}{\rho_S - \delta_{SC} - \rho_B} \text{ and } b_1 = B_0 - b_2 - b_3.$$

(b) If  $\rho_S - \delta_{SC} \neq \rho_C - \delta_{CB}$  and  $\rho_B = \rho_C - \delta_{CB}$ , then  $B$  writes as:

$$B(t) = (b_1 + b_2 t) e^{\rho_B t} + b_3 e^{(\rho_S - \delta_{SC})t},$$

$$\text{with } b_2 = \delta_{CB} c_1, b_3 = \frac{\delta_{CB} c_2}{\rho_S - \delta_{SC} - \rho_B} \text{ and } b_1 = B_0 - b_3.$$

(c) If  $\rho_S - \delta_{SC} \neq \rho_C - \delta_{CB}$  and  $\rho_B = \rho_S - \delta_{SC}$ , then  $B$  writes as:

$$B(t) = (b_1 + b_3 t) e^{(\rho_S - \delta_{SC})t} + b_2 e^{(\rho_C - \delta_{CB})t},$$

$$\text{with } b_2 = \frac{\delta_{CB} c_1}{\rho_C - \delta_{CB} - \rho_B}, b_3 = \delta_{CB} c_2 \text{ and } b_1 = B_0 - b_2.$$

2. If  $\rho_S - \delta_{SC} = \rho_C - \delta_{CB}$ , then:

$$\frac{dB}{dt}(t) - \rho_B B(t) = \delta_{CB} (c_1 + c_2 t) e^{(\rho_S - \delta_{SC})t}.$$

Then, there are two possible sub-cases depending on the relative values of  $\rho_S - \delta_{SC}$ ,  $\rho_C - \delta_{CB}$  and  $\rho_B$ :

(a) If  $\rho_S - \delta_{SC} = \rho_C - \delta_{CB}$  and  $\rho_B \neq \rho_S - \delta_{SC}$ , then  $B$  writes as:

$$B(t) = b_1 e^{\rho_B t} + (b_2 + b_3 t) e^{(\rho_S - \delta_{SC})t},$$

$$\text{with } b_3 = \frac{\delta_{CB} c_2}{\rho_S - \delta_{SC} - \rho_B}, b_2 = \frac{\delta_{CB} c_1 - b_3}{\rho_S - \delta_{SC} - \rho_B} \text{ and } b_1 = B_0 - b_2.$$

(b) If  $\rho_S - \delta_{SC} = \rho_C - \delta_{CB} = \rho_B$ , then  $B$  writes as:

$$B(t) = (b_1 + b_2 t + b_3 t^2) e^{\rho_B t},$$

$$\text{with } b_2 = \delta_{CB} c_1, b_3 = \frac{\delta_{CB} c_2}{2} \text{ and } b_1 = B_0$$

## 2 Convergence of the estimation

In both estimation steps, we minimized the -log likelihood with the Truncated Newton's algorithm implemented in scipy, with a maximum number of function evaluations of  $10^6$ . We used random sampling of the initial guesses for parameter values to assure convergence to the global optimum.

Figure S1 shows the distance to the minimal log-likelihood (sorted from highest to lowest) over large samples of initial guesses (200 initial guesses for the first step, 1000 initial guesses for the second one) for our SCB model with proportional error. It shows that with a relatively small sample, the estimated likelihood is already quite close to its minimal value and that increasing the sample size doesn't result in a better fit.

In order to balance the quality of the fit with the computational cost of the estimation, we used 100 different initial guesses for the first estimation step and 500 initial guesses for the second one for all of our models.

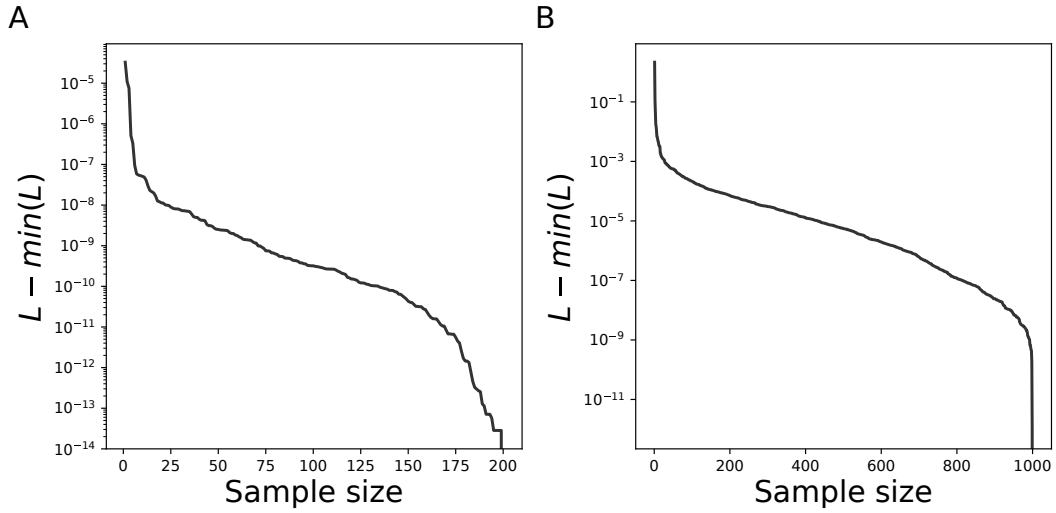


Figure S1: Influence of the initial guess sample size on the estimation. A: Sorted distance to the optimal likelihood over 200 runs of the estimation of  $\rho_S$  and  $b_1$  (SCB model with proportional error). B: Sorted distance to the optimal likelihood over 1000 runs of the estimation of  $\rho_C$ ,  $\delta_{CB}$ ,  $\rho_B$  and  $b_2$  (SCB model with proportional error).

### 3 Parameter values

The estimated parameter values for the 9 pairs of dynamic and error models are displayed in table S1

Dynamic	Error	$\rho_1$	$\delta_1$	$a_1$	$b_1$	$\rho_2$	$\delta_2$	$\rho_B$	$a_2$	$b_2$
SB	Constant	0.59	5.7	$2.8 \times 10^4$	-	-	-	0.62	$5.4 \times 10^4$	-
SB	Proportional	0.53	5.6	-	0.34	-	-	0.56	-	0.45
SB	Combined	0.53	5.6	0	0.34	-	-	0.56	0	0.45
S2B	Constant	0.59	5.7	$2.8 \times 10^4$	-	0.48	0.033	1.4	$1 \times 10^4$	-
S2B	Proportional	0.53	5.6	-	0.34	0.47	0.15	0.96	-	0.14
S2B	Combined	0.53	5.6	0	0.34	0.47	0.15	0.96	0x	0.14
SCB	Constant	0.59	5.7	$2.8 \times 10^4$	-	0.47	0.038	1.4	$1 \times 10^4$	-
SCB	Proportional	0.53	5.6	-	0.34	0.49	0.18	0.92	-	0.15
SCB	Combined	0.53	5.6	0	0.34	0.49	0.18	0.92	0	0.15

Table S1: Best-fit estimates of the parameters for the 9 pairs of error model and dynamic model.  $\rho_1$  is the net proliferation rate of the first compartment of the model (*i.e.*  $\rho_S$  for the SB and SCB models, and  $\rho_{LM1}$  for the S2B model).  $\delta_1$  is the differentiation rate of this compartment (*i.e.*  $\delta_{SB}$  for the SB model,  $\delta_{SC}$  for the SCB model, and it is not defined for the S2B model).  $\rho_2$  is the net proliferation rate of the second compartment, when it is different from the B compartment (*i.e.*  $\rho_{DM17}$  for the S2B model,  $\rho_C$  for the SCB model, and it is not defined for the SB model).  $\delta_2$  is its differentiation rate (*i.e.*  $\delta_{SB}$  for the S2B model,  $\delta_{CB}$  for the SCB model, and it is not defined for the SB model).  $\rho_B$  is defined in every model as in the SCB model.

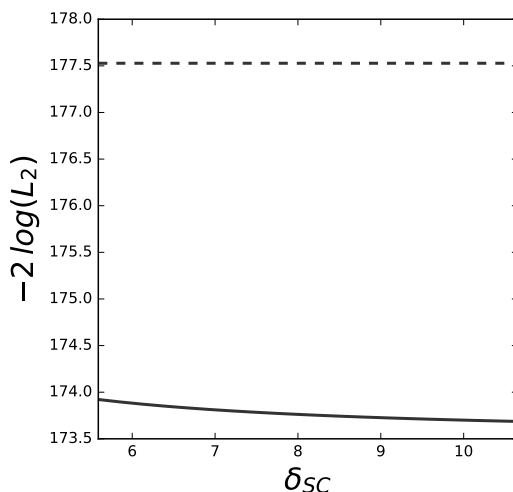


Figure S2: The choice of  $\delta_{SC}$  does not impact the quality of the fit of the model. The straight line represents the minimum  $-\log$  likelihood optimized in the last step of our estimation procedure as a function of the chosen value for  $\delta_{SC}$ . The dashed line gives the  $\chi^2$  significance threshold of a likelihood-ratio test.

#### 4 Importance of $\delta_{SC}$

In the estimation procedure described in the Methods section, every parameter of the dynamic model is estimated according to the experimental data, except  $\delta_{SC}$ , which is set to an arbitrary value between its two bounds (determined from the commitment experiment pictured on figure 1C). Though these bounds give precise limits to the values that  $\delta_{SC}$  can take, setting it to different values might result in different optimal parameter values for the second estimation step of the procedure.

Figure S2 displays the likelihood of the second estimation step for the range of values that  $\delta_{SC}$  can take. It does not vary significantly in this range, which means that the quality of the fit of the model is not influenced by the choice of the value of  $\delta_{SC}$ . This leaves two possible scenarios: either the value of  $\delta_{SC}$  has no influence on the estimated parameter values in the second estimation step, or it is possible to keep the likelihood high while changing the value of  $\delta_{SC}$  by adjusting the value of the other parameters (which would be a case of non-identifiability if the value of  $\delta_{SC}$  was optimized to fit the data).

Figure S3 displays the values of the parameters estimated in the step 3 of the procedure, for the range of values that  $\delta_{SC}$  can take. Since these value do not vary much, it seems reasonable to say that the choice of the value of  $\delta_{SC}$  does not impact the last estimation step of the procedure.

#### 5 Identifiability of the treatment parameters

Figure S4 displays the profile likelihood curves for the parameters that are affected by the rapamycin treatment. In the model of rapamycin treatment that we selected,  $b_1$  does not vary, so its value is not estimated from the data. It is also the case for  $\delta_{SC}$ , as in the control situation. It is thus impossible to define a profile likelihood for these two parameters. Thus,  $\rho_S$  is now the only parameter that is estimated with the LM1 data, so its identifiability threshold is  $\chi^2(0.95, 1) = 3.84$ . The other parameters ( $\rho_C$ ,  $\delta_{CB}$ ,  $\rho_B$  and  $b_2$ ) are all estimated together, so their identifiability threshold is  $\chi^2(0.95, 4) = 9.49$ , as in the control case.

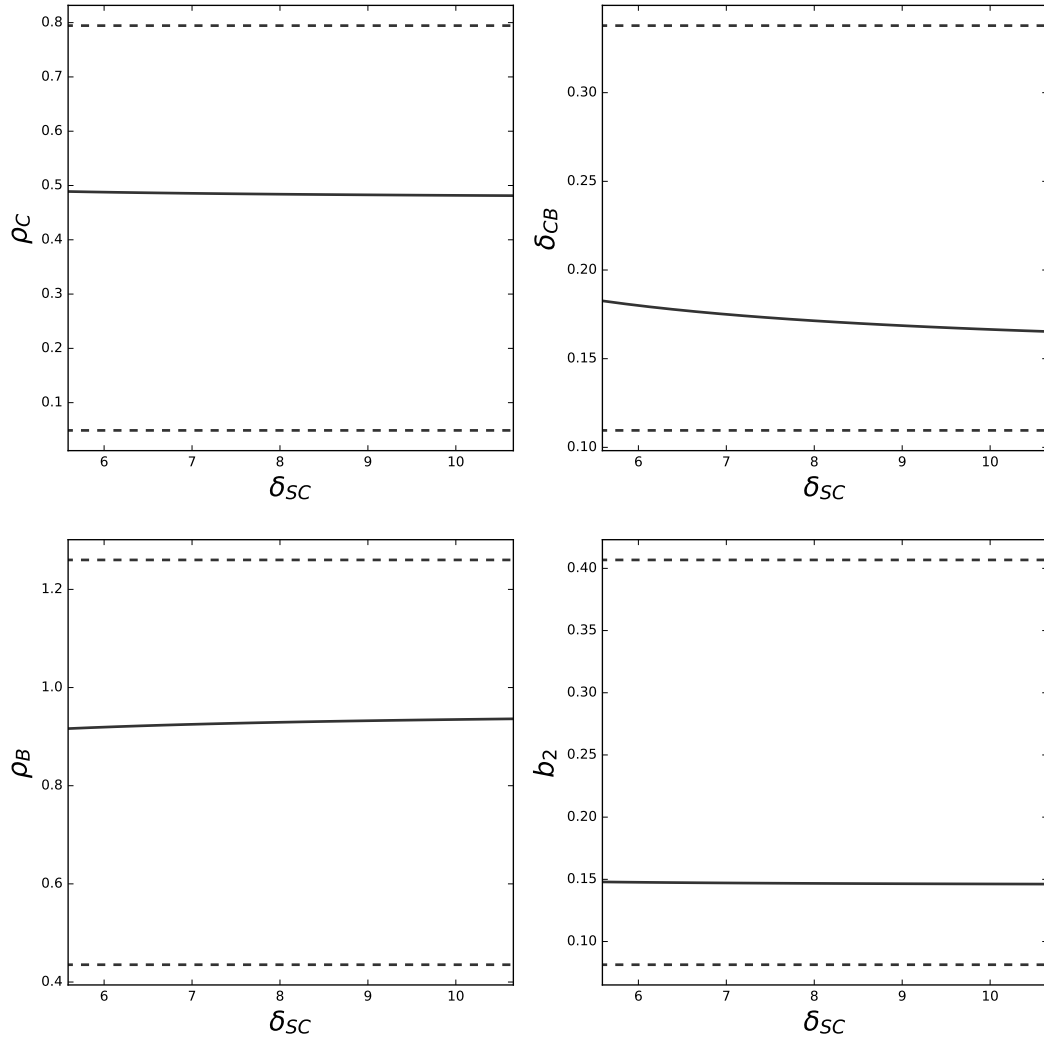


Figure S3: The choice of  $\delta_{SC}$  does not impact the value of the other parameters of the model. Solid lines represent the values of the parameters estimated in the last step of our procedure. Dashed lines represent the confidence interval of each parameter computed from figure 3.

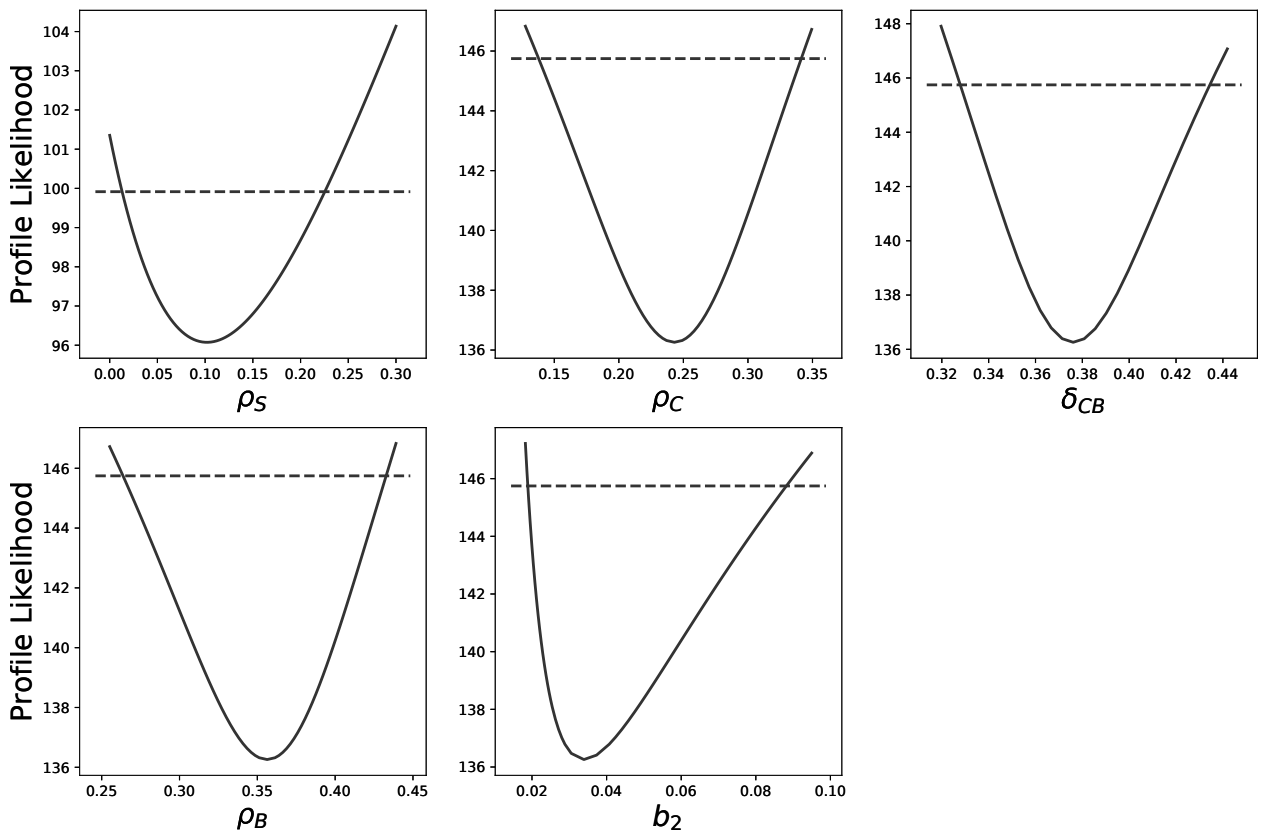


Figure S4: The values of the parameters under rapamycin treatment are identifiable. For each of the parameters which varied under the treatment, the solid line represents the profile likelihood with respect to that parameter, and the dashed line gives the  $\chi^2$  identifiability threshold (at  $\alpha = 0.95$ ).

### 2.3 Conclusion

We designed the first model of *in vitro* erythropoiesis. It is a linear ODE model describing the dynamics of three compartments which represent three different stages of differentiation (Section 2.2.1 in the paper). The S compartment comprises self-renewing cells which have not started differentiating. The B compartment comprises cells that are fully differentiated. Finally, the C compartment is an intermediary one, in which cells have started differentiating, and yet cannot come back to self-renewal. The matrix of this linear system is lower-triangular, which makes its simulation very quick and efficient. From this system of 3 linear ODE, we define a statistical likelihood by modeling the distribution of the model residuals, which combines an error model for the variance of the residuals to the dynamic model (Section 2.2.2 in the paper).

The parameters of this model are the three net self-renewal rates of the compartments ( $\rho_S$ ,  $\rho_C$  and  $\rho_B$ , which can be positive or negative), the two differentiation rates from one compartment to the next one ( $\delta_{SC}$  and  $\delta_{CB}$ , which are positive), and the two error parameters which quantify the standard deviation of the model residuals ( $b_1$  and  $b_2$ , which are positive). We present our estimation procedure in Section 2.3 of the paper. Basically we start by estimating  $\rho_S$  (and the corresponding error parameter  $b_1$ ) from the LM1 data. Then we choose the value of  $\delta_{SC}$  according to the results of the commitment experiment (which we explained in Section 1.1). Finally, we estimate  $\rho_C$ ,  $\delta_{CB}$ ,  $\rho_B$ , and the corresponding error parameter  $b_2$ , from the DM17 data. There are thus two error parameters, each describing the variance of the model residuals in each of the estimation steps.

We computed confidence intervals for these parameters in Section 3.2 of the paper, using the profile likelihood approach (which we presented in Section 1.3, Raue et al., 2009). This proved that our model is fully identifiable. We also tested its ability to account for the effects of rapamycin, a chemical drug which affects all stages of the erythroid differentiation, in Section 3.4 of the paper. We considered that under rapamycin treatment, each parameter could either be equal to its value in the control case, or to another value (estimated

## Chapter 2: A deterministic model of *in vitro* erythropoiesis

from the data). Since the model has 6 parameters that are estimated from the data, as  $\delta_{SC}$  is not estimated (see Section 2.3 of the paper), this defines  $2^6 = 64$  potential models of the rapamycin treatment. We estimated their parameter values, and selected the best ones using Akaike's weights (Burnham and Anderson, 2010). In the case of rapamycin, only one model was selected. We found that the estimated parameter values are consistent with previous experimental data, both in the control and in the rapamycin-treated conditions.

Now that we have designed our dynamic model of erythropoiesis, and tested some features of interest, we could use it to compute the effect of artemisinin, rapamycin and MB3 on the differentiation ability of the T2EC.

## Chapter 3

# Drugs that modulate SGE and differentiation

### 3.1 Introduction

In order to test our working hypothesis that there is a positive correlation between SGE and differentiation, Anissa Guillemin, who was at the time an experimentalist in the group, has searched for chemical drugs which affect both the level of SGE and the number of differentiated cells in a T2EC culture. She based her work upon a previous screen for drugs that would affect SGE in a different cellular system (Dar et al., 2014).

She quantified the effect of the drugs on the level of SGE by computing Shannon's entropy. Basically, this metric is minimal when the distribution of gene expression across cells is far from random (Shannon, 1948). She identified three drugs of interest in the T2EC cells: artemisinin and indomethacin both reduced the extent of SGE, while MB3 increased it.

Then, she tested the effect of the drugs on differentiation by performing the same *in vitro* differentiation experiment as in Chapter 2. She found that artemisinin and indomethacin both reduced the number of differentiated cells in the culture, whereas MB3 increased it (Guillemin et al., 2018).

However, this effect of the drugs might have several origins. The varia-

tion in the population of differentiated cells under treatment might be caused by a variation in the differentiation rate of the progenitors, as well as by another feature (e.g. mortality, or proliferation, of the differentiated cells). Since it is impossible to decipher between these different effects experimentally, we decided to quantify them using the dynamic model that we presented in Chapter 2 (Duchesne et al., 2018).

The challenge here was to calibrate the model for these cell culture experiments in the treated and untreated cases, and to conclude regarding the effect of the drugs on cellular kinetics. For each drug, the control was a culture in which DMSO was added at the same time as the drug (48h before inducing differentiation for artemisinin and indomethacin, and the same time as the induction for MB3). There are thus two different control conditions, depending on what treatment is being considered.

### **3.2 Paper**

# Drugs modulating stochastic gene expression affect the erythroid differentiation process

Anissa Guillemin<sup>1</sup>, Ronan Duchesne<sup>1,2</sup>, Fabien Crauste<sup>2</sup>, Sandrine Gonin-Giraud<sup>1</sup>,  
and Olivier Gandrillon<sup>1,2</sup>

<sup>1</sup>*Laboratoire de biologie et modélisation de la cellule. LBMC - Ecole Normale Supérieure - Lyon, Université Claude Bernard Lyon 1, Centre National de la Recherche Scientifique : UMR5239, Institut National de la Santé et de la Recherche Médicale : U1210 - Ecole Normale Supérieure de Lyon 46 allée d'Italie 69007 Lyon, France*

<sup>2</sup>*Institut Mathématiques de Bordeaux, CNRS UMR5251, Université de Bordeaux, Talence, France*

## Abstract

**Background:** To understand how a metazoan cell makes the decision to differentiate, we assessed the role of stochastic gene expression (SGE) during the erythroid differentiation process. Our hypothesis is that stochastic gene expression has a role in single-cell decision-making. In agreement with this hypothesis, we and others recently showed that SGE significantly increased during differentiation. However, evidence for the causative role of SGE is still lacking. Such demonstration would require being able to experimentally manipulate SGE levels and analyze the resulting impact of these variations on cell differentiation.

**Result:** We identified three drugs that modulate SGE in primary erythroid progenitor cells. Artemisinin and Indomethacin simultaneously decreased SGE and reduced the amount of differentiated cells. Inversely,  $\alpha$ -methylene- $\gamma$ -butyrolactone-3 (MB-3) simultaneously increased the level of SGE and the amount of differentiated cells. We then used a dynamical modelling approach which confirmed that differentiation rates were indeed affected by the drug treatment.

**Conclusion:** Using single-cell analysis and modeling tools, we provide experimental evidence that in a physiologically relevant cellular system, control of SGE can directly modify differentiation, supporting a causal link between the two.

## 1 Introduction

Cell-to-cell variability is intrinsic to all living forms, from prokaryotes [3, 1] to eukaryotes [30]. Such a variability originates from many sources, but arguably stochastic gene expression (SGE) is an important driving force in the generation of cell-to-cell variability among genetically identical cells [9], although additional regulation layers do exist [19]. Classically, SGE is separated into intrinsic and extrinsic sources [13, 26, 2, 25, 33] even if in many cases distinguishing between the two is difficult.

The very existence of SGE led to the concept of a probabilistic mapping between inputs (environment) and outputs (cell decisions) [34]. It is therefore clear that SGE has to be precisely tuned so as to tailor the biological process in which it is involved [11].

Numerous arguments suggest that SGE plays an important role in a wide range of biological processes ranging from bet hedging [36] to the fractional killing of cancer cells [4]. SGE is also involved in decision-making in viruses [39, 38, 40] and in prokaryotes [21, 8], but its role in the differentiation ability of metazoan cells remains an open question. We aim at assessing whether SGE is involved in differentiation or not [20, 18].

If one sees differentiation from the point of view of dynamical systems theory [5], undifferentiated cells are in an equilibrium state at first (self-renewal state). Once differentiation is activated, cells could increase their SGE, exploring a broader region of the state space. Such an exploratory behaviour would increase the probability for cells to attain the space region where they stabilize their gene expression pattern by reaching a new equilibrium state (differentiation state) [18].

We recently described a surge in cell-to-cell variability that accompanies the differentiation of normal primary chicken erythroid progenitors called T2EC [14], that is fully compatible with such a view [28]. Interestingly, these results have been confirmed in various settings, ranging from the differentiation of murine lymphohematopoietic progenitors [23] to the differentiation of murine embryonic stem cells [29, 32].

Nevertheless, a definitive demonstration of a causative role of SGE in differentiation is only starting to appear in the literature [24]. One way of demonstrating this link is the use of drugs that would on one hand modulate SGE and on the other modulate the differentiation process. It has recently been described that such drugs, identified using a large screening approach, were able to modulate the noise affecting the HIV Tat promoter [10]. Recently, drugs that directly inhibit promoter nucleosome remodelling were also shown to provide fine-tuning of SGE [22].

We therefore decided to explore how some of those drugs (Artemisinin and Indomethacin), together with a more general chromatin modifier (MB-3, [26]) could alter differentiation.

Here we show that the three selected drugs significantly modify levels of SGE simultaneously with the level of cell differentiation. We therefore provide the first evidence that in a physiologically relevant cellular system, the modulation of SGE results in a modification of differentiation.

## 2 Results

### 2.1 Drugs affect noise in transcriptomic level

In order to demonstrate a direct link between SGE and differentiation, we modified experimentally SGE in T2EC using three drug treatments: Artemisinin, Indomethacin and MB-3.

Artemisinin and Indomethacin are known to modify SGE of the HIV LTR promoter in human T-lymphocytes [10]. MB-3, a chromatin modifier, is known to modify stochastic gene expression in yeast [26] and in murine ES cells [24]. We first wanted to confirm that these drugs do indeed modify SGE in our cellular system and what are the mechanisms associated with this effect.

We treated T2EC with or without drugs and induced their erythroid differentiation. We then performed single-cell high-throughput RTqPCR on these cells at different time points after differentiation. We assessed a 92 gene panel, relevant for erythroid differentiation study, identical to those previously measured in untreated cells [28]. Single cell transcriptomics data were then analyzed using Shannon entropy as a measure of the heterogeneity among the cells for their gene expression profile [28, 32].

Entropy was affected by all treatments. Under Indomethacin or Artemisinin treatment, entropy significantly decreased after 2 days of erythroid differentiation. This effect was more pronounced with Indomethacin. The opposite effect is observed with MB-3 treatment where entropy was significantly increased after 12h of differentiation for T2EC treated with MB-3 (Figure 1A).

We then assessed whether the same genes vary their entropy under the different drug treatments. For this we computed a correlation value between the variations in entropy for each pair of drugs. If the same genes are affected by two drugs, then one would expect their entropy variations to be correlated. We observed a significant correlation only for the genes affected by Indomethacin and Artemisinin treatment. MB-3 treatment seemed to be affecting the variability of a different set of genes (Figure 1B).

The entropy variation could be achieved by modulating the global mean gene expression or the gene expression variance. Thus we finally wanted to test if our drug treatments affected entropy

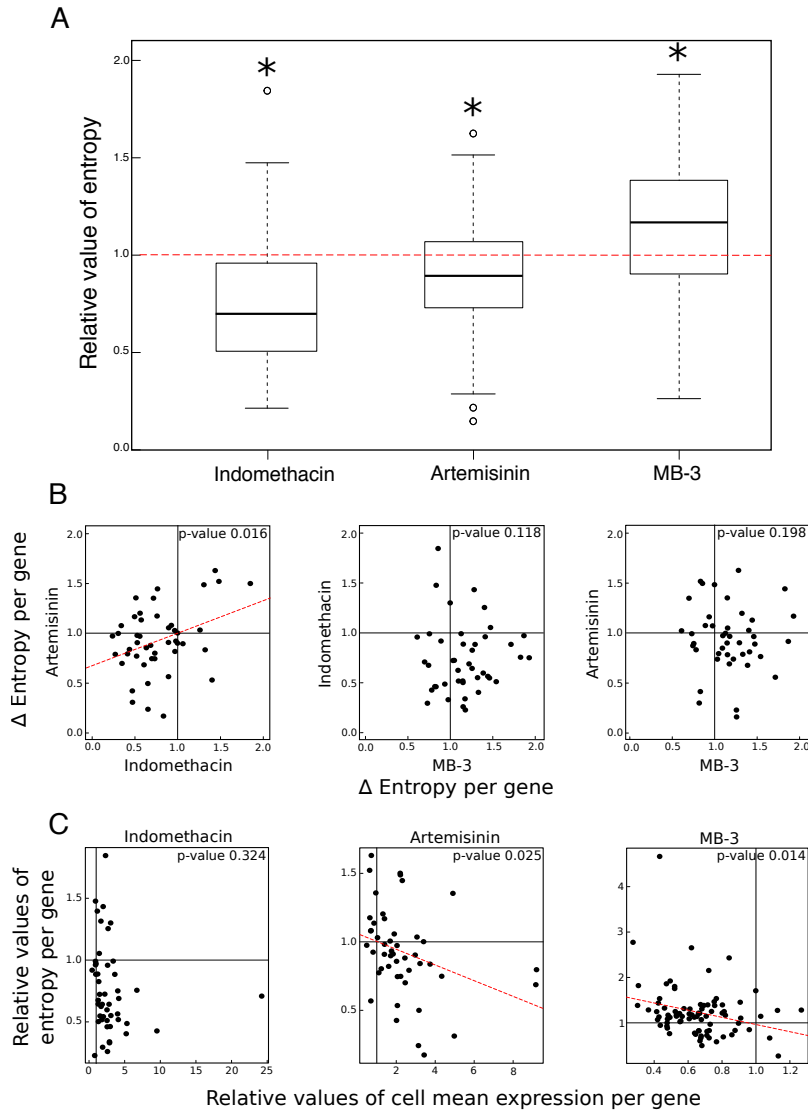


Figure 1: Relative effect of entropy and gene expression average under drug treatment during differentiation. (A) Boxplots representing values of entropy per gene for each treatment relative to control values (red dotted line). Some outliers are not displayed for readability. We assessed the significance of the differences between untreated and treated condition through a Wilcoxon test (tests with a  $p$ -value  $< 0.05$  are represented by a star above each boxplot). (B) Correlation plots representing relative values of entropy per gene for each pair of drugs. We assessed the significance of the differences between values for each drug through a Pearson test ( $p$ -value  $< 0.05$ ). When correlation is significant, we displayed the linear regression line for all points (red dotted lines). (C) Correlation plots representing relative values of entropy as a function of relative values of cell mean expression per gene. We assessed the significance of the differences between values for each drug through a Pearson test ( $p$ -value  $< 0.05$ ). When correlation is significant, we displayed the linear regression line for all points (red dotted lines).

through the modulation of the mean gene expression value. If so, one might expect to see a correlation between the variation of entropy and the mean expression level under drug treatment.

Indeed for two drugs out of three, Artemisinin and MB-3, one observed a significant inverse correlation between mean and entropy (Figure 1C). Nevertheless the effect of Indomethacin on entropy was not related to an effect on mean gene expression.

Here we have found three drugs that modulate SGE in T2EC cells. Indomethacin and Artemisinin decreased it whereas MB-3 increased it. All drugs involve a different set of genes and the effect of drugs was not strongly related to an effect on mean gene expression value. Entropy modulation is therefore the only common characteristic of our three drugs.

We next used these drugs to test their effect on the erythroid differentiation process.

## 2.2 Drugs affect differentiation process

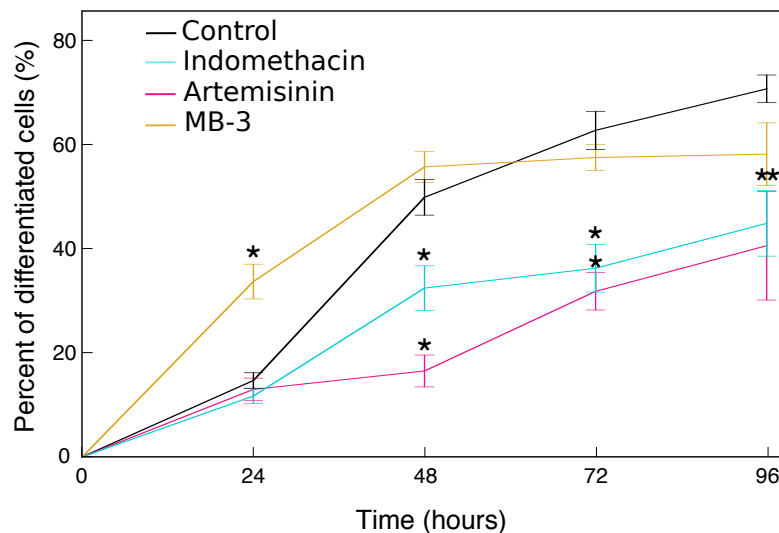


Figure 2: Drugs affected erythroid differentiation. Control conditions were averaged (black line) for readability. Shown is the percentage of differentiated cells for all conditions. Error bars represent the variation between experiments ( $n=3$ ). We assessed the significance of the differences between each treated condition with their own control condition through a student test ( $p$ -value  $< 0.05$ ).

In order to know if drugs modulating SGE also affect the differentiation process, we measured the percentage of differentiated cells in treated and untreated conditions during 96h of erythroid maturation.

A significant modulation in the percentage of differentiated cells was observed for all three drugs (Figure 2).

Indomethacin and Artemisinin decreased the percentage of mature cells from 48h of differentiation onward. MB-3 acted earlier: it significantly increased the percentage of differentiated cells by 24h before returning to somewhat below the control level.

Indomethacin and Artemisinin, two drugs that decreased SGE, reduced the percentage of differentiated cells. Inversely, MB-3 that increased SGE, enhanced the percentage of differentiated cells.

However, at this stage, we cannot conclude that drugs modifying SGE led to a change of the differentiation process itself. Indeed, these effects might have several origins including modification in growth or death rates of our cells. To decipher between these effects, we decided to use a mathematical model describing the dynamics of the *in vitro* erythroid differentiation [12].

## 2.3 Cellular basis of drug effect

Our model describes the dynamics of three cell populations related to three different stages of differentiation. The first one is the self renewing state (S) where differentiation has not started; the

third one is the differentiated state (B) where cells have finished differentiating. The second one is the committed state (C), comprising intermediary cells that are committed to differentiation but not yet fully differentiated (Figure 3).

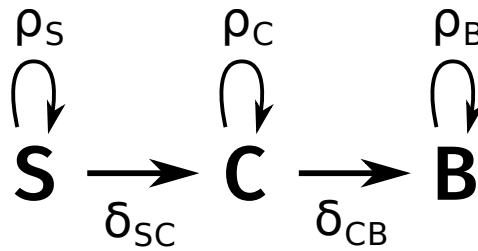


Figure 3: Schematic diagram of the model.

The dynamical model is characterized by a set of five parameters  $\theta = (\rho_S, \delta_{SC}, \rho_C, \delta_{CB}, \rho_B)$ :

- $\rho_i$  is the proliferation rate of compartment  $i$ , involving the balance between cell proliferation and cell death. This value can be either positive (more proliferation than death) or negative (more death than proliferation).
- $\delta_{ij}$  is the differentiation rate of cell type  $i$  into cell type  $j$ , which is positive.

Considering that there are no more self-renewing cells after 2 days of T2EC differentiation (Figure S1, [28]),  $\delta_{SC}$  is a fixed parameter fully determined by  $\rho_S$  [12].

In order to get the best description of the drugs effects with the fewest parameters, we used the same approach as described in [12] and section 4.3.

Using experimental data represented in Figure 2 and following this approach, numerous models are possible for each treatment. Among those, best models are selected by a criterion: Akaike's weights (Figure S2 & 4.3.3) and reproduced well the cellular kinetics during differentiation observed *in vitro* (Figure S3).

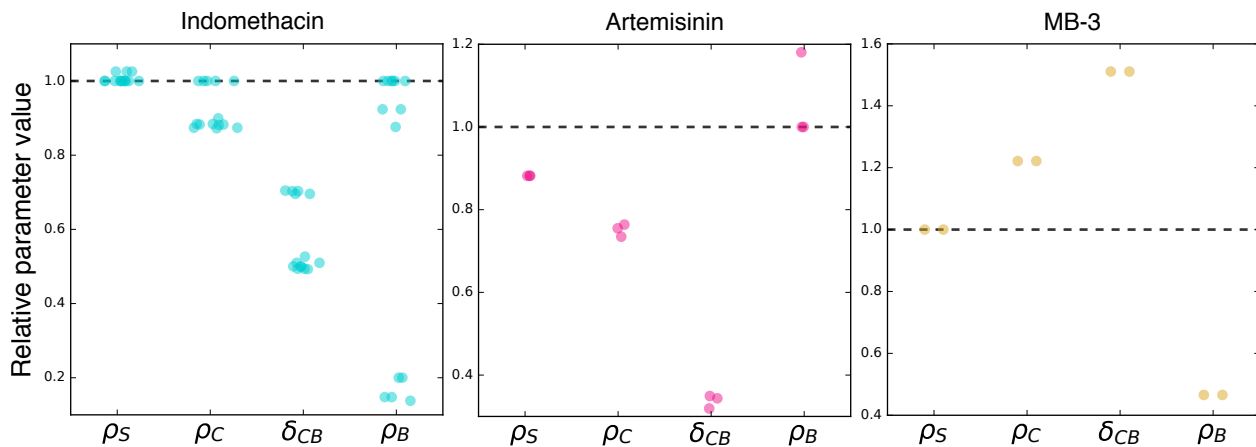


Figure 4: Relative parameter values. For each of the models selected by Akaike's weights (Figure S2), all the relative parameter values are represented by a dot for a treatment compared to the untreated condition (black dotted line). 14 models were selected for the Indomethacin treatment, 3 for the Artemisinin treatment and 2 for MB-3. The horizontal spacing between the values of each parameter was chosen randomly for readability.

For all of those best models, their parameter values for each treatment are displayed in Figure 4. Under Indomethacin or MB-3 treatment,  $\rho_S$  (net growth rate of the immature cells) was not affected in all models and slightly decreased under Artemisinin treatment. Therefore,  $\delta_{SC}$  was not affected by the treatments either (data not shown), since its value is entirely determined by the value of  $\rho_S$ .

Concerning  $\rho_C$ , the net growth rate of the committed compartment, its values were reduced compared to the untreated condition for the majority of models under Indomethacin or Artemisinin treatment, whereas for MB-3 its value increased in both models.

A more variable change between drug effect was observed with parameter  $\rho_B$ , which describes the net growth rate of differentiated cells. Under Indomethacin treatment, some of the best models did not show a different value when compared to untreated condition whereas some models displayed a reduced parameter value. Under Artemisinin treatment this value was unchanged for two models among three and increased for the other one. With MB-3 treatment,  $\rho_B$  decreased in both models.

Finally, we found that the  $\delta_{CB}$  parameter, representing the differentiation rate between committed compartment and mature cell compartment was affected by all three drugs: both Indomethacin and Artemisinin reduced this differentiation rate whereas MB-3 increased it in all best models.

These results demonstrate that all three drugs alter the differentiation process by modifying all dynamical parameters including the differentiation rate between committed and mature cells: it is clear that drugs that reduce SGE decrease differentiation rate and inversely that the drugs increasing SGE accelerate cell differentiation, in line with our initial hypothesis.

### 3 Conclusions & discussion

In this study, we assessed the existence of a direct link between the modulation of stochastic gene expression and a differentiation process. We tested drugs known to modulate SGE in different cellular systems [10, 26]. We showed that these drugs modify the level of SGE in our cells. We therefore tested their effect on the differentiation ability of avian erythropoietic progenitors. We identified which differentiation parameter were affected by drugs using a dynamical model of the *in vitro* erythroid differentiation [12]. We demonstrated that drugs modulating SGE level affected the differentiation process by impacting the differentiation rate between the two last compartments. We therefore demonstrated a direct link between SGE and a differentiation process supporting our starting hypothesis that stochastic gene expression participate positively in cell decision-making to differentiate.

Indomethacin, Artemisinin and MB-3 have clearly different functions. Artemisinin is an anti-malarial drug used against a parasitic infection [15]. Indomethacin is an anti-inflammatory drug that affects the prostaglandin pathway [17]. MB-3 is an inhibitor of GCN5, a histone acetyl transferase (HAT) that activates global gene expression [41]. Even in such a seemingly well-defined case, it should nevertheless be remembered that a very complex relationship may lie between the biochemical action of a drug (HAT inhibition) and its biological effect on SGE [40].

Considering these different functions, it is hard to imagine that all these drugs have in common anything else than their ability to modulate SGE in our cells.

The question then arises of the mechanisms through which these different drugs modulate SGE. We first assessed if these drugs affected the entropy of the same genes. For Indomethacin and Artemisinin, we showed that indeed the entropy of some of the same genes were affected but with a weak correlation. In contrast, MB-3 increased SGE through a different set of genes. This tends to indicate that cell-to-cell variability *per se*, relatively independently of the gene function involved, is participating to the differentiation process (see below).

We then investigated a potential role for variation in the mean gene expression that could explain the SGE level variation.

Modifying SGE level is accompanied by a variation in the mean gene expression level for two drugs out of three. The decrease of mean gene expression under MB-3 treatment has been shown in a different system not to be significant [24]. Also, it has not been reported that Artemisinin affect mean gene expression in any other cellular system. However, the fact that Indomethacin treatment decreased gene-wise entropy clearly without affecting the mean gene-wise expression level reinforces

the fact that the modification on the differentiation process is not due to a modification in mean gene expression but only to a non-specific modulation of SGE.

Collectively, these results suggest that neither common genes nor common mechanisms could explain the observed effect of the three drugs simultaneously. This reinforces the fact that modulation of cell-to-cell variability has a strong role in differentiation, independently of gene function or the specific mechanism involved.

This could be explained by adopting a dynamical systems view on the differentiation process, in the wake of Waddington's proposal [37]. In such a view, we could consider that in the highly dimensional gene expression space, an equilibrium cell state could be compared to a valley in an epigenetic landscape [18]. When we reduce SGE using Indomethacin or Artemisinin, we dig the valley, limiting the ability of cells to escape from a self-renewal equilibrium. Their probability to attain the new equilibrium state is reduced. Inversely, when we increase SGE using MB-3, we flatten the valley and improve the ability of cells to explore a larger dynamical landscape, and increase their probability to attain the new differentiated equilibrium state more quickly. Once cells achieved their journey, they stabilize their new gene expression pattern (the differentiated genetic profile) and return to a basal level of SGE [20, 18, 5]. In such a view, stochastic gene expression favours cells making the decision to differentiate, modifying the structure of the valley in which cells are moving. In a recent perspective, this same process of actively shaping the Waddington Landscape has been described in terms of a Plinko board, whose nail configuration, composition, and patterning can be modified towards forward stochastic design [11]. Similarly to our initial description [28], the variation of cell-to-cell gene expression in other differentiation systems has been recently described [31, 23, 29, 32, 24]. Furthermore, a functional link between transcriptional heterogeneity and cell fate transitions was demonstrated recently through manipulation of the histone acetylation landscape of mouse embryonic stem cells [24]. This is fully backed up by our own data that also demonstrate that the reverse (inhibiting differentiation by reducing SGE) can also be demonstrated.

In recent studies, it has been shown that active modulation of SGE is responsible for a modification of decision-making in viruses [10]. In primary erythroid progenitor cells, we show here that experimentally modifying SGE affects the differentiation process. It could therefore be important to study the potential use of SGE-modifying drugs in differentiation-related diseases such as tumoral cell progression [35], as exemplified by the chronic myeloid leukemia [16, 6, 11], paving the way to a "treatment by noise" of at least some cancer-related diseases.

## 4 Methods

### 4.1 Cell culture and treatment

T2EC were extracted from bone marrow of 19 days-old SPAFAS white leghorn chickens embryos (INRA, Tours, France). These cells were maintained in a medium called LM1. It is composed of  $\alpha$ -MEM medium supplemented with 10 % Foetal bovine serum (FBS), 1 mM HEPES, 100 nM  $\beta$ -mercaptoethanol, 100 U/mL penicillin and streptomycin, 5 ng/mL TGF- $\alpha$ , 1 ng/mL TGF- $\beta$  and 1 mM dexamethasone as previously described [14]. T2EC were induced to differentiate by removing the LM1 medium and placing cells into the DM17 medium ( $\alpha$ -MEM, 10% foetal bovine serum (FBS), 1 mM Hepes, 100 nM  $\beta$ -mercaptoethanol, 100 U/mL penicillin and streptomycin, 10 ng/mL insulin and 5% anemic chicken serum (ACS)). Differentiation kinetics were obtained by collecting cells at different times after the induction in differentiation. For Indomethacin and Artemisinin, cells in self-renewing medium are treated at respectively 25  $\mu$ M and 1  $\mu$ M 48h before switching into a differentiated medium in order to optimize their effects. For MB-3, cells are treated at 10  $\mu$ M just after inducing the differentiation. For each drug, a control treatment (0.1% DMSO) was added following the same conditions.

## 4.2 Counting of cell viability and cell differentiation

Cell population growth was evaluated by counting living cells using a Malassez cell and Trypan blue staining (SIGMA). Cell population differentiation was evaluated by counting differentiated cells using a counting cell and Benzidin (SIGMA) staining which stains haemoglobin in blue.

## 4.3 Dynamical model for erythroid differentiation

### 4.3.1 Calibration, selection and identifiability

This model has been selected among others and has been shown to be a relevant model for the *in vitro* erythroid differentiation process. Moreover, this model is fully identifiable meaning that there is only one parameter set  $\theta$  that corresponds to a dataset [27, 12]. This makes the reasoning on how drugs modify parameter values fully relevant. Details concerning the calibration, the selection and the identifiability analysis of the model are available in [12].

### 4.3.2 Estimating the parameters under drug treatments

For each parameter of the model, we considered two different cases: one in which the parameter value was unchanged compared to the untreated case (which would not change the number of parameters of the model), and one in which the treatment changed the value (which would introduce a new parameter in the model). Our model has 7 parameters: 5 dynamical parameters presented in 2.3 and 2 error parameters,  $b_1$  and  $b_2$ , which quantify the quality of the fit, and the amount of measurement error. These parameters do not influence the dynamics of the model. Only 6 out of these 7 parameters are estimated ( $\delta_{SC}$  is set by the value of  $\rho_S$ ), which defines  $2^6 = 64$  models for each drug treatment. We estimated the parameters of these 64 possible models and computed a selection criterion.

### 4.3.3 Model selection criterion

Estimating the parameters of all possible models under drug treatment needs to be accompanied by the computation of a selection criterion: the model weights based on their corrected Akaike's Information Criterion  $w_{AIC_c}$  [7]. The Akaike weight of a given model in a given set of models is a measure of the probability that the model is the best one in the set. Thus, selecting the best models of a set of models requires to sort them by their Akaike's weights. The best models in the set are those whose weights add up to a significance probability (95% in this study) [12].

## 4.4 Single cell high-throughput RTqPCR

Every experiment related to high-throughput microfluidic-based RT-qPCR was performed according to Fluidigm's protocol (PN 68000088 K1, p.157-172) and recommendations. All the following steps from single-cell isolation to high throughput RTqPCR of each cells are described in [28].

## 4.5 Entropy

We estimated the Shannon entropy of each gene  $j$  at each timepoint  $t$  as follows: we computed basic histograms of the genes with  $N = N_c / 2$  bins, where  $N_c$  is fixed for all tests, which provided the probabilities  $p_{j,k}^t$  of each class  $k$ . Finally, the entropies were defined by

$$E_j^t = - \sum_{k=1}^N p_{j,k}^t \log_2(p_{j,k}^t).$$

When all cells express the same amount of a given gene, this gene's entropy will be null. On the contrary, the maximum value of entropy will result from the most variable cell-to-cell gene expression level.

## 5 Acknowledgements

We thank R.D.Dar for his discussions, helpful advices and collaboration. This work was supported by funding from the French agency ANR (SinCity; ANR-17-CE12-0031) and La Ligue Contre le Cancer (Comite de Haute Savoie). We also thank the BioSyL Federation and the LabEx Ecofect (ANR-11-LABX-0048) of the University of Lyon for inspiring scientific events. We thank all members of the SBDM team for fruitful discussions.

## References

- [1] N. Q. Balaban. Persistence: mechanisms for triggering and enhancing phenotypic variability. *Curr Opin Genet Dev*, 21(6):768–75, 2011.
- [2] A. Becskei, B. B. Kaufmann, and A. van Oudenaarden. Contributions of low molecule number and chromosomal positioning to stochastic gene expression. *Nat Genet*, 37(9):937–44, 2005. p39.
- [3] S. Benzer. Induced synthesis of enzymes in bacteria analyzed at the cellular level. *Biochim Biophys Acta*, 11(3):383–95, 1953. 0006-3002 (Print) Journal Article.
- [4] F. Bertaux, S. Stoma, D. Drasdo, and G. Batt. Modeling dynamics of cell-to-cell variability in trail-induced apoptosis explains fractional killing and predicts reversible resistance. *PLoS Comput Biol*, 10(10):e1003893, 2014.
- [5] E. Braun. The unforeseen challenge: from genotype-to-phenotype in cell populations. *Rep Prog Phys*, 78(3):036602, 2015.
- [6] A. Brock, S. Krause, and D. E. Ingber. Control of cancer formation by intrinsic genetic noise and microenvironmental cues. *Nat Rev Cancer*, 15(8):499–509, 2015.
- [7] K. Burnham and D. Anderson. *Model selection and multimodel inference: a practical information-theoretic approach*. Springer, New York, 2010.
- [8] T. Cagatay, M. Turcotte, M. B. Elowitz, J. Garcia-Ojalvo, and G. M. Suel. Architecture-dependent noise discriminates functionally analogous differentiation circuits. *Cell*, 139(3):512–22, 2009.
- [9] J. R. Chubb. Symmetry breaking in development and stochastic gene expression. *Wiley Interdiscip Rev Dev Biol*, 2017.
- [10] R. D. Dar, N. N. Hosmane, M. R. Arkin, R. F. Siliciano, and L. S. Weinberger. Screening for noise in gene expression identifies drug synergies. *Science*, 344(6190):1392–6, 2014. p39.
- [11] R. D. Dar and R. Weiss. Perspective: Engineering noise in biological systems towards predictive stochastic design. *APL Bioengineering*, 2(2):020901, 2018.
- [12] R. Duchesne, A. Guillemin, O. Gandrillon, and F. Crauste. Calibration, selection and identifiability analysis of a mathematical model of the in vitro erythropoiesis in normal and perturbed contexts. *bioRxiv*, 2018.

- [13] M. B. Elowitz, A. J. Levine, E. D. Siggia, and P. S. Swain. Stochastic gene expression in a single cell. *Science*, 297(5584):1183–1186, 2002. p39.
- [14] O. Gandrillon, U. Schmidt, H. Beug, and J. Samarut. Tgf-beta cooperates with tgf-alpha to induce the self-renewal of normal erythrocytic progenitors: evidence for an autocrine mechanism. *Embo J*, 18(10):2764–2781, 1999. 0261-4189.
- [15] A. Ganguli, D. Choudhury, S. Datta, S. Bhattacharya, and G. Chakrabarti. Inhibition of autophagy by chloroquine potentiates synergistically anti-cancer property of artemisinin by promoting ros dependent apoptosis. *Biochimie*, 107 Pt B:338–49, 2014.
- [16] P. B. Gupta, C. M. Fillmore, G. Jiang, S. D. Shapira, K. Tao, C. Kuperwasser, and E. S. Lander. Stochastic state transitions give rise to phenotypic equilibrium in populations of cancer cells. *Cell*, 146(4):633–44, 2011. p39.
- [17] F. D. Hart and P. L. Boardman. Indomethacin: A new non-steroid anti-inflammatory agent. *Br Med J*, 2(5363):965–70, 1963.
- [18] S. Huang. Non-genetic heterogeneity of cells in development: more than just noise. *Development*, 136(23):3853–62, 2009. p39.
- [19] J. M. Keegstra, K. Kamino, F. Anquez, M. D. Lazova, T. Emonet, and T. S. Shimizu. Phenotypic diversity and temporal variability in a bacterial signaling network revealed by single-cell fret. *Elife*, 6, 2017.
- [20] J. J. Kupiec. A darwinian theory for the origin of cellular differentiation. *Mol Gen Genet*, 255(2):201–8, 1997. 97379979 0026-8925 Journal Article.
- [21] H. Maamar, A. Raj, and D. Dubnau. Noise in gene expression determines cell fate in bacillus subtilis. *Science*, 317(5837):526–9, 2007.
- [22] M. R. Megaridis, Y. Lu, E. N. Tevonian, K. M. Junger, J. M. Moy, K. Bohn-Wippert, and R. D. Dar. Fine-tuning of noise in gene expression with nucleosome remodeling. *APL Bioengineering*, 2(2):026106, 2018.
- [23] M. Mojtahedi, A. Skupin, J. Zhou, I. Castaño, R. Leong-Quong, H. Chang, A. Giuliani, and S. Huang. Cell fate-decision as high-dimensional critical state transition. *BioRxiv*, 2016.
- [24] N. Moris, S. Edri, D. Seyres, R. Kulkarni, A. F. Domingues, T. Balayo, M. Frontini, and C. Pina. Histone acetyltransferase kat2a stabilises pluripotency with control of transcriptional heterogeneity. *bioRxiv*, 2018.
- [25] A. Raj, C. S. Peskin, D. Tranchina, D. Y. Vargas, and S. Tyagi. Stochastic mrna synthesis in mammalian cells. *PLoS Biol*, 4(10):e309, 2006. p39.
- [26] J. M. Raser and E. K. O’Shea. Control of stochasticity in eukaryotic gene expression. *Science*, 304(5678):1811–4, 2004. p39.
- [27] A. Raue, C. Kreutz, T. Maiwald, J. Bachmann, M. Schilling, U. Klingmüller, and J. Timmer. Structural and practical identifiability analysis of partially observed dynamical models by exploiting the profile likelihood. *Bioinformatics*, 25(15):1923–1929, 2009.
- [28] A. Richard, L. Boullu, U. Herbach, A. Bonnafox, V. Morin, E. Vallin, A. Guillemin, N. Papi Gao, R. Gunawan, J. Cosette, O. Arnaud, J. J. Kupiec, T. Espinasse, S. Gonin-Giraud, and O. Gandrillon. Single-cell-based analysis highlights a surge in cell-to-cell molecular variability

- preceding irreversible commitment in a differentiation process. *PLoS Biol*, 14(12):e1002585, 2016.
- [29] S. Semrau, J. E. Goldmann, M. Soumillon, T. S. Mikkelsen, R. Jaenisch, and A. van Oudenaarden. Dynamics of lineage commitment revealed by single-cell transcriptomics of differentiating embryonic stem cells. *Nat Commun*, 8(1):1096, 2017.
- [30] A. Sigal, R. Milo, A. Cohen, N. Geva-Zatorsky, Y. Klein, Y. Liron, N. Rosenfeld, T. Danon, N. Perzov, and U. Alon. Variability and memory of protein levels in human cells. *Nature*, 444(7119):643–6, 2006.
- [31] Z. S. Singer, J. Yong, J. Tischler, J. A. Hackett, A. Altinok, M. A. Surani, L. Cai, and M. B. Elowitz. Dynamic heterogeneity and dna methylation in embryonic stem cells. *Mol Cell*, 55(2):319–31, 2014. p39.
- [32] P. Stumpf, R. Smith, M. Lenz, A. Schuppert, F.-J. Müller, A. Babbie, T. Chan, M. Stumpf, C. Please, S. Howison, F. Arai, and B. MacArthur. Stem cell differentiation as a non-markov stochastic process. *Cell Systems*, 5:268–282, 2017.
- [33] P. S. Swain, M. B. Elowitz, and E. D. Siggia. Intrinsic and extrinsic contributions to stochasticity in gene expression. *Proc Natl Acad Sci U S A*, 99(20):12795–800, 2002. p39.
- [34] O. Symmons and A. Raj. What’s luck got to do with it: Single cells, multiple fates, and biological nondeterminism. *Mol Cell*, 62(5):788–802, 2016.
- [35] K. Tzelepis, H. Koike-Yusa, E. De Braekeleer, Y. Li, E. Metzakopian, O. M. Dovey, A. Mupo, V. Grinkevich, M. Li, M. Mazan, M. Gozdecka, S. Ohnishi, J. Cooper, M. Patel, T. McKerrell, B. Chen, A. F. Domingues, P. Gallipoli, S. Teichmann, H. Ponstingl, U. McDermott, J. Saez-Rodriguez, B. J. P. Huntly, F. Iorio, C. Pina, G. S. Vassiliou, and K. Yusa. A crispr dropout screen identifies genetic vulnerabilities and therapeutic targets in acute myeloid leukemia. *Cell Rep*, 17(4):1193–1205, 2016.
- [36] M. Viney and S. E. Reece. Adaptive noise. *Proc Biol Sci*, 280(1767):20131104, 2013.
- [37] C. H. Waddington. The strategy of the genes. *London, UK: Allen and Unwin*, 1957.
- [38] L. Weinberger, R. Dar, and M. Simpson. Transient-mediated fate determination in a transcriptional circuit of hiv. *Nature Genetics*, 40(4):466–470, 4 2008.
- [39] L. S. Weinberger, J. C. Burnett, J. E. Toettcher, A. P. Arkin, and D. V. Schaffer. Stochastic gene expression in a lentiviral positive-feedback loop: Hiv-1 tat fluctuations drive phenotypic diversity. *Cell*, 122(2):169–82, 2005.
- [40] V. C. Wong, V. L. Bass, M. E. Bullock, A. K. Chavali, R. E. C. Lee, W. Mothes, S. Gaudet, and K. Miller-Jensen. Nf-kappab-chromatin interactions drive diverse phenotypes by modulating transcriptional noise. *Cell Rep*, 22(3):585–599, 2018.
- [41] Y. Wu, S. Ma, Y. Xia, Y. Lu, S. Xiao, Y. Cao, S. Zhuang, X. Tan, Q. Fu, L. Xie, Z. Li, and Z. Yuan. Loss of gcn5 leads to increased neuronal apoptosis by upregulating e2f1- and egr-1-dependent bh3-only protein bim. *Cell Death Dis*, 8(1):e2570, 2017.

# Drugs modulating stochastic gene expression affect the erythroid differentiation process

Anissa Guillemin<sup>1</sup>, Ronan Duchesne<sup>1,2</sup>, Fabien Crauste<sup>3</sup>, Sandrine Gonin-Giraud<sup>1</sup>,  
and Olivier Gandrillon<sup>1,2</sup>

<sup>1</sup>*Laboratoire de biologie et modélisation de la cellule. LBMC - Ecole Normale Supérieure - Lyon, Université Claude Bernard Lyon 1, Centre National de la Recherche Scientifique : UMR5239, Institut National de la Santé et de la Recherche Médicale : U1210 - Ecole Normale Supérieure de Lyon 46 allée d'Italie 69007 Lyon, France*

<sup>2</sup>*Inria Dracula, Villeurbanne, France*

<sup>3</sup>*Institut Mathématiques de Bordeaux, CNRS UMR5251, Université de Bordeaux, Talence, France*

## Supplementary data

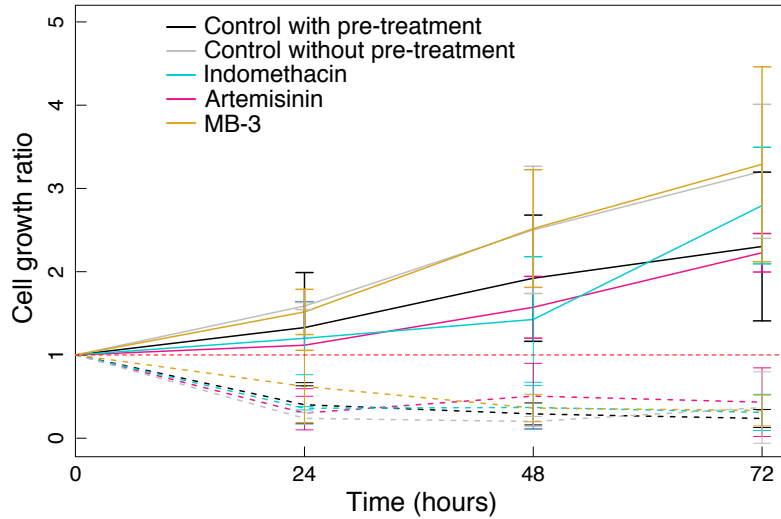


Figure S1: Drugs do not change the erythroid commitment. T2EC were induced to differentiate for 24 (solid lines) and 48 (dashed lines) hours and subsequently seeded back in self-renewal conditions. Cells were then counted every day for 3 days. The data shown are the mean  $\pm$  standard deviation calculated on the basis of three independent experiments. The growth ratio was computed as the cell number divided by the total cells at day 0.

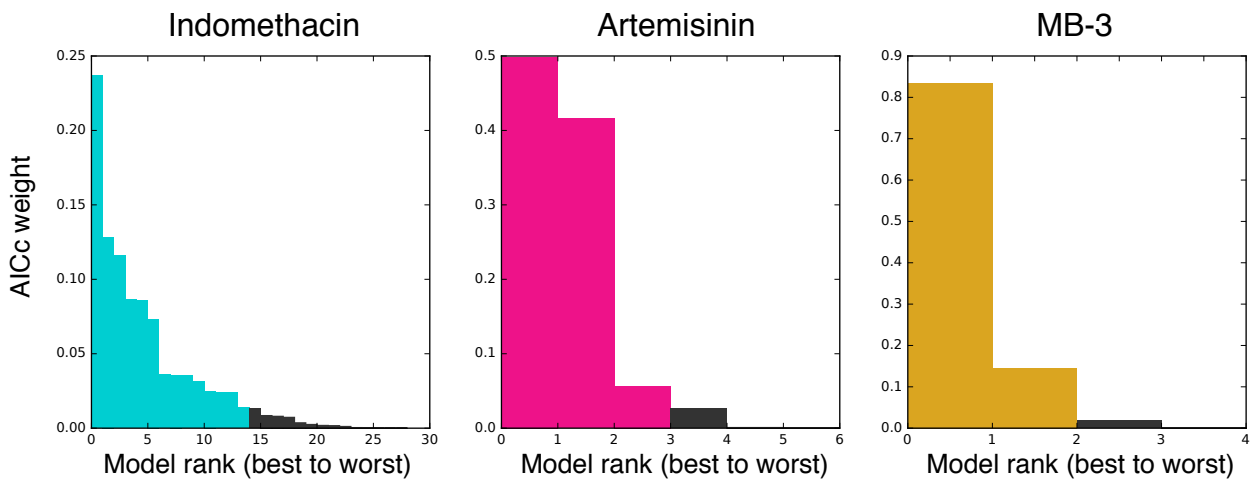


Figure S2: Model selection by Akaike weights. Shown are the Akaike weights of the models, sorted from best to worst. For readability, the worst models were omitted. For each drug, the coloured bars represent the models which amount to 95% of the overall Akaike's weight.

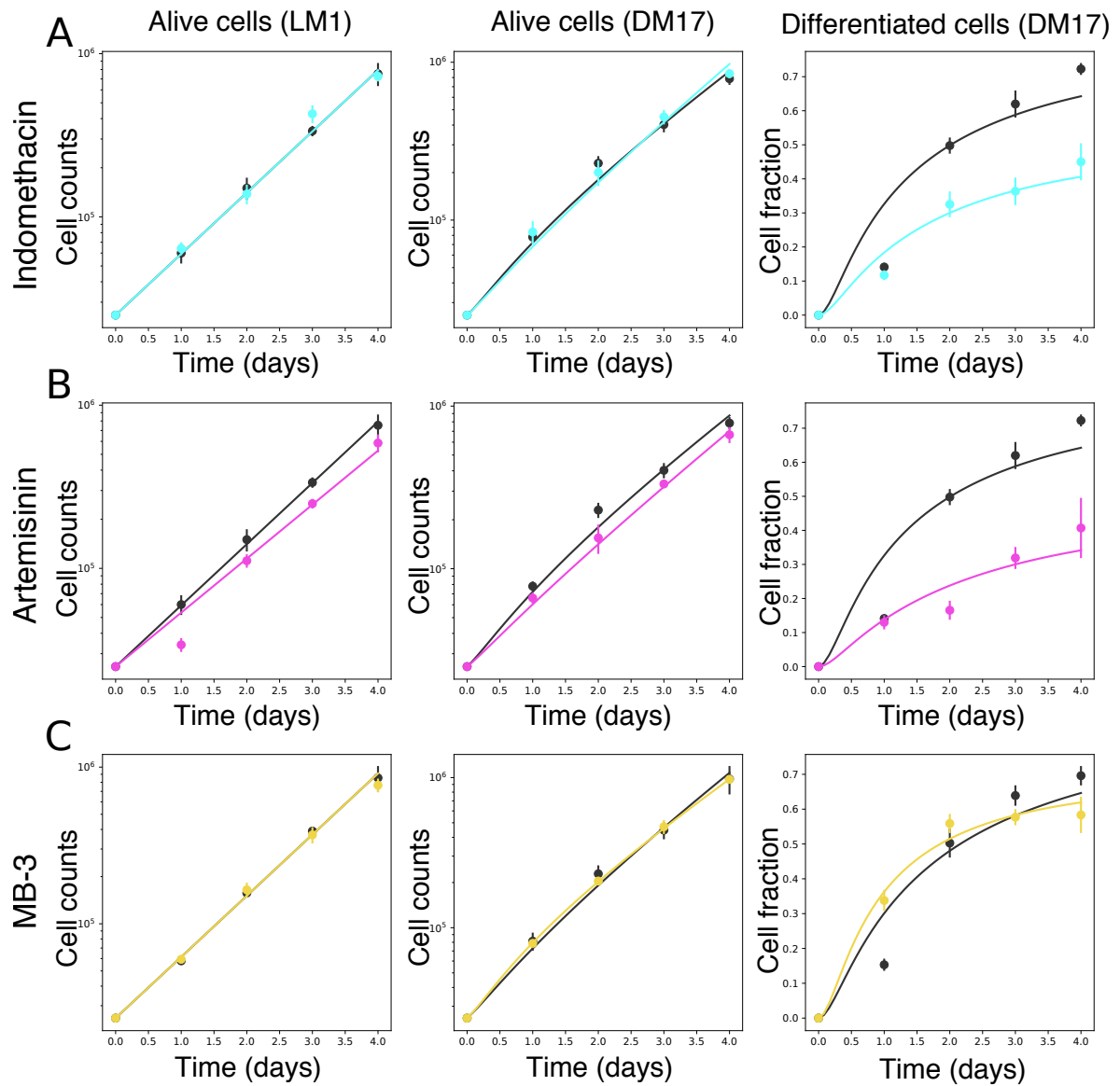


Figure S3: The model reproduces the cellular kinetics observed *in vitro*. Simulation of the model in the untreated (black) and treated cases (color). Solid lines represent a simulation of the best model selected by Akaike's weights. Dots are the experimental data. On the left and the center are respectively displayed the total number of living cells in self-renewing (LM1) and differentiated (DM17) media (in log-scale). On the right are displayed the fraction of differentiated cells in differentiated (DM17) medium.

### 3.3. Conclusion

## 3.3 Conclusion

In this paper, we identify three chemical drugs which affect both SGE and differentiation in the T2EC cells: artemisinin and indomethacin reduce both SGE and the number of differentiated cells, while MB3 increases both.

Then, using the deterministic model presented in Chapter 2, we assess the effects of these chemical drugs (which also affect SGE) on the parameters of cell growth kinetics. For artemisinin, we found 3 models of the treatment that fitted the data correctly, in which the differentiation rate  $\delta_{CB}$  was always decreased compared to the control. For indomethacin, we found 14 models of the treatment that fitted the data, in which  $\delta_{CB}$  was also always decreased compared to the control. For MB3, we found 2 models that fitted the data, in which  $\delta_{CB}$  increased compared to the control.

Consequently, it appears that artemisinin and indomethacin both reduced SGE and the differentiation rate of the T2EC, while MB3 increased both. We thus proved a positive correlation between the extent of SGE and differentiation.

At this point, it seems that we are able to compute the effect of any drug treatment on the differentiation kinetics of our T2EC cells, just by comparing the parameter values in the treated and control case. However, the precise values of the parameter in the control case seem to vary from Chapter 2 to Chapter 3. Such an experimental variability might contradict our conclusions regarding the effect of the drugs. Indeed, how can we compare the parameter values under treatments to the control ones if we can't even be sure of the control values? We thus decided to take more interest in this experimental heterogeneity.



# Chapter 4

## From a deterministic model to a mixed effects model - The Standard Two-States approach (STS)

### 4.1 Introduction

So far we have calibrated our deterministic model, that was defined in Chapter 2, on two different datasets, resulting from different experiments: the first one to carry out model selection, identifiability analysis and to compute the effect of rapamycin on differentiation (in Chapter 2), and the second one to compute the effect of artemisinin, indomethacin and MB3 on the erythroid differentiation (in Chapter 3). We were able to conclude regarding the effect of each drug on proliferation and differentiation by comparing the parameter values under treatment to their control values. Yet in the control condition, the two experiments did not render the same results, even though cells were cultured in the same conditions. We will refer to these differences between the outcomes of the same repeated experiment as *experimental heterogeneity*.

It is on this experimental heterogeneity that we will focus from this chapter on. Namely, we will try to assess the extent of experimental variability and its effect on the model outcome, in terms of parameter values and identifiability

(Section 1.3).

We will illustrate experimental heterogeneity using the experiments from the previous chapters as an example. Then we will introduce an extended dataset comprising 7 repetitions of the same experiment. Using this full dataset, we will try to calibrate our deterministic model on all experiments independently. In this setting, we consider that each repetition of the experiment is an individual sampled from a theoretical population. This approach, which consists in estimating the parameters of all individuals independently in order to characterize the population distribution of the parameters, is known as the *Standard Two-States Approach* (Karlsson et al., 2015), hereafter referred to as STS.

## 4.2 Some considerations on the results of the previous chapters

In the previous chapters, we have used different experimental datasets for different purposes. Yet all datasets were obtained from the exact same protocol, in terms of culture volume, duration, conditions, as well as medium composition or initial concentration of cells. We have already introduced it in Section 1.1.2, in Duchesne et al. (2018, Section 2.1) and in Guillemin et al. (2018, Section 4). The only feature that might have changed from an experiment to the other is the time at which drugs were added to the culture (or DMSO in the control). Artemisinin and indomethacin (and DMSO in the corresponding controls) were added 48h before inducing differentiation, which is referred to as *pre-treatment*. On the other hand, rapamycin and MB3 (and DMSO, in the corresponding control) were added upon induction. These timings were either optimized by Anissa Guillemin during her PhD, or taken from the literature (Dazy et al., 2003; Gonin-Giraud et al., 2008).

In Chapter 2, we used the result of a single experiment (which will be referred to as AG154<sub>2</sub>)<sup>1</sup> to design and select our dynamic model, as well as to

---

<sup>1</sup>The titles of all experiments in this work are obtained by concatenating the initials of the performing experimentalist, and a unique experiment identifier. AG154<sub>2</sub> is thus part of the

## 4.2. Some considerations on the results of the previous chapters

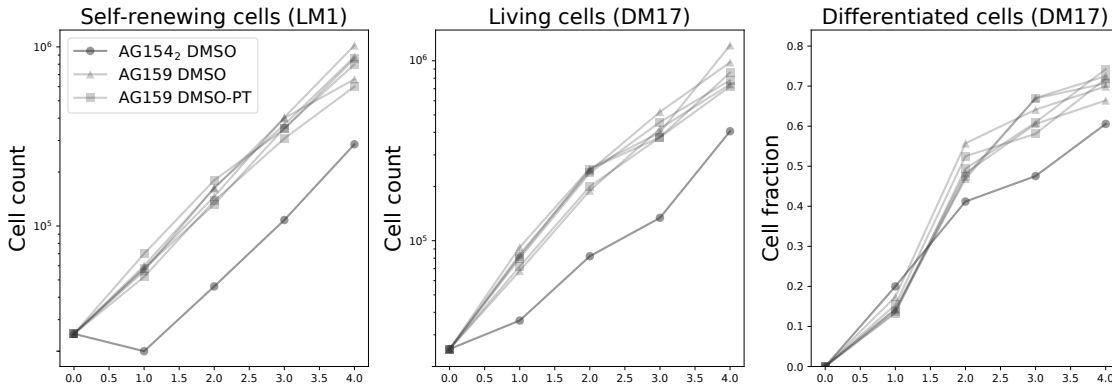


Figure 4.1: Experimental heterogeneity in the control condition. Displayed are the results of experiments AG154<sub>2</sub> (circles) and AG159<sub>1-3</sub> (with pre-treatment: squares, without pre-treatment: triangles) in the control case.

perform identifiability analysis and test the effect of rapamycin.

In Chapter 3, we used the results of three experiments (AG159<sub>1</sub>, AG159<sub>2</sub> & AG159<sub>3</sub>) to test the effect of artemisin, indomethacin and MB3 on the proliferation and differentiation of the T2EC.

We display the data of both experiments on Figures 4.1-4.2, and the corresponding parameter values and confidence intervals on Figure 4.3. These two datasets are different (Figure 4.1), because the protocol suffers some measurement error (for example in the sampling of the cells for counting, or at the initial insemination of the culture). This has already been discussed in Duchesne et al. (2018, Section 3.1), and should be accounted for by the error term of the likelihood of the model. An increased experimental error thus results in an increase in the error parameters  $b_1$  and  $b_2$ .

Our data are heterogeneous, yet the fit of our model is satisfying for every dataset (Figure 4.2). This means that the estimated parameter values, and their confidence intervals, depend on the data used for estimation (Figure 4.3). Moreover, the experimental error is averaged out when aggregating several datasets, as in Chapter 3: in AG159<sub>1-3</sub> the best-fit parameters of the dynamic model reproduce the average behaviour of the three replicates of the experiment (Figure 4.2B-D), while the heterogeneity between the replicates is

---

154<sup>th</sup> experiment performed by Anissa Guillemin.

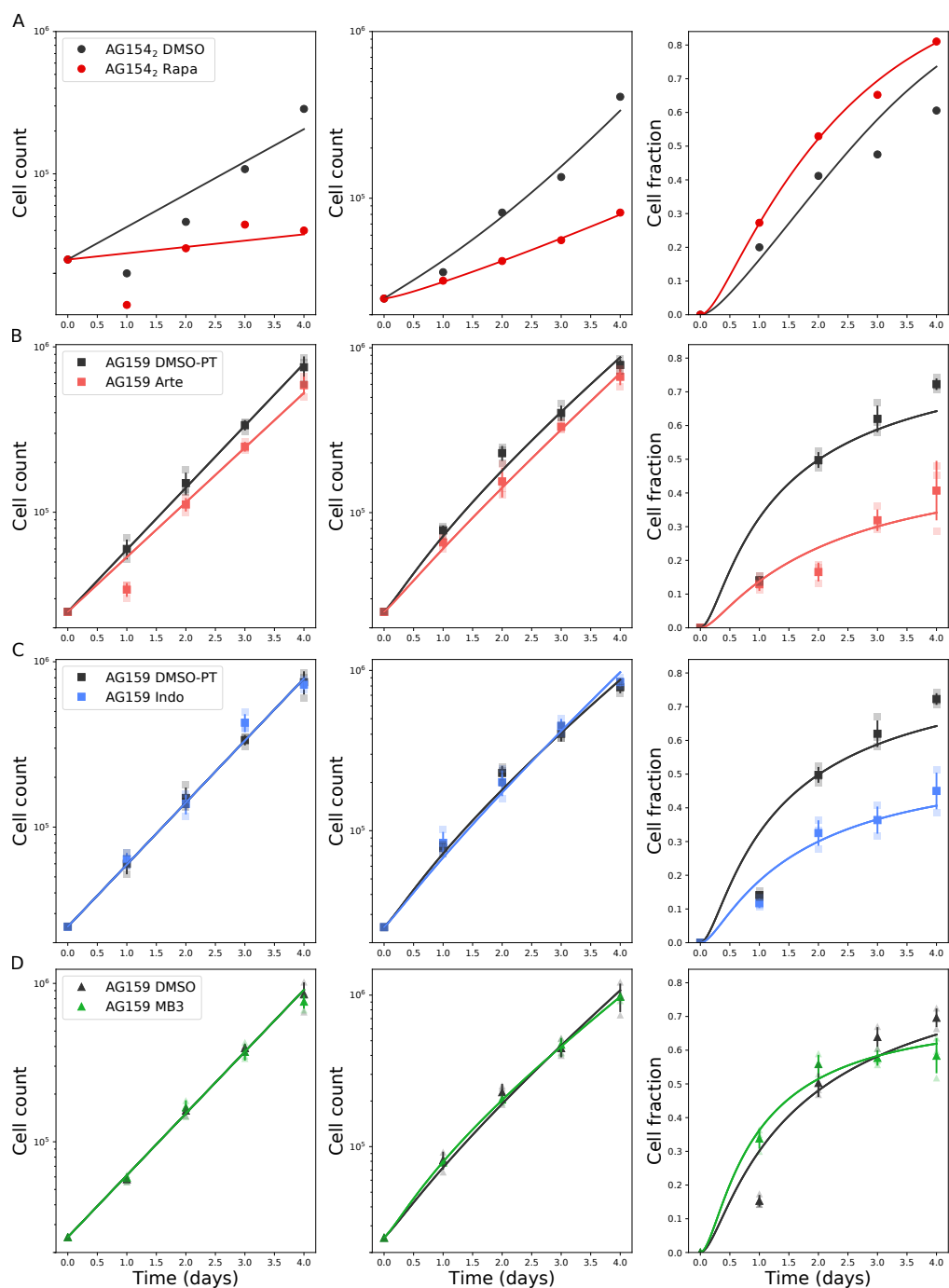


Figure 4.2: Experimental heterogeneity in the treated condition. Displayed are the results of experiments AG154<sub>2</sub> (circles) and AG159<sub>1-3</sub> (with pre-treatment: squares, without pre-treatment: triangles) in the control and treated conditions, as well as the best model fit (A: rapamicin, B: artemisinin, C: indomethacin, D: MB3). For AG159<sub>1-3</sub>, we display the average  $\pm$  standard deviation of the three replicates of the experiment, as well as the three replicates themselves in lighter colors.

## 4.2. Some considerations on the results of the previous chapters

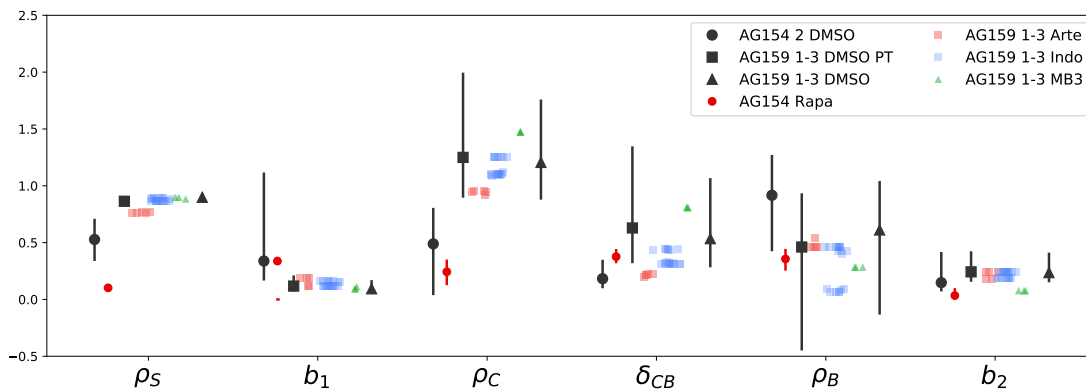


Figure 4.3: Parameter values from the previous chapters. Displayed are the best-fit values corresponding to experiments AG154<sub>2</sub> (circles) and AG159<sub>1-3</sub> (with pre-treatment: squares, without pre-treatment: triangles) in the control (black) and treated (colors) conditions. 95% confidence intervals are displayed when available. For rapamycin, we display only the parameter values of the best model of the treatment. For artemisinin, indomethacin and MB3, we display the parameters of the models selected by Akaike's weight (Chapter 3). The horizontal spacing between these values was chosen for readability.  $\delta_{SC}$  is not represented, because its value is entirely determined by the value of  $\rho_S$  (Chapter 1).

accounted for by the increased value of  $b_2$  compared to its value in AG154<sub>2</sub> (Figure 4.3). Moreover,  $b_1$  is higher in the control case for AG154<sub>2</sub> than for AG159<sub>1-3</sub>, because of the increased predictive error of the model regarding the number of cells in LM1.

This heterogeneity between the results of our experiments is unexpected, because the most interesting feature of our model is the comparison of parameter values in the treated and untreated cases. Yet it seems that we cannot be convinced by the values in the untreated case (Figure 4.3). So we decided to investigate it further, by using an extended dataset comprising more replicates of the experiments.

Anissa Guillemin obtained it by repeating the same protocol as we already described (Section 1.1), using the same cell culture to initiate the cultures for all treatments (comprising Artemisinin, Indomethacin and a DMSO control with pre-treatment). She changed the initial cell culture from an experiment to the

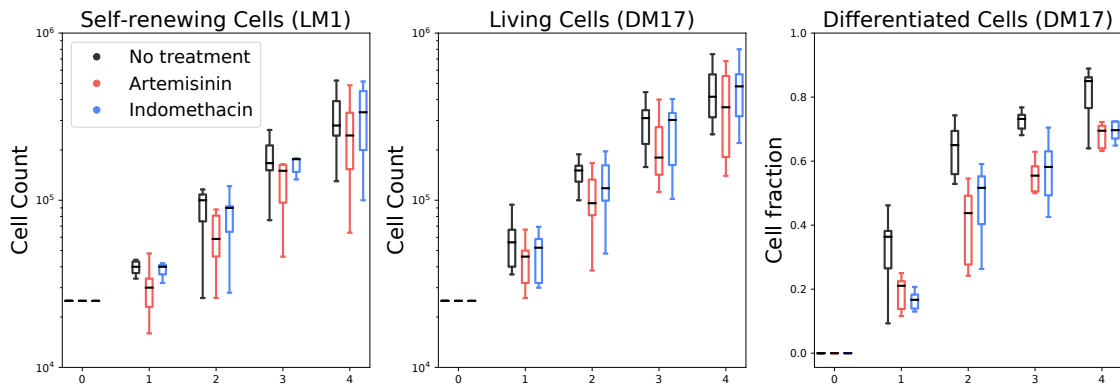


Figure 4.4: Boxplots of the full dataset. The figure displays the time evolution of the cell count distributions in the three conditions (black: control, red: artemisinin, blue: indomethacin)

next one, and she also had an intern (called Gaëlle Danancier) who did the same.

This extended dataset, which we will refer to as the *full dataset*, comprises 7 replicates of the experiment: AG111, AG112, AG139, AG142, GD14, GD15 & GD16.

### 4.3 Calibrating the deterministic model on a larger dataset

We show the full dataset on Figures 4.4-4.5, which confirms that artemisinin and indomethacin reduce the fraction of differentiated cells in the culture (MB3 was not tested in these experiments). Yet all observables are subject to some level of heterogeneity.

We then focused on the control situation, and estimated the parameter values of all individuals independently. They are displayed in Figure 4.6. We also computed their confidence intervals using the profile likelihood approach at 95% confidence level.

Figure 4.6 shows that all individuals are characterized (to some extent) by different parameter values, and that these values are not always identifiable.

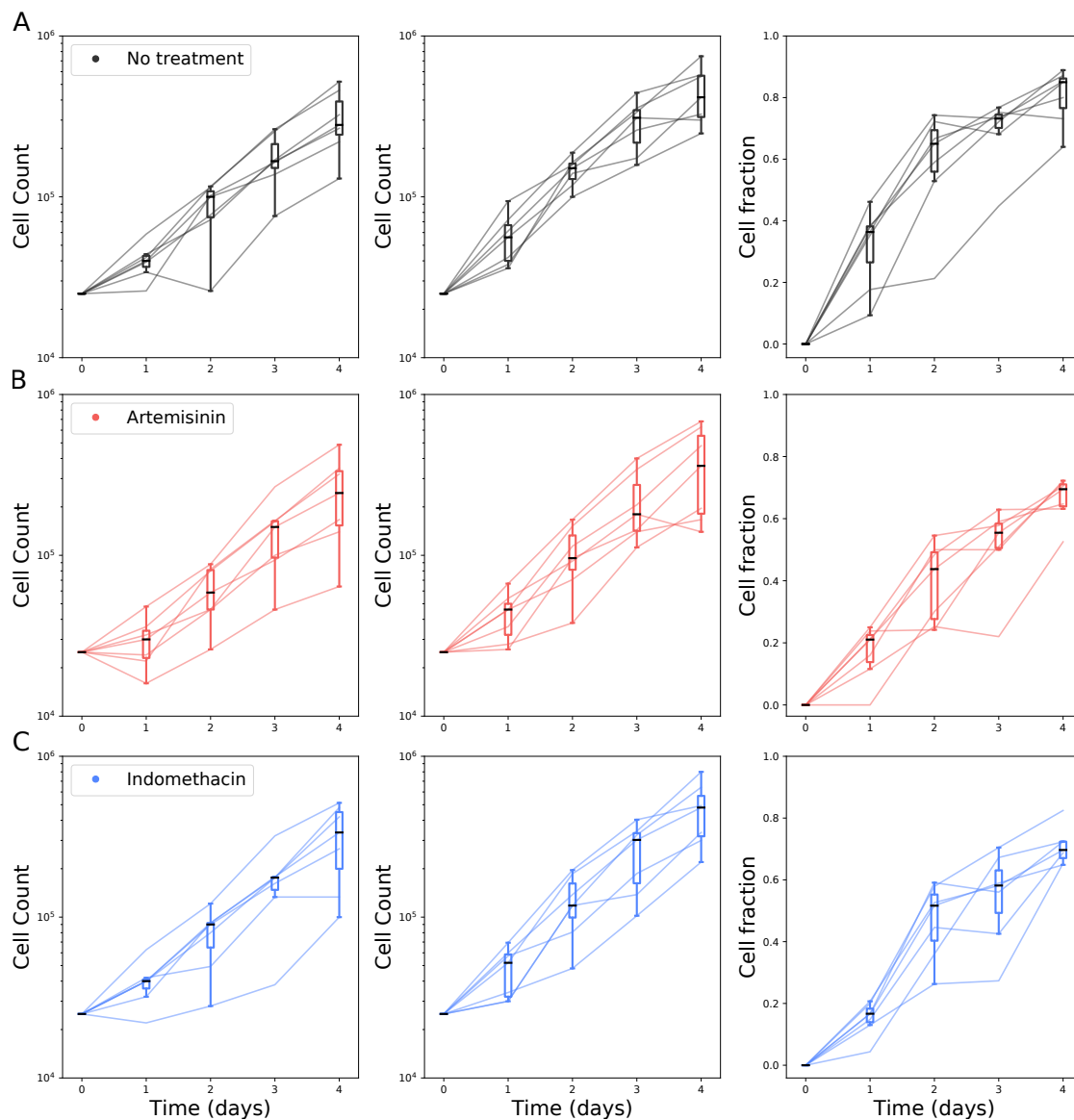


Figure 4.5: Spaghetti plots of the full dataset. The figure displays the cell count distributions and individual trajectories of the 7 replicates of the experiment in the control (A), artemisinin- (B) and indomethacin-treated (C) conditions.

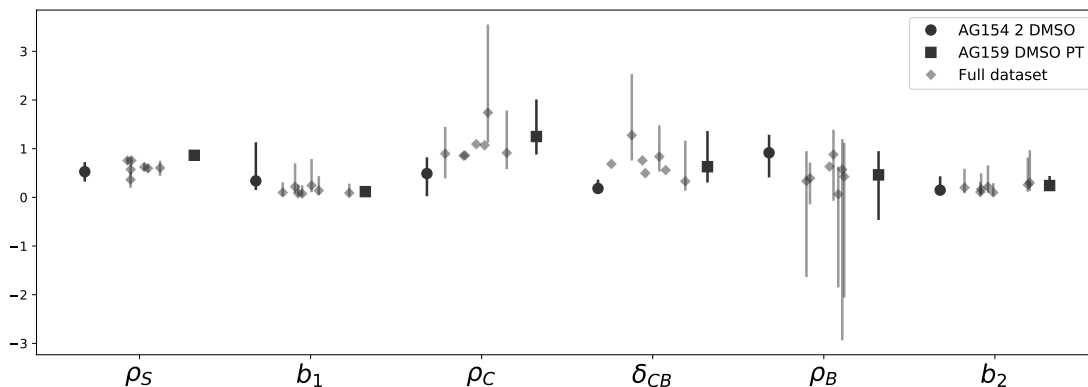


Figure 4.6: Parameter values in the full dataset. Displayed are the best-fit values corresponding to the 7 experiments of the full dataset (diamonds). 95% confidence intervals are displayed for the identifiable parameters. We also display the control values of the parameters in experiments AG154<sub>2</sub> and AG159<sub>1-3</sub> as a reminder, with their 95% confidence intervals. The horizontal spacing between the values was chosen randomly for readability.

## 4.4 Conclusion

Using the full dataset, we showed that despite experimental heterogeneity, artemisinin and indomethacin seem to have an effect on the differentiation of the T2EC cells. Yet, some of the experiments in the dataset are characterized by unidentifiable parameter values, and when they are identifiable, these values vary from an experiment to another.

As a consequence, it would seem difficult to compare the parameter values of the model under the different conditions, since it seems already difficult to assess these values in the control case.

In such cases where the dynamic model is unidentifiable for some of the individuals, it is possible instead to develop a Mixed Effect Model (MEM) based on the same dynamic model (Karlsson et al., 2015). Such an approach uses the data of all individuals to infer a population distribution for each parameter of the model. Then, it uses this population distribution to infer a value for each individual in a bayesian manner. It can thus provide some information to constrain the possible values of an unidentifiable individual parameter, compared

#### 4.4. Conclusion

to the STS approach which we have adopted so far (Karlsson et al., 2015).

This is why we decided to develop a mixed effect model of the *in vitro* erythropoiesis, considering that each replicate of the differentiation experiment from the full dataset is one individual, and that all experiments belong to the same population.



# Chapter 5

## Elaboration of a mixed effects model for the *in vitro* erythropoiesis

### 5.1 Introduction

We have defined a dynamic model of *in vitro* erythroid differentiation that is able to reproduce the result of one differentiation experiment (Chapter 2), as well as the average behaviour of several repetitions of the experiment (Chapter 3). Yet these repetitions are characterized by different parameter values (Chapter 4). As mentioned in Section 1.4, Mixed Effect Models (MEM) have been increasingly used to describe data exhibiting variability between individuals from the same population (Lavielle and Bleakley, 2014).

In order to define a MEM, one needs to define three different model components: a dynamic model (or structural model), an error model (or observation model) and a parameter model. The dynamic and error models were already defined in Chapter 2, so we need to define a parameter model in order to adapt our model to a "mixed effect" context. According to Equations (1.6) and (1.7) (Section 1.4.1), this means that for each parameter of the dynamic model, we have to define:

1. the fixed effect term in the population,

2. whether or not there is a random effect, and what its distribution is.

In this chapter, we first define a MEM for the full dataset that we introduced in Chapter 4, based upon the dynamic model from Chapter 2. To do so, we consider the full dataset as a population of experiments where each experiment is an individual characterized by its own parameter values. However, choosing the distribution of a parameter from raw data might not be straightforward, depending on what information we have on the parameter values. We illustrate this difficulty by defining different parameter models based on alternative sets of hypotheses about the parameter values. We then select the parameter model which fits our data best, using the criteria that we introduced in Section 1.4.3. Finally, since we are interested in the parameter variations of our model under drug treatments, we discuss the identifiability of our MEM using the criteria introduced in Section 1.4.4.

## 5.2 A first version of the model

We define our parameter model using the information that we have on the range of each parameter (see Section 2.3).

For the three proliferation rates  $\rho_S$ ,  $\rho_C$  and  $\rho_B$ , which can be positive or negative depending on the balance between cell proliferation and death (see Section 2.3 in this manuscript, or Section 2.2.1 in Duchesne et al., 2019), we choose a gaussian distribution.

For the differentiation rate  $\delta_{SC}$ , we use the bounds that can be inferred from the commitment experiment (see Section 1.1.2 in this manuscript, and Duchesne et al., 2019, Section 2.3):

$$\rho_S + 1/2\ln(S_0) \leq \delta_{SC} \leq \rho_S + \ln(S_0), \quad (5.1)$$

which link the individual parameters  $\rho_S$  and  $\delta_{SC}$  with the initial number of cells in the culture  $S_0$ .

One way of defining a bounded distribution for  $\delta_{SC}$  is by using a bounded

## 5.2. A first version of the model

transformation of the gaussian distribution, such as the probit-normal distribution that we presented in Section 1.4.1 (Lavielle and Bleakley, 2014). We thus introduce  $\tilde{\zeta}$ , the scaled value of  $\delta_{SC}$ :

$$0 \leq \tilde{\zeta}_k = \frac{\delta_{SC,k} - \rho_{S,k}}{2\ln(S_0)} \leq 1.$$

We then use a probit-normal distribution for  $\tilde{\zeta}$ , which describes the spreading of the individual values of  $\tilde{\zeta}$  between 0 and 1 across the population, and use it to define the distribution of  $\delta_{SC}$ :

$$\begin{cases} \tilde{\zeta}_k & \hookrightarrow \text{probit}\mathcal{N}(\tilde{\zeta}^{pop}, \omega_{\tilde{\zeta}}), \\ \delta_{SC,k} & = \rho_{S,k} + 1/2\ln(S_0)(1 + \tilde{\zeta}_k). \end{cases}$$

For the differentiation rate  $\delta_{CB}$ , which must be strictly positive, we choose a lognormal distribution that would also be positive, resulting in the following model for the individual parameters:

$$\begin{cases} \rho_{S,k} & \hookrightarrow \mathcal{N}(\rho_S^{pop}, \omega_{\rho_S}), \\ \tilde{\zeta}_k & \hookrightarrow \text{probit}\mathcal{N}(\tilde{\zeta}^{pop}, \omega_{\tilde{\zeta}}), \\ \delta_{SC,k} & = \rho_S + 1/2\ln(S_0)(1 + \tilde{\zeta}), \\ \rho_{C,k} & \hookrightarrow \mathcal{N}(\rho_C^{pop}, \omega_{\rho_C}), \\ \delta_{CB,k} & \hookrightarrow \log\mathcal{N}(\delta_{CB}^{pop}, \omega_{\delta_{CB}}), \\ \rho_{B,k} & \hookrightarrow \mathcal{N}(\rho_B^{pop}, \omega_{\rho_B}). \end{cases} \quad (5.2)$$

System (5.2), together with the dynamic model and the error model that we defined in Chapter 2, fully defines our first MEM of the *in vitro* erythropoiesis. It is characterized by thirteen parameters. The five fixed effects ( $\rho_S^{pop}$ ,  $\tilde{\zeta}^{pop}$ ,  $\rho_C^{pop}$ ,  $\delta_{CB}^{pop}$  and  $\rho_B^{pop}$ ) quantify the average behaviour of the population. The standard deviations of the five random effects ( $\omega_{\rho_S}$ ,  $\omega_{\tilde{\zeta}}$ ,  $\omega_{\rho_C}$ ,  $\omega_{\delta_{CB}}$  and  $\omega_{\rho_B}$ ) quantify the variability of the population around its average. The three error parameters ( $b_1$ ,  $b_2$  and  $b_3$ ) quantify the variance of the model residuals for each of its three observables.

Parameter	Initial guess	Unit
$\rho_S^{pop}$	$\mathcal{U}(-5, 5)$	$\text{d}^{-1}$
$\xi^{pop}$	$\mathcal{U}(0, 1)$	$\text{d}^{-1}$
$\rho_C^{pop}$	$\mathcal{U}(-5, 5)$	$\text{d}^{-1}$
$\delta_{CB}^{pop}$	$\mathcal{U}(0, 5)$	$\text{d}^{-1}$
$\rho_B^{pop}$	$\mathcal{U}(-5, 5)$	$\text{d}^{-1}$
$\omega_{\rho_S}$	5	$\text{d}^{-1}$
$\omega_{\xi}$	5	$\text{d}^{-1}$
$\omega_{\rho_C}$	5	$\text{d}^{-1}$
$\omega_{\delta_{CB}}$	5	$\text{d}^{-1}$
$\omega_{\rho_B}$	5	$\text{d}^{-1}$
$b_1$	1	-
$b_2$	1	-
$b_3$	1	-

Table 5.1: Initial guess values and distributions in our MEM (System (5.2)). The initial guesses of the fixed effects are sampled uniformly with respect to each parameter bounds. The initial guess of the variances of the random effects, and of the error parameters, are set to an arbitrary high value to improve the convergence of SAEM in the early phase of the estimation.

We try to estimate these population parameters using the SAEM algorithm implemented in Monolix. We run the algorithm 10 times, using a random sampling of the initial parameter guesses (Table 5.1). The optimal likelihood values estimated after these runs are displayed on Figure 5.1. The spreading of these estimated likelihood values over several dozens log-likelihood units indicates that the estimator did not always converge to the same likelihood optimum.

Moreover, for some of the SAEM runs, Monolix found parameters with a null sensitivity, either during the SAEM estimation, or while computing the Fisher Information Matrix (FIM, that we introduced in Section 1.3.4.2). In the former case, it means that Monolix is not able to estimate the values of the parameters. In the latter one, it means that Monolix is unable to compute

## 5.2. A first version of the model

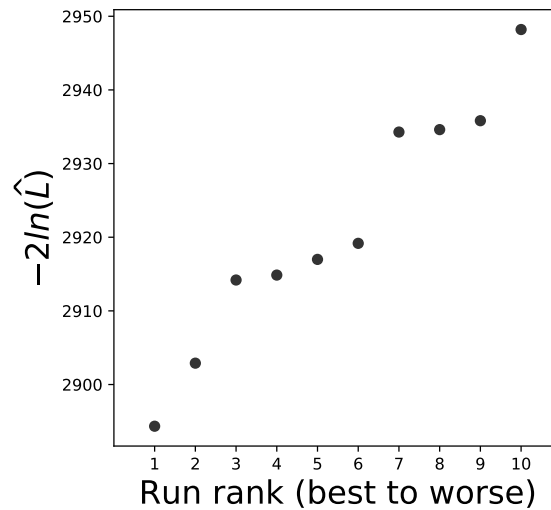


Figure 5.1: Distribution of the optimal likelihood values over 10 SAEM runs of our MEM (Equation (5.2)).

the standard errors of the estimated parameter values. These parameters that were not reliably estimated are summarized in Table 5.2, and have little to no influence on the model output, *i.e.* parameters for which the sensitivity is null near the estimated optimum. As a consequence, one would usually conclude that these parameters are unidentifiable. Yet, the likelihood values of all the SAEM runs are not the same (Figure 5.1), which might indicate that the algorithm failed at converging toward the global likelihood optimum because it got stuck in regions of the parameter space where the sensitivity to some parameter was null.

As a conclusion, the SAEM algorithm implemented in Monolix failed at estimating all the parameters of our model reliably, and even failed at converging to a global optimum. Since the dynamic model and the error model that we chose were selected based on their ability to fit our differentiation data (Chapter 2) in a variety of contexts (Chapters 2-4), it seems that our choice of distributions for the parameters of the model is responsible for the failure of their estimation. The parameter for which the estimation failed most frequently is  $\xi^{pop}$  (Table 5.2). Since  $\xi^{pop}$  defines the average value of  $\delta_{SC}$  in the population, our results suggest that we are not able to fit the differentiation data properly,

SAEM run	Parameters
1	$\zeta^{pop}, \omega_{\rho_C}$
2	-
3	$\zeta^{pop}, \rho_C^{pop}$
4	$\zeta^{pop}, \delta_{CB}^{pop}$
5	$\zeta^{pop}, \omega_{\delta_{CB}}$
6	$\delta_{CB}^{pop}, \omega_{\rho_C}, \omega_{\delta_{CB}}$
7	$\omega_{\rho_C}$
8	$\rho_C^{pop}, \omega_{\rho_C}, \omega_{\delta_{CB}}$
9	$\zeta^{pop}, \omega_{\rho_C}$
10	-

Table 5.2: Parameters with a null-sensitivity due to SAEM inability to compute the FIM, in the 10 SAEM runs. Displayed are the parameters for which Monolix cannot compute the standard error (s.e.), because it is infinite. Parameters which have a finite, but high, s.e. might also be considered but were not included in the table.

while at the same time respecting the bounds on the values of  $\delta_{SC}$  defined by the commitment experiment. Actually, Figure S2 in Duchesne et al. (2019) already showed that the likelihood of the model is not constant over the range of values allowed by the commitment experiment (Equation (5.1)). It is thus possible that the global optimal value of  $\delta_{SC}$  for fitting the differentiation data lies outside of this range, complicating the estimation of the population parameters of the MEM.

To verify this, we test different distributions for  $\delta_{SC}$  and try to find one that would fit our data correctly.

### 5.3 Selection of a distribution for $\delta_{SC}$

We thus define several alternative forms of the model (Table 5.3), which differ by their distribution for  $\delta_{SC}$ . To do so, we relax some of the constraints on the bounds of  $\delta_{SC}$  that we imposed when defining our MEM in System (5.2). We

### 5.3. Selection of a distribution for $\delta_{SC}$

Information	$\delta_{SC}$ bounds	$\delta_{SC}$ distribution
<i>Two bounds</i>	$1/2\ln(S_0) \leq \delta_{SC,k} - \rho_{S,k} \leq \ln(S_0)$	$\begin{cases} \xi_k \hookrightarrow \text{probit}\mathcal{N}(\xi^{pop}, \omega_{\xi}) \\ \delta_{SC,k} = \rho_{S,k} + 1/2\ln(S_0)(1 + \xi_k) \end{cases}$
<i>Lower bound</i>	$\rho_{S,k} + 1/2\ln(S_0) \leq \delta_{SC,k}$	$\begin{cases} \xi_k \hookrightarrow \log\mathcal{N}(\xi^{pop}, \omega_{\xi}) \\ \delta_{SC,k} = \rho_{S,k} + 1/2\ln(S_0) + \xi_k \end{cases}$
<i>Upper bound</i>	$\delta_{SC,k} \leq \rho_{S,k} + \ln(S_0)$	$\begin{cases} \xi_k \hookrightarrow \log\mathcal{N}(\xi^{pop}, \omega_{\xi}) \\ \delta_{SC,k} = \rho_{S,k} + \ln(S_0) - \xi_k \end{cases}$
<i>Rate</i>	$\delta_{SC,k} \geq 0$	$\delta_{SC,k} \hookrightarrow \log\mathcal{N}(\delta_{SC}^{pop}, \omega_{\delta_{SC}})$
<i>No information</i>	$\delta_{SC,k} \in \mathbb{R}$	$\delta_{SC,k} \hookrightarrow \mathcal{N}(\delta_{SC}^{pop}, \omega_{\delta_{SC}})$

Table 5.3: Alternative MEM defined by relaxing the bounds of  $\delta_{SC}$ .

refer to this model as the model with *two bounds* on the values of  $\delta_{SC}$ . In the *lower bound* (respectively *upper bound*) versions of the model, we only retain the lower bound (respectively the upper bound) on the value of  $\delta_{SC}$ , computed for each individual from Equation (5.1). In the *rate* version of the model, both bounds are forgotten, and we only consider the fact that as a differentiation rate,  $\delta_{SC}$  should be positive. In the last version of the model, we allow any value for  $\delta_{SC}$ . All these considerations define the five different distributions of  $\delta_{SC}$  that are presented in Table 5.3.

We estimate the population parameters of all these newly defined models the same way as we did for the first one in Section 5.2, by running the SAEM algorithm 10 times using a random sampling of the initial parameter guesses. We use the same distributions for the initial guesses as with the first model:

- the initial population mean of normally distributed parameters is sampled uniformly in  $[-5, 5]$ ,

$\delta_{SC}$ info	$-2\ln(\hat{L})$	AIC	BIC
Two Bounds	2894	2920	2918
Lower Bound	2899	2925	2923
Upper Bound	2824	2850	2848
Rate	<b>2811</b>	<b>2837</b>	<b>2835</b>
No Info	2816	2842	2840

Table 5.4: Selection criteria evaluated for our alternative  $\delta_{SC}$  distributions. Since all models have the same number of parameters, the selection is made solely on the likelihood values. The bold font indicates the model with the best likelihood.

- the initial population mean of log-normally distributed parameters is sampled uniformly in  $[0, 5]$ ,
- the initial population variances are set to  $5d^{-1}$  to ensure a quick convergence of the algorithm,
- the initial error parameters are set to 1.

For each model, we only keep the SAEM run which rendered the best likelihood, and we compute the selection criteria that are displayed in Table 5.4 (which were introduced in Section 1.4.3). The *rate* version of the model, with a log-normal distribution for  $\delta_{SC}$ , renders the best fit to the data, closely followed by the version with a gaussian distribution for  $\delta_{SC}$ . Since it makes more sense to use a positive distribution for a positive parameter, we will adopt the model with a log-normal distribution for  $\delta_{SC}$  in the following.

For the model with a log-normal distribution for  $\delta_{SC}$ , we also display the distribution of the likelihood values over the 10 runs of SAEM in Figure 5.2. The 10 SAEM runs have converged to very close likelihood values, which might mean that the algorithm found a global likelihood optimum.

Now that we have improved the convergence of our MEM, we will discuss its identifiability.

## 5.4. Identifiability analysis of our MEM

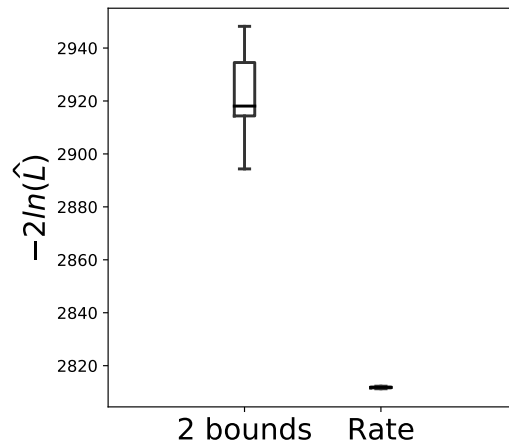


Figure 5.2: Boxplots of the optimal likelihood values over 10 SAEM runs of the model with two bounds and the rate model.

## 5.4 Identifiability analysis of our MEM

We have introduced identifiability in Section 1.3, and discussed it in the context of MEMs in Section 1.4.4. First, we should discuss the identifiability of the population parameters in the model, as their values are used for estimating the individual parameters (Section 1.4.2). Then we can move on to the identifiability of the individual parameters.

### 5.4.1 Population parameters: Initial Guess Sampling (IGS)

In order to assess the identifiability of the population parameters of our MEM, we adopted the following approach (Section 1.4.4):

1. We perform a random sampling of the initial parameter guesses, which provides us a sample of optimal parameter values.
2. We assess the convergence of the algorithm: we only want to consider the SAEM runs which reached the global optimum.
3. We compare the parameter values of these convergent runs. If they are not the same, then the model is unidentifiable (several different param-

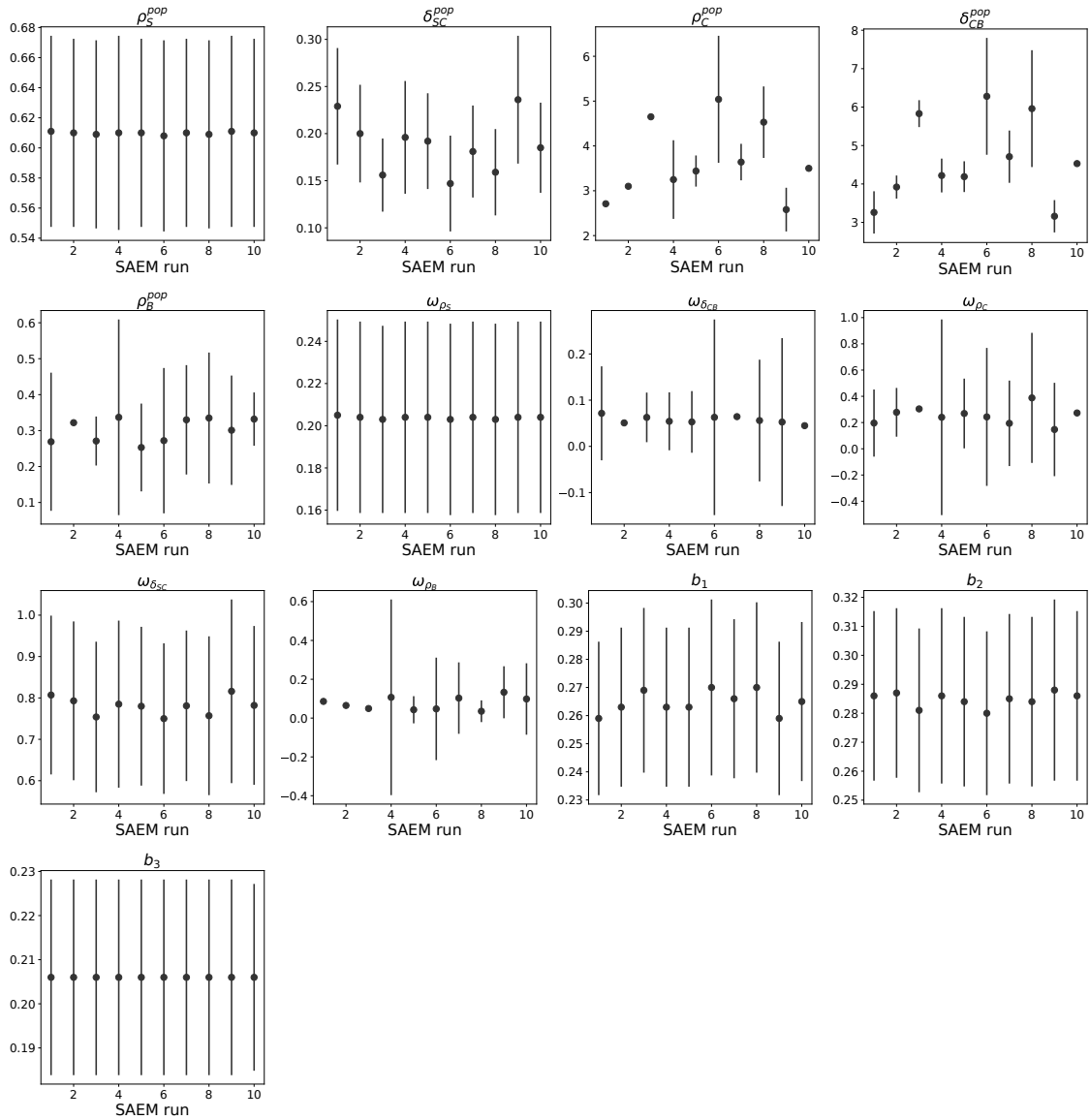


Figure 5.3: Initial guess sampling of the population parameters of the model with a lognormal  $\delta_{SC}$ . Displayed are the estimated values of each population parameter for 10 runs of the SAEM algorithm using different initial guess values (black dots). The error bars display the standard error of each parameter value, as computed from the FIM (when no error bar is displayed, it means that the FIM could not be computed).

## 5.4. Identifiability analysis of our MEM

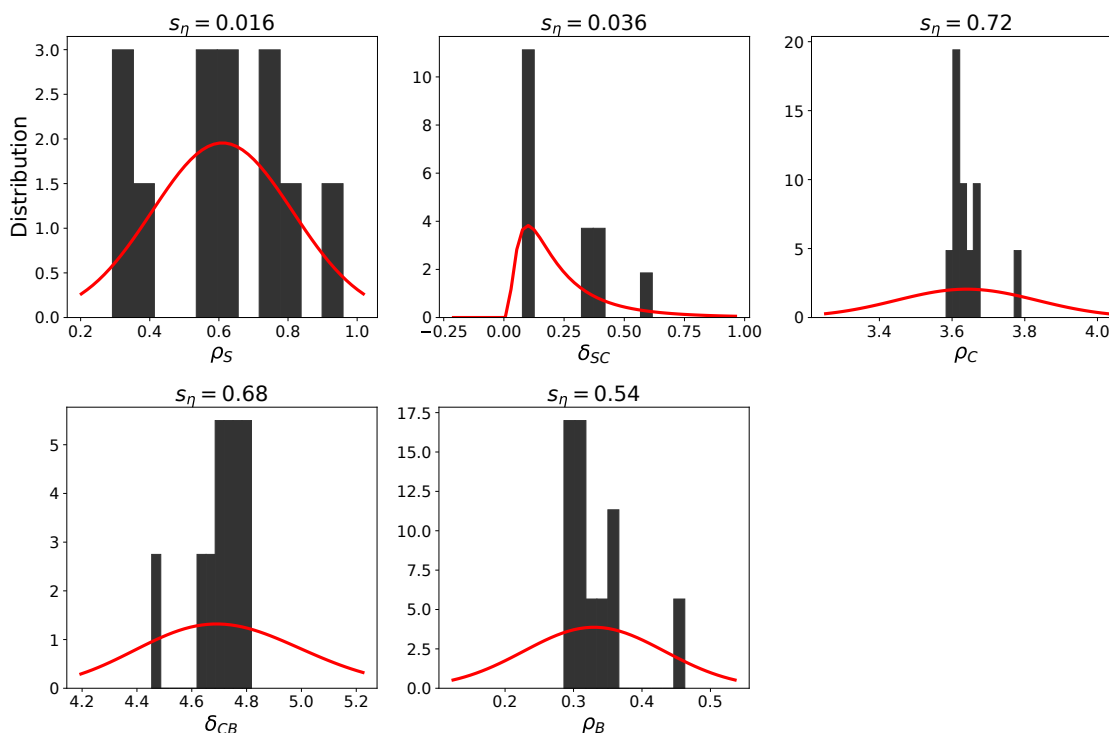


Figure 5.4: Parameter distributions for the *rate model*. Solid red lines indicate the population distribution. Black histograms represent the individual parameter distributions. For each parameter, we also display the amount of  $\eta$ -shrinkage as a fraction of the population variance (Equation (1.14))

eter values give the same likelihood). If they are, then we conclude that the model is identifiable.

We already showed with Figure 5.2 that the 10 SAEM runs that we have performed on the model with a log-normal  $\delta_{SC}$  converged to the same likelihood value. We display the associated parameter values in Figure 5.3.

Of all the parameters of the model,  $\rho_S^{pop}$ ,  $\omega_{\rho_S}$  and the three error parameters  $b_1$ ,  $b_2$  and  $b_3$  are estimated the most reliably, since their estimated values are conserved across all runs. All the other parameters are estimated with more variability, and since all runs rendered the same likelihood, it means that they are not identifiable.

### 5.4.2 Individual parameters: $\eta$ -shrinkage

A consequence of the lack of identifiability of individual parameters is the shrinking of their values toward the population average, which is measured by the  $\eta$ -shrinkage  $s_\eta$  (Equation (1.14), Section 1.4.4). A high value for  $s_\eta$  for a parameter means that individual data lack information for estimating it.

Figure 5.4 displays the distribution of the individual parameters in the SAEM run which rendered the lowest likelihood, and the associated shrinkage values. For  $\rho_S$  and  $\delta_{SC}$ , the low shrinkage values indicate that the data were sufficient to estimate a value for each individual. However  $\rho_C$ ,  $\delta_{CB}$  and  $\rho_B$  are more shrunk toward their population mean, which indicates that they could not be estimated for all individuals.

## 5.5 Conclusion

In this chapter, we have designed a MEM of the *in vitro* erythropoiesis, based on the selection of a distribution for  $\delta_{SC}$ :

$$\left\{ \begin{array}{l} \rho_S \quad \hookrightarrow \mathcal{N}(\rho_S^{pop}, \omega_{\rho_S}), \\ \delta_{SC} \quad \hookrightarrow \log\mathcal{N}(\delta_{SC}^{pop}, \omega_{\delta_{SC}}), \\ \rho_C \quad \hookrightarrow \mathcal{N}(\rho_C^{pop}, \omega_{\rho_C}), \\ \delta_{CB} \quad \hookrightarrow \log\mathcal{N}(\delta_{CB}^{pop}, \omega_{\delta_{CB}}), \\ \rho_B \quad \hookrightarrow \mathcal{N}(\rho_B^{pop}, \omega_{\rho_B}). \end{array} \right. \quad (5.3)$$

In our model, the three proliferation rates are normally distributed, and the two differentiation rates are log-normally distributed, resulting in five fixed effects ( $\rho_S^{pop}$ ,  $\delta_{SC}^{pop}$ ,  $\rho_C^{pop}$ ,  $\delta_{CB}^{pop}$  and  $\rho_B^{pop}$ ) and five population standard deviations ( $\omega_{\rho_S}$ ,  $\omega_{\delta_{SC}}$ ,  $\omega_{\rho_C}$ ,  $\omega_{\delta_{CB}}$  and  $\omega_{\rho_B}$ ). The model also incorporates three error parameters (one for each observable:  $b_1$ ,  $b_2$  and  $b_3$ ).

We have questioned the identifiability of this model using the methods introduced in Section 1.4.4, concluding that it is unidentifiable both at the popu-

## 5.5. Conclusion

lation and at the individual scale. At the population scale,  $\delta_{SC}^{pop}$ ,  $\rho_C^{pop}$ ,  $\delta_{CB}^{pop}$ ,  $\rho_B^{pop}$ ,  $\omega_{\delta_{SC}}$ ,  $\omega_{\rho_C}$ ,  $\omega_{\delta_{CB}}$  and  $\omega_{\rho_B}$  are the unidentifiable parameters. At the individual scale it seems that  $\rho_C$ ,  $\delta_{CB}$  and  $\rho_B$  are the unidentifiable parameters.

When confronted with an unidentifiable model, one essentially has two options:

- generating novel, more informative, data in order to characterize all parameters (which can usually be completed by using a step of experimental design),
- reducing the model in order to have fewer parameters to estimate, and ultimately improve their estimation.

The former one is the focus of Chapter 6, and the latter is treated in Chapter 7.



# Chapter 6

## Experimental design

In Chapter 5, we introduced a MEM for our *in vitro* erythropoiesis data, which was unidentifiable. Since the identifiability of a model depends on the definition of the model and on the quality and quantity of the data (Section 1.3.1), one solution to make a model identifiable, which is the focus of this chapter, is to design and perform new experiments, which would allow for a more precise estimation of the model parameters. For instance, it is possible that the structural model would make some additional timepoints or observables more informative than those of the original design, depending on the local sensitivity of the model outputs to the model parameters (Raue et al., 2010).

Mathematical modelling allows for a formal approach to experimental design, because one can use models to simulate data for a given process, and test *in silico* which experimental design would optimize a given feature of the model, or *design criterion*. For instance, one might want to minimize the model prediction error for some observables (Raue et al., 2009, 2010), or optimize some information criterion from the FIM (System (1.5) and Vanrolleghem and Dochain, 1998).

However, there is no *a priori* proof that a mathematical model properly accounts for the relevant microscopic mechanisms at play in a given biological process. As a consequence, the actual output of an optimally designed experiment might contradict what has been predicted *in silico* (A. White et al., 2016).

This is especially critical if the design optimizes a simplistic criterion. For instance, the FIM has been shown to render biased results when used to study parameter identifiability (Raue et al., 2009).

In the case of our previously defined MEM for *in vitro* erythropoiesis (Chapter 5), possibilities for optimal experimental design include measuring new observables, adding more timepoints to the individual measures, and observing more individuals, *i. e.* performing new replicates of the experiment in order to enlarge the dataset.

Our model already accounts for the number of self-renewing cells in the self-renewing medium, as well as the total number of cells and the number of differentiated cells in the differentiation medium (Chapter 2). Thus, the only way to add an observable would be to decipher between self-renewing and committed cells in the differentiation medium. However, since the committed compartment of the model is essentially hypothetical (Duchesne et al., 2019, Chapter 1), it is impossible for us to measure it experimentally. We conclude that if experimental design provides a way of improving the identifiability of our model, it is not through the definition of new observables.

Since our dataset comprises only 7 individuals (Chapter 4) in order to estimate the distribution of 5 random parameters in the population, we hypothesize that increasing the population size *–i.e.* performing new replicates of the experiment– should be more informative regarding parameter identifiability than adding new timepoints to the dataset.

In this chapter, we focus on experimental design in the context of our MEM for *in vitro* erythropoiesis. Specifically, we wonder if generating measuring new individuals *–i.e.* performing new replicates of the experiment with the same measurement timepoints– would allow for a better estimation of the model parameters.

Experimental design can be performed by maximizing the D-criterion of the FIM (Vanrolleghem and Dochain, 1998), and the FIM appears to be the fastest way of assessing parameter identifiability (Luzyanina et al., 2007). In MEM, experimental design is thus typically performed using the D-criterion

## 6.1. Methods

(Bazzoli et al., 2010) with specific optimization algorithms (Retout et al., 2007) in order to balance the computation time and the precision of the results.

However, since our structural model is very simple, it can be simulated without using any numerical integration (Chapter 2), and is thus quite fast to calibrate. We thus propose a more computationally-demanding, FIM-free approach for experimental-design, which we describe in the next section.

## 6.1 Methods

In order to assess if our model might become identifiable with a larger population size, we generated artificial datasets of varying population sizes and tried to calibrate our MEM on these artificial datasets. Our rationale is that if our model becomes identifiable above a certain population size, it can be measured using the methods that we introduced in Section 1.4.4.

### 6.1.1 Population size

We generated artificial datasets with the following population sizes:  $N \in \{3, 5, 7, 9, 11, 20\}$ . We tested 9 and 11 because conducting our *in vitro* differentiation experiments takes a lot of time, and we would not be able to add more than 4 individuals to our dataset without a considerable investment. We also tested datasets with 20 individuals as an arbitrary large sample, as well as datasets with 3, 5 or 7 individuals as a control, to verify that identifiability indeed improves with the sample size increasing.

### 6.1.2 Generation of artificial datasets

For each of the previously introduced population sizes, we generated 40 artificial datasets, using simulations from the model using the previously estimated parameters (Table 6.1). We drew the individual parameters with independent random effects, as specified in Model (5.3). We added experimental noise to

Parameter	True Value	Initial guess	Unit
<hr/> Population average <hr/>			
$\rho_S^{pop}$	0.612	$\mathcal{U}(-5, 5)$	$d^{-1}$
$\delta_{SC}^{pop}$	0.299	$\mathcal{U}(0, 5)$	$d^{-1}$
$\rho_C^{pop}$	4.82	$\mathcal{U}(-5, 5)$	$d^{-1}$
$\delta_{CB}^{pop}$	5.76	$\mathcal{U}(0, 5)$	$d^{-1}$
$\rho_B^{pop}$	0.259	$\mathcal{U}(-5, 5)$	$d^{-1}$
<hr/> Population variance <hr/>			
$\omega_{\rho_S}^{pop}$	0.118	5	$d^{-1}$
$\omega_{\delta_{SC}}^{pop}$	0.279	5	$d^{-1}$
$\omega_{\rho_C}^{pop}$	0.125	5	$d^{-1}$
$\omega_{\delta_{CB}}^{pop}$	0.0507	5	$d^{-1}$
$\omega_{\rho_B}^{pop}$	0.094	5	$d^{-1}$
<hr/> Error parameters <hr/>			
$b_1$	0.16	1	-
$b_2$	0.16	1	-
$b_3$	0.16	1	-

Table 6.1: Parameter values used to generate the artificial datasets, and calibrate the model on them. The table displays, for each parameter, the true value that was used to generate the *in silico* data, and the initial guess values and distributions used for estimation. The initial guess of the fixed effects are sampled uniformly with respect to each parameter bounds. The initial guess of the variances of the random effects, and of the error parameters, are set to an arbitrary high value to improve the convergence of SAEM in the early phase of the estimation.

## 6.2. Convergence

the individual trajectories, using our proportional error model with  $b = 0.16$  (Table 6.1).

### 6.1.3 Model calibration

For each artificial dataset, we ran the SAEM algorithm implemented in Monolix (Section 1.4.2.1 in this manuscript, and Kuhn and Lavielle, 2005) five times using uniformly drawn initial parameter guesses (Table 6.1).

## 6.2 Convergence

As we saw in the previous chapter, it is not sure that SAEM will converge for a given model and dataset. Since for all datasets, the estimated likelihood values differ from a SAEM run to another, we need a statistical tool in order to select the runs that reached the global likelihood optimum. We used a model selection method based on the Akaike's weights of the runs. We already defined this criterion earlier in the manuscript (Duchesne et al., 2019, Section 2.4, in Chapter 2) and we re-introduced it in Guillemin et al. (2018, section 4.3.3), in Chapter 3 :

$$w_i = \frac{\exp(-(AIC_i - \min(AIC))/2)}{\sum_{j=1}^R \exp(-(AIC_j - \min(AIC))/2)}, \quad (6.1)$$

where  $w_i$  is the Akaike's weight of the  $i$ -th run,  $AIC_i$  is its Akaike's Information Criterion (introduced in Section 1.4.3) and  $R$  is the number of SAEM runs (here  $R = 50$ ). The Akaike's weight of a given model in a given set of models can be seen as the probability that it is the best one among the set (Burnham and Anderson, 2010). In this setting, selecting the convergent SAEM runs means computing their Akaike's weights, sorting them, and keeping only the models whose weights add up to a significance probability (in our case, 95%).

The distributions of the number of convergent runs over the 40 artificial datasets are displayed on Figure 6.1. It shows an overall tendency of convergence to decrease as the population size increases, which is illustrated by the

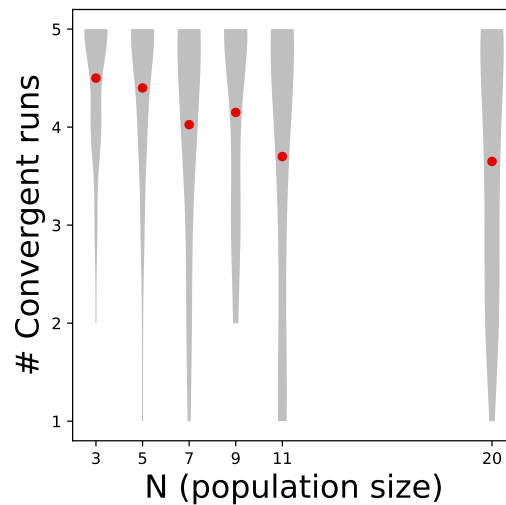


Figure 6.1: Number of convergent runs as a function of population size. The figure displays the violin plots of the distribution of the number of convergent runs of SAEM for the 40 simulated datasets for each population size. Violin plots display the density distribution of a measured variable based on kernel density estimation (Hintze and Nelson, 1998; Matplotlib 3.1.0 documentation, 2019) rather than showing the quantiles of a distribution like boxplots would do. Red dots display the mean of each distribution.

shift in the distribution of Figure 6.1.

This means that SAEM has more and more difficulty to converge as the population size increases. This implies that a proper exploration of the parameter unidentifiabilities would require more SAEM runs if we increased the population size. Conversely, the higher number of convergent runs with the smallest sample sizes indicates that the algorithm can easily reach a global likelihood optimum even with only 3 individuals in the dataset. This might imply that in small samples, an increased parameter uncertainty can result in improved convergence.

We then used the convergent runs of SAEM for each dataset in order to assess the identifiability of the model parameters for each sample size, both at the population and individual scales.

### 6.3. Identifiability of the population parameters

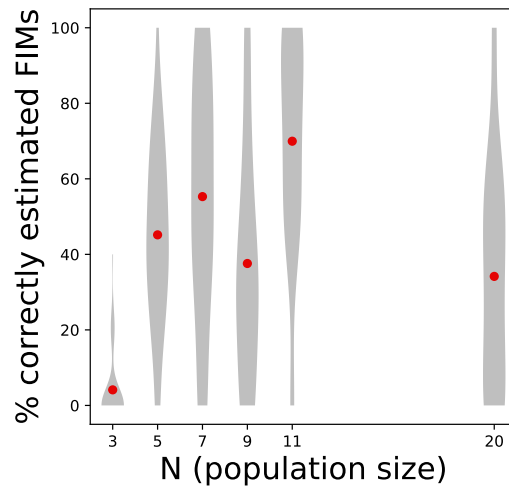


Figure 6.2: Fraction of correctly estimated FIMs as a function of population size. The figure displays the violin plots of the distribution of the SAEM runs for which the FIM could be computed, as a fraction of the convergent runs (Figure 6.1), for the 40 simulated datasets for each population size. Red dots display the mean of each distribution.

## 6.3 Identifiability of the population parameters

### 6.3.1 FIM-based identifiability

We already showed in the previous chapter (Figure 5.3), that even in cases where Monolix converges to the global likelihood optimum, it is not always able to compute the FIM. A failed attempt at computing the FIM usually results from parameters with infinite standard-errors.

With our artificial datasets, we display the fraction of the convergent runs for which the FIM could be computed in Figure 6.2. Even with  $N = 20$ , Monolix often fails at computing the FIM, which is a sign of parameter unidentifiabilities. However, since the largest populations are also associated to the poorest convergence (Figure 6.1), this result might also be due to the decreased number of convergent runs at high population sizes.

The various FIM-based design-criteria introduced in System (1.5), computed with our artificial datasets, are displayed in Figure 6.3. These FIM-based

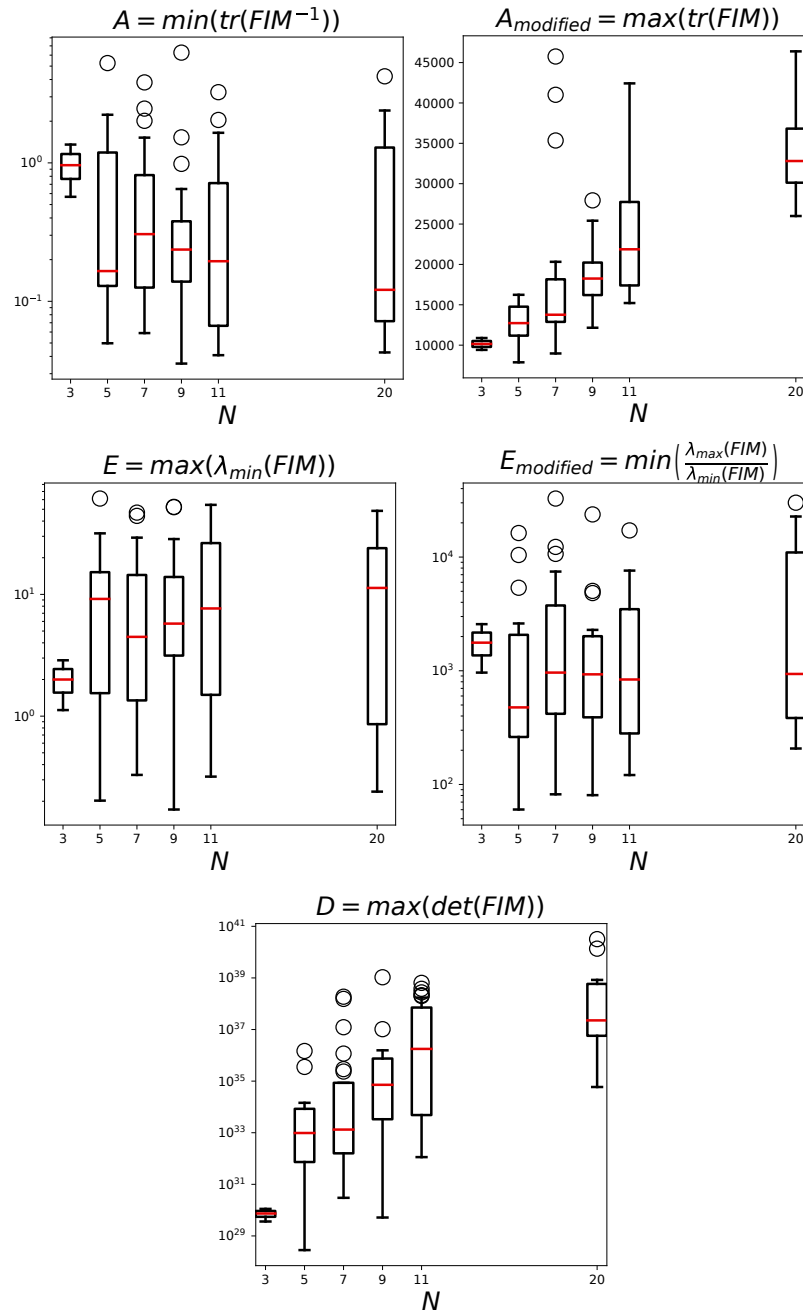


Figure 6.3: FIM-based identifiability criteria as a function of population size. Each panel displays the boxplots of a FIM-based identifiability criterion introduced in Equation (1.5) for the 40 simulated datasets for each population size. Criteria were computed based on the FIM of the best-likelihood SAEM run for each simulated dataset.

## 6.4. Identifiability of the individual parameters

criteria are not consistent between themselves, as increasing the population size does improve some of them (namely  $D$  and  $A_{modified}$ ) while for the others, this tendency is much weaker. This means that even with  $N = 20$ , we would not be sure to optimize these design criteria.

Since this can be due to the poor estimation of the FIM, as well as to a lack of identifiability of the population parameters, we decided to investigate the population parameters identifiability through other means.

### 6.3.2 Population parameter values.

The distributions of estimated population parameters in our artificial datasets are displayed in Figure 6.4. It shows that we cannot be sure to correctly estimate the model parameters even with 20 individuals in our data. Especially, only  $\rho_S^{pop}$  (Figure 6.4A) and  $\omega_{\rho_S}$  (Figure 6.4B) are estimated correctly with  $N = 20$ , in the sense that the average estimated values over all datasets are correct, and that their variances are relatively small. For all the other population parameters, either the variance of the estimated values are too high (Figure 6.4C), or there is a bias in the average parameter estimate over all datasets. For instance,  $\rho_B^{pop}$  is estimated in most cases with a negative value while the datasets were generated with a positive value (Figure 6.4D).

## 6.4 Identifiability of the individual parameters

Figure 6.5 displays the distributions  $\eta$ -shrinkage over all artificial datasets. It shows that even with  $N = 20$  the shrinkage remains higher than 30% in most datasets for  $\rho_C$ ,  $\delta_{CB}$  and  $\rho_B$ . This is the sign that individual parameters are not sufficiently constrained by the data, and are thus mostly determined by the population distribution.

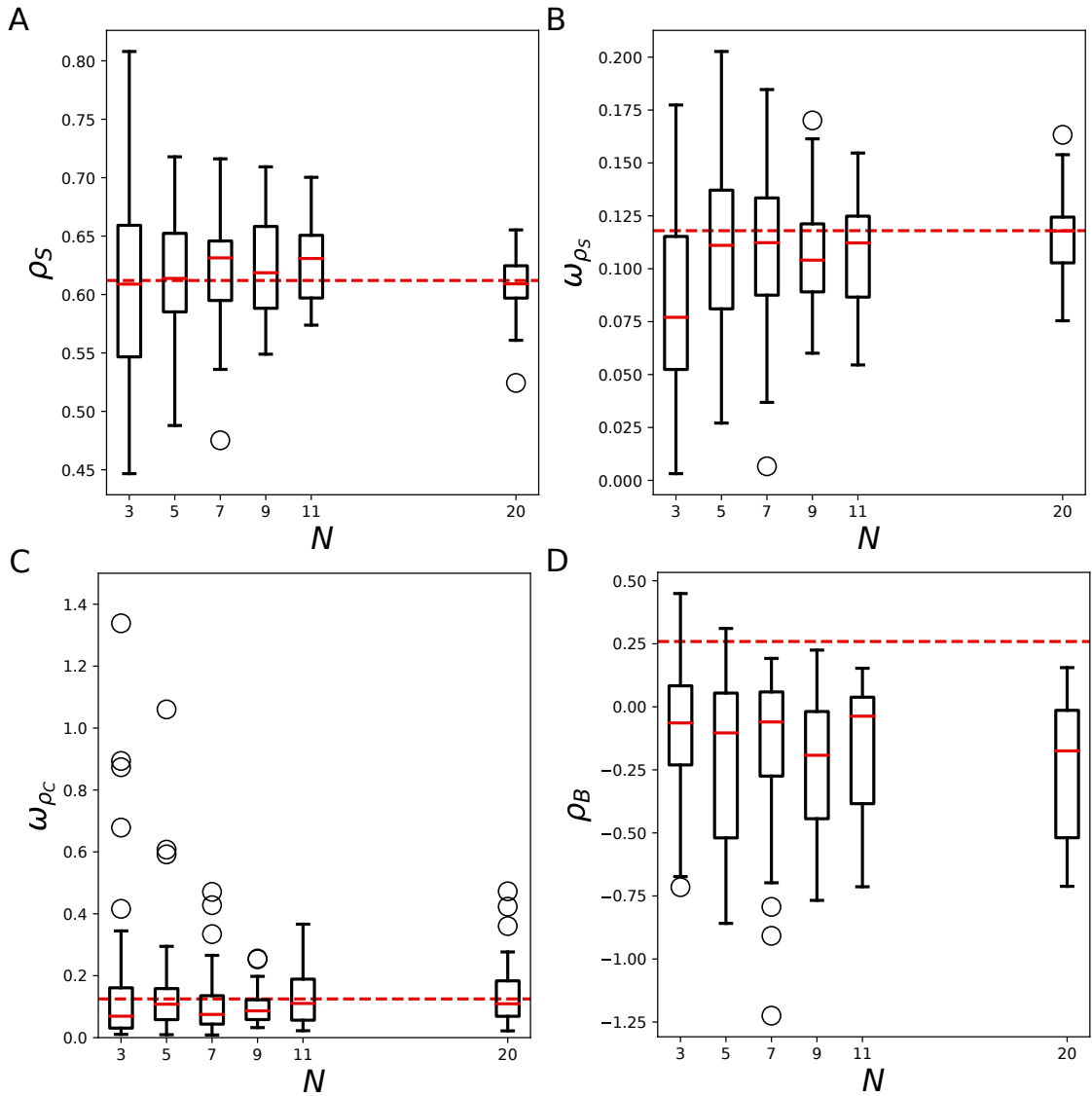


Figure 6.4: Estimated population parameters as a function of population size. The figure displays the boxplots of the estimated population parameter values with the 40 simulated datasets, as a function of population size, for  $\rho_S^{pop}$  (A),  $\omega_{\rho_S}$  (B),  $\omega_{\rho_C}$  (C) and  $\rho_B$  (D). Estimated parameter values are the average of the estimated parameter values over convergent runs, expressed in  $d^{-1}$ . The dashed red line indicates the parameter values used for generating the data.

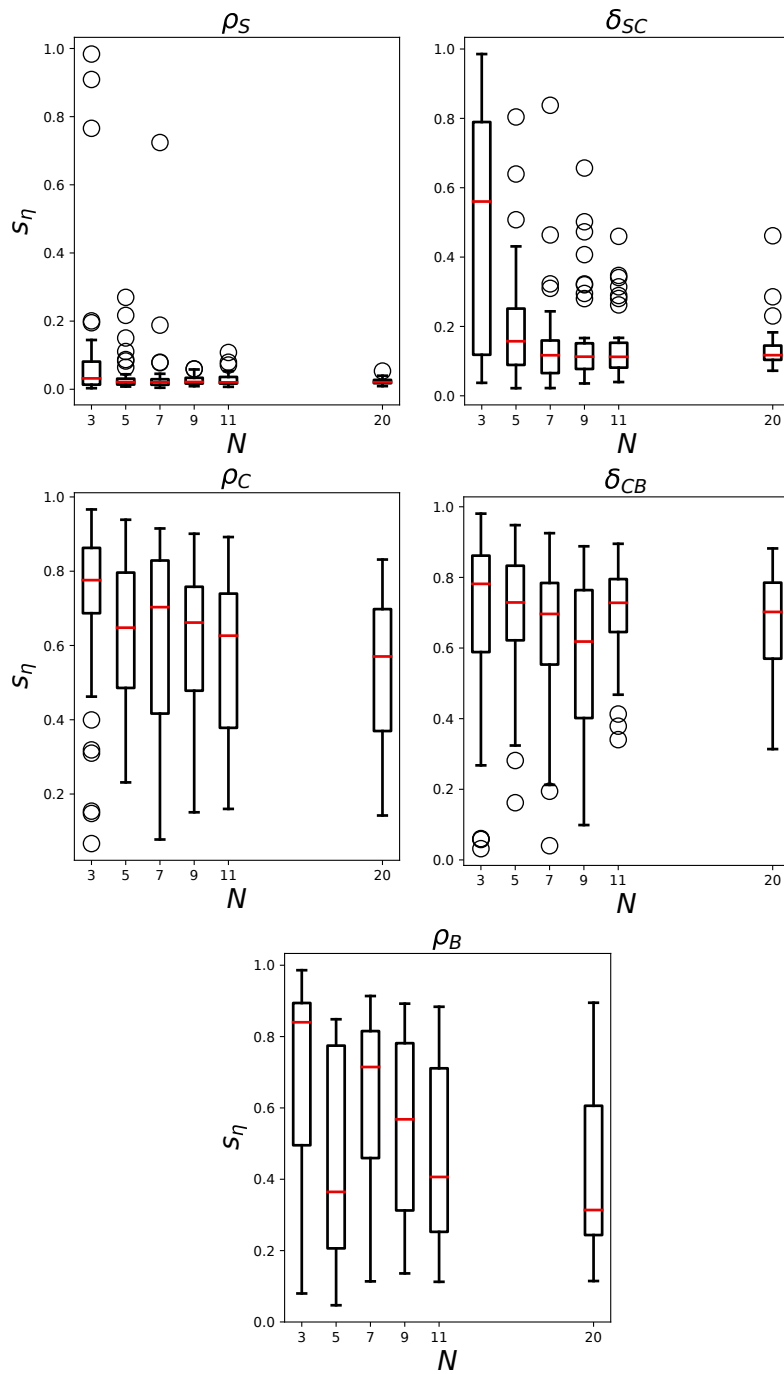


Figure 6.5:  $\eta$ -shrinkage as a function of population size. The figure displays the boxplots of  $s_\eta$  for the 40 simulated datasets for each population size. Shrinkage was computed using the SAEM run with the best-likelihood for each dataset.

## 6.5 Conclusion

In this chapter, we generated *in silico* datasets of varying sizes to investigate the ability of Monolix to identify the parameter values of our model. We showed that it was not possible to make our model identifiable, even by increasing the population size to 20 individuals, both at the level of population and individual parameters.

At the population scale, it seems that only  $\rho_S^{pop}$  and  $\omega_{\rho_S}$  might be estimated reliably by increasing the sample size, but they were already identifiable with our initial dataset (Chapter 5). Depending on the simulated dataset, the other parameters may or may not be correctly estimated, which suggests that increasing the population size might make the model identifiable. This would depend on the relevance of our model in terms of microscopic mechanisms (A. White et al., 2016).

At the individual scale, the  $\eta$ -shrinkage remains high even at the highest population size, which means that the individual parameters cannot be estimated correctly, since they were generated without shrinkage. This is not surprising, since Xu et al. (2012) showed that shrinkage does not directly depend on the population size.

As a consequence, we cannot assert that adding new individuals to our dataset will make the model identifiable, even if some of our simulated datasets did render the right parameter values upon estimation. In Section 5.5, we suggested model reduction as another solution to make a model identifiable. It will thus be the subject of the next chapter.

# Chapter 7

## Reduction procedure in mixed effect models

### 7.1 Introduction

In Chapter 5, we defined a MEM for the *in vitro* erythropoiesis which we proved to be unidentifiable. In Section 5.5, we presented two solutions to make it identifiable. The first one was to use the model to optimize the design of the experiments and perform new, more informative, experiments. It was presented in Chapter 6. In this chapter, we focus on the other option: reducing the number of model parameters in order to make their estimation easier.

Starting from the model defined in System (5.3) (which we will refer to as the *full model*), we will explore the correlations between population parameters estimates to ease their estimation. Then, we will measure the shrinkage of individual parameters to assess which random effects are the least important in determining the model output. This method will allow us to iteratively remove parameters from the model until they can all be estimated reliably, both at the population and individual scales.

## 7.2 Initial estimation of parameter values of the full model

In Section 1.4.4, we presented our approach for assessing the identifiability of the population parameters of the model, based on the random sampling of the initial parameter values:

1. We perform a random sampling of the initial parameter guesses, which provides us a sample of optimal parameter values.
2. We assess the convergence of the algorithm: we only want to consider the SAEM runs which reached the global optimum.
3. We compare the parameter values of these convergent runs. If they are not the same, then the model is unidentifiable (several different parameter values give the same likelihood). If they are, then we conclude that the model is identifiable.

### 7.2.1 Convergence over 50 SAEM runs

Figure 7.1 displays the likelihoods of 50 runs of the SAEM algorithm on the model defined in System (5.3). All the likelihood values differ from the optimal one by less than three units, which is a very small variation. For instance, the significance threshold of a Likelihood-ratio test (Section 1.4.3) for such a model with 13 parameters would be  $\chi^2(0.95, 13) = 22$  likelihood units, which means that we can reasonably consider that all these likelihood values are the same. Then, all of the 50 SAEM runs reached an equivalent likelihood optimum.

### 7.2.2 Population parameters

The distributions of estimated population parameter values in the 50 runs are represented in Figure 7.2. As we already exposed in Section 5.4,  $\rho_S^{pop}$ ,  $\omega_{\rho_S}$  and the three error parameters  $b_1$ ,  $b_2$  and  $b_3$  are estimated with the smallest

## 7.2. Initial estimation of parameter values of the full model

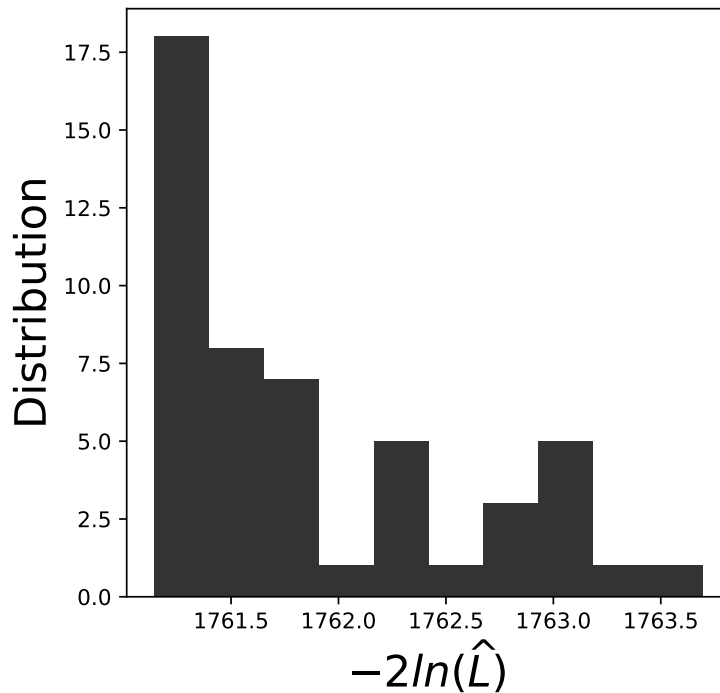


Figure 7.1: Likelihood distribution over 50 SAEM runs on the full model.

variance. For any of the other 8 parameters, the estimated values display more or less variance. For these parameters, the estimation is less reliable.

Figure 7.3 displays the value of Spearman's  $\rho^2$  for each pair of these 8 unidentifiable parameters. Spearman's  $\rho^2$  is a measure of the nonlinear correlation between two variables. There is a high correlation between  $\delta_{SC}^{pop}$ ,  $\rho_C^{pop}$  and  $\delta_{CB}^{pop}$  in our convergent runs, which is represented in Figure 7.4.

These results show that the optimal values of  $\delta_{SC}^{pop}$ ,  $\rho_C^{pop}$  and  $\delta_{CB}^{pop}$  are strongly correlated in the range of values of Figure 7.4. This range corresponds to the range of estimated values in the 50 SAEM runs. The correlations suggest that if we would replace two of these parameters by their expression as a function of the third one, we would also reduce the number of population parameters to estimate, and still allow them to reach their optimal value.

We found the following expressions for the correlations (Figure 7.4):

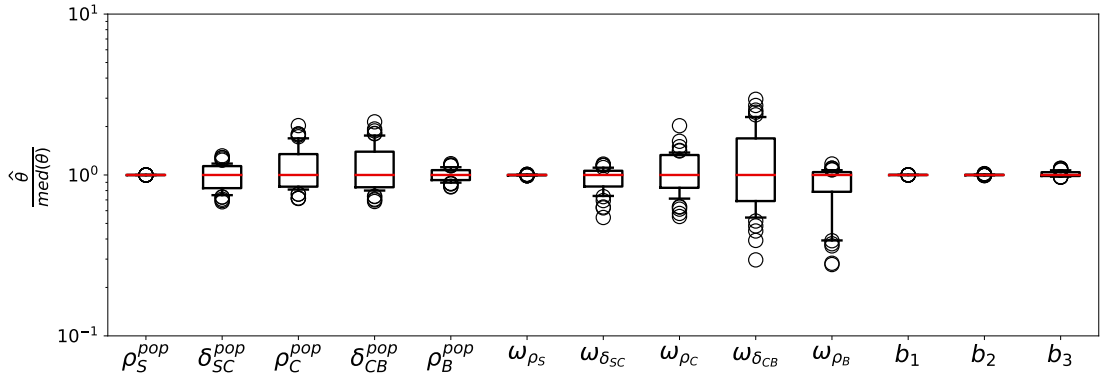


Figure 7.2: Normalized parameter values in the 50 runs of SAEM for the full model. Displayed are the distributions of estimated parameter values, normalized by their median.

$$\delta_{SC}^{pop} = 0.15 + \frac{1.2}{(\rho_C^{pop})^{1.3}}, \quad (7.1)$$

and

$$\delta_{CB}^{pop} = 1.3\rho_C^{pop} - 0.5. \quad (7.2)$$

We thus conclude that if we replace  $\delta_{SC}^{pop}$  and  $\delta_{CB}^{pop}$  by their expression as a function of  $\rho_C^{pop}$  in the model, it might help the estimation. Yet, such a reduction might affect the convergence of SAEM because the correlation might not hold outside of the parameter range of Figure 7.4. We define this reduced model and assess its identifiability in the next section.

### 7.3 Model with reduced $\delta_{SC}^{pop}$ and $\delta_{CB}^{pop}$

Replacing  $\delta_{SC}^{pop}$  and  $\delta_{CB}^{pop}$  in System (5.3) by their expression as a function of  $\rho_C^{pop}$  from Equations (7.1) and (7.2), we obtain the following reduced model:

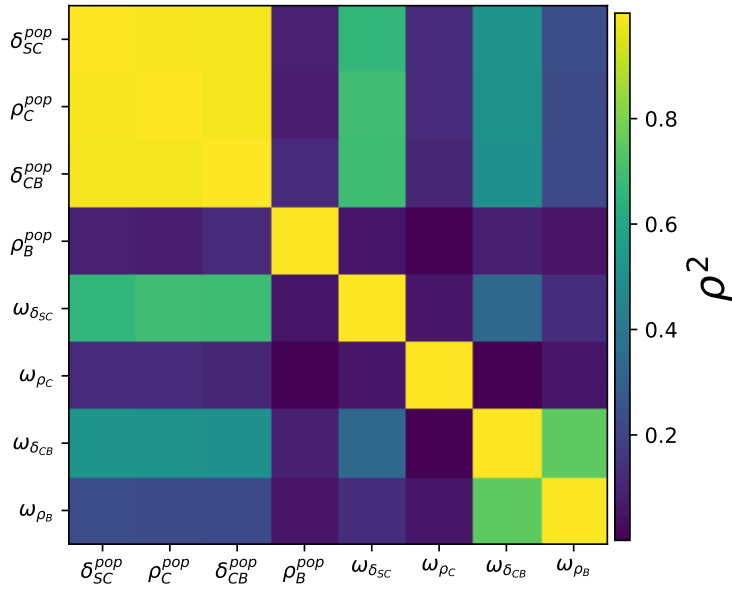


Figure 7.3: Correlation heatmap (Spearman's  $\rho^2$ ) of the 8 unidentifiable population parameters in the 50 runs of SAEM for the full model.

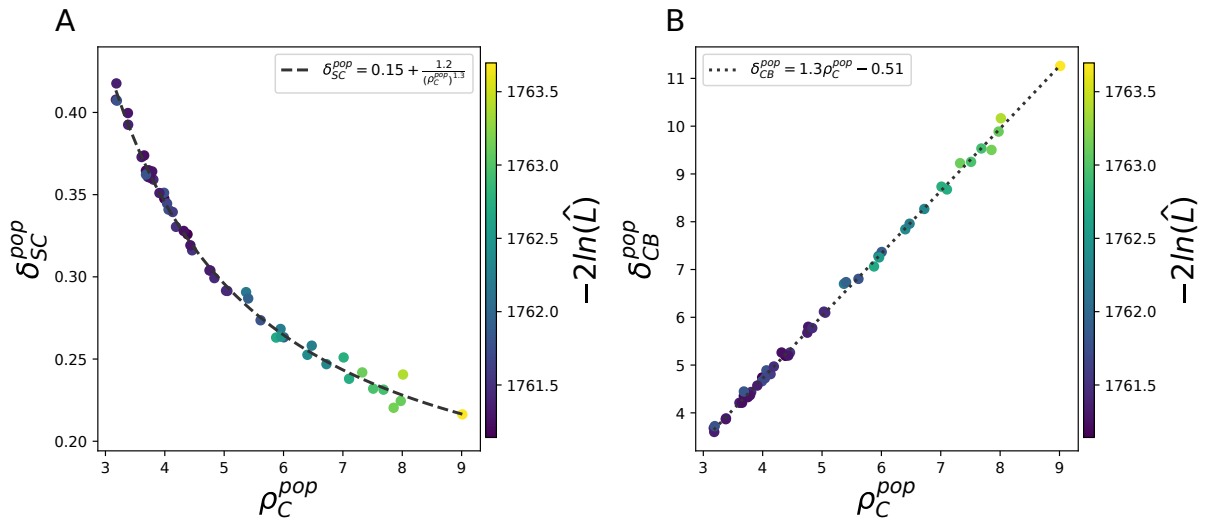


Figure 7.4: Correlations between population parameters in the full model. A: Nonlinear correlation between  $\delta_{SC}^{pop}$  and  $\rho_C^{pop}$ . B: Linear correlation between  $\delta_{CB}^{pop}$  and  $\rho_C^{pop}$ . Displayed are the estimated population parameter values over the 50 runs of SAEM, color-coded by likelihood. We also display the regression lines defined by Equations (7.1) and (7.2).

$$\begin{cases} \rho_S & \hookrightarrow \mathcal{N}(\rho_S^{pop}, \omega_{\rho_S}), \\ \delta_{SC} & \hookrightarrow \log\mathcal{N}\left(0.15 + \frac{1.2}{(\rho_C^{pop})^{1.3}}, \omega_{\delta_{SC}}\right), \\ \rho_C & \hookrightarrow \mathcal{N}(\rho_C^{pop}, \omega_{\rho_C}), \\ \delta_{CB} & \hookrightarrow \log\mathcal{N}(1.3\rho_C^{pop} - 0.5, \omega_{\delta_{CB}}), \\ \rho_B & \hookrightarrow \mathcal{N}(\rho_B^{pop}, \omega_{\rho_B}), \end{cases} \quad (7.3)$$

in which we removed two fixed effects from the estimation problem, without modifying the definition of the random effects. Although the typical values of  $\delta_{SC}$  and  $\delta_{CB}$  in the population are now related to the value of  $\rho_C^{pop}$ , their individual random effects are still independent. This means that the model still comprises 5 population variances that we have to estimate. In total, the model has 11 population parameters (3 fixed effects, 5 standard deviations, and the 3 error parameters that were unaffected by the reduction).

### 7.3.1 Convergence over 50 SAEM runs

Following the same approach as for the *full model*, we ran the SAEM algorithm on this model 50 times using uniformly sampled initial guesses for the population parameters. The resulting optimal likelihood distribution is displayed on Figure 7.5A. Most of the runs reached the same likelihood optimum as in the previous model (Figure 7.1), but 11 of them found higher likelihood values.

Since all the estimated likelihood values are different, we need a statistical tool in order to select the runs that reached the global likelihood optimum. As in the previous chapter, we used the Akaike's weights of the runs, which we defined in Equation (6.1).

In the case of our reduced model, Akaike's weights select only 37 runs as the best ones (Figure 7.5B), that we will consider as the runs that reached the global likelihood optimum.

### 7.3. Model with reduced $\delta_{SC}^{pop}$ and $\delta_{CB}^{pop}$

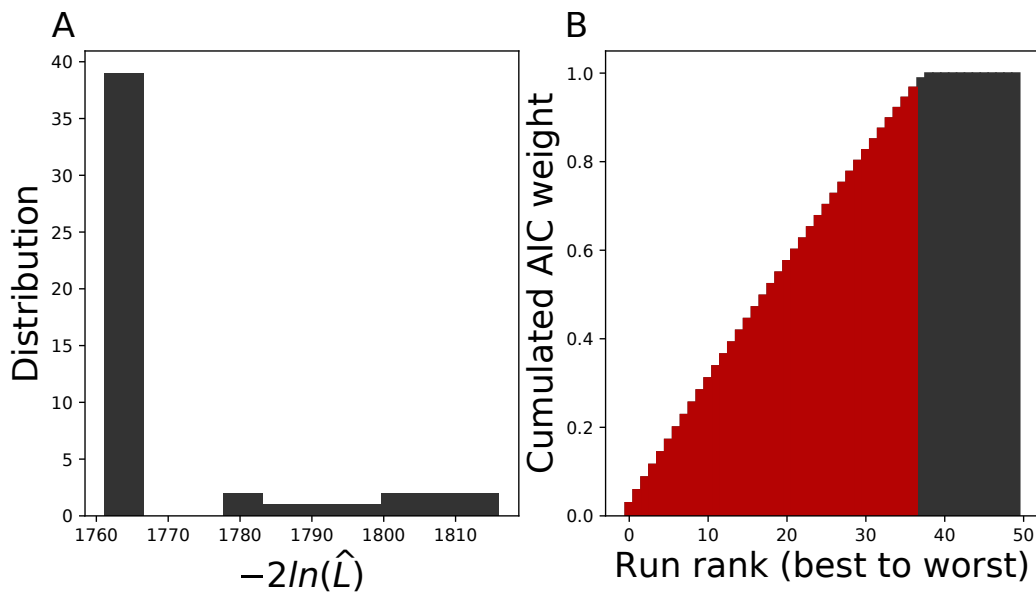


Figure 7.5: Likelihood distribution over 50 SAEM runs on the model with reduced  $\delta_{SC}^{pop}$  and  $\delta_{CB}^{pop}$ . (A) and the corresponding cumulated AIC weights (B). The 37 runs associated to the lowest likelihood values (*i.e.* those that add up to 95% of the total weight of the 50 runs) are coloured in red.

#### 7.3.2 Population parameters

The parameter values estimated in these 37 runs are displayed on Figure 7.6. First, it shows that the reduction of the model did not affect the accuracy of the estimation for the five parameters that were identifiable in the *full model*. Then, the population means  $\rho_C^{pop}$  and  $\rho_B^{pop}$  are estimated more precisely in the reduced model (7.3) than in the *full model*. However the three standard deviations  $\omega_{\rho_C}$ ,  $\omega_{\delta_{CB}}$  and  $\omega_{\rho_B}$  are still estimated with some variability.

Figure 7.7A displays Spearman's correlation coefficient  $\rho^2$  for each pair of the parameters that were unidentifiable in the *full model*. It shows that our reduction approach successfully removed all correlations from the model, except a weak one between  $\omega_{\rho_B}$  and  $\omega_{\delta_{CB}}$ , that was already present in the *full model* (Figure 7.3). Figure 7.7B shows that there is indeed a linear, negative correlation between the two parameters.

Since  $\omega_{\rho_C}$ ,  $\omega_{\delta_{CB}}$  and  $\omega_{\rho_B}$  define the distributions of three random effects,

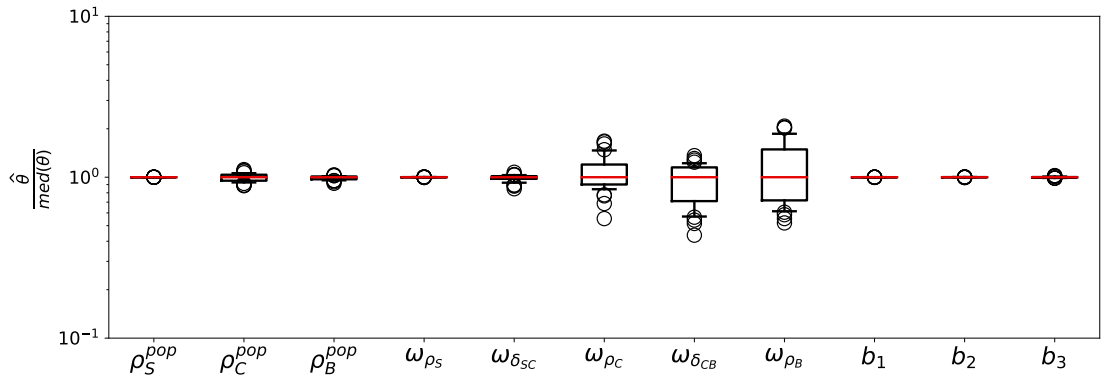


Figure 7.6: Estimated parameter values in the 37 convergent runs of SAEM for the model with reduced  $\delta_{SC}^{pop}$  and  $\delta_{CB}^{pop}$ . Displayed are the distributions of estimated parameter values, normalized by their median.

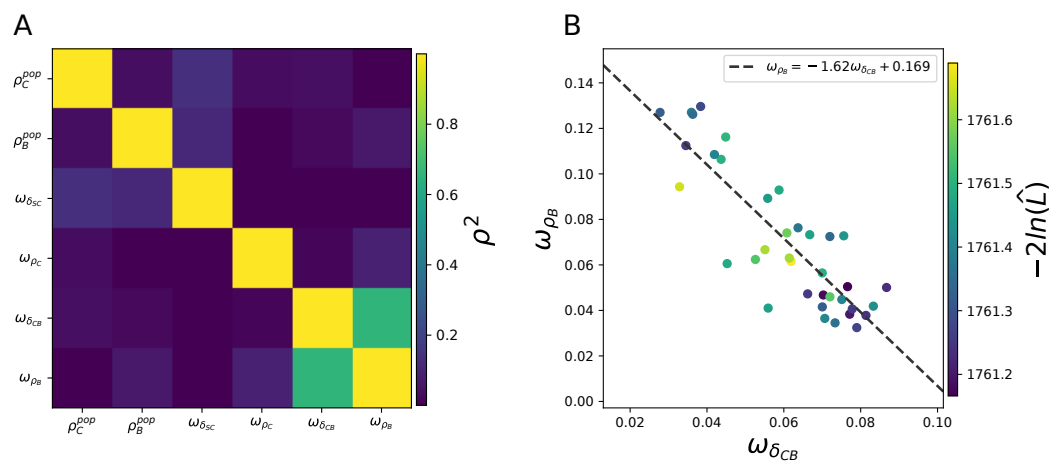


Figure 7.7: Correlations between population parameters in the model with reduced  $\delta_{SC}^{pop}$  and  $\delta_{CB}^{pop}$ . A: Correlation heatmap (Spearman's  $\rho^2$ ) of the population parameters in the 37 convergent runs of SAEM. B: Negative linear correlation between  $\omega_{\rho_B}$  and  $\omega_{\delta_{CB}}$  ( $r^2 = 0.73$ ).

### 7.3. Model with reduced $\delta_{SC}^{pop}$ and $\delta_{CB}^{pop}$

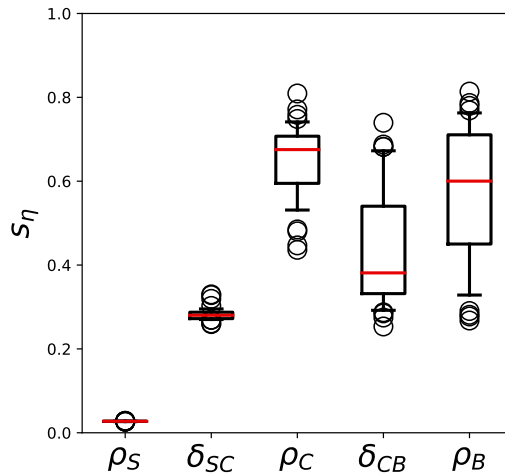


Figure 7.8: Distribution of  $s_\eta$  values for the individual parameters in the 37 convergent runs of SAEM.

their unidentifiability might indicate an overparameterization of the random effects. We investigate this using the  $\eta$ -shrinkage (cf. Section 1.4.4) of the individual random effects in the next section.

#### 7.3.3 Individual random effects

The shrinkage of the individual random effects in the 50 SAEM runs is displayed on Figure 7.8. The values of shrinkage for  $\rho_C$ ,  $\delta_{CB}$  and  $\rho_B$  range from 30 to 80% depending on the run, which indicates a clear discordance between the population distribution of the parameters and the actual distribution of the individual parameters. We thus conclude that the individual data are not informative enough to estimate all random effects for each individual.

We conclude that our first reduction step improved the estimation of the fixed effects, but that neither the individual values of the random effects nor their variance are identifiable. As a solution for the overparameterization of the individual random effects, we propose to further reduce our model by removing one of them. Since  $\rho_C$  shows the highest average shrinkage among the 37 convergent runs of SAEM, we will remove its random effect first.

## 7.4 Model with reduced $\delta_{SC}^{pop}$ , $\delta_{CB}^{pop}$ and a fixed $\rho_C$

Removing the individual effect on  $\rho_C$  in our previous model leads to a model with one constant parameter over the population:

$$\begin{cases} \rho_S & \hookrightarrow \mathcal{N}(\rho_S^{pop}, \omega_{\rho_S}), \\ \delta_{SC} & \hookrightarrow \log\mathcal{N}\left(0.15 + \frac{1.2}{(\rho_C^{pop})^{1.3}}, \omega_{\delta_{SC}}\right), \\ \rho_C & = \rho_C^{pop}, \\ \delta_{CB} & \hookrightarrow \log\mathcal{N}(1.3\rho_C^{pop} - 0.5, \omega_{\delta_{CB}}), \\ \rho_B & \hookrightarrow \mathcal{N}(\rho_B^{pop}, \omega_{\rho_B}), \end{cases} \quad (7.4)$$

which has 10 parameters in total (the 3 fixed effects, 4 standard-deviations for the random effects, and 3 error parameters). We followed the same approach as for the previous models when estimating the parameters of System (7.4).

### 7.4.1 Convergence over 50 SAEM runs

The distribution of the estimated likelihood values over 50 runs of the SAEM algorithm, and the corresponding AIC weights, are displayed on Figure 7.9. Among the 50 runs, 40 seem to have reached the same likelihood optimum, while the 10 others reached local optima at higher likelihood values. The AIC weights select the 38 first models among the 40, and we will consider in the following that these 38 runs are those that converged to the global likelihood optimum.

### 7.4.2 Population parameters

The estimated parameter values in the convergent SAEM runs are displayed in Figure 7.10. Among the remaining parameters of the model, only  $\omega_{\delta_{CB}}$  and  $\omega_{\rho_B}$  show some level of variability, with some parameter values being estimated as far as 80% from the median of the distribution. The other parameters of the

7.4. Model with reduced  $\delta_{SC}^{pop}$ ,  $\delta_{CB}^{pop}$  and a fixed  $\rho_C$

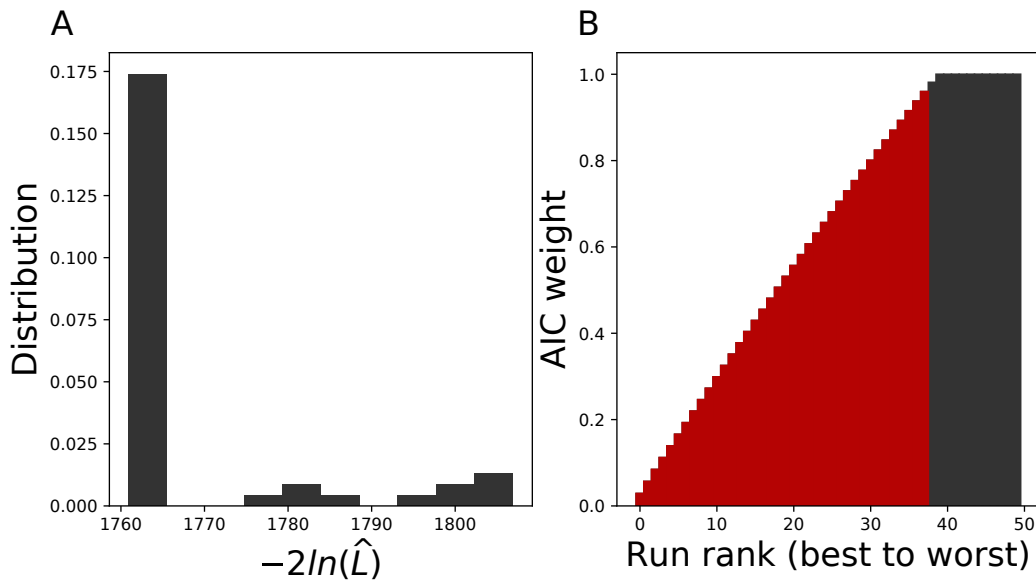


Figure 7.9: Likelihood distribution over 50 SAEM runs on the model with reduced  $\delta_{SC}^{pop}$ , and  $\delta_{CB}^{pop}$ , and no variability on  $\rho_C$ . (A) and the corresponding cumulated AIC weights (B). The 38 runs associated to the lowest likelihood values (*i.e.* those that add up to 95% of the total weight of the 50 runs) are coloured in red.

model are estimated at the same value for all the runs. The correlation coefficients between parameter pairs are displayed on Figure 7.11A. The negative correlation between  $\omega_{\delta_{CB}}$  and  $\omega_{\rho_B}$ , which was already present in the previous models, is stronger in this reduced model (Figure 7.11B). It seems impossible to estimate both variances from the data, because when one variance is estimated far from 0 then the other one shrinks towards 0 and vice-versa. Moreover, the runs associated to the lowest log-likelihoods are those where the two variances are the most different, with one variance being 4 to 7 times higher than the other one.

Since it is possible to keep the log-likelihood minimal while lowering the value of one of the two variances, it seems that the model is still overparameterized and that we might remove one more random effect in order to make it identifiable.

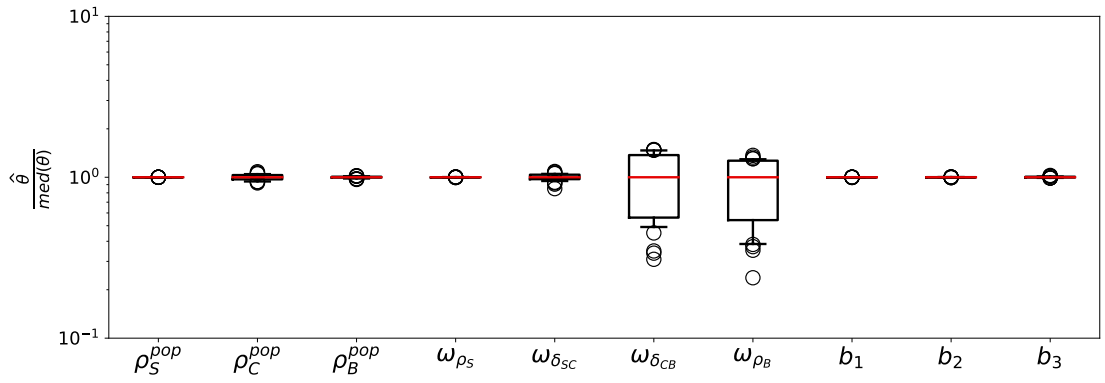


Figure 7.10: Estimated parameter values in the 38 convergent runs of SAEM for the model with reduced  $\delta_{SC}^{pop}$  and  $\delta_{CB}^{pop}$ , and no variability on  $\rho_C$ . Displayed are the distributions of estimated parameter values, normalized by their median.

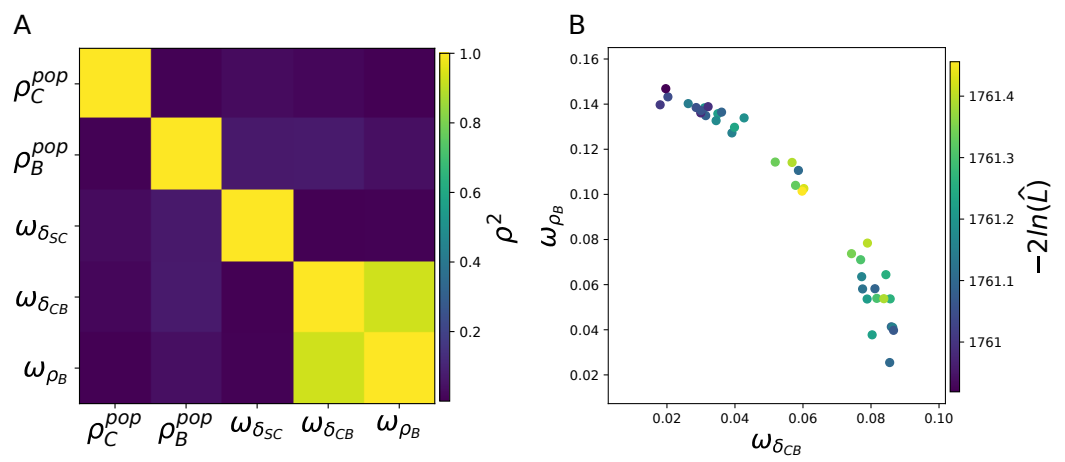


Figure 7.11: Correlations in the model with reduced  $\delta_{SC}^{pop}$  and  $\delta_{CB}^{pop}$ , and no variability on  $\rho_C$ . A: Correlation heatmap (Spearman's  $\rho^2$ ) of the population parameters in the 38 convergent runs of SAEM. B: Negative correlation between  $\omega_{\rho_B}$  and  $\omega_{\delta_{CB}}$ .

#### 7.4. Model with reduced $\delta_{SC}^{pop}$ , $\delta_{CB}^{pop}$ and a fixed $\rho_C$

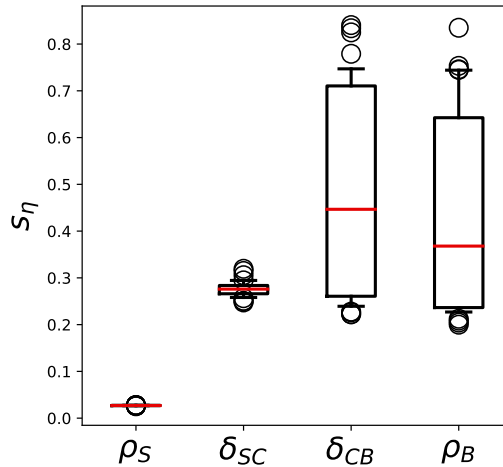


Figure 7.12: Distribution of  $s_\eta$  values for the individual parameters in the 38 convergent runs of SAEM.

### 7.4.3 Individual parameters

We investigated this overparameterization using the shrinkage of the remaining random effects (Figure 7.12), which indeed shows that  $\delta_{CB}$  and  $\rho_B$  are associated to more than 30% of shrinkage. We thus conclude that this reduced model is still unidentifiable, and we propose to remove one more random effect from it.

Since  $\delta_{CB}$  displays the largest shrinkage on average, it would seem reasonable to remove its random effect rather than the one of  $\rho_B$ . However,  $\delta_{CB}$  is involved in the dynamics of both the committed and the differentiated cells in the model (Chapter 2, and Equation (3) in Duchesne et al., 2018), while  $\rho_B$  can only influence the number of differentiated cells. Thus, we hypothesize that varying  $\delta_{CB}$  instead of  $\rho_B$  in the population might result in more flexibility for the individual fits. We test the reduced model where we remove the variability on  $\rho_B$  in the next section.

## 7.5 Final model with reduced $\delta_{SC}^{pop}$ , $\delta_{CB}^{pop}$ , and fixed $\rho_C$ and $\rho_B$

Removing the individual effect on  $\rho_B$  in our previous model leads to a model with one more constant parameter:

$$\begin{cases} \rho_S & \hookrightarrow \mathcal{N}(\rho_S^{pop}, \omega_{\rho_S}), \\ \delta_{SC} & \hookrightarrow \log\mathcal{N}\left(0.15 + \frac{1.2}{(\rho_C^{pop})^{1.3}}, \omega_{\delta_{SC}}\right), \\ \rho_C & = \rho_C^{pop}, \\ \delta_{CB} & \hookrightarrow \log\mathcal{N}(1.3\rho_C^{pop} - 0.5, \omega_{\delta_{CB}}), \\ \rho_B & = \rho_B^{pop}, \end{cases} \quad (7.5)$$

which has 9 parameters in total (the 3 fixed effects, 3 standard-deviations for the random effects, and the 3 error parameters).

### 7.5.1 Convergence over 50 SAEM runs

Figure 7.13 displays the distribution of the estimated likelihoods and the corresponding Akaike's weights over 50 runs of the SAEM algorithm. The best 26 runs reached likelihood values that are very close to the optimal one. The other likelihood optima are spread across several dozens likelihood units. Akaike's weights select the best 25 runs, and we will consider these runs as those that reached the global likelihood optimum in the following.

However, as we remove more and more parameters from the *full model*, it seems harder to be sure of the convergence of the algorithm, since we find fewer runs in the global optimum with this model than with the previous ones. This might prove critical for applying this approach to other models, as will be discussed later (Section 8.3).

### 7.5. Final model with reduced $\delta_{SC}^{pop}$ , $\delta_{CB}^{pop}$ , and fixed $\rho_C$ and $\rho_B$

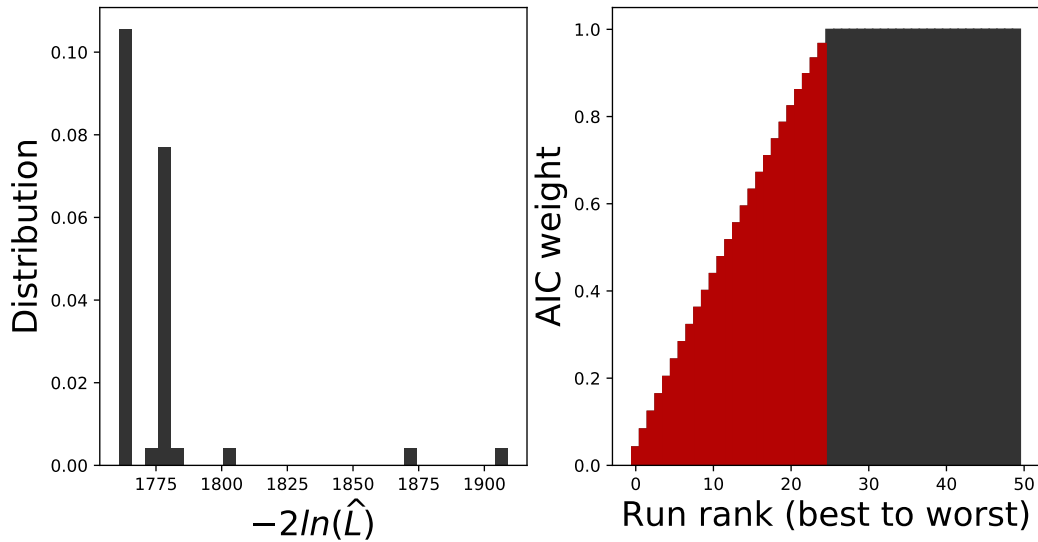


Figure 7.13: Likelihood distribution over 50 SAEM runs on the model with reduced  $\delta_{SC}^{pop}$ , and  $\delta_{CB}^{pop}$ , and no variability on  $\rho_C$  and  $\rho_B$ . (A) and the corresponding cumulated AIC weights (B). The 25 runs associated to the lowest likelihood values (*i.e.* those that add up to 95% of the total weight of the 50 runs) are coloured in red.

#### 7.5.2 Population parameters

The normalized values of the population parameters in the convergent runs are displayed in Figure 7.14, showing that in this model, all the population parameter values are estimated precisely. This proves that our reduction approach led successfully to the design of a model where all the parameters can be estimated with a single value.

#### 7.5.3 Individual parameters

We computed the shrinkage of the individual parameters in the convergent runs to verify the agreement of the population parameter distributions (estimated with the population parameters) with the distribution of estimated individual parameter values. The three parameters  $\rho_S$ ,  $\delta_{SC}$  and  $\delta_{CB}$  respectively showed an average shrinkage of 3%, 28% and 21% (Figure 7.15), with very

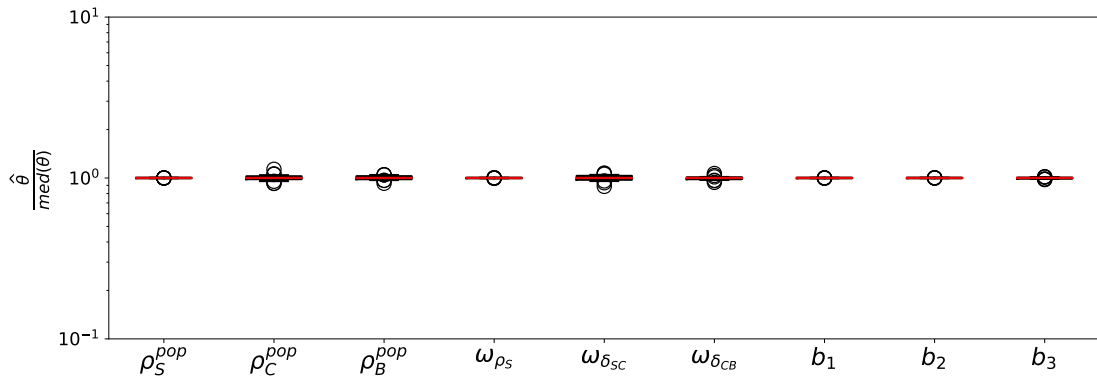


Figure 7.14: Normalized parameter values in the 25 convergent runs of SAEM for the model with reduced  $\delta_{SC}^{pop}$  and  $\delta_{CB}^{pop}$ , and no variability on  $\rho_C$  and  $\rho_B$ . Displayed are the distributions of estimated parameter values, normalized by their median.

small variations between the convergent SAEM runs (the most variable shrinkage is the one on  $\delta_{SC}$ , which varies between 26% and 32% depending on the run). This corresponds to a much lower shrinkage than in the previous models, which is the sign that the data contain enough information for the model to sample the individual parameters across the whole population distribution.

Now that we verified the accuracy of the estimation for both the population and the individual parameters of the reduced model, we verify that it is still able to fit the data.

### 7.5.4 Quality of the fit

Since the global minimum of the log-likelihood was not affected by the reduction (Figures 7.1, 7.5A, 7.9A and 7.13A), the fit of the model to the data should not be worsened. The individual observation/prediction diagram of the reduced model defined in System (7.5) is displayed in Figure 7.16, which shows that the model is able to faithfully reproduce the behaviour of each individual in the population.

## 7.6. Discussion

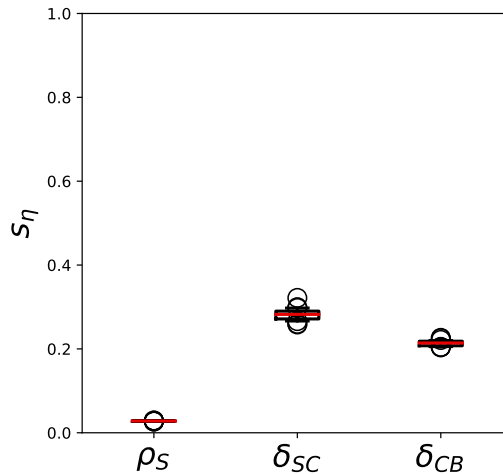


Figure 7.15: Distribution of  $s_\eta$  values for the individual parameters in the 25 convergent runs of SAEM.

## 7.6 Discussion

### 7.6.1 Parameter values in the final model

The absolute parameter values estimated in the 25 convergent runs of SAEM for the final model of System (7.5) are displayed in Figure 7.17. The average proliferation rate  $\rho_S^{pop}$  is estimated at  $0.61 d^{-1}$ . The doubling time of the self-renewing cells (*i.e.* the time it would take to double their population in the absence of proliferation) is thus  $27 h$  in the average experiment. The average experiment is the predicted outcome of the model with individual parameters chosen equal to their population average. Proliferation in the committed compartment is much faster ( $\rho_C^{pop} = 4.0 d^{-1}$ ), which gives the committed cells a doubling time of  $4 h$ . Even though T2EC cells are known to proliferate faster in the differentiation medium than in the self-renewal medium (Gandrillon et al., 1999), such a difference in proliferation times is rather intriguing. However, the quality of the fit of our reduced model (Figure 7.16) and the reliability of our parameter estimates (Figure 7.17) seem to indicate that the parameters of the model are well estimated.

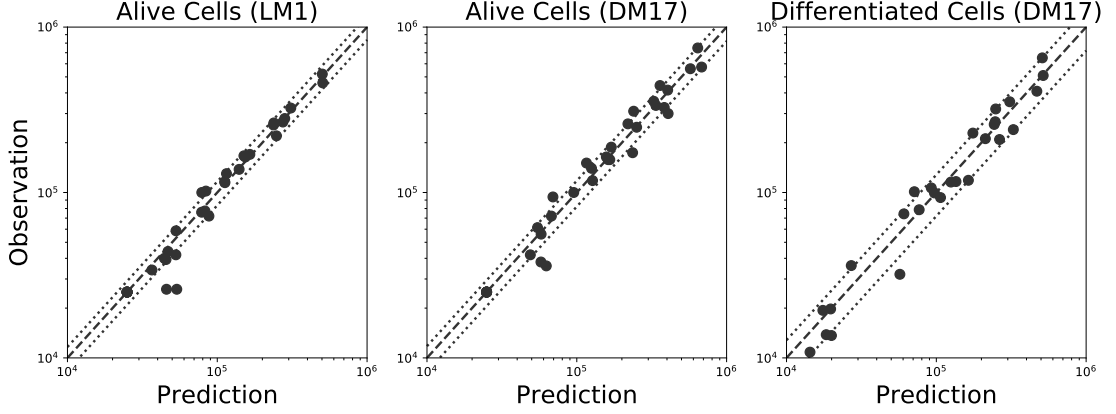


Figure 7.16: Observation/Prediction Diagram of the reduced model. Displayed are the individual data and prediction from the individual parameters estimates in the SAEM run with the lowest log-likelihood. The dashed line is the diagonal. Dotted lines represent one standard deviation of the error model.

Moreover,  $\rho_B^{pop}$  is estimated at  $0.25 d^{-1}$ , giving the differentiated cells a doubling time of  $66 h$ . This means that their proliferation is almost invisible at the timescale of the experiments, as might be expected from differentiated cells.

From Equation (7.1), the value of  $\rho_C^{pop}$  sets  $\delta_{SC}^{pop}$  to  $0.35 d^{-1}$ . The half-life of the self-renewing cells (*i.e.* the time it would take to differentiate half of the population in the absence of proliferation) is thus  $48 h$ . Respectively, from Equation (7.2),  $\delta_{CB}^{pop}$  is estimated at  $4.8 d^{-1}$ , which gives the committed cells a half-life of  $3.6 h$  in the average experiment.

Apart from this average behaviour, three parameters of the final model can vary across the population (Figure 7.18), and are estimated at different values for each individual experiment. The first one is  $\rho_S$ , which has the estimated variance  $\omega_{\rho_S} = 0.12 d^{-1}$ . This translates into the individual values of  $\rho_S$  being estimated between  $0.38 d^{-1}$  and  $0.75 d^{-1}$  depending on the experiment (Figure 7.18), which corresponds to doubling times between  $22 h$  and  $44 h$ . Then,  $\omega_{\delta_{SC}}$  is estimated at  $0.25 d^{-1}$  with the individual parameter values of  $\delta_{SC}$  estimated from  $0.25 d^{-1}$  to  $0.48 d^{-1}$ , which means that the corresponding half-life ranges from  $34 h$  to  $66 h$  depending on the experiment. Finally,  $\omega_{\delta_{CB}}$  is es-

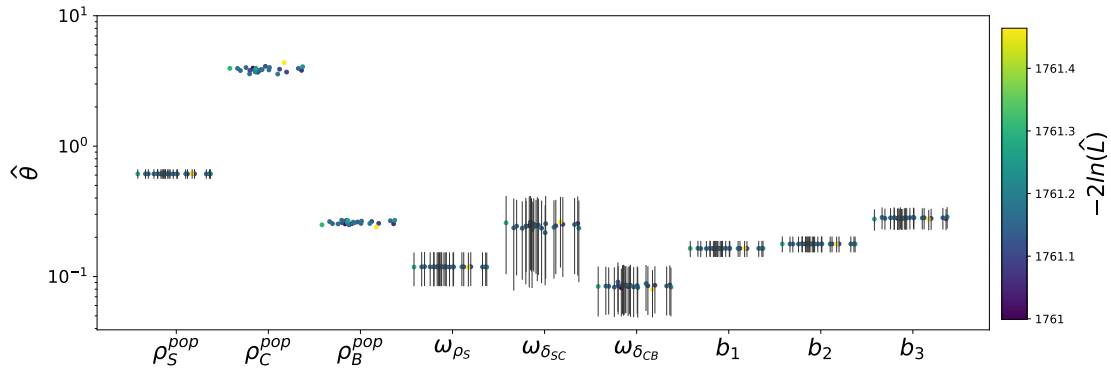


Figure 7.17: Estimated parameter values in the 25 convergent runs of SAEM for the model with reduced  $\delta_{SC}^{pop}$  and  $\delta_{CB}^{pop}$ , and no variability on  $\rho_C$  and  $\rho_B$ . Displayed are the estimated parameter values, color-coded by log-likelihood. Error bars are the FIM-derived standard errors of the estimates when available (when there is no error bar for a parameter value in a given run, it means that it was impossible for Monolix to invert the FIM). The population means and standard deviations are expressed in  $d^{-1}$ . The error parameters are unitless.

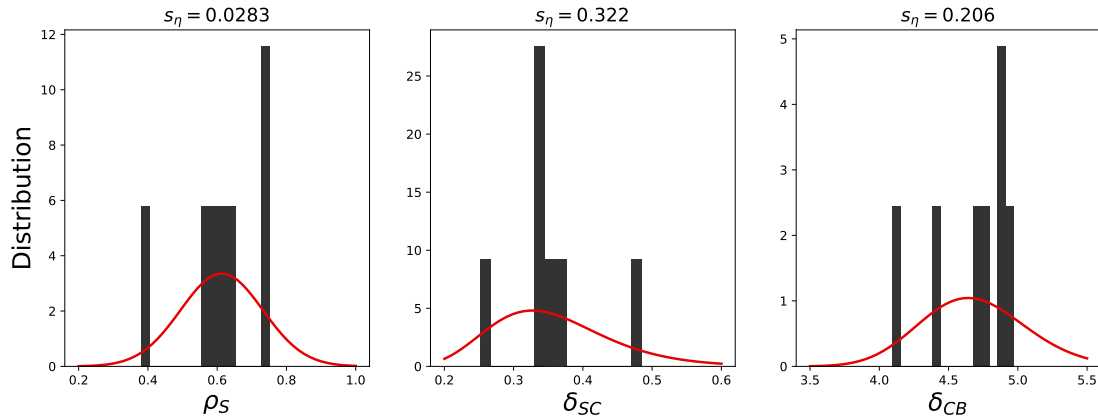


Figure 7.18: Parameter distributions in the SAEM run with the lowest log-likelihood. Histograms display the distribution of the estimated individual parameters. Red lines display the theoretical population distribution of the parameters (defined by the population parameter values). For each parameter we also give the  $\eta$ -shrinkage  $s_\eta$ .

estimated at  $0.082 d^{-1}$ , with individual parameter values for  $\delta_{CB}$  ranging from  $4.1 d^{-1}$  to  $5.0 d^{-1}$  and the corresponding half-life ranges from  $3 h$  to  $4 h$ .

The consequences of these parameter values for each replicate of the experiment are illustrated on Figure 7.19, which displays the total number of cells in the culture and the proportion of cells in each compartment of the model in each individual of the population. Because of differentiation, each compartment does not grow according to its net growth rate but to the difference of the two parameters. As a consequence, the committed compartment is smaller than the two others because despite their greater proliferation rate, committed cells also have a higher differentiation rate. The culture comprises on average 60% of differentiated cells by day 4, consistently with experimental measurements (Guillemin et al., 2018). It should also be noted that Figure 7.19 is very different from its equivalent in our deterministic model from Chapter 2 (Figure 4B in Duchesne et al., 2018), because in order to estimate the parameters of our MEM in Chapter 5, we had to relax the constraint that the model should reproduce the results of commitment experiments (cf. Section 1.1.2).

All these parameters are identifiable according to the criteria that we introduced in Section 1.4.4: each population parameter is estimated at a unique value (Figure 7.17), and the distribution of individual parameters matches the population distribution (Figure 7.18). However, identifiability analysis in Monolix is based on the FIM, and it was impossible to compute the FIM of our final model in any of the SAEM runs that we performed (Figure 7.17):  $\rho_C^{pop}$  and  $\rho_B^{pop}$  have an infinite standard error when computed from the FIM (Section 1.3.4.2). Based on the FIM, these two parameters thus appear as unidentifiable, while the others are all identifiable with a standard error which seems consistent between the SAEM runs (Figure 7.17). This means that the method used for identifiability analysis in MEM has an impact on the outcome of the analysis. However, since the FIM is proven to render biased confidence intervals when studying practical identifiability (Raue et al., 2009), our FIM-free method for identifiability analysis and model reduction, used in this chapter, appears as a reasonable approach with MEM.

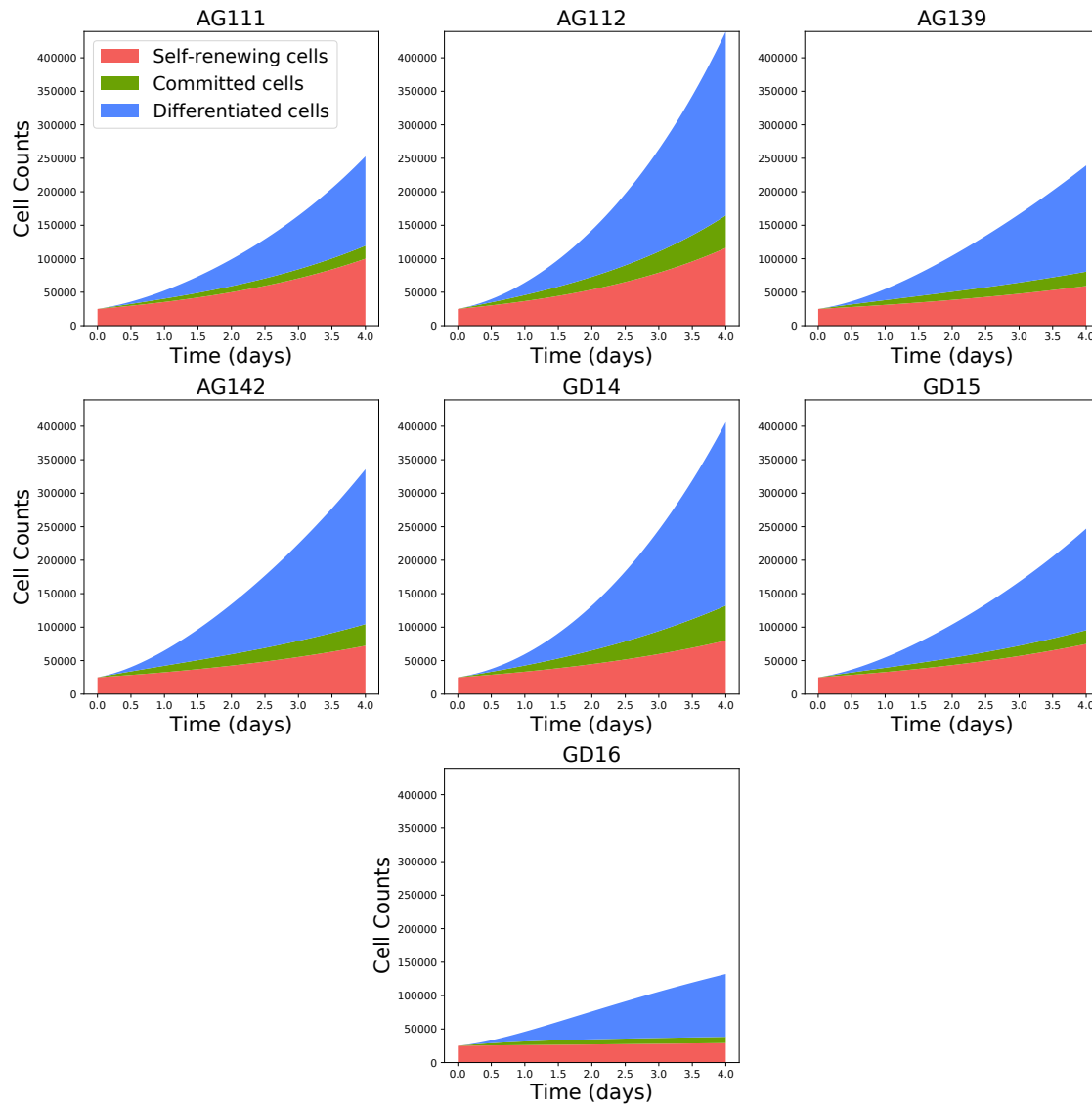


Figure 7.19: Cell distributions in each replicate of the experiment. The figure displays the number of cells in each compartment as shaded areas.

## 7.6.2 About the final model

In Section 7.6.1, we discussed the estimated values of the parameters and their biological relevance in terms of the timescales of the associated processes. But what did we actually learn from the reduction of the *full model*? Does it make sense that some parameters of the model should vary across experiments and not the others?

Actually, since we are using an experimental dataset with 7 individuals, it would be overly optimistic to state that the model that we constructed by reducing our *full model* reflects the true origin of heterogeneity in the experiments of *in vitro* differentiation. Nevertheless, the reduction approach that we adopted still allowed us to accurately determine which parameter values best describe the experimental heterogeneity in a small dataset. As a consequence, it seems that testing different combinations of fixed and random effects somehow optimized the potential of mixed effect modelling for reproducing experimental heterogeneity, with the little information on the observables that we had. Our approach thus appears as a promising attempt to address the problem of identifiability analysis in MEM (Lavielle and Aarons, 2016).

Still, the approach currently suffers one major drawback: it seems somewhat arbitrary to start reducing the *full model* by addressing the correlations between the fixed effects rather than the overparameterization of the random effects. What would have happened if we had reduced the model the other way around, starting by the random effects and addressing the correlations of the fixed effects next? Since varying the number of random effects in the model would not affect the structure of the fixed effects, the first reduction step should not address the problem of the correlations between fixed effects. Moreover, the correlations between the fixed effects in the *full model* describe a tendency for the average experiment, which should not be affected by the number of random effects in the model. As a consequence, there is no *a priori* reason that reducing the model the other way around would have resulted in a different final model.

And what if we had chosen to remove the random effect on  $\delta_{CB}$  instead

## 7.6. Discussion

of the one on  $\rho_B$  as a last step in the reduction? As we already argued, it makes more sense to remove the random effect on  $\rho_B$  rather than  $\delta_{CB}$ . Because the values of  $\delta_{CB}$  can be tuned to fit two variables of the system while  $\rho_B$  can fit only one variable, it seems reasonable to consider that the alternate model with a random effect on  $\rho_B$  and none on  $\delta_{CB}$  would give a worse fit to the data than our *final model*. However, as is often the case with MEM, the best solution would be to test both options.

### 7.6.3 Conclusion

In this chapter, we have iteratively reduced our mixed effect model until we could precisely estimate all of its parameters. First, we noticed correlations in the optimal values of the fixed effect parameters, and used them to simplify the estimation. Then, we detected an overparameterization of the random effects using their shrinkage. Removing two random effects from the initial model led to the model defined in System (7.5), which has 3 fixed effects (as the fixed effects on  $\delta_{SC}$  and  $\delta_{CB}$  are entirely determined by the one on  $\rho_C$ ), 3 random effects (on  $\rho_S$ ,  $\delta_{SC}$  and  $\delta_{CB}$ ) and three error parameters (one for each observable).

This model is able to fit the data from *in vitro* differentiation experiments, and is associated to identifiable parameter values. It might thus be confronted with the data obtained under treatment that we introduced in Chapter 4 in order to better characterize which parameters of cellular kinetics are affected by the drugs. The possible approaches for assessing the influence of the drugs on each parameter will be discussed in the next chapter.



# Chapter 8

## Discussion and prospects

### 8.1 A mathematical model of *in vitro* erythropoiesis

As we already mentioned in Section 1.1.3, a substantial amount of literature has been focusing on the modelling of erythropoiesis *in vivo* during the last decades (Pujo-Menjouet, 2016), while to our knowledge no modelling work has focused on the *in vitro* erythropoiesis so far. The main objective of this thesis was thus to develop a dynamic mathematical model of the *in vitro* erythropoiesis introduced in Section 1.1.2.

We presented our model in Chapter 2. It is a set of 3 linear ODEs describing the dynamics of three cell populations: the self-renewing compartment (S), the differentiated compartment (B), and a hypothetical intermediary compartment, also referred to as the committed compartment (C). Each compartment can proliferate and differentiate with its own rate, as depicted on Figure 8.1.

Although the C compartment is essentially hypothetical, its introduction can be justified by two arguments. First, the commitment experiment that we presented in Section 1.1.2 suggests that some cells in the culture have lost their self-renewing ability, and yet are not fully differentiated. Moreover, we showed in Duchesne et al. (2019) that a model without this intermediary compartment cannot fit the data as well as the model with three compartments.

More generally, the existence of such an intermediary state between the un-

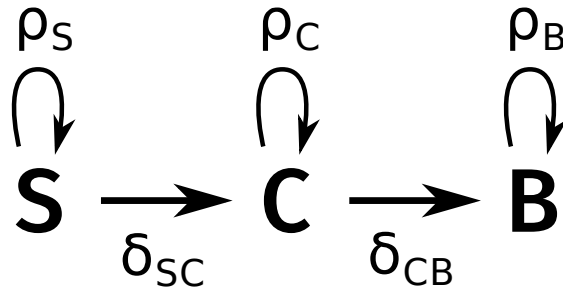


Figure 8.1: Diagram of the model designed in Chapter 2. S: self-renewing cells. C: committed cells. B: Benzidine-positive (*i.e.* differentiated) cells.  $\rho_i$  denotes the proliferation rate of compartment  $i$  and  $\delta_{ij}$  is the differentiation rate of compartment  $i$  into compartment  $j$ .

differentiated and differentiated states has been discussed (Moris et al., 2016), and does not seem specific to the erythropoietic system. In this transition state, the variability of gene expression increases, and then decreases back to its base level once cells are differentiated (Richard et al., 2016).

All the debate regarding the existence of a transition state has led to the hypothesis that differentiation happens through stochastic transitions between discrete states (Moris et al., 2016; Stumpf et al., 2017). An alternative point of view would consider differentiation as a continuous process with an infinite number of intermediary states. For instance, PDE-based models structured by the levels of differentiation factors have been developed to describe the differentiation of immune cells (Friedman et al., 2009; Barbarroux et al., 2016). Such an approach might be beneficial to describe our data, since PDE models (mostly structured by age) have been extensively used to describe erythropoiesis, as we already exposed in Section 1.1.3.

As a conclusion, our dynamic model accounts well for all the data at our disposal, and is in line with the contemporary view of cell differentiation. We thus conclude that it is a relevant basis for modelling *in vitro* erythropoiesis. Moreover, it is analytically solvable, which makes its simulation and calibration very fast.

## 8.2 Stochasticity of gene expression and differentiation

Over the past few years, several independent studies have highlighted that SGE increases during various differentiation processes (Mojtahedi et al., 2016; Richard et al., 2016; Semrau et al., 2017; Stumpf et al., 2017). Following these observations, we hypothesized that in T2EC cultures, increasing SGE should increase the differentiation rates of the cells (Section 1.2.2).

We addressed this question by identifying chemical drugs that modulate SGE in other biological systems (Dar et al., 2014; Moris et al., 2018) and applying them on T2EC cultures (Section 1.2.3). We found two drugs that reduced SGE and the number of differentiated cells in the culture (indomethacin and artemisinin, from Dar et al., 2014), as well as one drug that increased both the extent of SGE and the number of differentiated cells (MB3, from Moris et al., 2018). Then, using the mathematical model defined in Chapter 2, we proved that the effect of the drugs on differentiation was indeed due to altered values of differentiation rates (Chapter 3 and Guillemin et al., 2018). Namely, artemisinin and indomethacin led to decreased values of differentiation rates in our model, while MB3 led to increased values.

As a consequence, we provide the first experimental argument in favour of the theory that SGE is a driver of cell fate-decision events. This observation has been confirmed by Moris et al. (2018), who tested the effect of MB3 on another cellular system (mouse embryonic stem cells).

In bacteria and cancer cells, SGE has been shown to be involved in bet-hedging (Kreso et al., 2013; Pradhan and Chatterjee, 2014), that is an evolutionary strategy which enhances the survival of some cells in a varying environment (or against a treatment). Actually, since our *in vitro* differentiation experiment is driven by a change of the cells environment (that is their culture medium, as explained in Section 1.1.2), it would make sense to imagine an increased SGE allows cells to explore their state space and to adapt to their new environment.

### 8.3 Generalizing our reduction approach for mixed effect models

In Chapter 7, we developed an identifiable MEM of *in vitro* erythropoiesis by reducing the model defined in Chapter 5. Our approach for model reduction is based on initial guess sampling to detect correlations between population parameters, and on the  $\eta$ -shrinkage of the random effects to detect overparameterizations of the individual parameters.

This approach is based on extensive parameter estimations, and we were able to apply it to our model because it is analytically solvable and is thus very fast to simulate and calibrate. In this section, we discuss what features might complicate the application of our approach on other MEM.

In Section 7.2, we first used the correlations between population parameters to define a reduced model with constraints on the fixed effects. Using Spearman's  $\rho$ , we measured non-linear correlations between pairs of parameters, which allowed us to identify a cluster of highly correlated parameters (comprising  $\delta_{SC}^{pop}$ ,  $\rho_C^{pop}$  and  $\delta_{CB}^{pop}$ ). The exact shape of the likelihood landscape and the resulting unidentifiability is related to the structure of the model, and the quality of the data. This means that we were able to explore the parameter space near the likelihood optimum using pairwise correlations (Figure 7.4). Yet, in more complex nonlinear MEM, it is possible that the correlations would involve more than two parameters at a time. This means that detecting these complex correlations would require some kind of multivariate correlation analysis (Allison, 1999).

Throughout Chapter 7, we highlighted the fact that model reduction affects the convergence of SAEM. For instance, the first reduction step, which replaced  $\delta_{SC}^{pop}$  and  $\delta_{CB}^{pop}$  by their expression as function of  $\rho_C^{pop}$ , affected 11 SAEM runs out of 50. As we already mentioned, this is due to the fact that the approximation that we use to reduce the model is valid only near the range of parameter values on which it was defined. Outside of this range, the reduced model might not be a valid approximation of the full model, so that the estimator

#### 8.4. Computing the effect of the drugs with the mixed effect model

might get stuck in local optima that were absent from the full model.

Globally, the more parameters we removed from the full model, the fewer SAEM runs converged to the global optimum. However, the number of convergent SAEM runs is critical to the assessment of population parameters identifiability. This means that depending on the model under study, 50 SAEM runs might not be sufficient to assess parameter identifiability and allow for model reduction.

This is not a limit in the case of our model, since we use the analytical solution of the ODEs to reduce computation time. However, with more complex nonlinear dynamic models, computation time might become an issue, even though the latest versions of Monolix make profit of parallelization.

## 8.4 Computing the effect of the drugs with the mixed effect model

In Section 1.2.3, we introduced chemical drugs that influence both the extent of SGE and the number of differentiated cells in the culture. Now that we have defined an identifiable MEM of *in vitro* erythropoiesis, the next step would be to assess the effect of the drugs on the MEM parameters, using the full dataset that we introduced in Chapter 4.

In Chapter 3, we used a non-optimized approach to select the best models of treatments based on which parameters could vary in each treatment, without overfitting each treatment. This approach would be cumbersome with our MEM, since the estimation time of our MEM is much longer than for our deterministic model from Chapter 2. In the case of MEM, at least two methods could be used to identify which parameters vary under treatments, *i.e.* which combinations of parameters best explain each treatment.

First, Delattre and Poursat (2016) proposed a step-by-step approach for the selection of covariates and random-effects based on the BIC derived for MEM (Delattre et al., 2014). Covariates are parameters which describe variations in the individual parameters between different groups of individuals. In our case,

adding a covariate to a parameter of the model for one treatment would shift the population value of this parameter under the treatment, and the BIC would select the best combinations of covariates for each treatment. However, the BIC defined in Delattre and Poursat (2016), that we introduced in Equation (1.11), is based on the decomposition of the individual parameters into fixed individual parameters and random individual parameters. Since our reduced MEM from Equation (7.5) has a constant  $\rho_C$  over the population,  $\rho_C^{pop}$  would count as a population parameter that sets the value of a fixed parameter in Equation (1.11). However,  $\rho_C^{pop}$  is also used to set the population values of  $\delta_{SC}$  and  $\delta_{CB}$ , which are random in the final model. As a consequence, it is not obvious how to compute the BIC of our reduced model, so that using the BIC to select covariates would not be trivial either.

Another option would be to use a fused Lasso-penalized maximum-likelihood estimation (Ollier et al., 2015) in order to estimate the parameters of each treatment with a penalization proportional to the difference between the value under treatment and the control value. This would allow for the fitting of the model parameters to each treatment while avoiding overfitting. However, this method works under the hypothesis that the variance-covariance matrix of the random effects is diagonal and that all variances are non-null. Since only three parameters have random effects in our final MEM, it seems that this approach cannot be applied to our final model either.

## 8.5 Source of experimental heterogeneity

We introduced the concept of experimental heterogeneity in Chapter 4, and we used it a lot in the rest of the manuscript, but we did not really discuss how and why the outcome of our differentiation experiment should be variable.

In the introduction of this manuscript (Section 1.2.1), we mentioned the observation that heterogeneity is a fundamental feature of single-cell biology. For instance, *in vivo*, substantial variations have been observed in the self-renewal and potency of single haematopoietic stem cells and progenitors (Haas

## 8.6. Conclusion

et al., 2018). Since our T2EC are actual progenitors from the bone marrow of chick embryos, it is possible that similar heterogeneity might be observed in our *in vitro* experiments. In this setting, fluctuations in the self-renewal and differentiation rates of the culture at the macroscopic scale might be due to the random sampling of the progenitors at the microscopic scale when the culture is initiated.

However, our cultures were initiated with 25000 cells, so that cellular heterogeneity should be averaged out by the initial size of the culture. It is then possible that uncertainty on the initial condition of the model might be the cause of the apparent variability of the cell kinetics. Indeed, an error in the initial number of cells would affect the model prediction at all timepoints, which would result in an increased prediction error (and in turn to an increased value of the error parameters). It is possible to test this hypothesis by designing alternative forms of our MEM where the initial condition could vary between individuals. For instance, using model selection tools would allow to assess which model best describes experimental heterogeneity, among the reduced model of Chapter 7, the same model where the initial condition could vary, and the alternative model where only the initial condition could vary.

## 8.6 Conclusion

In this manuscript, we have defined a deterministic dynamic model of avian *in vitro* erythropoiesis (Chapter 2) and proved its identifiability. We then applied it to the data obtained under the drug treatments that influence SGE (Chapter 3). We proved that the drugs which decrease SGE also decrease the differentiation rate of the T2EC, and that the drug which increases the extent of SGE also increases the differentiation rate.

Then, we introduced the notion of experimental heterogeneity in Chapter 4 and proved that our deterministic model was not identifiable for all the replicates of the experiment. This motivated the elaboration of a first version of our MEM, or full model in Chapter 5, which we proved to be unidentifiable

according to the FIM, and to our own identifiability criteria.

In Chapter 6, we used experimental design to prove that increasing our sample size might not make our full model identifiable. Finally, we introduced in Chapter 7 an approach to reduce our full model in order to make it identifiable, without using the FIM.

This work provides strong arguments in favour of the theory that SGE can influence cell decision-making. In order to better characterize this influence at the single-cell level, an interesting prospect is provided by the single-cell transcriptomic data that were generated by Guillemin et al. (2018). These data, when confronted to proper models of gene expression (Herbach et al., 2017; Bonnaffoux et al., 2018), could be used to characterize the Gene Regulatory Networks that underlie differentiation in the control and drug-treated conditions. This would allow to disentangle more precisely how our chemical drugs modulate SGE and differentiation at the molecular level.

Following this description, one might also simulate artificial differentiation experiments, through the design of a multi-scale model of differentiation, in which cell decisions are taken based on realistic molecular mechanisms. These artificial experiments could then be compared to our original differentiation data, in order to verify if simulated experiments are characterized by the same kinetic parameter values as those that were estimated herein. This approach would allow to test the validity of our MEM without requiring more replicates of the experiments that would be too costly to perform. It would also link our work on the mixed effect modelling of differentiation to the biological functions of SGE.

# Bibliography

- Allison, P. D. (1999). *Multiple regression: a primer*. eng. Open Library ID: OL378019M. Thousand Oaks, Calif: Pine Forge Press. ISBN: 978-0-7619-8533-4.
- Andersen, S. W. and Millen, B. A. (2013). "On the practical application of mixed effects models for repeated measures to clinical trial data". en. In: *Pharmaceutical Statistics* 12.1, pp. 7–16. ISSN: 1539-1612. DOI: 10.1002/pst.1548.
- Apgar, J. F., Witmer, D. K., White, F. M., and Tidor, B. (2010). "Sloppy models, parameter uncertainty, and the role of experimental design". en. In: *Mol. BioSyst.* 6.10, pp. 1890–1900. ISSN: 1742-2051. DOI: 10.1039/B918098B.
- Bagiella, E., Sloan, R. P., and Heitjan, D. F. (2000). "Mixed-effects models in psychophysiology". en. In: *Psychophysiology* 37.1, pp. 13–20. ISSN: 1469-8986. DOI: 10.1111/1469-8986.3710013.
- Barbarroux, L., Michel, P., Adimy, M., and Crauste, F. (2016). "Multi-scale modeling of the CD8 immune response". en. In: AIP Publishing, p. 320002. DOI: 10.1063/1.4952106.
- Baron, M. H. and Maniatis, T. (1991). "Regulated expression of human alpha and beta-globin genes in transient heterokaryons." en. In: *Molecular and Cellular Biology* 11.3, pp. 1239–1247. ISSN: 0270-7306, 1098-5549. DOI: 10.1128/MCB.11.3.1239.
- Bauer, R. J. (2019). "NONMEM Tutorial Part II: Estimation Methods and Advanced Examples". en. In: *CPT: Pharmacometrics & Systems Pharmacology* 8.8, pp. 538–556. ISSN: 2163-8306. DOI: 10.1002/psp4.12422.
- Bazzoli, C., Retout, S., and Mentré, F. (2010). "Design evaluation and optimisation in multiple response nonlinear mixed effect models: PFIM 3.0". eng.

- In: *Comput Methods Programs Biomed* 98.1, pp. 55–65. ISSN: 1872-7565. DOI: 10.1016/j.cmpb.2009.09.012.
- Becskei, A., Kaufmann, B. B., and Oudenaarden, A. v. (2005). “Contributions of low molecule number and chromosomal positioning to stochastic gene expression”. en. In: *Nat Genet* 37.9, pp. 937–944. ISSN: 1546-1718. DOI: 10.1038/ng1616.
- Bélaïr, J., Mackey, M. C., and Mahaffy, J. M. (1995). “Age-structured and two-delay models for erythropoiesis”. In: *Mathematical Biosciences* 128.1, pp. 317–346. ISSN: 0025-5564. DOI: 10.1016/0025-5564(94)00078-E.
- Bernard, S. (2013). “How to Build a Multiscale Model in Biology”. en. In: *Acta Biotheoretica* 61.3, pp. 291–303. ISSN: 0001-5342, 1572-8358. DOI: 10.1007/s10441-013-9199-z.
- Bertin, E. (2012). *A concise introduction to the statistical physics of complex systems*. en. SpringerBriefs in complexity. OCLC: ocn771939627. Heidelberg ; New York: Springer. ISBN: 978-3-642-23922-9.
- Bessonov, N., Crauste, F., Demin, I., and Volpert, V. (2009). “Dynamics of Erythroid Progenitors and Erythroleukemia”. en. In: *Math. Model. Nat. Phenom.* 4.3, pp. 210–232. ISSN: 0973-5348, 1760-6101. DOI: 10.1051/mmnp/20094309.
- Bolker, B. M., Brooks, M. E., Clark, C. J., Geange, S. W., Poulsen, J. R., Stevens, M. H. H., and White, J.-S. S. (2009). “Generalized linear mixed models: a practical guide for ecology and evolution”. In: *Trends in Ecology & Evolution* 24.3, pp. 127–135. ISSN: 0169-5347. DOI: 10.1016/j.tree.2008.10.008.
- Bonnaïffoux, A., Herbach, U., Richard, A., Guillemin, A., Giraud, S., Gros, P.-A., and Gandrillon, O. (2018). “WASABI: a dynamic iterative framework for gene regulatory network inference”. en. In: *bioRxiv*, p. 292128. DOI: 10.1101/292128.
- Bouchnita, A., Eymard, N., Koury, M., and Volpert, V. (2014). “Initiation of erythropoiesis by BFU-E cells”. In: *Mathematical biology in life sciences*. Sidi bel Abbes, Algeria. DOI: 10.1051/itmconf/20150401002.
- Bresson-Mazet, C., Gandrillon, O., and Gonin-Giraud, S. (2008). “Stem cell antigen 2: a new gene involved in the self-renewal of erythroid progenitors”. en.

## Bibliography

- In: *Cell Proliferation* 41.5, pp. 726–738. ISSN: 1365-2184. DOI: 10.1111/j.1365-2184.2008.00554.x.
- Brown, G., Bunce, C. M., and Guy, G. R. (1985). “Sequential determination of lineage potentials during haemopoiesis.” In: *Br J Cancer* 52.5, pp. 681–686. ISSN: 0007-0920.
- Brown, K., Hill, C., Calero, G., Myers, C., Lee, K., Sethna, J., and Cerione, R. (2004). “The statistical mechanics of complex signaling networks: nerve growth factor signaling”. en. In: *Phys. Biol.* 1.3, pp. 184–195. ISSN: 1478-3975. DOI: 10.1088/1478-3967/1/3/006.
- Brown, K. and Sethna, J. (2003). “Statistical mechanical approaches to models with many poorly known parameters”. In: *Phys. Rev. E* 68.2, p. 021904. DOI: 10.1103/PhysRevE.68.021904.
- Burnham, K. and Anderson, D. (2010). *Model selection and multimodel inference: a practical information-theoretic approach*. OCLC: 934366523. New York: Springer. ISBN: 978-0-387-95364-9 0-387-95364-7.
- Busetto, A., Hauser, A., Krummenacher, G., Sunnåker, M., Dimopoulos, S., Ong, C., Stelling, J., and Buhmann, J. (2013). “Near-optimal experimental design for model selection in systems biology”. en. In: *Bioinformatics* 29.20, pp. 2625–2632. ISSN: 1367-4803. DOI: 10.1093/bioinformatics/btt436.
- Chang, H., Hemberg, M., Barahona, M., Ingber, D., and Huang, S. (2008). “Transcriptome-wide noise controls lineage choice in mammalian progenitor cells”. eng. In: *Nature* 453.7194, pp. 544–547. ISSN: 1476-4687. DOI: 10.1038/nature06965.
- Chis, O., Banga, J., and Balsa-Canto, E. (2011). “Structural Identifiability of Systems Biology Models: A Critical Comparison of Methods”. In: *PLOS ONE* 6.11, e27755. ISSN: 1932-6203. DOI: 10.1371/journal.pone.0027755.
- Conrado, D. J., Karlsson, M. O., Romero, K., Sarr, C., and Wilkins, J. J. (2017). “Open innovation: Towards sharing of data, models and workflows”. In: *European Journal of Pharmaceutical Sciences*. Special issue in honour of Professor Meindert Danhof 109, S65–S71. ISSN: 0928-0987. DOI: 10.1016/j.ejps.2017.06.035.

- Crauste, F., Pujo-Menjouet, L., Génieys, S., Molina, C., and Gandrillon, O. (2008). “Adding self-renewal in committed erythroid progenitors improves the biological relevance of a mathematical model of erythropoiesis”. eng. In: *J. Theor. Biol.* 250.2, pp. 322–338. ISSN: 1095-8541. DOI: 10.1016/j.jtbi.2007.09.041.
- Dar, R. D., Hosmane, N. N., Arkin, M. R., Siliciano, R. F., and Weinberger, L. S. (2014). “Screening for noise in gene expression identifies drug synergies”. en. In: *Science* 344.6190, pp. 1392–1396. ISSN: 0036-8075, 1095-9203. DOI: 10.1126/science.1250220.
- Davila-Velderrain, J., Martinez-Garcia, J., and Alvarez-Buylla, E. (2015). “Modeling the epigenetic attractors landscape: toward a post-genomic mechanistic understanding of development”. English. In: *Front. Genet.* 6. ISSN: 1664-8021. DOI: 10.3389/fgene.2015.00160.
- Dazy, S., Damiola, F., Parisey, N., Beug, H., and Gandrillon, O. (2003). “The MEK-1/ERKs signalling pathway is differentially involved in the self-renewal of early and late avian erythroid progenitor cells”. In: *Oncogene* 22.58, pp. 9205–9216. ISSN: 0950-9232, 1476-5594. DOI: 10.1038/sj.onc.1207049.
- Delattre, M., Lavielle, M., and Poursat, M. (2014). “A note on BIC in mixed-effects models”. EN. In: *Electron. J. Statist.* 8.1, pp. 456–475. ISSN: 1935-7524. DOI: 10.1214/14-EJS890.
- Delattre, M. and Poursat, M. (2016). “BIC strategies for model choice in a population approach”. In: *arXiv:1612.02405 [stat]*. arXiv: 1612.02405.
- Dempster, A. P., Laird, N. M., and Rubin, D. B. (1977). “Maximum Likelihood from Incomplete Data Via the EM Algorithm”. en. In: *Journal of the Royal Statistical Society: Series B (Methodological)* 39.1, pp. 1–22. ISSN: 2517-6161. DOI: 10.1111/j.2517-6161.1977.tb01600.x.
- Dolznic, H., Bartunek, P., Nasmyth, K., Müllner, E. W., and Beug, H. (1995). “Terminal differentiation of normal chicken erythroid progenitors: shortening of G1 correlates with loss of D-cyclin/cdk4 expression and altered cell size control”. eng. In: *Cell Growth Differ.* 6.11, pp. 1341–1352. ISSN: 1044-9523.

## Bibliography

- Drylewicz, J., Commenges, D., and Thiebaut, R. (2012). “Maximum a Posteriori Estimation in Dynamical Models of Primary HIV Infection”. In: *Statistical Communications in Infectious Diseases* 4.1. ISSN: 1948-4690. DOI: 10.1515/1948-4690.1040.
- Duchesne, R., Guillemin, A., Crauste, F., and Gandrillon, O. (2019). “Calibration, Selection and Identifiability Analysis of a Mathematical Model of the in vitro Erythropoiesis in Normal and Perturbed Contexts”. en. In: *ISB* 13.1-2, pp. 55–69. ISSN: 13866338, 14343207. DOI: 10.3233/ISB-190471.
- Duchesne, R., Guillemin, A., Gandrillon, O., and Crauste, F. (2018). “Calibration, Selection and Identifiability Analysis of a Mathematical Model of the in vitro Erythropoiesis in Normal and Perturbed Contexts”. In: *bioRxiv*. DOI: 10.1101/314955.
- Efron, B. and Tibshirani, R. (1986). “Bootstrap Methods for Standard Errors, Confidence Intervals, and Other Measures of Statistical Accuracy”. EN. In: *Statistical Science* 1.1, pp. 54–75. ISSN: 0883-4237, 2168-8745. DOI: 10.1214/ss/1177013815.
- Eldar, A. and Elowitz, M. B. (2010). “Functional roles for noise in genetic circuits”. eng. In: *Nature* 467.7312, pp. 167–173. ISSN: 1476-4687. DOI: 10.1038/nature09326.
- Elowitz, M., Levine, A., Siggia, E., and Swain, P. (2002). “Stochastic Gene Expression in a Single Cell”. en. In: *Science* 297.5584, pp. 1183–1186. ISSN: 0036-8075, 1095-9203. DOI: 10.1126/science.1070919.
- Faller, D., Klingmüller, U., and Timmer, J. (2003). “Simulation Methods for Optimal Experimental Design in Systems Biology”. en. In: *SIMULATION* 79.12, pp. 717–725. ISSN: 0037-5497, 1741-3133. DOI: 10.1177/0037549703040937.
- Fidler, M., Wilkins, J. J., Hooijmaijers, R., Post, T. M., Schoemaker, R., Trame, M. N., Xiong, Y., and Wang, W. (2019). “Nonlinear Mixed-Effects Model Development and Simulation Using nlmixr and Related R Open-Source Packages”. In: *CPT: Pharmacometrics & Systems Pharmacology* 0.0. ISSN: 2163-8306. DOI: 10.1002/psp4.12445.

- Fischer, S., Kurbatova, P., Bessonov, N., Gandrillon, O., Volpert, V., and Crauste, F. (2012). "Modeling erythroblastic islands: using a hybrid model to assess the function of central macrophage". eng. In: *J. Theor. Biol.* 298, pp. 92–106. ISSN: 1095-8541. DOI: 10.1016/j.jtbi.2012.01.002.
- Foley, C. and Mackey, M. (2009). "Dynamic hematological disease: a review". eng. In: *J Math Biol* 58.1-2, pp. 285–322. ISSN: 0303-6812. DOI: 10.1007/s00285-008-0165-3.
- Friedman, A., Kao, C., and Shih, C. (2009). "Asymptotic phases in a cell differentiation model". In: *Journal of Differential Equations* 247.3, pp. 736–769. ISSN: 0022-0396. DOI: 10.1016/j.jde.2009.03.033.
- Fröhlich, F., Kessler, T., Weindl, D., Shadrin, A., Schmiester, L., Hache, H., Muradyan, A., Schütte, M., Lim, J., Heinig, M., Theis, F., Lehrach, H., Wierling, C., Lange, B., and Hasenauer, J. (2018). "Efficient Parameter Estimation Enables the Prediction of Drug Response Using a Mechanistic Pan-Cancer Pathway Model". English. In: *cels* 0.0. ISSN: 2405-4712. DOI: 10.1016/j.cels.2018.10.013.
- Fröhlich, F., Theis, F., and Hasenauer, J. (2014). "Uncertainty Analysis for Non-identifiable Dynamical Systems: Profile Likelihoods, Bootstrapping and More". In: *CMSB*. Ed. by P. Mendes, J. Dada, and K. Smallbone. Cham: Springer International Publishing, pp. 61–72. ISBN: 978-3-319-12982-2.
- Gandrillon, O., Schmidt, U., Beug, H., and Samarut, J. (1999). "TGF-beta cooperates with TGF-alpha to induce the self-renewal of normal erythrocytic progenitors: evidence for an autocrine mechanism". eng. In: *EMBO J.* 18.10, pp. 2764–2781. ISSN: 0261-4189. DOI: 10.1093/emboj/18.10.2764.
- Goetz, J. J. and Trimarchi, J. M. (2012). "Transcriptome sequencing of single cells with Smart-Seq". en. In: *Nature Biotechnology* 30.8, pp. 763–765. ISSN: 1546-1696. DOI: 10.1038/nbt.2325.
- Gonin-Giraud, S., Bresson-Mazet, C., and Gandrillon, O. (2008). "Involvement of the TGF- $\beta$  and mTOR/p70S6Kinase pathways in the transformation process induced by v-ErbA". In: *Leukemia Research* 32.12, pp. 1878–1888. ISSN: 01452126. DOI: 10.1016/j.leukres.2008.05.010.

## Bibliography

- Gonzalez, A. M., Uhlenhof, J., Schaul, J., Cinquemani, E., Batt, G., and Ferrari-Trecate, G. (2013). "Identification of biological models from single-cell data: A comparison between mixed-effects and moment-based inference". en. In: *2013 European Control Conference (ECC)*. Zurich: IEEE, pp. 3652–3657. ISBN: 978-3-033-03962-9. DOI: 10.23919/ECC.2013.6669366.
- Görgens, A., Radtke, S., Möllmann, M., Cross, M., Dürig, J., Horn, P. A., and Giebel, B. (2013). "Revision of the Human Hematopoietic Tree: Granulocyte Subtypes Derive from Distinct Hematopoietic Lineages". In: *Cell Reports* 3.5, pp. 1539–1552. ISSN: 2211-1247. DOI: 10.1016/j.celrep.2013.04.025.
- Guedj, J., Thiébaud, R., and Commenges, D. (2007). "Maximum Likelihood Estimation in Dynamical Models of HIV". en. In: *Biometrics* 63.4, pp. 1198–1206. ISSN: 1541-0420. DOI: 10.1111/j.1541-0420.2007.00812.x.
- Guillemain, A., Duchesne, R., Crauste, F., Gonin-Giraud, S., and Gandrillon, O. (2018). "Drugs modulating stochastic gene expression affect the erythroid differentiation process". en. In: *bioRxiv*. DOI: 10.1101/371666.
- Haas, S., Trumpp, A., and Milsom, M. D. (2018). "Causes and Consequences of Hematopoietic Stem Cell Heterogeneity". In: *Cell Stem Cell* 22.5, pp. 627–638. ISSN: 1934-5909. DOI: 10.1016/j.stem.2018.04.003.
- Haldermans, P., Shkedy, Z., Van Sanden, S., Burzykowski, T., and Aerts, M. (2007). "Using Linear Mixed Models for Normalization of cDNA Microarrays". In: *Statistical applications in genetics and molecular biology* 6, Article 19. DOI: 10.2202/1544-6115.1249.
- Heitzler, P. and Simpson, P. (1991). "The choice of cell fate in the epidermis of *Drosophila*". eng. In: *Cell* 64.6, pp. 1083–1092. ISSN: 0092-8674. DOI: 10.1016/0092-8674(91)90263-x.
- Herbach, U., Bonnafox, A., Espinasse, T., and Gandrillon, O. (2017). "Inferring gene regulatory networks from single-cell data: a mechanistic approach". In: *BMC Systems Biology* 11, p. 105. ISSN: 1752-0509. DOI: 10.1186/s12918-017-0487-0.

- Hintze, J. L. and Nelson, R. D. (1998). "Violin Plots: A Box Plot-Density Trace Synergism". In: *The American Statistician* 52.2, pp. 181–184. ISSN: 0003-1305. DOI: 10.1080/00031305.1998.10480559.
- Huang, S. (2009). "Non-genetic heterogeneity of cells in development: more than just noise". eng. In: *Development* 136.23, pp. 3853–3862. ISSN: 1477-9129. DOI: 10.1242/dev.035139.
- Huang, S. (2010). "Cell Lineage Determination in State Space: A Systems View Brings Flexibility to Dogmatic Canonical Rules". In: *PLoS Biol* 8.5. ISSN: 1544-9173. DOI: 10.1371/journal.pbio.1000380.
- Kalmar, T., Lim, C., Hayward, P., Muñoz-Descalzo, S., Nichols, J., Garcia-Ojalvo, J., and Arias, A. M. (2009). "Regulated Fluctuations in Nanog Expression Mediate Cell Fate Decisions in Embryonic Stem Cells". en. In: *PLOS Biology* 7.7, e1000149. ISSN: 1545-7885. DOI: 10.1371/journal.pbio.1000149.
- Karin, O., Alon, U., and Sontag, E. (2017). "A note on dynamical compensation and its relation to parameter identifiability". en. In: *bioRxiv*, p. 123489. DOI: 10.1101/123489.
- Karin, O., Swisa, A., Glaser, B., Dor, Y., and Alon, U. (2016). "Dynamical compensation in physiological circuits". en. In: *Molecular Systems Biology* 12.11, p. 886. ISSN: 1744-4292, 1744-4292. DOI: 10.15252/msb.20167216.
- Karlsson, M., Janzén, D., Durrieu, L., Colman-Lerner, A., Kjellsson, M., and Cedersund, G. (2015). "Nonlinear mixed-effects modelling for single cell estimation: when, why, and how to use it". en. In: *BMC Sys. Biol.* 9.1. ISSN: 1752-0509. DOI: 10.1186/s12918-015-0203-x.
- Karlsson, M. and Savic, R. (2007). "Diagnosing Model Diagnostics". en. In: *Clinical Pharmacology & Therapeutics* 82.1, pp. 17–20. ISSN: 1532-6535. DOI: 10.1038/sj.clpt.6100241.
- Kauffman, S. (1969). "Homeostasis and Differentiation in Random Genetic Control Networks". en. In: *Nature* 224.5215, pp. 177–178. ISSN: 0028-0836. DOI: 10.1038/224177a0.

## Bibliography

- Kennedy, W. (1980). "New Developments in Statistical Computing". In: *The American Statistician* 34.2, pp. 115–121. ISSN: 0003-1305. DOI: 10.1080/00031305.1980.10483014.
- Kowalski, A. and Palyga, J. (2011). "Chromatin compaction in terminally differentiated avian blood cells: the role of linker histone H5 and non-histone protein MENT". en. In: *Chromosome Res* 19.5, pp. 579–590. ISSN: 1573-6849. DOI: 10.1007/s10577-011-9218-3.
- Kreso, A., O'Brien, C. A., Galen, P. v., Gan, O. I., Notta, F., Brown, A. M. K., Ng, K., Ma, J., Wienholds, E., Dunant, C., Pollett, A., Gallinger, S., McPherson, J., Mullighan, C. G., Shibata, D., and Dick, J. E. (2013). "Variable Clonal Repopulation Dynamics Influence Chemotherapy Response in Colorectal Cancer". en. In: *Science* 339.6119, pp. 543–548. ISSN: 0036-8075, 1095-9203. DOI: 10.1126/science.1227670.
- Krinner, A., Roeder, I., Loeffler, M., and Scholz, M. (2013). "Merging concepts - coupling an agent-based model of hematopoietic stem cells with an ODE model of granulopoiesis". In: *BMC Systems Biology* 7, p. 117. ISSN: 1752-0509. DOI: 10.1186/1752-0509-7-117.
- Kuhn, E. and Lavielle, M. (2005). "Maximum likelihood estimation in nonlinear mixed effects models". In: *Computational Statistics & Data Analysis* 49.4, pp. 1020–1038. ISSN: 0167-9473. DOI: 10.1016/j.csda.2004.07.002.
- Lavielle, M. and Aarons, L. (2016). "What do we mean by identifiability in mixed effects models?" en. In: *J Pharmacokinet Pharmacodyn* 43.1, pp. 111–122. ISSN: 1567-567X, 1573-8744. DOI: 10.1007/s10928-015-9459-4.
- Lavielle, M. and Bleakley, K. (2014). *Mixed Effects Models for the Population Approach: Models, Tasks, Methods and Tools*. Chapman & Hall/CRC Biostatistics Series. Boca Raton, Florida: CRC Press/Taylor & Francis Group. ISBN: 978-1-4822-2650-8.
- Li, C. and Wang, J. (2013). "Quantifying Cell Fate Decisions for Differentiation and Reprogramming of a Human Stem Cell Network: Landscape and Biological Paths". In: *PLOS Computational Biology* 9.8, e1003165. ISSN: 1553-7358. DOI: 10.1371/journal.pcbi.1003165.

- Liang, H., Wu, H., and Zou, G. (2008). "A note on conditional aic for linear mixed-effects models". In: *Biometrika* 95.3, pp. 773–778. ISSN: 0006-3444. DOI: 10.1093/biomet/asn023.
- Liepe, J., Filippi, S., Komorowski, M., and Stumpf, M. (2013). "Maximizing the Information Content of Experiments in Systems Biology". en. In: *PLOS Comp. Biol.* 9.1, e1002888. ISSN: 1553-7358. DOI: 10.1371/journal.pcbi.1002888.
- Lindstrom, M. and Bates, D. (1990). "Nonlinear Mixed Effects Models for Repeated Measures Data". en. In: *Biometrics* 46.3, p. 673. ISSN: 0006341X. DOI: 10.2307/2532087.
- Lixoft (2019). *Feature of the week #45: Understanding how SAEM works*. URL: <https://www.youtube.com/watch?v=3DfgPWWuvk4> (visited on 08/28/2019).
- Loeffler, M., Pantel, K., Wulff, H., and Wichmann, H. E. (1989). "A mathematical model of erythropoiesis in mice and rats. Part 1: Structure of the model". eng. In: *Cell Tissue Kinet* 22.1, pp. 13–30. ISSN: 0008-8730.
- Luzyanina, T., Mrusek, S., Edwards, J., Roose, D., Ehl, S., and Bocharov, G. (2007). "Computational analysis of CFSE proliferation assay". eng. In: *Journal of Mathematical Biology* 54.1, pp. 57–89. ISSN: 0303-6812. DOI: 10.1007/s00285-006-0046-6.
- Machta, B., Chachra, R., Transtrum, M., and Sethna, J. (2013). "Parameter Space Compression Underlies Emergent Theories and Predictive Models". en. In: *Science* 342.6158, pp. 604–607. ISSN: 0036-8075, 1095-9203. DOI: 10.1126/science.1238723.
- Mackey, M. C. and Dörmer, P. (1982). "Continuous maturation of proliferating erythroid precursors". eng. In: *Cell Tissue Kinet* 15.4, pp. 381–392. ISSN: 0008-8730.
- Matplotlib 3.1.0 documentation (2019). *Violin plot basics*. URL: <https://matplotlib.org/3.1.0/gallery/statistics/violinplot.html> (visited on 08/28/2019).
- Mojtahedi, M., Skupin, A., Zhou, J., Castaño, I., Leong-Quong, R., Chang, H., Trachana, K., Giuliani, A., and Huang, S. (2016). "Cell Fate Decision as

## Bibliography

- High-Dimensional Critical State Transition". In: *PLOS Biology* 14.12, e2000640. ISSN: 1545-7885. DOI: 10.1371/journal.pbio.2000640.
- Moris, N., Pina, C., and Arias, A. (2016). "Transition states and cell fate decisions in epigenetic landscapes". In: *Nature Reviews Genetics* 17.11, pp. 693–703.
- Moris, N., Edri, S., Seyres, D., Kulkarni, R., Domingues, A. F., Balayo, T., Frontini, M., and Pina, C. (2018). "Histone Acetyltransferase KAT2A Stabilizes Pluripotency with Control of Transcriptional Heterogeneity". en. In: *STEM CELLS* 36.12, pp. 1828–1838. ISSN: 1549-4918. DOI: 10.1002/stem.2919.
- Nooney, G. C. (1965). "Iron kinetics and erythron development". eng. In: *Biophys. J.* 5.6, pp. 755–765. ISSN: 0006-3495. DOI: 10.1016/S0006-3495(65)86750-9.
- O'Brien, R. M., Hudson, K., and Stockard, J. (2008). "A Mixed Model Estimation of Age, Period, and Cohort Effects". en. In: *Sociological Methods & Research* 36.3, pp. 402–428. ISSN: 0049-1241. DOI: 10.1177/0049124106290392.
- Ollier, E., Samson, A., Delavenne, X., and Viallon, V. (2015). "A SAEM Algorithm for Fused Lasso Penalized Non Linear Mixed Effect Models: Application to Group Comparison in Pharmacokinetic". In: *arXiv:1502.07458 [stat]*. arXiv: 1502.07458.
- Ozbudak, E., Thattai, M., Kurtser, I., Grossman, A., and Oudenaarden, A. van (2002). "Regulation of noise in the expression of a single gene". eng. In: *Nat. Genet.* 31.1, pp. 69–73. ISSN: 1061-4036. DOI: 10.1038/ng869.
- Pillai, G., Mentré, F., and Steimer, J. (2005). "Non-linear mixed effects modeling - from methodology and software development to driving implementation in drug development science". eng. In: *J Pharmacokinet Pharmacodyn* 32.2, pp. 161–183. ISSN: 1567-567X. DOI: 10.1007/s10928-005-0062-y.
- Pinheiro, J. C. and Bates, D. M. (1995). "Approximations to the Log-Likelihood Function in the Nonlinear Mixed-Effects Model". In: *Journal of Computational and Graphical Statistics* 4.1, pp. 12–35. ISSN: 1061-8600. DOI: 10.1080/10618600.1995.10474663.

- Pohjanpalo, H. (1978). "System identifiability based on the power series expansion of the solution - ScienceDirect". In: *Mathematical Biosciences* 41.1-2, pp. 21–33. DOI: 10.1016/0025-5564(78)90063-9.
- Pradhan, B. B. and Chatterjee, S. (2014). "Reversible non-genetic phenotypic heterogeneity in bacterial quorum sensing". In: *Molecular Microbiology* 92.3, pp. 557–569. ISSN: 0950-382X. DOI: 10.1111/mmi.12575.
- Prague, M., Commenges, D., Guedj, J., Julia, D., and Thiébaud, R. (2013). "NIMROD: a program for inference via a normal approximation of the posterior in models with random effects based on ordinary differential equations." In: *Comput Methods Programs Biomed.* 111.2, pp. 447–458. DOI: 10.1016/j.cmpb.2013.04.014.
- Pujo-Menjouet, L. (2016). "Blood Cell Dynamics: Half of a Century of Modelling". en. In: *Math. Model. Nat. Phenom.* 11.1, pp. 92–115. ISSN: 0973-5348, 1760-6101. DOI: 10.1051/mmnp/201611106.
- Raser, J. M. and O'Shea, E. K. (2004). "Control of Stochasticity in Eukaryotic Gene Expression". en. In: *Science* 304.5678, pp. 1811–1814. ISSN: 0036-8075, 1095-9203. DOI: 10.1126/science.1098641.
- Raue, A., Becker, V., Klingmüller, U., and Timmer, J. (2010). "Identifiability and observability analysis for experimental design in nonlinear dynamical models". In: *Chaos* 20.4, p. 045105. ISSN: 1054-1500. DOI: 10.1063/1.3528102.
- Raue, A., Kreutz, C., Maiwald, T., Bachmann, J., Schilling, M., Klingmüller, U., and Timmer, J. (2009). "Structural and practical identifiability analysis of partially observed dynamical models by exploiting the profile likelihood". In: *Bioinformatics* 25.15, pp. 1923–1929. ISSN: 1367-4803, 1460-2059. DOI: 10.1093/bioinformatics/btp358.
- Raue, A., Kreutz, C., Theis, F., and Timmer, J. (2013). "Joining forces of Bayesian and frequentist methodology: a study for inference in the presence of non-identifiability". en. In: *Phil. Trans. R. Soc. A* 371.1984, p. 20110544. ISSN: 1364-503X, 1471-2962. DOI: 10.1098/rsta.2011.0544.
- Raue, A., Schilling, M., Bachmann, J., Matteson, A., Schelke, M., Kaschek, D., Hug, S., Kreutz, C., Harms, B., Theis, F., Klingmüller, U., and Timmer, J.

## Bibliography

- (2013). "Lessons learned from quantitative dynamical modeling in systems biology". eng. In: *PloS One* 8.9, e74335. ISSN: 1932-6203. DOI: 10.1371/journal.pone.0074335.
- Retout, S., Comets, E., Samson, A., and Mentré, F. (2007). "Design in nonlinear mixed effects models: Optimization using the Fedorov-Wynn algorithm and power of the Wald test for binary covariates." en. In: *Statistics in Medicine*, p. 2007. DOI: 10.1002/sim.2910.
- Richard, A., Boullu, L., Herbach, U., Bonnafoux, A., Morin, V., Vallin, E., Guillemin, A., Papili Gao, N., Gunawan, R., Cosette, J., Arnaud, O., Kupiec, J., Espinasse, T., Gonin-Giraud, S., and Gandrillon, O. (2016). "Single-Cell-Based Analysis Highlights a Surge in Cell-to-Cell Molecular Variability Preceding Irreversible Commitment in a Differentiation Process". eng. In: *PLoS Biol.* 14.12, e1002585. ISSN: 1545-7885. DOI: 10.1371/journal.pbio.1002585.
- Rinott, R., Jaimovich, A., and Friedman, N. (2011). "Exploring transcription regulation through cell-to-cell variability". en. In: *PNAS* 108.15, pp. 6329–6334. ISSN: 0027-8424, 1091-6490. DOI: 10.1073/pnas.1013148108.
- Roeder, I., Horn, K., Sieburg, H., Cho, R., Muller-Sieburg, C., and Loeffler, M. (2008). "Characterization and quantification of clonal heterogeneity among hematopoietic stem cells: a model-based approach". en. In: *Blood* 112.13, pp. 4874–4883. ISSN: 0006-4971, 1528-0020. DOI: 10.1182/blood-2008-05-155374.
- Rowland, M. (2005). "Editorial to the First Issue Dedicated to Lewis Sheiner". en. In: *J Pharmacokinet Pharmacodyn* 32.2, pp. 157–159. ISSN: 1573-8744. DOI: 10.1007/s10928-005-9502-y.
- Rué, P. and Martínez Arias, A. (2015). "Cell dynamics and gene expression control in tissue homeostasis and development". In: *Molecular Systems Biology* 11.2, p. 792. ISSN: 1744-4292. DOI: 10.15252/msb.20145549.
- Savic, R. and Karlsson, M. (2009). "Importance of Shrinkage in Empirical Bayes Estimates for Diagnostics: Problems and Solutions". In: *AAPS J* 11.3, pp. 558–569. ISSN: 1550-7416. DOI: 10.1208/s12248-009-9133-0.

- Schirm, S., Engel, C., Loeffler, M., and Scholz, M. (2013). "A Biomathematical Model of Human Erythropoiesis under Erythropoietin and Chemotherapy Administration". In: *PLOS ONE* 8.6, e65630. ISSN: 1932-6203. DOI: 10.1371/journal.pone.0065630.
- Schwarz, G. (1978). "Estimating the Dimension of a Model". In: *The Annals of Statistics* 6.2, pp. 461–464. ISSN: 0090-5364.
- Seita, J. and Weissman, I. L. (2010). "Hematopoietic stem cell: self-renewal versus differentiation". en. In: *Wiley Interdisciplinary Reviews: Systems Biology and Medicine* 2.6, pp. 640–653. ISSN: 1939-005X. DOI: 10.1002/wsbm.86.
- Semrau, S., Goldmann, J., Soumillon, M., Mikkelsen, T., Jaenisch, R., and Oude-naarden, A. (2017). "Dynamics of lineage commitment revealed by single-cell transcriptomics of differentiating embryonic stem cells". En. In: *Nature Communications* 8.1, p. 1096. ISSN: 2041-1723. DOI: 10.1038/s41467-017-01076-4.
- Sepúlveda, L. A., Xu, H., Zhang, J., Wang, M., and Golding, I. (2016). "Measurement of gene regulation in individual cells reveals rapid switching between promoter states". en. In: *Science* 351.6278, pp. 1218–1222. ISSN: 0036-8075, 1095-9203. DOI: 10.1126/science.aad0635.
- Shannon, C. (1948). "A Mathematical Theory of Communication". en. In: *Bell Syst. Tech. Jour.* 27, pp. 379–423.
- Sharney, L., Wasserman, L. R., Schwartz, L., and Tendler, D. (1963). "Multiple pool analysis as applied to erythro-kinetics". eng. In: *Ann. N. Y. Acad. Sci.* 108, pp. 230–249. ISSN: 0077-8923.
- Singh, H. (1996). "Gene targeting reveals a hierarchy of transcription factors regulating specification of lymphoid cell fates". In: *Current Opinion in Immunology* 8.2, pp. 160–165. ISSN: 0952-7915. DOI: 10.1016/S0952-7915(96)80053-7.
- Sontag, E. (2017). "Dynamic compensation, parameter identifiability, and equivariances". English. In: *PLoS Comp. Biol.* 13.4. WOS:000402542900012, e1005447. ISSN: 1553-734X. DOI: 10.1371/journal.pcbi.1005447.

## Bibliography

- Stumpf, P., Smith, R., Lenz, M., Schuppert, A., Müller, F., Babbie, A., Chan, T., Stumpf, M., Please, C., Howison, S., Arai, F., and MacArthur, B. (2017). “Stem Cell Differentiation as a Non-Markov Stochastic Process”. en. In: *Cell Systems* 5.3, 268–282.e7. ISSN: 24054712. DOI: 10.1016/j.cels.2017.08.009.
- Süel, G. M., Garcia-Ojalvo, J., Liberman, L. M., and Elowitz, M. B. (2006). “An excitable gene regulatory circuit induces transient cellular differentiation”. en. In: *Nature* 440.7083, pp. 545–550. ISSN: 1476-4687. DOI: 10.1038/nature04588.
- Transtrum, M., Machta, B., Brown, K., Daniels, B., Myers, C., and Sethna, J. (2015). “Perspective: Sloppiness and emergent theories in physics, biology, and beyond”. In: *The Journal of Chemical Physics* 143.1, p. 010901. ISSN: 0021-9606. DOI: 10.1063/1.4923066.
- Vaida, F. and Blanchard, S. (2005). “Conditional Akaike information for mixed-effects models”. In: *Biometrika* 92.2, pp. 351–370. ISSN: 0006-3444. DOI: 10.1093/biomet/92.2.351.
- Vajda, S., Godfrey, K. R., and Rabitz, H. (1989). “Similarity transformation approach to identifiability analysis of nonlinear compartmental models”. eng. In: *Mathematical Biosciences* 93.2, pp. 217–248. ISSN: 0025-5564. DOI: 10.1016/0025-5564(89)90024-2.
- Vanrolleghem, P. A. and Dochain, D. (1998). “Bioprocess model identification”. In: *Advanced instrumentation, data interpretation, and control of biotechnological processes*. Springer, pp. 251–318.
- Venzon, D. J. and Moolgavkar, S. H. (1988). “A Method for Computing Profile-Likelihood-Based Confidence Intervals”. In: *Journal of the Royal Statistical Society. Series C (Applied Statistics)* 37.1, pp. 87–94. ISSN: 0035-9254. DOI: 10.2307/2347496.
- Villarreal, C., Padilla-Longoria, P., and Alvarez-Buylla, E. (2012). “General Theory of Genotype to Phenotype Mapping: Derivation of Epigenetic Landscapes from N-Node Complex Gene Regulatory Networks”. In: *Phys. Rev. Lett.* 109.11, p. 118102. DOI: 10.1103/PhysRevLett.109.118102.

- Villaverde, A. and Banga, J. (2017). "Dynamical compensation and structural identifiability of biological models: Analysis, implications, and reconciliation". In: *PLOS Comp. Biol.* 13.11, e1005878. ISSN: 1553-7358. DOI: 10.1371/journal.pcbi.1005878.
- Villaverde, A. and Barreiro, A. (2016). "Identifiability of Large Nonlinear Biochemical Networks". In: 76, pp. 259–296.
- Viñuelas, J., Kaneko, G., Coulon, A., Vallin, E., Morin, V., Mejia-Pous, C., Kupiec, J.-J., Beslon, G., and Gandrillon, O. (2013). "Quantifying the contribution of chromatin dynamics to stochastic gene expression reveals long, locus-dependent periods between transcriptional bursts". In: *BMC Biology* 11.1, p. 15. ISSN: 1741-7007. DOI: 10.1186/1741-7007-11-15.
- Waddington, C. (1957). *The strategy of the genes: a discussion of some aspects of theoretical biology*. en. Allen & Unwin.
- Walter, E. and Lecourtier, Y. (1982). "Global approaches to identifiability testing for linear and nonlinear state space models - ScienceDirect". In: *Mathematics and Computers in Simulation* 24, pp. 472–482.
- Wang, J., Xu, L., Wang, E., and Huang, S. (2010). "The potential landscape of genetic circuits imposes the arrow of time in stem cell differentiation". eng. In: *Biophys. J.* 99.1, pp. 29–39. ISSN: 1542-0086. DOI: 10.1016/j.bpj.2010.03.058.
- Wang, Y. (2007). "Derivation of various NONMEM estimation methods". en. In: *J Pharmacokinet Pharmacodyn* 34.5, pp. 575–593. ISSN: 1567-567X, 1573-8744. DOI: 10.1007/s10928-007-9060-6.
- Waterfall, J., Casey, F., Gutenkunst, R., Brown, K., Myers, C., Brouwer, P., Elser, V., and Sethna, J. (2006). "Sloppy-Model Universality Class and the Vandermonde Matrix". In: *Phys. Rev. Lett.* 97.15, p. 150601. DOI: 10.1103/PhysRevLett.97.150601.
- Weber, P., Kramer, A., Dingler, C., and Radde, N. (2012). "Trajectory-oriented Bayesian experiment design versus Fisher A-optimal design: an in depth comparison study". en. In: *Bioinformatics* 28.18, pp. i535–i541. ISSN: 1367-4803. DOI: 10.1093/bioinformatics/bts377.

## Bibliography

- Weissman, I. L. and Shizuru, J. A. (2008). “The origins of the identification and isolation of hematopoietic stem cells, and their capability to induce donor-specific transplantation tolerance and treat autoimmune diseases”. en. In: *Blood* 112.9, pp. 3543–3553. ISSN: 0006-4971, 1528-0020. DOI: 10.1182/blood-2008-08-078220.
- White, A., Tolman, M., Thames, H., Withers, H., Mason, K., and Transtrum, M. (2016). “The Limitations of Model-Based Experimental Design and Parameter Estimation in Sloppy Systems”. In: *PLOS Computational Biology* 12.12, e1005227. ISSN: 1553-7358. DOI: 10.1371/journal.pcbi.1005227.
- White, A. K., VanInsberghe, M., Petriv, O. I., Hamidi, M., Sikorski, D., Marra, M. A., Piret, J., Aparicio, S., and Hansen, C. L. (2011). “High-throughput microfluidic single-cell RT-qPCR”. en. In: *PNAS* 108.34, pp. 13999–14004. ISSN: 0027-8424, 1091-6490. DOI: 10.1073/pnas.1019446108.
- Wikimedia Commons (2019a). *File:Hematopoiesis (human) diagram en.svg* — *Wikimedia Commons, the free media repository*. [Online; accessed 15-August-2019]. URL: [https://commons.wikimedia.org/w/index.php?title=File:Hematopoiesis\\_\(human\)\\_diagram\\_en.svg&oldid=360847125](https://commons.wikimedia.org/w/index.php?title=File:Hematopoiesis_(human)_diagram_en.svg&oldid=360847125).
- Wikimedia Commons (2019b). *File:Hematopoiesis simple.svg* — *Wikimedia Commons, the free media repository*. [Online; accessed 15-August-2019]. URL: [https://commons.wikimedia.org/w/index.php?title=File:Hematopoiesis\\_simple.svg&oldid=338900399](https://commons.wikimedia.org/w/index.php?title=File:Hematopoiesis_simple.svg&oldid=338900399).
- Wong, V. C., Bass, V. L., Bullock, M. E., Chavali, A. K., Lee, R. E. C., Mothes, W., Gaudet, S., and Miller-Jensen, K. (2018). “NF- $\kappa$ B-Chromatin Interactions Drive Diverse Phenotypes by Modulating Transcriptional Noise”. In: *Cell Reports* 22.3, pp. 585–599. ISSN: 2211-1247. DOI: 10.1016/j.celrep.2017.12.080.
- Xu, X. S., Yuan, M., Karlsson, M. O., Dunne, A., Nandy, P., and Vermeulen, A. (2012). “Shrinkage in nonlinear mixed-effects population models: quantification, influencing factors, and impact”. eng. In: *AAPS J* 14.4, pp. 927–936. ISSN: 1550-7416. DOI: 10.1208/s12248-012-9407-9.

Zhou, J. X., Aliyu, M. D. S., Aurell, E., and Huang, S. (2012). "Quasi-potential landscape in complex multi-stable systems". In: *Journal of The Royal Society Interface* 9.77, pp. 3539–3553. DOI: 10.1098/rsif.2012.0434.